# Procedures for the analysis and use of multiple view angle image data

Simon A.W. Kay

Submission for the degree of Doctor of Philosophy

University College London
December 1989

ProQuest Number: 10609869

All rights reserved

INFORMATION TO ALL USERS
The quality of this reproduction is dependent upon the quality of the copy submitted.

In the unlikely event that the author did not send a complete manuscript
and there are missing pages, these will be noted. Also, if material had to be removed,
a note will indicate the deletion.

ProQuest 10609869

Published by ProQuest LLC (2017). Copyright of the Dissertation is held by the Author.

All rights reserved.
This work is protected against unauthorized copying under Title 17, United States Code
Microform Edition © ProQuest LLC.

ProQuest LLC.
789 East Eisenhower Parkway
P.O. Box 1346
Ann Arbor, MI 48106 – 1346

## Abstract

It is recognised that the majority of vegetative cover types have anisotropic reflectance characteristics that are largely a function of their canopy geometry. Several studies have made attempts at formulating methods for the use of data remotely sensed from off-nadir directions. The best of these methods attempt to utilise the "extra" information implicitly contained in off-nadir image datasets. In this study, an attempt is made to extract information concerning agro-physical parameters of a number of vegetative cover types using imagery acquired by an airborne sensor, the Daedalus Airborne Thematic Mapper (ATM).

It is also recognised in the literature that the nature of spatial variance in images is related to the size and distribution of the objects in the scene and the sampling characteristics of the sensor. In previous work this relationship has been explored by examining scenes using images of varying spatial resolutions, using a number of measurements of spatial variance. The underlying trend of these measurements is then used to interpret the nature of the objects in the scene.

No previous work exists which attempts to utilise the change in variance of images acquired at different off-nadir view angles. In this study, the understanding of this relationship is developed by examining the change in variance of a number of vegetative cover types from multiple view angle image datasets. The geometry of the ATM sensor is derived to allow an understanding of the sampling characteristics of the instrument. Two important geometric factors are established: first, the area of the ground resolution element increases with view angle, which effectively reduces spatial resolution at off-nadir angles; and second, overlap between adjacent ground resolution elements increases with view angle, increasing the spatial auto-correlation between these samples.

The effects of illumination, atmosphere and topography can all influence variance in an image. A parametric procedure for normalising multiple view angle (and therefore multitemporal) datasets for these factors is developed, based upon the production of reflectance images using a sky radiance model of the spectral and

spatial distributions of irradiance, ground measurements of irradiance, and a digital terrain model of the study site.

Finally, it is shown that image variance is likely to decrease at off-nadir view angles, the magnitude of this decrease being related to the sensor geometry and (more importantly) the geometry of the canopy. By a simple statistical analytical procedure it is possible to construct broad classes within which the nature of the canopy can be classified.

# Contents

## Main Sections

## Chapter 3: Data collection and pre-processing



## Chapter 4: The use of reflectance images to process and correct ATM image data

## Tables

### Chapter 3



### Chapter 4



### Chapter 5



### Chapter 6

## Figures

### Chapter 1



### Chapter 2



### Chapter 3



### Chapter 4

**Chapter 5**



**Chapter 6**

# Preface

'Space exploration has always served as a convenient whipping-boy to those needing money for some worthy cause, yet it is far less expensive than many a stuck-in-the-mud, down-to-earth technological failure. Unfortunately, the apologists for space science always seem over-impressed by the engineering trivia and make far too much of non-stick frying pans and perfect ball-bearings. To my mind, the outstanding spin-off from space research is not new technology. The real bonus has been that for the first time in human history we have had a chance to look at the Earth from space, and the information gained from seeing from the outside our azure-green planet in all its global beauty has given rise to a whole new set of questions and answers.'

(J.E. Lovelock, *Gaia*)

Figure 2.1: A full-swath Daedalus ATM image, band 1.

# Acknowledgments

It is always difficult to start a list acknowledging support from such a large number of people - except that of course in the creation of a thesis, a research student will have his or her supervisor to thank the most once the document is bound and buried. I am indebted to Mike Barnsley for many things, beginning with his judgement that my attempt to complete this thesis in the short time available to me was possible. I have been allowed to develop the study in most any manner that I desired, the careful aspects of contingency and caution introduced into the study being mostly his. The less-than-perfect passages remaining in my thesis are more often than not a result of my intransigence and idleness, and in no way a reflection of Mike's careful, zealous attention to my script.

Without a farm study site that I knew, had superb access to, and was run by helpful and enthusiastic friends, I could never had completed this study in the time I have. For this I owe Joe Henson and John Neave a lot more than they got for me trampling their crops, and even more for the knowledge I picked up for being around with them (and listening more closely this time). I also much appreciated the cups of tea, coffee, toast, sandwiches, lunches... the list is endless. Many thanks, Gill.

Graham Sadler and Don Monteith helped collect data at various times; I would also like to thank Terry Elsey for early discussions concerning image processing, and Paul Smyth for his later assistance. Paul Schooling, as well as being an amenable and generous system manager, also provided valuable expertise in assisting me with many of the mathematical and programming problems I faced, making up for any lack of confidence or ability of my own in these areas.

The opportunity to discuss and present one's own work to others is an invaluable event that helps spur development and generate further ideas; for such occasions I would like to thank (in alphabetical order) Tony Allan, Ciska Borry, James Cutler, Phil Eales, Phil Lewis, Ted Milton, Kevin Morris, Peter Muller, Andy Newton, James Pearson, Allison Reid, Liz Rollin, Wells Small, among others, who attended workshops and seminars where I was presenting work.

In the production of the thesis I would like to thank first Prof. Ron Cooke, for the recognition that good equipment may help to produce a better thesis; I hope this one benefits as a result. Most of the diagrams were drawn on an Apple Macintosh, for the use of which I must thank Tim Aspden and Robert Bradbrook of UCL Geography, and Mike Durant for finding not just one, but *two* Mac's *and* a PC that I could finish up on. Kevin Morris also provided one of the diagrams. Bill Campbell provided helpful advice with statistics, Mapics, and various mid-project crises, again many thanks for letting me through the open door. I also owe many small favours to other staff at UCL, who I have come to bother at some time or other. Anne Oxenham, Chris Cromarty and Claudette John have all made my access to a variety of things much simpler.

The Natural Environment Research Council funded both my time at UCL and my field work, including the airborne data acquisition. I would like to make due recognition of this, and hope that they continue to fund data collection by research students as comprehensively.

All of my friends deserve some mention; Paul, Estelle, Tim, Steve, James, Louise and Colin, Mary, Helen, Wells, Peter Wood, Peter Jackson, Alun, Clare, plus all the geography post-grads, have all put up with a griping and introspective research student for long enough.

Finally, I have Ciska to thank for pulling me over these last few hurdles, her hard work correcting my manuscripts where I had given up, and providing the real reason for finishing as soon as I could.

Simon Kay, November 1989

# CHAPTER 1: Introduction

## 1.1: Aims and objectives

- To provide a comprehensive and practicable method for the analysis and utilisation of multiple view angle image data, to allow the application of these data in agriculture for crop inventory and management uses, with particular reference to wheat and barley crops in southern England.

- To assess the suitability of using component models of atmospheric, topographic and illumination effects in the correction of multiple view angle imagery, and to move towards the development of an holistic physical modelling strategy for image correction in general.

- To develop a modelling strategy capable of using the 'additional' information that may be contained in off-nadir data.

- To demonstrate that such data are useful in the context of mapping agrophysical parameters in the United Kingdom.

### 1.1.1: Background

Remote sensing can provide valuable information to the agricultural community, at a local level to farm managers and agricultural materials suppliers (Wiegand *et al.*, 1986, Jackson *et al.*, 1986), and at a regional scale to agricultural business conglomerates, federal and national governments, such as in this country the Ministry of Agriculture, Fisheries and Food (MAFF) (MacDonald and Hall, 1980, Heydorn and Takacs, 1986, Wiegand *et al.*, 1986, Gallo and Fesch, 1989), and international organisations, for example the European Community, United Nations Food and Agriculture Organisation (Tucker *et al.*, 1985, Townshend and Justice, 1986, Henricksen, 1986, Tucker and Choudhury, 1987). Each organisation will have its own requirements as to the nature of the information; scale, data presentation, accuracy, timeliness, and frequency of coverage are all considerations

that must be made (Jackson *et al.*, 1986). Farmers and farm managers are always interested in a tool which may aid them to increase yield, and therefore income and hopefully profitability. Remote sensing could contribute in two ways: first, it can help improve the statistical collection of data used in compiling regional or national figures for production; and second, it can be used to identify parcels where production is sub-optimal, and bring attention to these regions.

While a role for remote sensing in UK agriculture could be visualised, it would be almost impossible to realise it at the present time, considering the complex political and educational changes that would have to take place. In the future, however, farm management and government or consultative bodies could be trained to exploit this valuable data resource. It is in anticipation of this demand that the Remote Sensing community must explore the possibilities opened by new sensors, and in particular reference to the UK, oblique imaging sensors such as SPOT, NOAA AVHRR, HIRIS, MODIS-N and MODIS-T. So-called *off-nadir*[1] geometric configurations provide a major advantage over other low-orbit satellite sensors, since theoretical imaging opportunities for locations on the Earth's surface are increased. This improves temporal resolution of the instruments, an important factor in temperate, cloudy regions. The SPOT High Resolution Visible (HRV) sensor has a ±27°off-nadir pointing capability across track, and the Advanced Very High Resolution Radiometer (AVHRR) sensors, on board the NOAA series of satellite platforms, gather off-nadir data from a track 2700km wide with a 111° field of view (FOV) (figure 1.1). Further planned oblique imaging sensors include HIRIS and MODIS, to be launched in the 1990s as part of the NASA EOS campaign. Thus, it is no longer feasible to consider imagery to be collected under uniform geometric conditions.

A change of image geometry presents a challenge to the remote sensing community, namely to examine the nature of the reflectance of targets more closely, and also to examine the associated effect of view angle upon detected reflectance. Several studies have already been carried out with this intention (Salomonson and Marlatt, 1971, Barnsley, 1984a and b, 1985, Irons *et al.*, 1987),

---

[1]*Italicised* terms, used for the first time, are explained further in the Glossary.

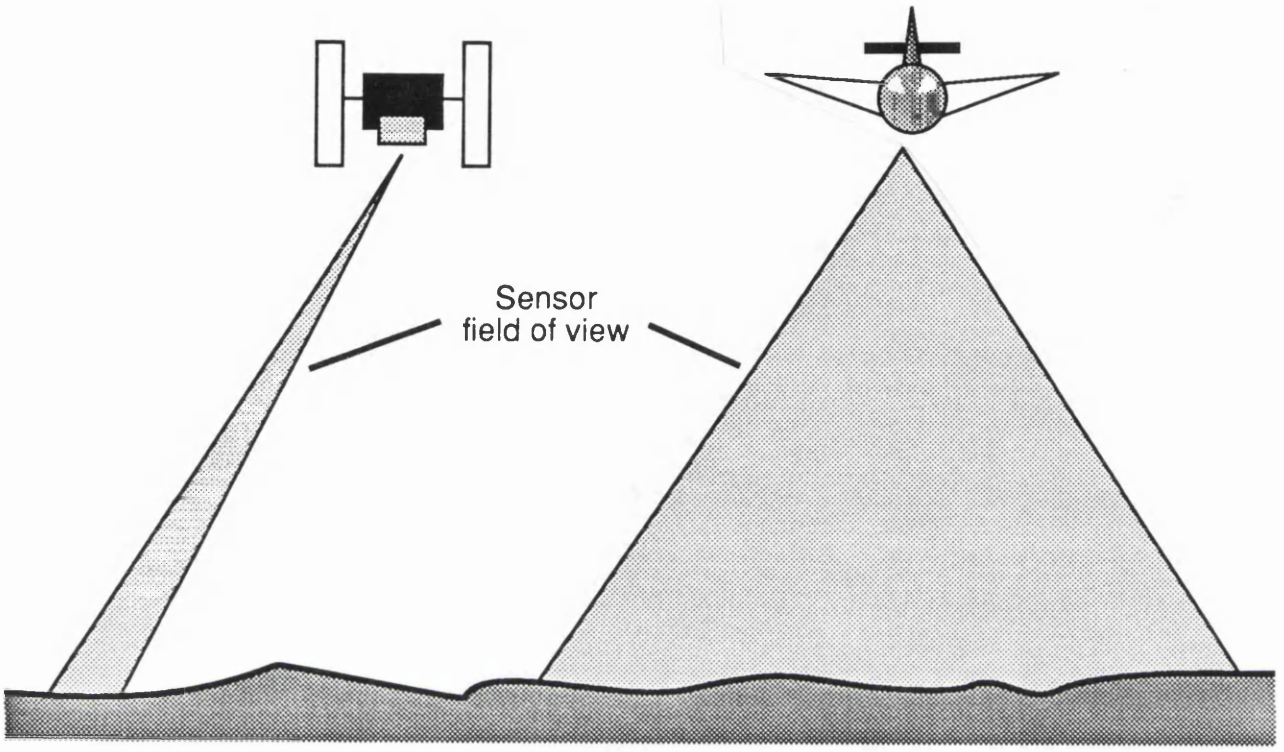


Figure 1.1: Off-nadir pointing and view geometries. Examples of off-nadir pointing sensors (left) are SPOT and HIRIS; off-nadir viewing instruments have wide fields of view, such as the AVHRR and the Daedalus ATM used in this study.

and many ideas have been postulated about the usefulness of directional reflectance data, and about how the effects may be normalised (to preserve the current remote sensing paradigm) or enhanced and utilised (to examine a new dimension).

The aim of this study is to produce a practicable method for the use of multiple view angle data to measure agrophysical parameters for a restricted number of cover types. The result, the examination of change in image variance with increasing view angle, may not be the definitive solution, but it is a step towards the acceptance of the fact that off-nadir view angle data cannot be used in the current, conventional remote sensing framework for image analysis and interpretation.

## 1.2: Directional Reflectance

*Directional reflectance* is the general term used to describe the concept of angular reflectance properties of objects in a scene. Other specific terms are also used to describe this effect: 'ideal' targets may be *diffuse* - a property otherwise termed *Lambertian* or *isotropic* - or *specular* in their angular reflectance characteristics, although in reality they are usually a combination of the two properties, or *anisotropic*. Hypothetical descriptions of angular reflectance properties of targets are usually referenced as the *Bidirectional Reflectance Distribution Function* (BRDF) (Nicodemus, 1970) which is the theoretical description of reflectance from a target over infinitesimally small solid angles, and so therefore cannot be measured directly. Conventional remote sensing strategies have tended to ignore the directional reflectance properties of targets on the Earth's surface, because the geometric configuration of sensors has, in general, been of predominantly one type, namely nadir-pointing, and therefore only ever recorded one 'direction', ignoring seasonal effects changing solar illumination geometry.

### 1.2.1: The interaction of directional reflectance and image geometry

Variable image geometry means variable effects on scene radiance due to atmosphere, illumination, topography, and canopy geometry. This must be

recognised before multi-scene analysis can be made (Moran *et al.*, 1988). The differences between any two images of the same scene can be explained by the temporal variation in any of these factors between data acquisition, and the differences in the geometry of Sun, target and sensor, the latter of which is detailed in chapter 3. Popular current thought assumes that given "minor" differences in geometry these differences can be wholly explained by time (giving rise to multi-temporal models, Kauth and Thomas, 1976, Pinter *et al.*, 1981, and Kalayeh and Landgrebe, 1986, Campbell *et al.*, 1987), i.e. that image geometry has little effect on the radiance detected by the sensor (Curran and Williamson, 1985 and 1987, Jones *et al.*, 1988). This is shown to be a false assumption in chapter 4, by eliminating temporal variations between scenes of the same location acquired from different angles, such that the remaining differences in detected response are due to geometric differences in data collection. Chapter 5 then proceeds to analyse changes in image variance as a function of view angle, in an attempt to extract agrophysical parameters from multiple view-angle imagery. These three related themes constitute the major experiment in this study.

As yet, modulation of radiance due to view angle effect is not fully understood, despite numerous experimental measurement studies (section 2.2.2), and theoretical examinations and simulations of the problem (section 2.2.3). In this study, the differences due to view angle are identified and analysed for several canopies on a single farm (sections 3.1, 4.1.1), with a selection of planting dates and variety of topographic orientations. The radiometric differences are explained to as large a degree as is possible by the differences in atmosphere, illumination, topography and view angle (chapter 4). The remaining differences are then analysed to devise a strategy for the utilisation of multiple view-angle image data (chapter 5).

### 1.2.2: Present and future sensors

The Landsat series of sensors has a FOV of 14°; at the edge of the image data are acquired at a moderate view angle of 7° off-nadir. While with some illumination geometries (i.e. small solar zenith angles) this is unlikely to have any great effect, with low illumination the effect of image geometry could be greater. In general

Landsat imagery does not present a major problem with regards to directional reflectance, indeed is probably the major reason for the tenacious existence of vertical geometry paradigms.

The SPOT HRV sensor provides a current example of off-nadir data collection. Although the FOV is more restricted than that of Landsat[2], the ability to view up to ±27° (Chevrel *et al.*, 1981) means that off-nadir radiometric effects are more pronounced (for scene by scene comparison). However, some studies have claimed that the Sun-Target-Sensor (S-T-S) geometry for this sensor are not as bad (with regards view angle effect) as they could be for other future sensors (Barnsley and Muller, 1989).

### 1.2.3: Strategies for the use of off-nadir data

Two distinct strategies exist for the utilisation of multiple view angle data. The first, *normalisation*, attempts to correct data to a given "normal", usually taken to be the nadir view value - although occasionally the minimum value may be regarded as a datum. The second strategy, *utilisation*, emphasises that the relationship between view angle and data is determined by the interaction of the radiant flux and the canopy, summarised by the Bidirectional Reflectance Distribution Function of the surface, and that by understanding this process further information concerning the target can be extracted.

Normalisation strategies often take the form of *non-parametric* solutions, that is those that do not attempt to model the flux/canopy interaction, using knowledge of how reflectance is modulated by view angle, but instead concentrate on *a posteriori* predictions of the relationship between view angle and the parameter under investigation. Statistical techniques, such as the regression of polynomial functions are typical examples of these methods (Royer *et al.*, 1985, Morris and Barnsley, 1989, figure 2.7). Attempts at utilisation are usually *parametric*, trying to use an understanding of canopy geometry, and the consequent effects upon

---

[2]4.3° (Baudoin and Brossier, 1983)

reflectance, in model inversions that provide some information about the target. Normalisation techniques are unlikely ever to become parametric, since such methods would discard much of the valuable information that current remote sensing models can only divulge indirectly; essentially, parametric normalisation "throws out the baby with the bath water". The more logical approach, therefore, is to work towards a new, parametric, utilisation strategy that will allow the direct interpretation of agrophysical parameters that can be used as inputs for modelling of crop development and classification.

## 1.3: Application of remote sensing in agriculture

### 1.3.1: The use of remote sensing products in agriculture

Remote sensing has the capability to provide a synoptic "snapshot" of the Earth; it is well suited to overviews of larger areas than act as the focus for point studies, i.e of specific features. This is due to the quantised nature of the image, and the relative coarseness of the spatial resolution of most civilian sensors. Certainly with current satellite imagery, and to a lesser extent airborne data, the spectral and spatial characteristics of the sensors demand an interpretation of the data based upon models and inference (i.e. examination of band ratios, indices, spatial variations, classification) in order to extract meaningful information. High resolution sensors (in either spectral or spatial domain) could reduce this dependency upon inference, by allowing a more direct path to information extraction - at the expense of increased data quantities and processing times. This problem is discussed in chapter 6, where a new data collection strategy is proposed which would allow multiple view angle data to enhance the information already provided by remote sensing to agriculture.

On a small farm, the farm manager can inspect crops quickly and frequently, independent of weather conditions, programme requests *etc*, from the seat of a Land Rover. In Britain, this technique is highly satisfactory, and it is unlikely that any farmer should wish to exchange such a useful vehicle for a ground receiving

station and an image processor. Crop inspection usually demands greater attention to detail than current sensors are capable of providing, and often indirect indicators (e.g. aphids, root inspections) are used to assess crop health and disease. Remote sensing therefore is likely to provide an interpretive tool for the consultant, perhaps in assessing drainage, nutrient supply, and management strategies on a farm or region basis. Of great significance is the type of information required for farm management, and the consequent timeliness of the data supply.

The exact nature of the information required by farmers and farm managers, therefore, is greatly dependent upon the management strategy adopted on each individual farm. Considering only the production of wheat or barley, for example, in the USA much of this crop is grown in semi-arid regions, and is heavily dependent upon irrigation. It is important that the farm management optimises the irrigation, to minimise costs and maximise yields. The timeliness of the remotely sensed data which could warn of water stress in a canopy is of great significance; for example, Jackson *et al.* (1986) cite a few hours as being the period of time after which the data has little value.

### 1.3.2: The need for remote sensing in agronomy

From a conventional remote sensing objective, classification, indices production and thematic mapping can be all carried out in an automatic or semi-automated manner, given ground and image data availability. These data are not of direct use to farmers; however, they are of great use to larger planning agencies, such as ministries, development agencies, or financial speculators in the agricultural produce market. The ability to predict and quantify future yields of crops, bought and sold on the global commodity market, is an extremely valuable one to certain groups of people. While it could help to solve, and more importantly avoid, regional shortages and major crop failures and their consequent devastating effects upon populations in marginal farming regions, the western world has also developed a powerful tool for the fine tuning of exploitation of these commodities, and the people who produce them. A final irony is that the populations most affected by agricultural catastrophies are usually without access to such technology,

and therefore rely upon the generosity of the developed countries to provide them with forecasts or "now-casts" of impending disasters.

It is interesting, therefore, to note that economic decisions are cited as being of greatest importance for the development of the United States Department of Agriculture (USDA) LACIE program:

> 'International trade decisions based on inadequate information regarding the global food supply can have severe economic and social effects. In 1972 and again in 1977, advance knowledge of the shortfall in the Soviet grain crop could have had a positive effect on the US economy, rather than the negative effect that resulted from the lack of good information.'
>
> (MacDonald and Hall, 1980, p670)

That is, better forecasts would have resulted in more dollars. But in other cases, accurate, *timely*, agro-meteorological forecasting could be more than just beneficial to the US economy, and the emphasis could be shifted onto the "social", or more literally humanitarian, effects of disaster avoidance. Good forecasting, and even now-casting, can contribute effectively to the planning and execution of relief and aid programmes, avoiding unnecessary suffering caused often by "inadequate information" and delayed action. Two such examples are presented in the use of NOAA AVHRR data to analyse drought conditions in Ethiopia and the Sahel for the years 1983-1986 (Henricksen, 1986, Tucker and Choudhury, 1987). It is worth recalling, however, that the use of such image data demands the understanding of the implications of the distortions inherent in such a broad swath, high oblique view angle sensor.

### 1.3.3: Agriculturally oriented products

Until remote sensing comes to terms with understanding what farmers and consultants want, rather than publishing on what they can provide, remote sensing will remain peripheral to operational arable farming. A major stumbling block is the perception of a farmer's tasks; these are complex and numerous on a large modern farm, the inter-relations of each decision in terms of the overall effect on

the operability and profitability of the farm being close and fundamental. However, it might be noted that farms at present suffer from a substantial lack of management tools that could be a considerable aid; and that more sophisticated management tools could help the organisation of a farm, and indeed remote sensing could provide one of these tools.

While farmers are unlikely to take on the task of image interpretation themselves, they can benefit from particular products that remote sensing could offer. Among these that could at present be available are:

- Annually derived images showing relative productivity, or some simpler index such as percentage cover - this would help identify areas within fields which are sub-optimal in production; it is likely that farmers are able to identify the reasons for such anomalies better than a remote sensing interpreter.

- Tailored data provided to farmers to help them plan more efficient use of resources.

- Regional assessments of agricultural production, to enhance GIS database management systems.

It is important to recall that, at the present, remote sensing seems unlikely to provide an automated method of crop assessment, and hence such products will remain too expensive for many farmers for some time. Some steps towards automation have been made; however, the first successful systems integrating remote sensing (for example LACIE, *cf.* MacDonald and Hall, 1980, Wiegand *et al.* 1986, and AgRISTARS, May *et al.*, 1986) involved a considerable degree of manual image interpretation and person hours, and was best done by someone familiar with the agronomy of the region (farm and topography). While this may well actually be the farmer, the data, and the system used to produce it, must be able to produce information simple enough for the farmer or consultant to understand, interpret and include in their management analysis and decision making.

## 1.4: Summary

This chapter has briefly examined some of the requirements of agriculture for data collection that could, conceivably, be provided by remote sensing. In order to carry out these tasks in this country (and many others), full use must be made of the off-nadir viewing capabilities of current and future sensors. For these data to be applied successfully, the anisotropic directional reflectance properties of Earth surface materials must be better understood. Chapter 2 begins to review this problem, along with the associated effects of the atmosphere, topography and solar geometry upon image data. In conclusion, this section outlines a new strategy, based upon the collection of multiple view angle image data of parcels on the Earth surface, which attempts to utilise the anisotropic reflectance effects for information extraction.

Chapter 3 describes the chosen study site, in Gloucestershire, and the ground data collection strategy employed. Next, it is explained how the sensor used in this study, the Daedalus 1268 Airborne Thematic Mapper, can be used for a multiple view angle data collection task, and also how the geometry of the sensor is likely to effect such data. As well as deriving the operating geometry of the sensor, the chapter gives a first illustration of the relationship between view angle and image variance, discusses methods for geometric correction of airborne image data, and describes the method of radiometric calibration applied to the imagery.

In chapter 4, the use of reflectance images to remove the effects of different atmosphere, illumination geometry and topography between the different flightlines of data is explained and developed. It is demonstrated that the relationship between view angle and image variance is the same before and after conversion to reflectance data, indicating that the method used in this study to measure image variance - the coefficient of variation of parcels - gives a normalised measure for the sites used here. The problems of quantisation and the resultant corruption of sample population distributions is highlighted.

In the following section, chapter 5, the effect of scene variance and the sampling frequency of a sensor is discussed. A framework of models is outlined, derived

from work by Woodcock (Woodcock and Strahler 1987, Woodcock, 1985), within which the results of the variance analysis can be interpreted. The effect of differing spatial resolutions upon image variance is tested for the data used in this study, prior to the analysis of the relationship between view angle and the coefficient of variation of test parcels for a number of different vegetative cover types. It is found that canopy structure has a significant effect upon the variance of an image when viewed from different angles, and a simple model is developed relating the general canopy type to this relationship, based upon the non-linear regression of these two variables. Possible extensions and improvements to this model conclude this chapter.

Chapter 6 discusses the possible application of multiple angle image data analysis using current and future sensor data. While most current sensors are not capable of providing data of adequate quality, in the future two sensors on the NASA EOS platform should provide high quality data that represent a significant improvement over current instruments for such analysis. Finally, chapter 7 summarises the findings and main conclusions of this study.

# CHAPTER 2: Remotely sensing directional reflectance properties of Earth surface materials

## 2.0: Introduction

Previous work has highlighted the importance of understanding the radiometric effects of viewing vegetation canopies at various angles if such data are to be used effectively for reflectance, classification or indices studies (Barnsley, 1984a, Wardley, 1984). Despite this, image data are frequently used without correct reference to, or acknowledgement of, these effects (see Curran and Williamson, 1987, Callison *et al.*, 1987, Jones *et al.*, 1988, and Williamson, 1989). With some remotely sensed data, it may be very apparent from the raw image data that the intensity of any pixel is a function of its sample number (i.e. related to view angle), as is the case with airborne MSS imagery (figure 2.1, 2.2). However, while the effects can be severe on a full scene scale, they may not be readily appreciated at a subscene level. For example, the field of view (FOV) of Landsat TM is approximately 14°; thus, 512x512 subscenes from either side of the full scene are not only 7° off nadir, but ±14° of each other. It is therefore unreasonable to expect detected radiance from similar cover types in these two subscenes to be the same.

SPOT-HRV data provide a more extreme example of the same problem. Although the FOV is more restricted (4.3°, Baudoin and Brossier, 1983), the ability to view off-nadir by up to 27° (Chevrel *et al.*, 1981) means that off-nadir radiometric effects are (for a scene by scene comparison) worse than that for Landsat TM. Data acquired using scanners with a broad FOV, such as the NOAA-AVHRR series or airborne instruments like the Daedalus ATM, represent another level of image data attenuation and modulation (figure 1.1). All the problems experienced with SPOT-HRV data will be evident in a single image, since the sensor geometry for broad swath scanners causes each sample in a line to be acquired at a different view angle over a wide range of off-nadir angles. A greater understanding of these view angle effects, and how they are manifested in the image, must be obtained for off-nadir multispectral data to be used effectively.

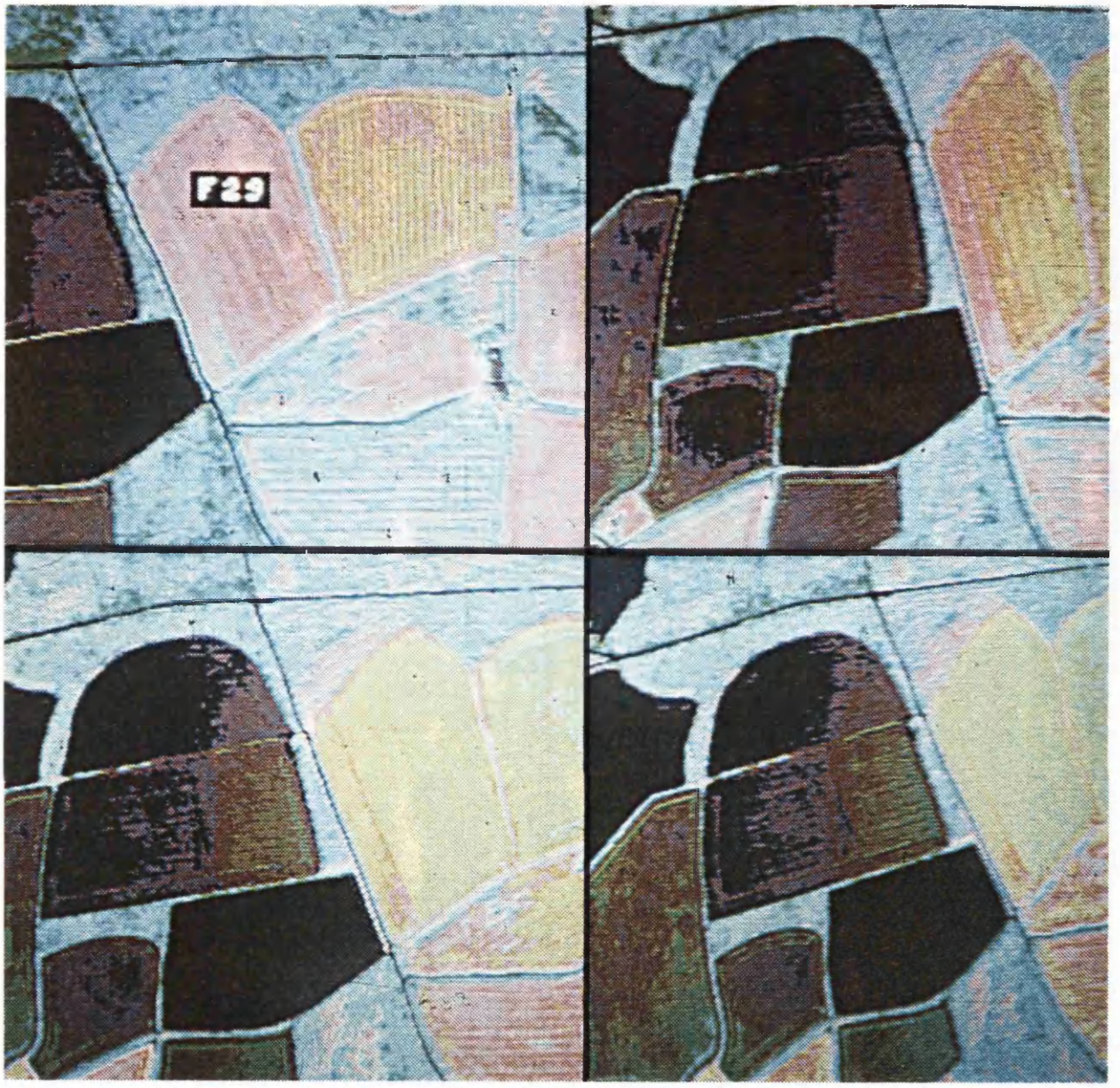


Figure 2.1: (see Preface, page 11) View angle effects in Daedalus ATM data, band 1. Differences in contrast and mean DN values are evident across the swath, mainly as a result of atmospheric effects in this short waveband. Illumination from right of diagram. Flightline direction in all images is up the page.

Figure 2.2: (above) View angle effects on vegetation indices; field 29 going through changes in tone between view angles -28° (top left, viewing towards the Sun), -19° (top right), 5.5° (bottom left), and 27° (bottom right).

In this study, a Daedalus ATM sensor (sec. 3.3) is used to examine the effects of broad-swath geometric configuration in a controlled field experiment. It is intended, as a result of these analyses, to demonstrate one possible strategy for the utilisation of anisotropic characteristics of canopy reflectance. This is a complex and, as yet, unsolved problem. As a result, much previous work has concentrated on the description of the factors affecting the radiance detected at the sensor, and several correction or normalisation (*cf.* 1.2.3) procedures developed. Section 2.1 gives a general overview of the correction methods used, and the breakdown of these methods into "component" factors, while the following sections (2.2-2.5) will deal with each of these components in turn.

After this review, however, it will become apparent that image correction, based upon physical modelling, demands a high level of understanding of the processes that cause the anisotropic reflectance characteristics of most Earth surface materials. If this understanding is achieved, then it is a logical step to utilise this information, rather than ignore the extra dimension represented by such an advancement in image interpretation (Kimes, 1984, Kimes *et al.*, 1984, 1986, Gerstl and Simmer, 1986, and Goel and Reynolds, 1989).

## 2.1: Image correction methods

Many general image correction strategies have been presented in the remote sensing literature. These range from non-parametric methods (Holben and Justice, 1981, Crippen, 1987, 1988) to more physically-based analytical models (Woodham and Gray, 1987). As the understanding of the processes modifying scene reflectance has developed, there has been a move toward the latter approach (Woodham, 1989). An early paper, incorporating this ideology and perhaps instigating a move towards an holistic understanding of the general image correction problem, was published by Teillet (1986), and describes a general method for radiometric scene correction, based upon "component" physical models. These component models describe sensor characteristics, atmospheric transmittance and attenuation to light energy, reflectance characteristics of Earth surface materials, and modifications caused by topography. Other information may be

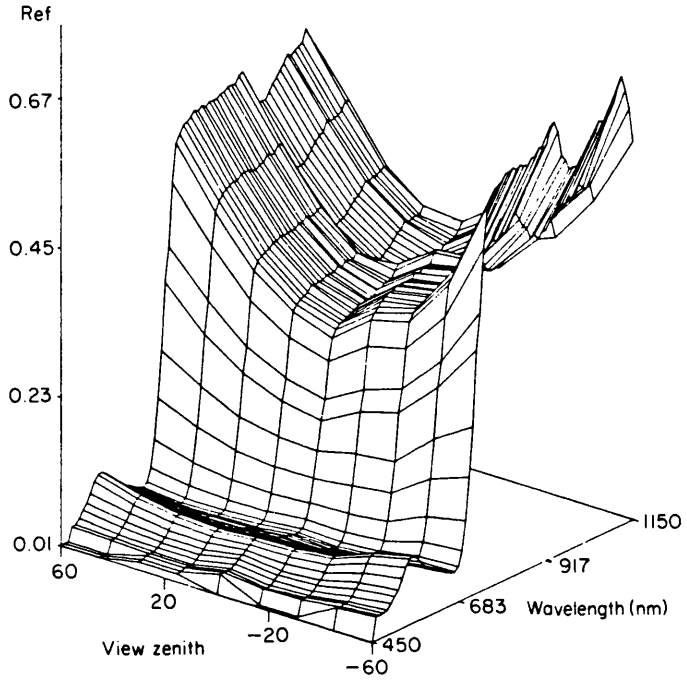


Figure 2.3: Wavelength dependent and view zenith angle dependence of bidirectional reflectance factor for wheat at boot stage, for solar zenith and azimuth angles typical for NOAA-6 (AVHRR sensor) ephemeris. Negative view zenith angle is down-Sun. (From Duggin, 1985)

required to complete the models, such as component models upon climatological effects (wind speed, Lord *et al.*, 1985, precipitation Hinzman *et al.*, 1986).

Although such "component" models are inter-related (Teillet, 1986), for the purpose of this chapter it is convenient to assess the earlier work, leading to the development of a more integrated approach to image correction, in four major topics; reflectance effects (sec. 2.2), atmospheric effects (2.3), topographic effects (2.4) and view angle effects (2.5). All these factors have a common link through the geometry of the sensor and the image. Thus it is, in reality, difficult to model one factor without controlling any, or all, of the others. This is the basis for the requirement of a more holistic strategy to account for these problems in image correction.

## 2.2: Reflectance properties of Earth surface materials

### 2.2.1: Anisotropic characteristics of Earth surface materials

The anisotropic nature of Earth surface materials should be related to characteristics of the object under observation, as well as a number of other factors (such as illumination angle and topography, which will be discussed below). As an illustration of the kind of directional reflectance patterns that are presented later in this study, figure 2.3 indicates the relationship between view angle and reflectance for the red and near-infrared spectrum, of wheat at boot stage (pre-flag leaf emergence) for NOAA-6 AVHRR data with a 45° solar elevation (from Duggin, 1985, page 9). This type of view-angle related response is typical of the results presented in this study and elsewhere.

A initial summary of the anisotropic behaviour of targets is made by Duggin (1985), and includes experimental evidence of directional reflectance characteristics of materials (Kriebel, 1978, Ranson *et al.*, 1985a and b), theoretical calculations and hypotheses (Suits, 1972a), and experimental confirmation of these models (Kimes *et al.*, 1986). Salomonson and Marlatt (1971) investigated the reflectance of

solar radiation over soils and vegetation in an early airborne study (1965/6). This investigation was prompted by a more general requirement, namely for radiation balance measurements to account for the anisotropic reflectance of various land surfaces. This need was highlighted because:

> '...the majority of satellite radiometers have a limited field of view and, as a result, a prior knowledge of the anisotropy in reflected solar radiation must be combined with measurements by these instruments from a single direction in order to determine the total energy reflected in all directions.'
>
> (Salomonson and Marlatt, 1971, p1)

This simple but general observation has many implications. Although in this case the measurements are being used for radiation balance calculations, any interpretation of data based upon single directional measurements of radiance must take into account the effect of canopy anisotropy if they are to be consistent between one experiment and the next. This basic assumption, reported by Salomonson and Marlatt nearly 20 years ago, has not always been recognized by many more recent authors. This is almost certainly due to the dominance through the 1970's of fixed geometry satellite sensors, typified by the Multispectral Scanning System (MSS) on-board the early Landsat satellite platforms. The data collected by these instruments are characterised by a restricted field of view, low spatial resolution, and static, nadir-pointing geometry. As a result, Earth scientists did not have the means by which to measure surface anisotropy from space, and in any case greater emphasis was placed upon the development of numerous models which quasi-quantitatively related radiance measurements with, for example, leaf area index (LAI) or biomass.

Such non-parametric models originating in this era have provided some significant results, for example, MacDonald and Hall (1980), Tucker *et al.* (1985), Townshend and Justice (1986), on global vegetation mapping, although in many cases the results were still of an unacceptably low accuracy for operational purposes[1]. The

---

[1]Tucker *et al.* (1985) were only able to validate their results against supposedly inaccurate maps - no field checks were used initially in the presentation of this work.

limitation of this paradigm, which makes little reference to the "real world" of non-homogeneous, systematically distributed vegetation canopies which exhibit anisotropic reflectance, is acknowledged by Tucker and Sellers (1986). More recently, other sensor data with different image viewing geometry have become commonly available, including aircraft data (with broad swath view angle effects) and SPOT variable geometry data. Nevertheless, researchers have continued to apply these models, without consideration for what were once recognised as fundamental understandings of plant/radiation canopy interactions.

### 2.2.2: Characterising the directional reflectance properties of vegetative surfaces

Many researchers have measured the directional reflectance properties of various vegetation canopies over the last two decades, primarily as an empirical basis upon which to build and elaborate physical reflectance models. As well as Salomonson and Marlatt's (1971) study, Kimes and co-workers have measured directional reflectance distributions of forest canopies (Kimes *et al.* 1984, 1987, Kimes and Newcomb, 1987) and homogeneous vegetation canopies (Kimes *et al.*, 1980). Different strategies have been employed in obtaining such datasets. Middleton *et al.* (1987) examined surface anisotropy for semi-arid cover types, using specialised ground based instrumentation (the PARABOLA sensor). Airborne scanner studies include Barnsley (1984a), who assessed the effect of view angle on the detected spectral response for a number of complete and partial canopies, and Irons *et al.* (1987), who made multiple angle observations of reflectance anisotropy from an airborne sensor, again using bespoke equipment. Most recently, Goel and Reynolds (1989) have measured bidirectional canopy reflectance for soybean, shinnery oak, orchard grass and corn, and tried to relate these data to vegetation type and growth stage. At a micro-vegetation scale, Grant (1987) summarises the processes and characteristics of anisotropic leaf reflectance. All these studies have contributed to the growing evidence of the importance of considering anisotropic reflectance properties, and begun to identify routes to solve the 'problem' that it causes.

2.2.2.1: External factors affecting reflectance anisotropy

Much work has taken place to measure canopy directional reflectance distributions and build reflectance models for various Earth surface cover types. For example, Kirchner *et al.* (1981) simulated directional radiance of vegetation from satellite platforms using a stochastic model, accounting for off-nadir viewing, canopy effects, solar geometry and atmospheric conditions in two wavelengths (0.68μm and 0.80μm). Polar plots were used to describe trends for different view and zenith angles; effects were found to be more pronounced in the red than infrared, canopy geometry (in particular leaf orientation distribution) being a critical factor. Atmospheric haze was established as attenuating anisotropy for the targets, but the use of multiple view-angle imagery was noted as a potential method for measuring and correcting atmospheric conditions. Holben and Fraser (1984) examined the red and near-infrared (i.e. similar to Kirchner *et al.* above) sensor response to off-nadir viewing, using simulated NOAA AVHRR data. Both view and illumination geometry were varied. Variable response to a range of soil and vegetation targets were found as a function of view and illumination geometry. Sensor response to atmospheric path length was substantial for normalised difference vegetation index (NDVI) values as well as individual channels. These could be minimised by high Sun and clear atmosphere viewing. Holben *et al.* (1986) again examined directional reflectance response with particular reference to AVHRR data, for bare soil, orchard and fescue grass surfaces. Vegetation indices were found to be more reliable than the response from individual channels. The inclusion of scan angle data improved interpretability. It was recommended that atmospheric optical thickness data also be collected on a global basis for operational vegetation indices extraction.

Models that relate simple measurements of detected radiance to canopy parameters (Hatfield *et al.*, 1985, Asrar *et al.*, 1986) without incorporation of other factors impinging upon the scene will produce invalid results. Many studies exist which indicate the significance of such factors in the use of models to interpret image data. For example, Pinter *et al.* (1985) undertook field experiments, measuring canopy spectral reflectance over six cultivars of spring wheat, at 30-45min intervals over a day, simulating Landsat MSS and TM bands. Major differences were

observed between the measurements despite similarities in green leaf area and green biomass; erectophile canopies varied more with Sun zenith and azimuth angles than planophile ones. It was concluded that spectral reflectance was strongly dependent upon the direction of incident radiation. Ranson *et al.* (1985a and b) also compared spectral responses of soybean and corn canopies with respect to illumination, view and canopy geometry, finding greater anisotropy with incomplete canopies and in the red (0.6-0.7 μm) wavelength band. For incomplete maize canopies, a decrease in contrast between soil and vegetation (due to shadowing) was the major cause of change in reflectance factor. Shibayama and Wiegand (1985) also examined winter wheat canopies over the second to sixth growth stages, making five daily measurements on four dates. Although 70% of the variation in NIR was explained by a simple regression model, most error occurred with large solar zenith angles. Other studies have also attempted to incorporate these external factors into the reflectance modelling. Walthall *et al.* (1985) developed a simple three term equation modelling bidirectional reflectance of some vegetation canopies and soil surfaces as a function of view and solar azimuth and zenith angles. Clear sky (isotropic atmospheric) conditions were assumed.

Such studies again confirm the complexity of characterising the directional reflectance properties of Earth surface materials, and the unsatisfactory results that might be derived from attempts to produce general descriptions. Thus, a non-parametric, non-physical process modelling strategy would be unlikely to produce an acceptable method for the correction of image data for anisotropic reflectance. This is one of the major reasons for moving towards other, parametric, strategies that consider the physical processes more holistically in their approach to extracting information from remotely sensed images.

2.2.2.2: Effect of canopy geometry upon reflectance anisotropy

Suits (1972a) indicated that changing canopy geometries would cause variations in reflectance of that target; inverting this argument, changes in reflectance, from either an expected level or over a sequence of dates, could be inferred to be the result of differences in canopy architecture and geometric distribution of canopy

components (Jackson and Pinter, 1986), *ceteris paribus*. Alterations to canopy structure are often associated with canopy stress (Jackson *et al.*, 1986), and therefore such an interpretation could have a useful purpose. The major problem with Suits' hypothesis is that there are many causes of canopy stress, often with similar symptoms; water, biological and salinity stress all produce similar geometrical canopy response (wilting, leaf curl), which would, again, not enable the cause to be determined without considerable knowledge of the ground conditions. This, combined with the problem of the timeliness of data, may cause such information to become of limited value for crop management. This strengthens the case therefore of taking account of the canopy geometry when interpreting reflectance data.

A second problem is that, in order to identify whether or not the detected radiance from a parcel of land is that of a healthy or stressed crop, a standard expectation or reference must be established. This reference is extremely dependent upon local environmental conditions and farm management practices, to the point where not even the same field can be expected to give consistent results at similar dates, year after year. For example, how many years a field has been given over to a single crop, or at what stage in a rotation cycle it is in, will greatly determine the development of a crop, and hence its reflectance. It will, therefore, be impossible to distinguish background variations from actual stress artifacts, leading to difficulties of interpreting image data correctly in the assessment of canopy characteristics.

### 2.2.3: Earth surface reflectance modelling

It is recognised that in order to understand remotely sensed images and extract quantitative information about the object under consideration, hypotheses and methods must be developed to relate scene characteristics to the image. Several works illustrate the construction of models defining the effects of illumination, topography and view angle in a scene (Temps and Coulson, 1977, Pinter *et al.*, 1985, Hugli and Frei, 1983, Justice *et al.*, 1981). Often a general descriptive reflectance model of the surface is used, i.e. Lambertian, non-Lambertian (Justice

*et al.* 1981, Jones *et al.*, 1988) for sand, snow etc. The choice of such models for correcting for these effects, and the implicit assumptions that are made to justify their use, has been questioned (Smith *et al.*, 1980), and shown to be valid only over a restricted range of illumination and slope angles (for a given cover type). The choice of reflectance model is obviously critical to the success or failure of the attempt to correct data, particularly for view angle, since diffuse reflectance models, or even simple anisotropic models, bear little resemblance to the reflectance distributions common to the majority of land cover types.

While the use of general reflectance models for image corrections is limited, there are also problems when cover type-specific models are applied. An empirical, non-parametric, model based upon measurements of one cover type is unlikely to work when applied to a different cover type (Jones *et al.*, 1988, Morris and Barnsley, 1989). Paradoxically, if the application of specific directional reflectance models can be cover-type specific, then the scene is already classified, or other data are available to describe the spatial distribution of cover types within the scene (for example ground survey data). It is a frustrating but inevitable fact that a detailed description of the bi-directional reflectance distribution function (BRDF) is required to understand target reflectance in a scene (and hence predict detected radiance at the sensor) (see Hugli and Frei, 1983). Goel and Reynolds (1989) also highlight an important concept, postulated much earlier by Suits (1972a); that is, remote sensing is hardly 'remote' if numerous ground measurements of leaf angle distributions need to be made for modelling, as indeed would have to be made for the operational application of models like Suits'. If such detailed information exists *a priori*, then what new information can be obtained from such an image?

2.2.3.1: The use of vegetation canopy reflectance models in image understanding

The conceptual starting point for the understanding of vegetation canopy directional reflectance is the Suits' model, originating with his work published in the early 1970's (Suits, 1972a & b, Suits and Safir, 1972). Suits developed his model from earlier work by a chain of other researchers, beginning with Kubelka and Munk (1931), through Duntley (1942), ending with Allen, Gayle and Richardson (1970).

His resulting three-dimensional model is well known and understood, and treats the canopies as infinitely extended horizontal layers, the components of which are randomly distributed and homogeneously mixed. Each component is 'idealised as a combination of vertically oriented and horizontally oriented flat diffusely reflecting and transmitting panels.' (Suits, 1972a, p 118.) The distribution of these components is derived from field or laboratory measurements, and used to calculate reflectance. Suits' major extensions to the earlier body of work were to incorporate canopy layers comprised of different biological components (commonly stalks, leaves, ears), to take into account laboratory measurements of scattering and absorption coefficients, to permit consideration of the canopy 'hot spot' and, most importantly, to allow the calculation of non-Lambertian canopy reflectance.

The main thrust of this work, therefore, is to allow an understanding of the processes that cause directional reflectance anisotropy, and to invert such models that may be developed as a result (Woodham, 1989); this would allow the estimation of canopy parameters solely from the remotely sensed data. For example, Suits (1972a, p. 118) makes the tentative suggestion that for crop monitoring purposes, plant stress inducing changes in canopy geometry could be detected by measuring directional reflectance changes, given no change in other factors affecting reflectance. In general, though, it would be desirable to identify agro-physical parameters for a whole range of purposes (Woodham, 1989).

2.2.3.2: The use of models to extract agro-physical parameters from image data

Other workers have been more ambitious in attempting to extract useful, quantitative, agro-physical parameters. Li and Strahler (1985, 1986, 1988) have modelled bidirectional reflectance of a conifer forest, utilising simple geometric figures casting shadows on a planar surface (from an idea by Egbert, 1977). Inversion of this three-dimensional model yields predictions of tree size and density within 10% of actual values (Kimes *et al.* 1986) for sparse forest in northern California. In turn, the model was adapted by Franklin (Franklin and Strahler, 1988) and inverted to provide (less satisfactory) estimates of average tree size and density for regions of semi-arid *Acacia* woodland in Mali, using Landsat

TM data. These results are compared with those of a coniferous forest in Oregon, U.S.A., by Strahler *et al.* (1988), where better results were obtained. Prince (1987) also modelled the canopy interception of sparse *Acacia* woodland in Sudan, using a three-dimensional canopy model incorporating sensor view direction, with relation to primary production estimates (of great importance in estimating firewood reserves and production on the continent). However, while none of these studies explicitly examines the directional reflectance properties of such canopies, they do initiate the use of an understanding of the physical processes involved in determining reflectance.

Several attempts at inverting canopy reflectance models, in order to extract canopy parameters, have been made. Goel and Deering (1985) used the SAIL model (*cf.* Badhwar *et al.*, 1985, Verhoef, 1984, 1985, Reyna and Badhwar, 1983) to estimate LAI for soybean and orchard grass canopies, following earlier work by Goel and Thompson (1984a) to estimate agronomic variables. Clevers (1986, 1988) adapted the SAIL model to account for illumination of the substrate when estimating canopy parameters such as LAI. Goel *et al.* (Goel and Strebel, 1983, Goel and Thompson, 1984a and b) inverted the Suits model (Suits, 1972a) to produce similar estimates. Much of this work is reviewed by Goel (1988), and a derivation of the Suits' model, named TRIM, is outlined to model radiative transfer in heterogeneous three-dimensional canopies, to cope with the problems presented by orchards and other similar canopies (Goel and Grier, 1986, 1987, 1988).

In the application of remote sensing for quantitative studies, these papers represent an important step, albeit one that is hindered by the complex problems of determining directional reflectance. Most agronometric modelling requires inputs of two parameters which (it is postulated) can be derived from remote sensing; area estimates (mostly from classification and thematic mapping) and canopy parameters, such as growth stage, height, total biomass, percentage cover. Both estimates are distorted by anisotropic reflectance (Barnsley, 1984a and b, 1985), but in this study the effect of anisotropy upon estimated canopy parameters will be the main area of discussion.

## 2.3: Atmospheric effects

Corrections to images for atmospheric effects are among the most complicated attempted in remote sensing. Atmospheric corrections are a prerequisite to proper scene radiometric corrections (Teillet, 1986). The task of collecting valid data for a continuously varying medium, both spatially (in three dimensions) and temporally, is virtually impossible given current technology. This problem is compounded by the scale of remote sensing projects, often covering regions or even continents. For these reasons, many of the correction strategies used are based upon estimates, assumptions and point data, sampled at the Earth's surface.

### 2.3.1: Atmospheric effects on incoming radiation

It is assumed here, for the purpose of clarity, that we are dealing with a plane, level, target, viewing a hemispherical sky. This facet on the ground receives energy, or flux, radiated from the sky. Given no atmosphere, the sky irradiance would be related to the energy emitted from the Sun, the Sun-Earth distance, and the zenith angle of the Sun, modified with respect to the band-pass that we are concerned with.

The Earth, however, is enclosed by a thin atmosphere made up of a number of mixed gases, including $N_2$, $O_2$, CO, $CO_2$, $CH_4$, $N_2O$, unmixed gases such as $H_2O$, $O_3$, $HNO_3$, and includes considerable quantities of aerosols (Prasad *et al.*, 1987). The proportion of the unmixed gases in the atmosphere and of the aerosols is neither vertically nor horizontally constant (Steven and Rollin, 1985, 1986, Prasad *et al.*, 1987), and can vary considerably over short time periods. The main controlling factor of the relative proportion of direct to diffuse flux is the content and particle size of aerosols in the atmosphere, as well as the spectral absorption caused by the unmixed gases.

The atmosphere, therefore, scatters and absorbs radiation, attenuating the direct illumination component, and causing diffuse skylight to impinge upon a target. Both these processes are wavelength dependent, molecular (Rayleigh) scattering

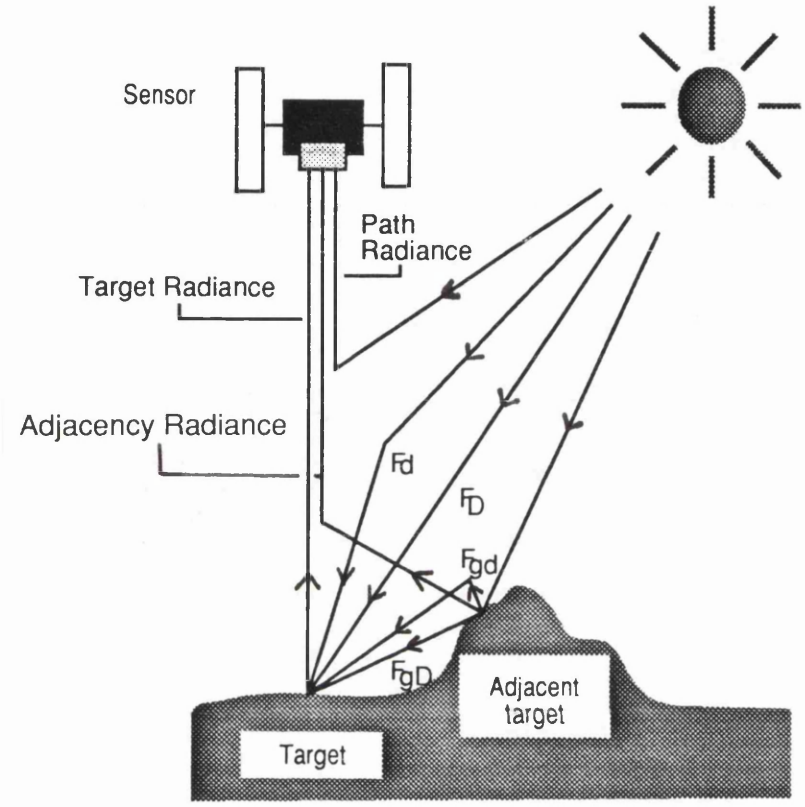


Figure 2.4: Component modelling of sky radiance - direct sky component $F_D$, diffuse sky component $F_d$, direct ground component $F_{gD}$, diffuse ground component $F_{gd}$. (After Woodham and Gray, 1987.)

varying as $l^4$, aerosol scattering between $l^1$ and $l^3$ (Kaufman, 1988). Absorption in clear sky conditions in the visible spectrum and out to 0.8μm is negligible (Slater, 1980), but in hazy or polluted atmospheres aerosols also act to absorb radiation in this spectrum. Absorption due to ozone takes place below 0.29μm, and a number of absorption bands arise in the infrared spectrum due to water vapour and carbon dioxide. Combined with the problems of temporal and spatial variability of the atmosphere, atmospheric scattering and absorption affects the multi-spectral classification of surface features, and also the extraction of vegetation indices (Holben and Fraser, 1984, Fraser and Kaufman, 1985).

Several attempts to classify target irradiance have been made (for example, Temps and Coulson, 1977), but essentially four components can be identified (Woodham and Gray, 1987) (figure 2.4). First, the attenuated direct solar beam illuminates the target; second, radiation scattered by the atmosphere, that is diffuse skylight; third, radiation reflected directly to the target from adjacent terrain; and fourth, radiation reflected skyward from adjacent terrain that is scattered back from the atmosphere onto the target. It is apparent that in areas of low reflectance that these last two factors will become less significant, and that in areas of low slope the third will become minimal (Woodham and Gray, 1987, Hall-Könyves, 1987, 1988).

### 2.3.2: Atmospheric effects on the radiance detected by the sensor

The detected radiance at the sensor from a target is attenuated and augmented by the atmosphere in three ways (figure 2.4). First, direct radiance from the target is scattered and absorbed by the atmosphere. Second, radiation from adjacent resolution elements is scattered into the IFOV of the sensor (the adjacency effect). Third, incoming radiation from the Sun is scattered into the IFOV of the sensor (path radiance). These three factors are a function of the optical density of the atmosphere and the path length through it. Hence, while low altitude[2] airborne data may be considered to minimise atmospheric effects, this is an oversimplification

[2]With respect to satellite sensors.

since most of the aerosol content of the atmosphere is in the bottom 1000m, and also aircraft data do not have constant path length due to the large FOV's in use.

The most commonly observed effect of atmosphere upon image data then is contrast reduction. For vegetative cover types, this is most important in the visible part of the spectrum (Slater, 1980); first because scattering is greatest in this part of the spectrum, and second because reflectance is low (by comparison with the near infrared). The simple explanation for contrast reduction in this part of the spectrum is a combination of reduced dynamic range of the data, due to increased "noise" from the scattered flux (Woodham and Gray, 1987).

It has been reported that the angular distribution of the surface reflectance measured remotely (through the atmosphere) is smoother than at the surface (Lee and Kaufman, 1986). Atmospheric effects are of particular relevance to off-nadir data (Gratzki and Gerstl, 1989), and although strong local extremes such as the hotspot are retained through the atmosphere, observations with varying view zenith angles are most affected due the varying path lengths of the radiation through the atmosphere to the sensor (Simmer and Gerstl, 1985). It is recognized that this attenuation is wave-length dependent (Barnsley, 1984a and b). In the visible (shorter) wavelengths, the angular pattern of reflectance, due to the anisotropic nature of the target, may be degraded near to extinction; in longer wavelengths (near-infrared and beyond) the higher reflectance of vegetative canopies ensures that the angular effects are retained (Simmer and Gerstl, 1985). This implies that the offset ratio strategy suggested by Crippen (1988), proposed for a wide selection of image corrections (see 2.4 and 2.5 below), would not be applicable to the solution of atmospheric effects caused by differing path lengths within a scene (i.e. as is the case with airborne data such as used in this study), since attenuation of radiance with view angle is not identical in all bands. It may however work if a selection of bands is made, for example only the NIR/MIR bands, or for selected cover types (Lee and Kaufman, 1986).

Lee and Kaufman (1986) also report that the dominant modifications to the detected radiance are a result of the atmosphere, not target anisotropy, a conclusion made elsewhere (Kirchner *et al.*, 1981, Holben and Fraser, 1984, Holben, 1986),

when considering three cover types (savannah, pasture and coniferous forest). They conclude that the use of the Normalised Difference Vegetation Index would eliminate most of these effects, a point reiterated by Fraser and Kaufman (1985), although this is also due to the sampling strategy devised for the compilation of Global Vegetation Maps (Tucker and Sellers, 1986).

### 2.3.3: Empirical measurements and modelling

As with the development of plant canopy directional reflectance models, spatial and spectral sky radiance models have relied heavily on empirical data input. Even the more sophisticated models, such as the 5S algorithm used in this study (Tanré *et al.*, 1986), depend upon large matrices of data from which interpolated estimates of sky radiance can be made. In many respects, there is also a distinction between the modelling of direct and diffuse sky radiance, and this is reflected in the studies made to understand the problem.

Direct solar radiance can either be measured (Hämälainen *et al.*, 1985) or modelled using scattering and absorption data (derived from meterological measurements), for example SOLTRAN (Bird, 1982, Bird and Hulstrom, 1983). Diffuse skylight radiation is a more complicated problem. In cloudless conditions (i.e. those optimal for visible and infrared remote sensing), the diffuse solar flux contributes around 15% of the total incoming radiation (Prasad *et al.*, 1987). The distribution of this diffuse sky radiance, however, is not isotropic, nor is it a constant proportion of the measured flux with respect to wavelength (otherwise the sky would be white, not blue). Empirical studies have been carried out to address this problem, using a variety of instruments such as those listed in Oke (1978), or more specialised instrumentation such actinometers (spectral pyranometers) and custom built instruments (Hämälainen *et al.*, 1985, Ahmad *et al.*, 1987). Early work, such as Kondratyev (1969), records measurements of both spectral and angular distributions of clear sky conditions. Steven (1977) attempted to measure and standardise angular distributions of clear sky radiance in Britain, based upon a series of 69 measurements over a year long period; Hämälainen *et al.* (1985) designed a multisensor pyranometer to allow measurements of the direct component and the

angular distribution of solar radiation in Finland. Both of these studies examined broad spectral categories; but Ahmad *et al.* (1987), and Deering (1987, 1988) used the PARABOLA instrument to make rapid hemispherical scans of upwelling and downwelling flux in three selected wavebands, validating the results for the 0.65-0.67μm and 0.81-0.84μm bands. McDowell (1974) measured spectral irradiance upon a horizontal plane for total sky radiance and diffuse radiance alone, for two types of atmosphere ('hazy' and 'clear'[3]); results indicate that the ratio of diffuse to total radiation varies by nearly an order of magnitude (≈0.75 to ≈0.08) over the 350nm-1100nm wavelength range. The ratio is more variable for clear sky conditions, although it is markedly wavelength dependent across the full measured spectrum, but is fairly constant for the wavelength range 0.7μm-1.1μm.

Several solar spectral data sets have been published; for example Kondratyev (1969), Dave (1978), Bird and Hulstrom (1983), Riordan *et al.* (1989). These can go into considerable detail; some focus specifically upon diffuse sky radiance (eg Forgan, 1980, Zangvil and Aviv, 1987, and Sirén, 1987). Such measurements are useful for radiation engineers applying models to assess insolation on tilted surfaces for building purposes (for example Lewis, 1987, Kouremenos *et al.* 1987, Ineichen *et al.*, 1987, Gueymard, 1987). These datasets, however, are not of great relevance to remote sensing, since they are presented over a limited spectral coverage (usually no longer than 0.9μm wavelength) and record measurements for particular days and times, often with specific atmospheric conditions (including cloud cover, for example Riordan *et al.*, 1989).

Solar engineers, moreover, are not usually concerned with spectral distributions of sky radiance nor of spectral reflectance (*cf.* albedo), whereas for remote sensing purposes an understanding of atmospheric properties at a minimum of band-pass resolution is required. While estimates of exoatmospheric irradiance have been

---

[3]The first, 'hazy', measurement 'was made in Rochester, New York, on August 14, 1970, under extremely hazy but cloudless conditions. The measurements were made at 2:45 p.m., which corresponds to a sun angle of 55°.' [Probably elevation angle, though this is not clear from the text.] The 'clear' measurement 'was made at the White Sands Missile Range in New Mexico on October 30, 1970, 12.06 p.m. The sun angle was 43° and the atmosphere was extremely clear'. (McDowell, 1974, p. 569)

published for individual sensors (Markham and Barker, 1985, 1987, Woodham and Gray, 1987), the data to modify these for particular atmospheric conditions are not so easy to find. One solution is to measure spectral profiles of irradiance at times of imaging (Baret *et al.*, 1987). This presents a further data collection problem, virtually impossible to resolve with the collection of satellite data on a regular basis since it demands contemporaneous fieldwork.

## 2.4: Topographic effects

### 2.4.1: Identification of radiometric effects of topography in images

Several investigations have been carried out on radiometric effects of topography on various cover types (e.g. Holben and Justice, 1980, 1981, Justice *et al.*, 1981, Hugli and Frei, 1983, Hall-Könyves, 1987). In the first of a series of articles, Holben and Justice (1980) indicate that a single cover type may have a wide range of associated pixel values, due solely to variations in slope and aspect throughout the scene. The magnitude of this effect was found to vary as a function of the solar elevation, azimuthal orientation of the terrain facet, and the terrain facet inclination (slope). This is a result of variations in the irradiance incident on facets of different orientations and inclinations, and the geometric relation between the illumination source and sensor.

Holben and Justice (1980) also found that the lowest solar elevations were found to produce the greatest contrast in radiance values, and greatest variations in sensor response were found for slopes oriented in the principal plane (i.e. in the plane defined by the zenith, the Sun and the target, figure 2.5). This is due to the effect of the surface being illuminated up- or down-Sun[4], and the associated anisotropic behaviour of natural surfaces. For example, a grass surface is composed of many individual leaves, usually with a preferred orientation. Given a description of this

[4]Respectively looking towards and away from the Sun when viewing the target.

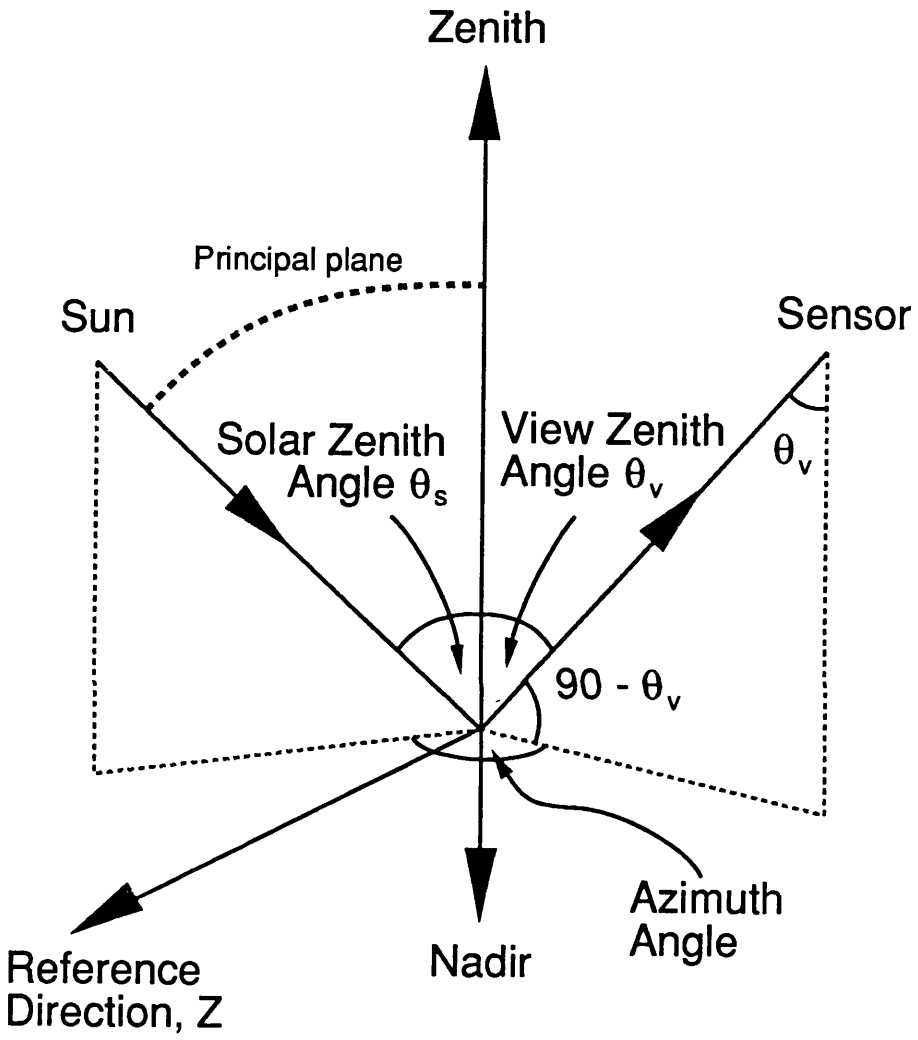


Figure 2.5: Sun target sensor geometry

orientation distribution (say, mostly vertical, erectophile), the surface will be composed of a distribution of illuminated or shadowed leaves. This distribution will not change for any terrain facet oriented perpendicular to the principal plane, whatever the inclination, but for all other facets the proportions of the illuminated surfaces and the shaded surfaces on a facet will alter, hence altering the radiance. For a nadir-viewing sensor, zenith illumination would of course produce no topographic effect (the principal plane cannot be defined). Indeed, for a Lambertian type surface, no topographic effect will be perceived if the sensor has the same orientation as the Sun.

### 2.4.2: Non-parametric corrections for the radiometric effects of topography

Holben and Justice (1981) examined the use of spectral band ratioing to reduce the topographic effect. Red and photographic infrared data were collected using a ground radiometer, and ratios of these wavebands were found to reduce the effect by more than a factor of six. Band ratios (typically Landsat MSS 5/7) are commonly specified as a simple solution to reducing topographically induced radiometric distortion (Lillesand and Kiefer, 1979, Schowengerdt, 1983). This is because reflectance in each band is assumed to be proportionally related to the strength of illumination. It is noted, however, that such a technique is likely to be less successful when applied to airborne or satellite data because of problems with sensor calibration, quantization effects, additive wavelength-dependent scattered atmospheric effects and radiation from adjacent facets. These introduce, additive rather than multiplicative effects on the received signal (Crippen 1988), which are difficult to determine empirically. Crippen (1988) also considers band ratioing to be the optimum method for minimizing image effects attributable to topography, provided that correct adjustments are made for data offsets (Crippen 1987).

Dymond (1988) attempted to model radiance in hilly terrain using training datasets to characterise the radiance over the range of topographic conditions in the scene. Target irradiance was factorised as proportional to the cosine of the solar incident angle and the proportion of sky and neighbouring hills that is "seen" by the target (diffuse sky radiance component). Reflectance, therefore, was a function of

topography, the BRDF of the target and viewing geometry. Mistakenly, Dymond includes the slope vector as part of the geometry describing the reflectance function - in the same manner as Jones *et al.* (1988) (*cf.* 2.4.3). Mis-classification was reduced from 23% to 13.5% for classes of forest and pasture. Dymond (1988) notes that non-parametric techniques are capable of modelling a variety of spatially variable effects, provided that there are sufficient training sets for each category to characterise the model, and that visual interpretation of the imagery permits their accurate identification.

The problem of using non-parametric techniques for the correction of topographic effects is that the proportion of diffuse and direct illumination is not constant for all wavelengths. If the proportions of diffuse and direct flux are altered (as they will be in undulating terrain), so the topographic effect will be dependent upon the waveband in use. Woodham and Gray (1987), for example, illustrate this effect of topography upon the spectral shift of peak detected response; the Minnaert function was modelled to show that changing facet orientations (but *not* slope angle) will alter the spectral composition of the target reflectance. Diffuse sky radiance compounds the problem, since the spectral distribution of skylight is different from that of the direct beam. This spectral shift is identified as being towards the blue as the target faces further away from the sun, since a greater component of the irradiance is made up of diffuse (scattered) flux (Woodham and Gray, 1987). These sort of effects cannot be dealt with effectively by non-parametric techniques, such as band ratios, alone. They demand explicit analytical solutions to the problems of sky radiance spectral and spatial distributions.

### 2.4.3: Parametric corrections for the radiometric effects of topographic

Non-parametric solutions to topographic correction produce, in general, normalised data. Apart from such products being inconvenient to work with (Hook and Donoghue, 1988, sec. 2.5.2), other methods of correction can produce more effective results (Holben and Justice, 1981, Woodham 1989). The application of terrain and reflectance modelling may prove a more sensible, parametric, approach. This has been attempted by Justice *et al.* (1981), Sjoberg and Horn (1983), and

Franklin *et al.* (1986) over a variety of terrain types, with some success. With the increased availability of digital terrain data, and the software to process it, such techniques are now more practicable. Geocoded data, however, are a prerequisite for this method, in order to identify topographic parameters.

Jones *et al.* (1988) attempted to follow the method of Justice and Holben in using Lambertian and non-Lambertian functions (in particular the Minnaert function) and a DTM to correct SPOT-HRV multi-spectral imagery of semi-natural upland vegetation in North Wales for topographic effects. The results showed that the Lambertian adjusted scenes over-compensated for shadowing (and presumably also highlighting). This can be explained by the absence of a model of the sky radiance distribution (*cf.* 4.2.3, and Kay, 1989), since the Lambertian function only incorporates a direct component factor related to the solar incidence angle. The Minnaert-corrected imagery was judged to be more successful, by improving classification accuracies by the greatest margin. Four criticisms, however, can be levelled against this work. First, the method of adjusting the function using an empirically-determined constant is questionable, so far as generality of the model is concerned (i.e. with regard to different cover types or different scenes, or even different topographic regimes). Second, the inclusion of the exitant angle in the function should allow for viewing geometry, although it is not clear that this is taken into account. Third, the function is used as an approximation to the BRDF for all the cover types within the scene[5], and fourth, the exitant angle is modified by the slope angle for each pixel.

Leprieur *et al.* (1988) attempted to utilise digital terrain data to examine the relationship between reflectance, forest stand parameters, and the local Sun/target/sensor (STS) geometry, in multi-date Landsat TM imagery of Vosges, Eastern France. The major aim of the work was to generate reflectance maps based upon a knowledge of standardised illumination parameters, terrain modelling and sensor radiometric calibration. A 30m resolution DTM was derived from 1:50,000 scale 100m interval contour maps, smoothed and interpolated to produce separate

[5]The inherent weakness of this approach will be discussed in section 4.1

images of slope angle, aspect, and cosine of the solar incident angle[6]. Illumination effects and also, more unusually for the application of Landsat TM data, directional effects dependent upon view angle were accounted for in the radiometric processing. They observed correctly, however, that trees do not grow perpendicular to the slope, as is often assumed in the implicit use of a DTM to orient a BRDF (*cf.* Jones *et al.*, 1988). Leprieur *et al.* (1988) conclude that S/T/S geometry is significant for forestry sites, particularly in the middle-infrared part of the spectrum.

The correct interpretation of the way in which slope and aspect modulate the BRDF of a surface is made by Strahler (Strahler, 1988, Strahler *et al.*, 1988). He concludes that it is not possible to assume that a sloping vegetated surface has the same BRDF as a flat surface with the same vegetation cover, since plants grow upright and the three-dimensional structure of the canopy will become a function of topography (figure 2.6).

Jones *et al.* (1988) conclude that 'models for the correction of multispectral data for terrain effects are not independent of the nature of the ground cover.' (p. 677). This is hardly surprising. The assumption by Jones *et al.* (1988, 1989), however, that one function can describe the angular reflectance characteristics of a scene, made up of many cover types, contradicts with their own conclusions. Angular reflectance distributions cannot be corrected without knowledge of what canopy is being corrected for. This is one cause of the low classification accuracies recorded in their work.

Other ecological factors may also prevail that are indirectly associated with topography. Franklin *et al.* (1986) used a transformation to adjust image data for aspect using a DTM, by shifting the azimuth axis; this is based upon observations of increased productivity of forests on north-west slopes when compared to south-east slopes, due to increased moisture availability, by Hartung and Lloyd (1969). Strahler (1977, 1978) also conducted similar biogeographic studies, using binary discriminant analysis to assess relationships between tree species to topographic

[6]The Solar incident angle is defined as the angle between the surface normal and the incident beam.

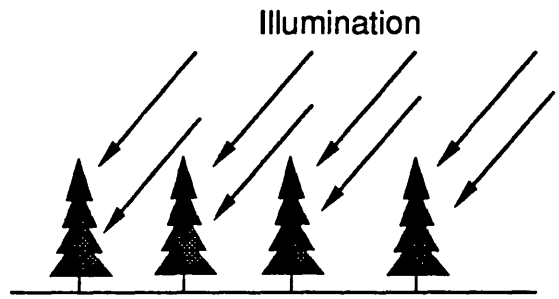


Canopy on flat ground - only shadows understorey

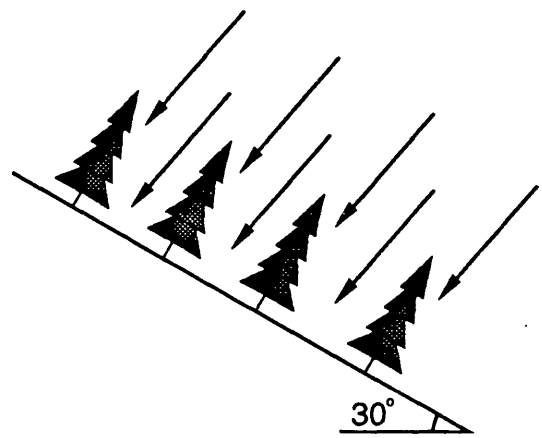


Orienting the BRDF according to DTM - but this does not account for changing tree spacing (along ground) and the direction of tree growth

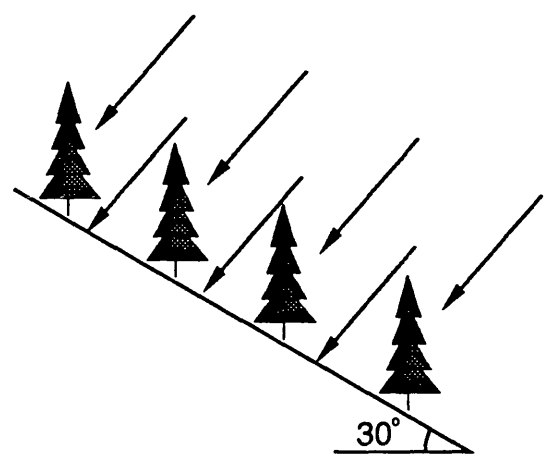


The true effect of topography upon this canopy is more subtle

Figure 2.6: Effect of topography upon the BRDF of a surface.

site factors, finding significant stratification by elevation. These relationships, of ecological association of topography and plant development, are often over-looked by the remote sensing community, in an attempt to construct image correction techniques. It may well be the case, in some instances, that two regions have a different spectral response, despite being dominated by the same species, as a result of local environmental conditions (such as slope, aspect, and therefore indirectly light and water availability) pertaining plant canopy development.

### 2.4.4: Methods for topographic correction - comments and conclusions

Because the topographic effect can be visualised as a problem of the distribution of irradiance in the scene, and not therefore necessarily determined by any surface reflectance properties, independence from cover reflectance model should be maintained if at all possible in devising a method for the radiometric correction of topography in an image. Cover type will not alter the perceived topographic effect, although sensor/Sun geometry will. Since the anisotropic reflectance of most natural targets is also affected by sensor/Sun geometry, these two separate effects (of topography and directional reflectance) upon images are often confused. This can be illustrated more clearly if the construction of a target is considered; a coniferous forest, for example, grows in a nominal vertical direction, not at a normal to the facet on which it is located. Consequently, given distant sensor and illumination sources (or a fixed view angle to the target from the sensor), no significant change in Sun-target-sensor geometry will take place due to topography, and hence no topographic effect will be manifested in the image because of a 'non-Lambertian' target. It is, therefore, incorrect to use a reflectance model in the description of the topographic effect, since this effect is a product of different spatial distributions of irradiance within a scene[7] and not the directional reflectance properties of the cover types within it. The correct modelling of these spatial distributions, for example with parametric illumination algorithms (Woodham and Gray, 1987, Kay 1989, Dozier and Frew, 1989), combined with the use of reflectance imagery (Kay, 1989, Yang and Vidal, 1989, Woodham, 1989), is a

[7]Although the angular distribution is constant, measured from the illumination source

better and more effective procedure, since these techniques will isolate the anisotropic reflectance properties of the targets, allowing further analysis of the physical properties of the targets to take place.

## 2.5: View angle corrections

### 2.5.1: Identification of view angle effects

The conventional remote sensing strategy governing the application of off-nadir image data relates to the paradigm that remote sensing is about the collection, interpretation and application of multispectral measurements of radiance reflected or emitted from a remote object. The ideal remote sensing system for this strategy gathers a constant signal (in a given wave-band) for a target as a function of view angle (Kimes *et al.*, 1984). The community has been provided with this type of system by Sun-synchronous nadir viewing satellites such as the Landsat series. However, the desire for sensors with increased spatial and temporal resolutions has led to the development and launch of SPOT-1, which partially resolves these problems by collecting data off-nadir. Such a capability does not provide data that can be used easily within the current strategy of the remote sensing community, because of the view angle effects (Barnsley, 1984a and b, Foody, 1988).

### 2.5.2: Non-parametric corrections for view angle effects

There have been several attempts to develop non-parametric corrections for view angle effects, which are manifested as systematic differences in detected spectral radiance across the image (Hook and Donoghue, 1988, figure 2.1). Most of these attempt to model this variation in radiance by some ratio procedure, or by fitting a polynomial to the image data (figure 2.7).

Ratio techniques considered to be suitable to correct for view angle effects are the conventional band ratios (Holben and Justice, 1981) and the more refined offset

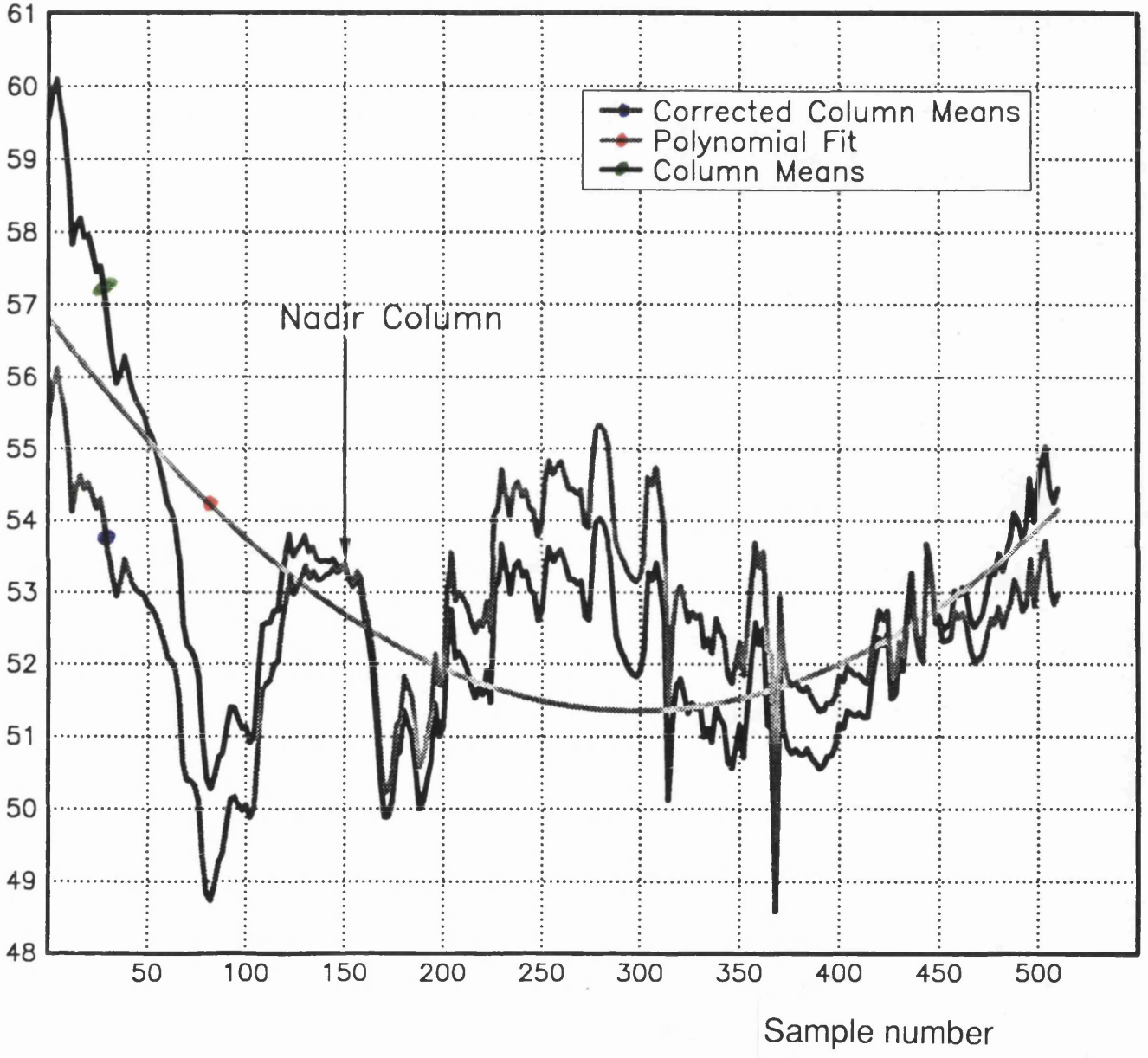


Figure 2.7: Fitting a polynomial to multiple view angle data (from Morris and Barnsley, 1989).

ratio method of Crippen (1987, 1988), both of which are normally used to correct for topographic effects (sec. 2.4.2). The major disadvantage of these techniques is that the products cannot be related to reflectance directly, limiting the scope of their application (Hook and Donoghue, 1988). A further difficulty is that the implicit assumption of this technique - i.e. the view angle effect is spectrally constant, at least over small parts of the spectrum - is plainly incorrect. Inspection of almost any dataset, including those presented in this work, indicates that this is false (for example, figure 2.8, section 4.1, Barnsley 1984a, 1985, Foody 1988).

Corrections using a polynomial fit (Irons and Labovitz, 1982, Royer *et al.*, 1985) have proved useful in image classification. Hook and Donoghue (1988) found improvements in classifications of '30%', Danson (1987) up to '85%'. In some cases, however, this was because classifications were extremely poor to begin with[8]. The moderate success of these techniques is easier to explain; polynomial fitting assumes that the view angle effect is systematic across the image, and thus independent of cover type. The anisotropic reflectance, however, is dependent upon cover type, and therefore if no attempt is made to model *explicitly* anisotropic canopy reflectance, the spatial distribution of these parcels (with different reflectance characteristics) within the scene will have an important impact upon the polynomial fit (Morris and Barnsley, 1989).

An objective test of these methods was carried out by Morris and Barnsley (1989), in which three polynomial correction methods proposed by Royer *et al.* (1985), plus a further method based upon proportional distance of column means from the calculated polynomial values, were implemented on a Sun workstation. Each of these methods was tried on the basis of calculating column means for the full image, and also for sections of the image defined by specifying a range of scan lines over which the column means would be calculated. This has the effect of improving the sensitivity of the technique to the spatial distributions of the different land cover types in the image (Morris and Barnsley, 1989). Accuracy improvements of the order of 2-10% points are typical, although accuracies are still very low unless view angle is restricted. A major reason for this is that class

[8]For example, Danson's (1987) most marked improvement is from 8% to 25% for identification of percentage canopy cover in a coniferous woodland.

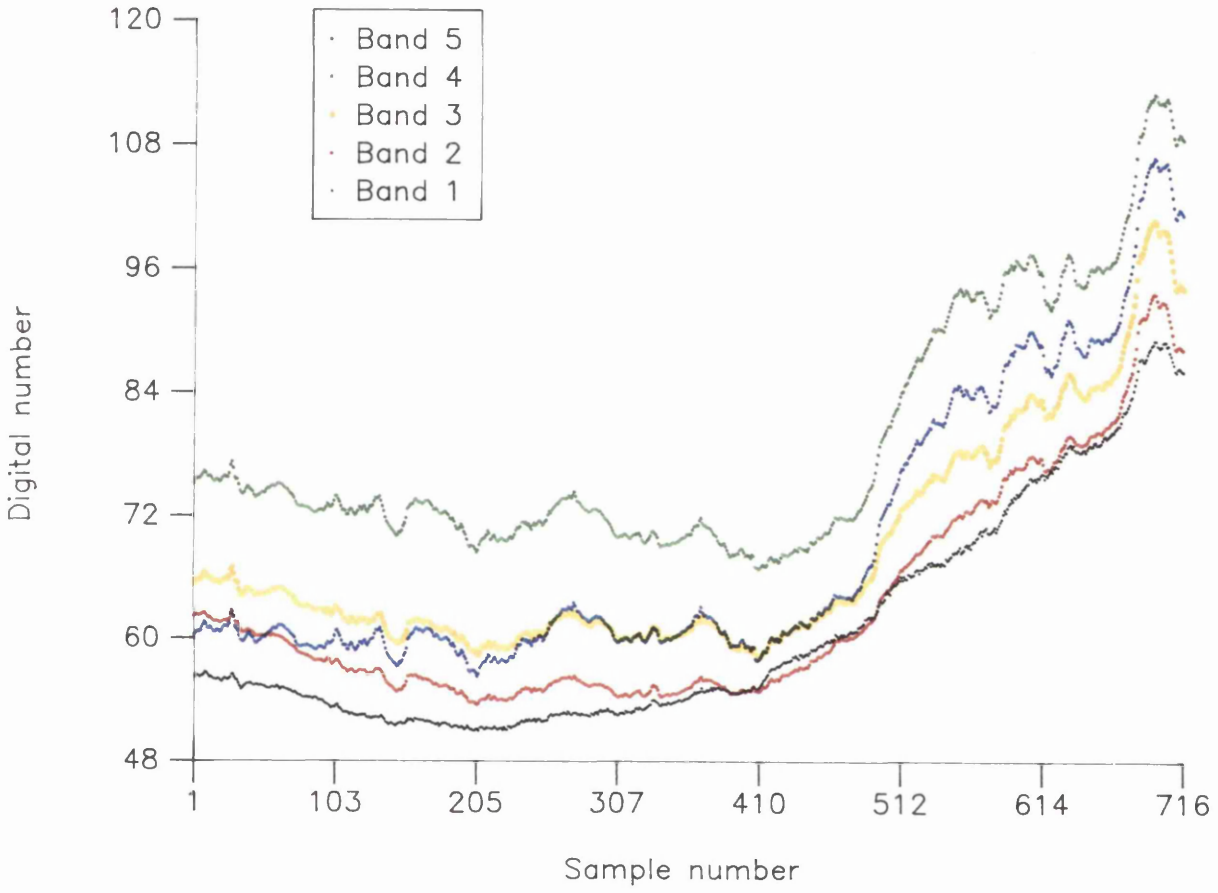


Figure 2.8:Column mean values for flightline 4, bands 1-10, in this study. The figure above illustrates the relationship between sample number and DN for the visible bands; overleaf, the top graph gives the relationship for the NIR bands, and the lower graph for the MIR bands.

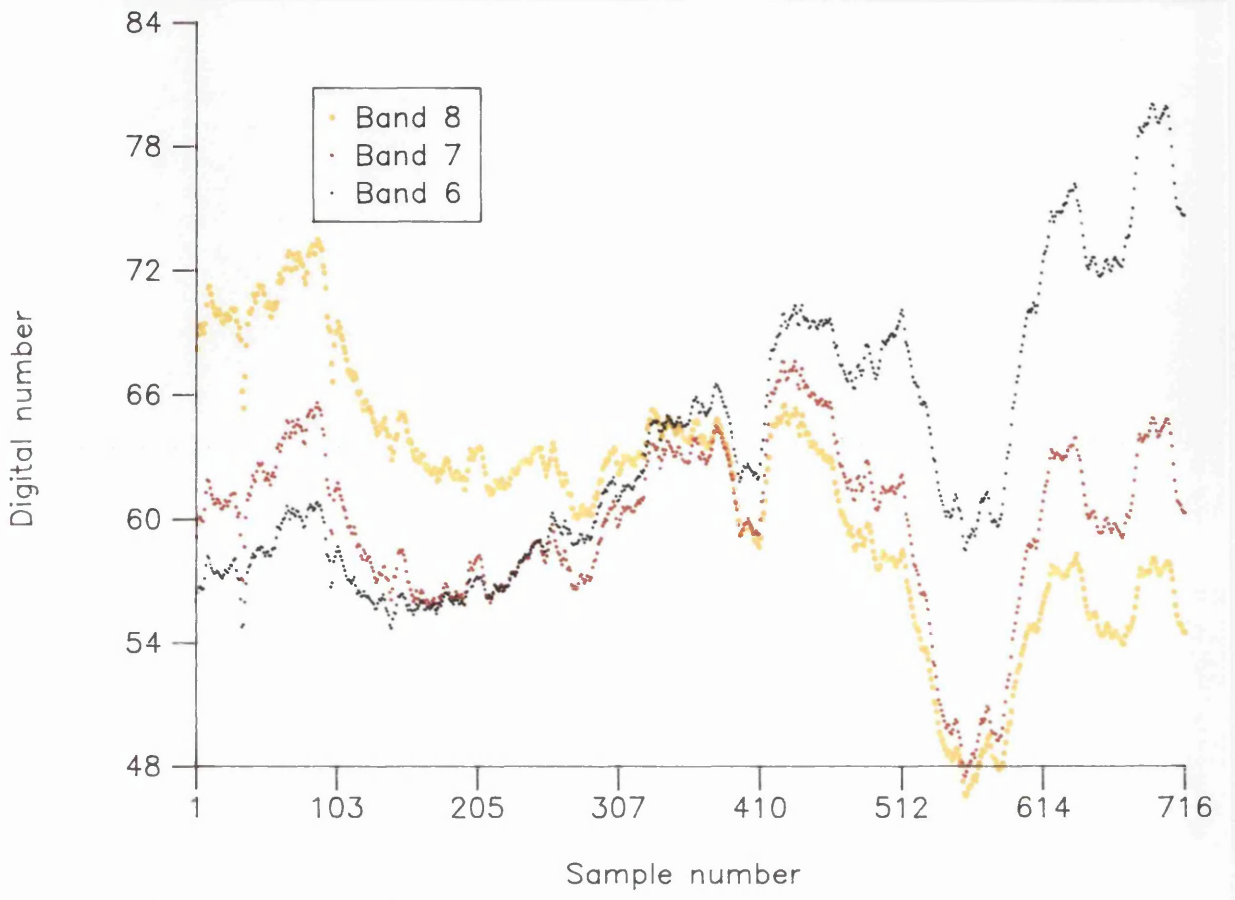
Band 8
Band 7
Band 6
Digital number
84
78
72
66
60
54
48
1
103
205
307
410
512
614
716
Sample number

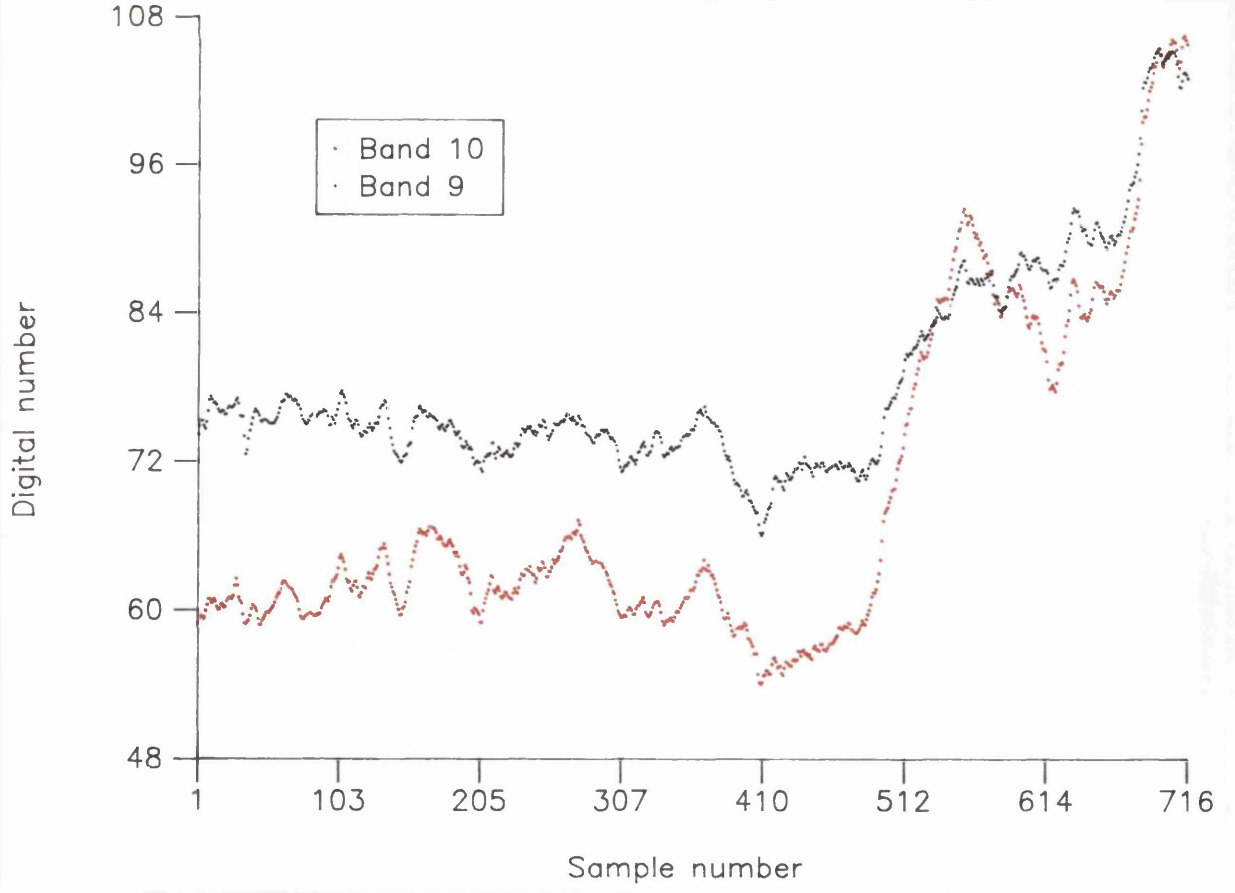
Band 10
Band 9
Digital number
108
96
84
72
60
48
1
103
205
307
410
512
614
716
Sample number

discrimination is degraded by the inclusion of multiple view angle training data, since the variance of the training data sets will increase, increasing the likelihood of overlap in feature space of different classes (Barnsley, 1985, Foody, 1988). A second factor is that while non-parametric corrections account for changes in mean value of training sets, they can make no correction for the distribution of these datasets. Kay and Barnsley (1989) and Barnsley and Kay (1989) have demonstrated that the variability of data is likely to decrease (for spatially heterogeneous cover types) towards the edge of the image (due to sensor and canopy geometry, *cf.* sec. 4.1). Thus a training set from the edge of an image (off-nadir) will tend to produce more errors of omission, and one from the centre (nadir) would produce more errors of commission. This has important implications for the application of multispectral classification algorithms to wide angle sensor data (such as AVHRR, MODIS-N and MODIS-T) (Morris and Barnsley, 1989), and for the inclusion of variance data in classification routines (such as the Coefficient of Variation, for example Williamson, 1989).

Non-parametric models can provide a useful solution to some sensor geometry radiometric effects. The technique, however, is limited by the different anisotropic reflectance properties of different canopies within the scene (polynomial fitting), or by the fact that the view angle effect is dependent on the choice of spectral channels (band ratios). Holistic approaches to these problems, taking into account an understanding of the mechanisms behind the effects, while holding little hope for improving simple image correction for view angle effects, will allow the development of alternative strategies for processing off-nadir data sets. In this instance it is the residual 'noise' remaining after the 'corrections' that is the information of interest, since this can only be explained by canopy geometry effects if all other effects are normalised. It is this information that is sort after in this study, in an attempt to extract canopy agro-physical parameters from multiple view angle image data.

### 2.5.3: Approaches to utilising canopy reflectance anisotropy for information extraction

Some workers (e.g. Hugli and Frei, 1983) have examined which view angles optimise the advantages of off-nadir viewing given differing Sun and view azimuth and zenith angles. Two options are presented: the first utilises a vertical view angle, with a small FOV to avoid both hotspot and specular reflectance peaks. The second uses high oblique views. In this case the view angle would be so great as to give unfavourable geometric distortions and increased atmospheric attenuation and scattering. Others have been bolder and more forward in thought. In an important paper, Kimes *et al.* (1984) show how multi-angle data are useful when considering the effect of view angle. A new strategy is outlined for the gathering of such data, to provide additional information about the physical characteristics of the target. The choice of view angles would reflect not the desire to minimize these effects, but to maximize the information gained from a particular target. The strategy is analogous to the multispectral strategy in that the additional information increases as the number of view angles increase and the number of data sets collected under different Sun angles increases.

A further approach is the analysis of the canopy 'hotspot'; this is the peak radiance value measured (in a multidirectional dataset) at a view angle equal in both the zenith and azimuth planes to the illumination angle. When the view and illumination angles are the same, shadowed components within the canopy and background will not be visible, and thus are not included in part of the scene. As the viewing angle moves away from this position, an increasing proportion of shadowed components will contribute to scene radiance, and net radiance from the surface diminishes (Strahler, 1988). It is considered that the rate of decrease in radiance with view angle is a direct function of size, shape, and spacing of leaves in the canopy, and that analysis of this change could reveal information about the geometry of the canopy. Indeed, this has been attempted, and to some extent verified, by Goel and various co-workers (for example, Goel and Strebel, 1983, Goel and Grier, 1988, Goel, 1988).

Ideally, a multiple view angle strategy would require (near) simultaneous imaging of a target from different positions, with a spatially constant (or predictable) atmospheric component. SPOT-1 is unable to provide such a capability, giving rise to problems of atmospheric modelling (Moran *et al.*, 1988) and variations in target characteristics over time, for example precipitation events and lodging (Hinzman *et al.*, 1986), different wind (Lord *et al.*, 1985) and illumination regimes, and even canopy architecture changes due to growth and maturity of the target (Pinter *et al.*, 1985). Looking to the near future, ERS-1 with the Along Track Scanning Radiometer (ATSR) will provide a capability of two near-simultaneous images of the same target, but without the high frequency of coverage that SPOT provides, and of course with only seasonally related alterations of Sun azimuth and zenith angle. The EOS platforms, however, with the pointable MODIS-T and HIRIS image spectrometers will provide a much more valuable source of data in the 1990's (NASA, 1986, 1987, chapter 6).

## 2.6: Summary and conclusions

This review of previous work, in fields related to the directional reflectance properties vegetative canopies, reveals that normalisation strategies are only useful for a paradigm that continues to demand the application of current modelling techniques for information extraction. In order for better, quantitative, information to be collected using current and planned remote sensing instruments, new strategies which make allowances for, and utilisation of, off-nadir capabilities must be developed. Additive, component or piece-meal approaches to image-understanding are unlikely to produce very successful results; however, current knowledge and the status of technology demands relatively simple non-parametric procedures for the development of these new, holistic, methods. Thus, a strategy which accounts for the integrated effects of atmosphere, topography and illumination will allow the artifacts of directional reflectance to be isolated. New methods can then be derived to analyse these artifacts to extract information concerning agro-physical parameters of the target.

Several major paradoxes arise in the development of new multiple view angle strategies. These new data analysis and processing procedures cannot be dependent upon extensive ground "truth". More complex techniques and models, however, often demand more complex and comprehensive data. In order to preserve the advantages of remotely sensed data collection strategies, these new model inputs must also be collected remotely whenever possible. Examination of the procedures used to extract information concerning the physical properties of the target also brings into question the validity of the current paradigm for data collection.

In chapter 3, it is recognised that conventional image corrections (such as radiometric calibration of the data) must be made and the sensor geometry derived before more complicated image analysis can be made. Some of the special features of the ATM sensor (evident in other sensors also) provide the continuity and development to Chapter 4. In this section, after an introduction to the view angle artifacts in this data set, an attempt at devising a practicable preprocessing system for multiple view angle imagery, in order to isolate these artifacts, is made; the resultant combined sky and terrain, spectral and spatial, illumination model is applied to the experimental data set. The aim of this section is to isolate directional effects of the canopy, which are then examined in greater detail in chapter 5.

Once it is possible to identify view angle artifacts in the image data with certainty, analysis of what causes them and what importance the canopy has in controlling them can be made. Chapter 5 attempts to identify relationships between image variance in a qualitative way to achieve this understanding. The chapter then goes on to explore a new method for extracting information, by examining the coefficient of variation of parcels in the image, concerning basic physical parameters for a number of cover types. In chapter 6, the suitability of current remote sensing instruments is explored with regard to their capability for collecting multiple view angle data sets. The options for the development of new data collection strategies opened by the use of planned sensors, such as MODIS-T and HIRIS, are also examined.

# CHAPTER 3: Data collection and preprocessing

## 3.0: Introduction

In chapter 2, the factors which influence the directional reflectance properties of Earth surface materials measured by spaceborne and airborne sensors were examined. A suitable approach for the remote sensing of these surfaces, attempting to utilise the additional information given by observing the target from different view angles, was outlined. One of the prerequisites of such a method is suitably processed input image data, in which corrections for radiometric calibration, geometric corrections, and some sensor geometry artefacts are made, in order to isolate those artefacts due to the physical properties of the target.

In this chapter the study area is described (section 3.1), techniques for the collection of ground and remotely sensed data outlined (3.2), and details of the operation and geometry of the Daedalus ATM scanner discussed (3.3). In particular, the correct derivation for the view angle for a given sample in ATM imagery obtained with the S-bend system correction is given (3.4), in order to identify accurately view angle dependent relationships, and the effects of view angle upon image data in this study introduced (3.5). Section 3.6 discusses geometric problems and corrections to airborne imagery, explaining how this can become a limiting factor on the quality of data, and section 3.7 details the method of radiometric correction applied to the data.

## 3.1: Study area

The chosen field site for the study is Bemborough Farm, near Guiting Power, Gloucestershire (Lat. 51 56' 30" N, Long. 1 50' 30" W) (figure 3.1). This is a large homogeneous farm cropping mainly wheat and barley, with occasional fields of rye and triticale, and some winter crops such as sugar beet (Langer and Hill, 1982). Several varieties of the dominant crops are sown as an insurance against varietal epidemics. As well as 800 acres of these crops, Bemborough also has 250 acres devoted to sheep pasture, and several large stands of deciduous, coniferous

Figure 3.1: Location of study site

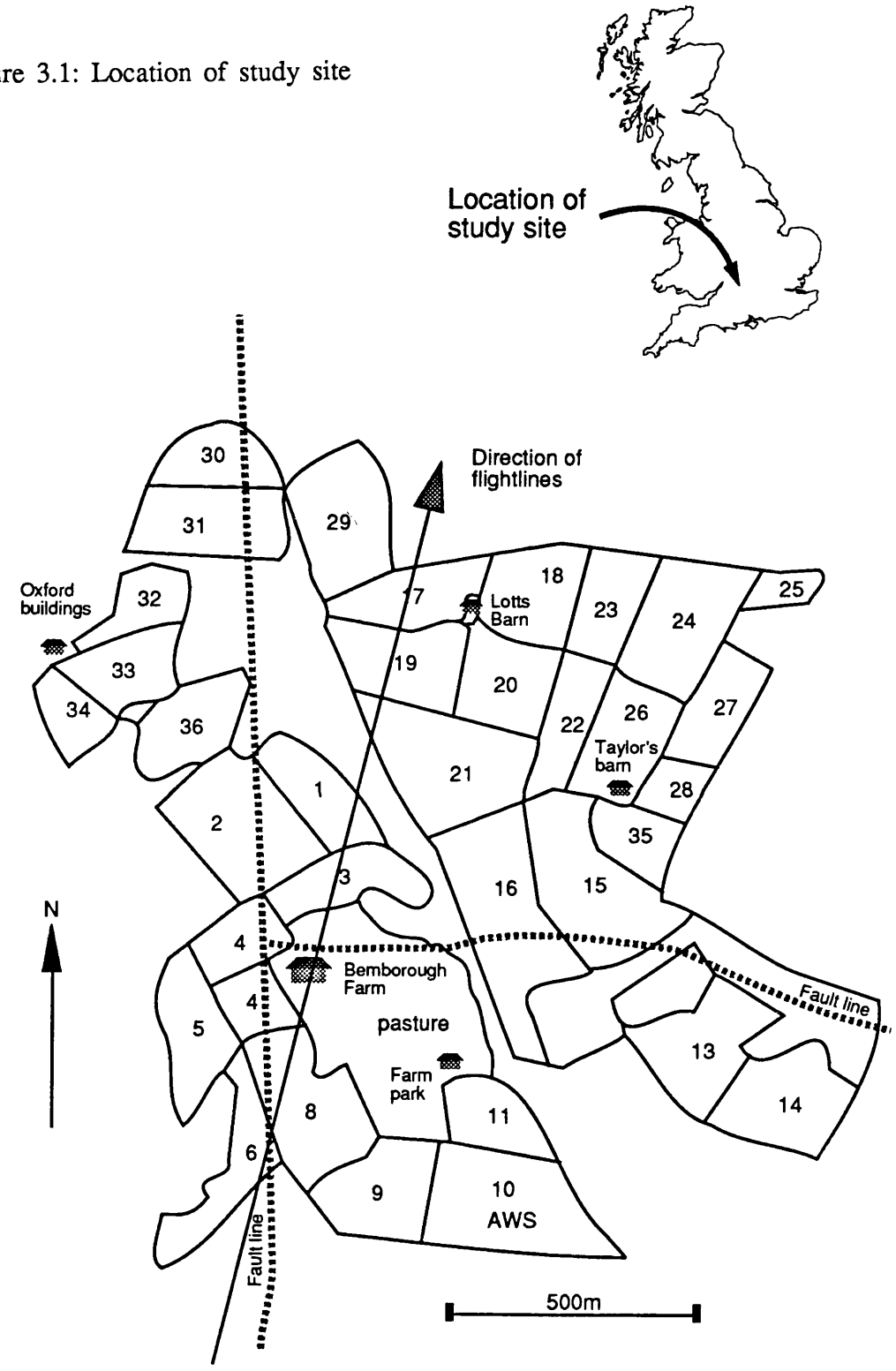


Figure 3.2: Map of study site, including field index (see Appendix 1)

and mixed woodland. The predominant agriculture on neighbouring farms is the same.

The farm is situated on a large (270m altitude) downland ridge, running approximately NW-SE (figures 3.2 and 3.3), the solid geology comprised in general of sandy oolitic limestones, with some calcareous sandstones (Chipping Norton Limestone, Inferior Oolite, and Great Oolitic Limestone (Stonesfield formation) (Geological Survey of Great Britain, 1:50,000 series, 1981)). A major surface fault, running north-south, divides the farm in two, and is easily identified on the imagery. The soils also follow the division of this fault line; to the east they are classed as Elmton 1 [1], to the west as Sherborne [2]. Annual precipitation for the region is 32.5" (827mm), of which 45% falls during the summer months (April to September)[3]. Precipitation distribution is not influenced greatly by season, and is of low variability.

Full cooperation with the farm managers in terms of permission for overflight, facilities for instrumentation, and information relating to sowing dates, varieties, application of fertilizers etc. was obtained at an early stage.

## 3.2: Ground data collection

### 3.2.1: Automatic Weather Station

An automatic weather station (AWS) collected data from early April through until late August 1988 (figure 3.2). The variables measured were wet and dry bulb

---

[1]Elmton 1: subdivision 343a, shallow well drained brashy calcareous fine loamy soils over limestone. Some similar deeper soils and some non-calcareous and calcareous clayey soils. Associated landuse: Cereals, sugar beet and potatoes; winter cereals and dairying in South West. (Soil Survey England and Wales, 1983)

[2]Sherborne: subdivision 343d, shallow well drained brashy calcareous clayey soils over limestone, associated with permeable clayey soils. Associated landuse: cereals, short term and permanent grassland with dairying and stock rearing. (Soil survey England and Wales, 1983)

[3]Precipitation estimates based upon annual averages between 1916 and 1950, as published by the Ordnance Survey, 1967.

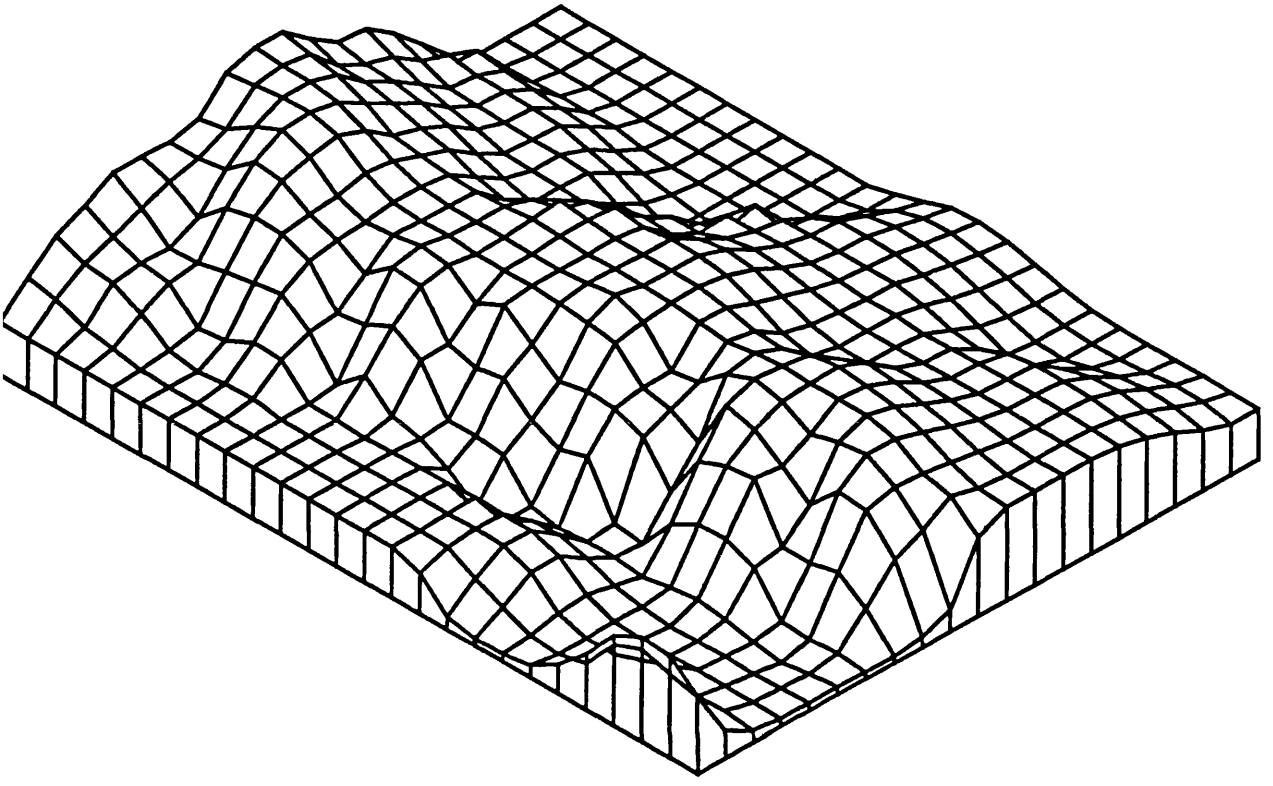

Figure 3.3: Wire frame DEM of study area, viewed from South-West.

temperature, wind run, wind direction, precipitation (using a tilting bucket rain gauge), and irradiance (using a pyranometer) (Oke, 1978). The collection interval was set to 5 minutes, in order to guarantee a measurement close to a SPOT image collection time, since this was the original image data that the study was intending to use. The meteorological data, stored by the automatic logger, were supplemented by manual readings on the day of the aircraft data collection that was actually used in the study.

The main purpose of the AWS was to provide data concerning the ground-level meterological conditions at the time of imaging, although it was acknowledged in advance that extrapolation from point to area for these measurements would present difficulties. Vegetation canopy reflectance is known to be affected by wind (strength, gusts) (Lord *et al.*, 1985), and soil reflectance affected by the time elapsed since the last precipitation event (Richardson and Wiegand, 1977, Huete *et al.*, 1985, Escadafal *et al.*, 1989). The meteorological data would, however, also provide important information regarding the development of crops; this had originally been one of the main intended study topics. For example, the major limiting factor in crop development (especially on thin, well drained, limestone soils, such as at Bemborough) is precipitation amount and frequency.

### 3.2.2: Management records

Farm records provide all the management decisions concerning care and development of crops. Dates and details of spraying, fertilizer applications and yields are recorded on a per field basis. Historical records for this farm extend back 15 years. However, the data referenced most frequently by this study were the variety, sowing date and sowing density of each field, as well as the final yield. Consideration of external factors[4] is also made when assessing crop productivity. These records are used in conjunction with other field observations, outlined in section 3.2.3 below.

---

[4]For example infestations of brome grass, which significantly reduce yields, and are usually restricted to individual fields.

### 3.2.3: Other ground data

In addition to the meteorological data, and the use of farm management records, detailed observations of crops were made. These have been carried out in three ways. First, regular measurements have been made of crops in four sample fields; these data are most relevant to the airborne image data. Second, an assessment of the growth stage of the crop in each field on the farm was also made regularly throughout the summer until harvest. Third, observations and discussions with the farm managers and a visiting consultant were made at intervals over this period. This final source has been of great importance, much being learnt about the complexity of decision-making that takes place on a modern farm.

The ground data relevant to the ATM data comprised both simultaneous field measurements, and data collected subsequent to the aircraft overflights. The simultaneous measurements were restricted to a point location, using the instrumentation at the AWS site (3.2.1). A limited number of observations were made for one field (number 10) on the day of the overflight, more extensive observations were carried out the next day.

After the success of the over-flight was confirmed, the scene "quick-looks" were collected to allow identification of suitable fields for study. These could not be chosen until after the over-flight had been completed, as it was critical that they should be viewed from as many different flightlines as possible. As a result, four fields were chosen. Measurements of parameters in these fields could not be made until the following day, by which time some precipitation had occurred, and the general meteorological conditions had changed (overcast, wet, quite windy). Measurements of crop plant height, flag leaf length and crop cover were made at three sample locations in each field. Ten measurements were made of each parameter at each location. Percentage ground cover was assessed using a 50x50cm quadrat. Photographic measurements were also made, along and across the flightline direction, to allow analysis of leaf angle distribution. Photographs of individual plants were also taken to provide a record of plant physiology.

The crops in the sample fields were harvested to provide an estimate of biomass, again at three locations within each field. The area harvested in each case was $1m^2$. Because of the precipitation during the day and between the flights and the data collection, only dry biomass has been estimated. Larger harvest areas were required to overcome the spatial variability of the cover in the field; this is a function of the row spacing and the efficiency of germination. Results are summarised as follows:

**Table 3.1: Field data, Bemborough Farm, April 27 1988**

| | Leaf length | | Leaf width | | | |
|---|---|---|---|---|---|---|
| Field | mean | sd | mean | sd | cover | sd |
| 10 | 156.50 | 15.32 | 14.07 | 1.55 | 58.17% | 10.63 |
| 21 | 169.50 | 20.57 | 13.27 | 1.53 | 21.67% | 7.58 |
| 29 | 183.17 | 19.76 | 15.07 | 2.43 | 56.00% | 8.14 |
| 30 | 77.80 | 19.26 | 5.73 | 0.83 | 6.17% | 3.13 |

| Field | Plant height | spacing | orientation |
|---|---|---|---|
| 10 | 307 | 104 | 260°/80° |
| 21 | 275 | 104 | 270°/90° |
| 29 | 415 | 104 | 350°/170° |
| 30 | 90 | 104 | 98°/278° |

(measurements in millimetres)

Other data were also collected over the summer for use with the anticipated SPOT image data. In addition to measuring the same variables on two further occasions for the same four fields over the period, more frequent observations were made of all of the grain fields on the farm. Each round of observations took a full day. The assessment of crop growth was made using the MAFF standardised growth stage chart. This does not always provide a precise definition of the crop state, as

variability will exist within a single field in terms of both the maturity and the health of the crop, but it does provide an objective standard of comparison. Varietal differences would also have to be considered in the final analysis of these data.

### 3.2.4: Map data

Map data were obtained from several sources:

- Farm sketch maps, providing information on field names, and referencing the farm records to fields.

- Ordnance Survey (OS) 1:10,000 maps for the area were used to produce a digital ground control point data set for the geometric correction of the airborne imagery (sec. 3.6). OS 1:25,000 and 1:50,000 maps were used in the field and for the ATM flightline planning.

- Geology, soils and precipitation maps were referenced for site description purposes (sec. 3.1).

- Digital terrain data were acquired from the OS, originally derived from digitised 1:50,000 Landranger contour map series. These data were used to calculate the illuminated terrain models produced as part of the Terrain Lite algorithm, developed in chapter 4.

## 3.3: The Daedalus Airborne Thematic Mapper (ATM) simulator

### 3.3.0: The use of airborne remote sensing devices

Airborne scanner development often precedes the development of space borne sensors in order to test design and technology (for example, AIS, AVIRIS, HIRIS).

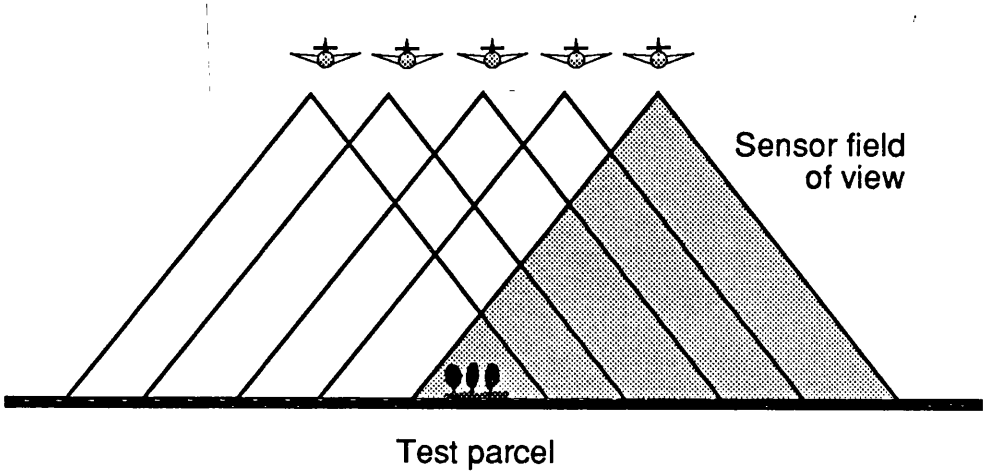


Figure 3.4: Multiple view angle data collection strategy using the ATM.

They are, however, also useful in their own right as sources of data. An aircraft is directly under the control of the researcher, and as such, small specialised sites may be imaged at short notice and under conditions dictated by the scientist. The airborne scanner may have a greater number of spectral channels than its airborne counterpart, often as a result of no telemetry of data being required. Moreover, higher spatial resolutions may be obtained, by controlling the flying height. For these reasons it is ideal for research applications.

New airborne data were collected, as part of the NERC 1988/9 airborne campaign, in order to develop and test the methods described in this study (chapters 4 and 5). These image data provide several useful functions:

- ability to simulate SPOT wavebands
- relatively precise control over view angle
- repeated passes over one cover type within short time
- greater number of view angles than current satellite sensors

Several passes from different view angles over sample test areas were made in order to assess the effect of viewing a canopy from different zenith angles (figure 3.4).

### 3.3.1: Characteristics of the Daedalus ATM sensor

The Daedalus AADS 1268 Airborne Thematic Mapper (ATM) is the sensor which has been chosen by the Natural Environment Research Council (NERC) for the past eight years (1982-89) of airborne campaigns. The ATM is an eleven channel digital system, covering the spectral bands used by Landsat TM, and (by combinations of bands) also Landsat MSS, SPOT-HRV, and NOAA-AVHRR. The multispectral scanner system is a passive sensor collecting and recording data ranging from the visible blue to the thermal infra-red (see table 3.2).

**Table 3.2: ATM and TM specifications**

| ATM | | Bandwidth (μm's) | Equivalent Landsat band |
|---|---|---|---|
| Channel 1 | : | 0.42 - 0.45 | |
| Channel 2 | : | 0.45 - 0.52 | (TM Channel 1) |
| Channel 3 | : | 0.52 - 0.60 | (TM Channel 2) |
| Channel 4 | : | 0.605 - 0.625 | |
| Channel 5 | : | 0.63 - 0.69 | (TM Channel 3) |
| Channel 6 | : | 0.695 - 0.75 | |
| Channel 7 | : | 0.76 - 0.90 | (TM Channel 4) |
| Channel 8 | : | 0.91 - 1.05 | |
| Channel 9 | : | 1.55 - 1.75 | (TM Channel 5) |
| Channel 10 | : | 2.08 - 2.35 | (TM Channel 7) |
| Channel 11* | : | 8.50 - 13.00 | (TM Channel 6) |

*Not used in this study

Channels 1 to 5 are in the visible part of electromagnetic spectrum, 6 to 8 near infrared, 9 and 10 the short wave infrared and channel 11 the thermal infrared. (Source Huntings Technical Document, and Williams, 1984).

Simulation of other sensors can be achieved by combining several channels of the ATM sensor, although this does not take into account the difference in the spectral response curves of the sensors in question. For example, simulation of the SPOT-HRV channels can be achieved as follows:

**Table 3.3: Simulation of SPOT-HRV channels using Daedalus ATM**

| SPOT channel | ATM Channel |
|---|---|
| S1 | 3 |
| S2 | 4+5 |
| S3 | 7 |
| P1 | 3+4+5+6 |

### 3.3.2: Image data

Daedalus Airborne Thematic Mapper 11 channel data, at 5m nominal IFOV were requested as part of the NERC 1988 airborne remote sensing campaign. Eight flightlines were flown (date 26 April 1988), the spacing of which resulted in a nominal 80% overlap. These gave multiple view angle on sites on the farm within a 40 minute period. The airborne data acquired are of excellent quality, nearly cloud free and excessive roll. Although the day was only average visibility (approx 10-15km visibility on the ground), the image is clear and of high contrast in each band. However, the flightlines were not always in the same parallel, and are certainly not simultaneous observations of the sample test areas from different view angles, as they should be ideally. This apart, the airborne data provide the key data input to the study, especially since no SPOT data were acquired as was initially intended for the study.

Panchromatic aerial photography was acquired for the site, simultaneous with the Daedalus imagery, on three of the flightlines. These photographs provide a useful reference for interpretation and familiarisation with the imagery. Some schemes for using the photographs to orient the airborne data have been suggested, and these are discussed elsewhere (3.6).

No SPOT data have been acquired. It is understood that no cloud free days occurred when the sensor was available for pointing at the study area. Cushnie (1988) reports that only one or two images per scene per year can be expected from the present system. This is despite the off-nadir pointing capability, which should allow 11 opportunities to sample every 26 days. Cushnie calls for a more efficient method of obtaining cloud free cover (using SPOT), either through systematic coverage or the use of meteorological data to help predict cloud free areas. In any case, the ability of SPOT to produce data with the qualities of 'reliability, timeliness, adequacy of coverage, efficiency and effectiveness' (MacDonald and Hall, 1980, p.671), must certainly be questioned here.

### 3.3.3: Geometric properties of ATM image data

Aircraft data suffer from severe geometric distortions due to the instability of the platform, as well as due to the geometric configuration of sensors designed to operate (relatively) close to the object. This is mainly because the aircraft is flying through an unstable medium (heated air) and in order to keep the aircraft on track, corrections to yaw, pitch and roll must be made continuously by the pilot. These distortions are exaggerated by the geometric configuration which, in particular the wide FOV (74°), is extreme. Relief displacement is also increased, since this is inversely proportional to altitude of the sensor (*cf.* 3.6.2), and also because the view angles with aircraft imagery are larger since the FOV is greater (see 3.6). Airborne scanner data distortions can be classified as follows:

**Table 3.4: Airborne scanner geometric distortions**

| | |
|---|---|
| Platform movement: | orientation<br>position |
| Sensor operation: | panoramic effect<br>rotation of mirror<br>non-linearity of mirror movement |
| Imaging geometry: | oblique view angles<br>relief |

(Adapted from Dowman, 1985, p106)

With ATM data, all of these parameters can be considered to be effective at all times, and constantly changing. For this reason, airborne scanner data geometry is particularly hard to model parametrically (*cf.* 3.6 below). It should be noted that airborne data is unique in combining the worst elements of distortion in a single geometry.

Each line in an ATM image is scanned using a rotating scan mirror which traverses the FOV of the sensor. Line scan rate can be set at 12.5, 25 or 50 lines per second, depending upon flying height and speed of the aircraft used as a

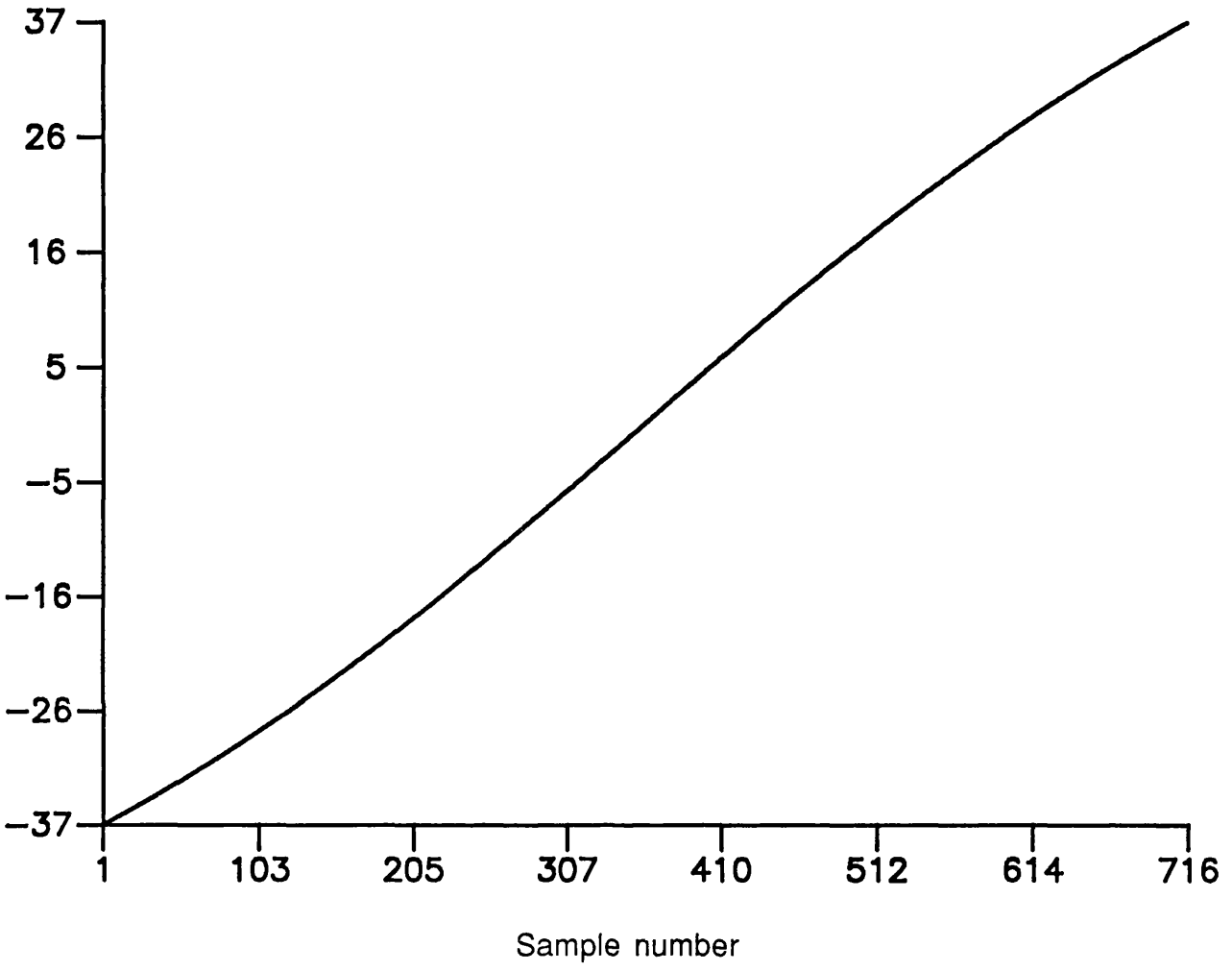


Figure 3.5: S-bend curve; sample number vs view angle. The S-bend correction makes this relationship linear.

platform. The IFOV of the sensor is 2.5 mrad. A typical configuration such as that normally flown on the NERC campaigns is a flying height of 2000m, 25 scans per second, at a velocity of 150 knots. This gives a GRE of 5x5m at nadir, and a pixel size of 4.21m by 3.29m (Table 3.5).

**Table 3.5: Configuration of NERC ATM scanner used in this study**

| | |
|---|---|
| Instantaneous field of view (IFOV) | 2.5 mrad |
| FOV after S-bend correction | 74° |
| Scan rate | 25 scans $s^{-1}$ |
| Nominal flying height | 2000m above ground level |
| Nominal ground track velocity | 82.22 $m.s^{-1}$ |
| Pixel size (across track) | 4.21m |
| Pixel size (along track) | 3.29m |

(From Barnsley and Kay, 1989)

However, several factors must be taken into consideration when examining the geometry of ATM imagery:

- First, a degree of overlap between successive scan lines is desirable, to ensure that there are no gaps.

- Second, a system geometric correction (known as 'S-bend' correction) is applied in flight to preserve scale across track in the image (figure 3.5).

- Third, aircraft motion (change in velocity and altitude, roll, yaw and pitch) must all be taken into consideration. Roll correction up to ±6° is applied automatically using a gyro mechanism linked to the digitizer unit.

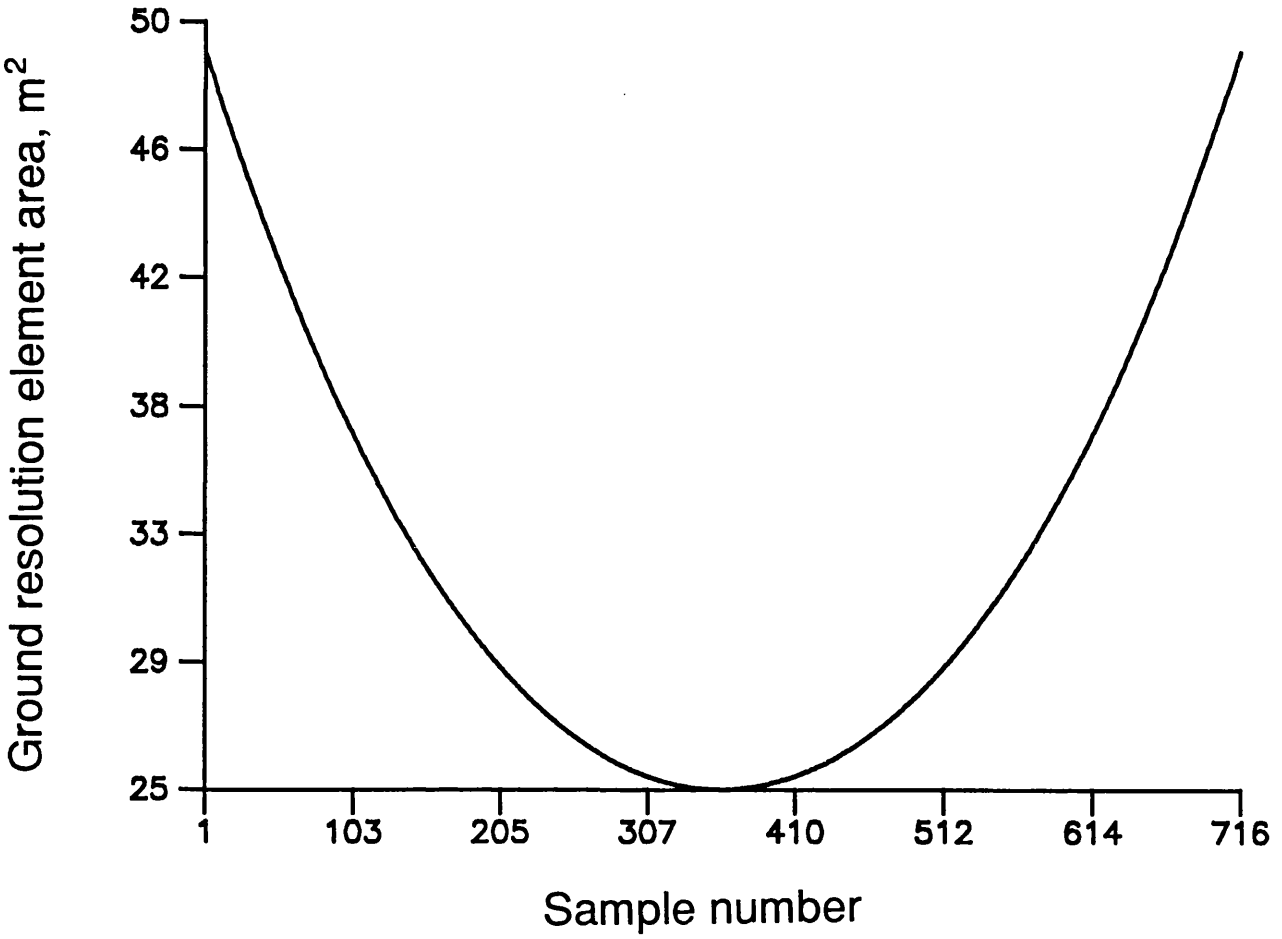


Figure 3.6: Ground Resolution Element (GRE) area increase with sample number. Samples 358/359 are nadir viewing.

A further complication of ATM data is that the very wide FOV of the sensor distorts the GRE of the IFOV at the edge of the image, so that the GRE increases in both dimensions, and therefore area (figure 3.7, table 3.6) for samples towards the edges of an image. This has considerable effect on the overlap between adjacent IFOV's and the spatial autocorrelation between pixels in the image (*cf.* 3.4 below).

**Table 3.6: Size and area of the GRE for the NERC ATM scanner used in this study**

| GRE | Nadir | 10° | 20° | 30° | 37° |
|---|---|---|---|---|---|
| Across | 5m | 5.16m | 5.66m | 6.67m | 7.84m |
| Along | 5m | 5.08m | 5.32m | 5.77m | 6.26m |
| Area | $25m^2$ | $26.21m^2$ | $30.11m^2$ | $38.49m^2$ | $49.08m^2$ |

(From Barnsley and Kay, 1989)

Nominal overlap between successive lines is easily calculated with reference to the parameters above. Oversampling increases from 15.8% at nadir to 46.3% at 37° (off-nadir) in the across-track direction, and from 36.2% to 47.4% in the along-track direction (Barnsley and Kay, 1989). This will be affected by changes in velocity and pitch. It is impossible to calculate the exact overlap between any two lines in an image, since not all the information required is available[5].

[5]Exact modelling of the ephemeris of the aircraft is not possible given the system corrections to the ATM imagery; these render the normal use of ground control to construct a parametric model (space resection) of the aircraft's path useless. The simultaneous photography could be used to define a generalised model, but is not frequent enough to provide high enough quality data for the correction of the digital data (only one photo-pair every 250 lines). Inertial navigation may have provided the data necessary, and has been used for such purposes.

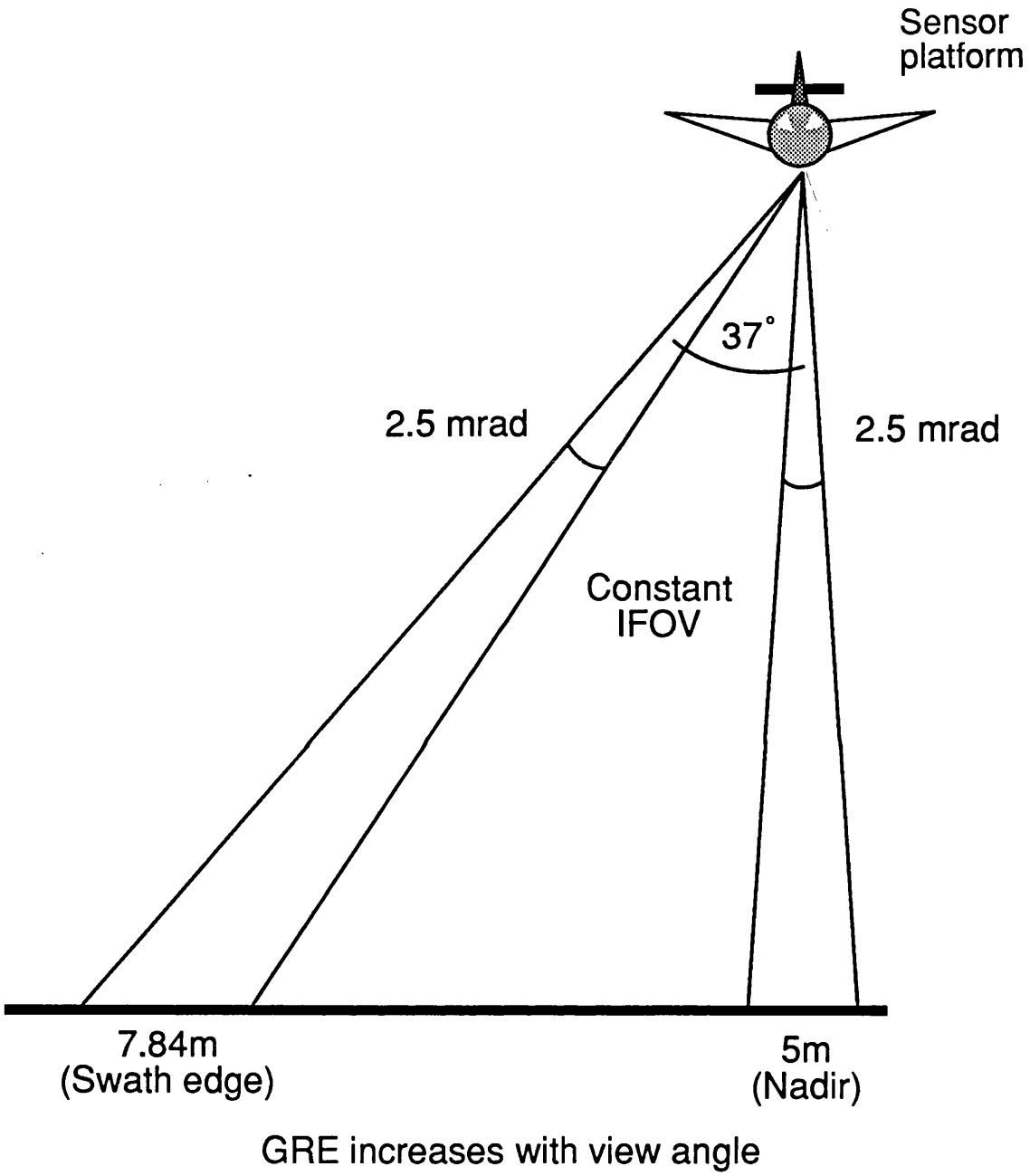


Figure 3.7: GRE increase with view angle; geometry of the ATM sensor.

## 3.4: S-Bend correction

The S-bend system correction is a hardware adjustment unique to the Daedalus ATM scanner system. None of the effects of applying this correction, other than the principal intention of preserving image scale across the swath, have been considered in previous published work with these data. This section, therefore, will examine in greater detail the exact mechanism, nature and effects of this correction on the data used in this study.

If the sampling rate of the ATM scanner was a constant angular rate, the image would suffer from compression towards the edges, since a greater area on the ground would be represented by one pixel. This is because the dimensions of the GRE increase towards the edge of an image (figure 3.7, table 3.6). By default the sensor is operated with the S-bend system correction in operation. This functions by restricting the field of view of the sensor to 74°, and controlling the sampling interval using a Read-Only Memory (ROM) chip in the instrument. This has the angular position for each sample already determined, and preserves the scale in the across-track direction, assuming no other external distortions (such as relief, changes in aircraft altitude). However, it also provides for a (variable) degree of over-sampling between IFOV's along the line; the angular difference between the centre of IFOV's at nadir being 2.1 mrad, as against 2.5 mrad for the full IFOV. This over-sampling increases towards the edge of the image, as the angle between the centre of IFOV's reduces, while the GRE increases.

### 3.4.1: Definitions

The correct calculation of the ground resolution element and sensor geometry for the Daedalus ATM scanner, in a standard configuration[6], is outlined below (3.4.2) and in Barnsley and Kay (1989). The results of these calculations are used to

[6]The common configuration of the Daedalus ATM scanner on NERC campaigns has been a flying height of 2000m, an IFOV of 2.5 mrad, and with S-bend correction applied.

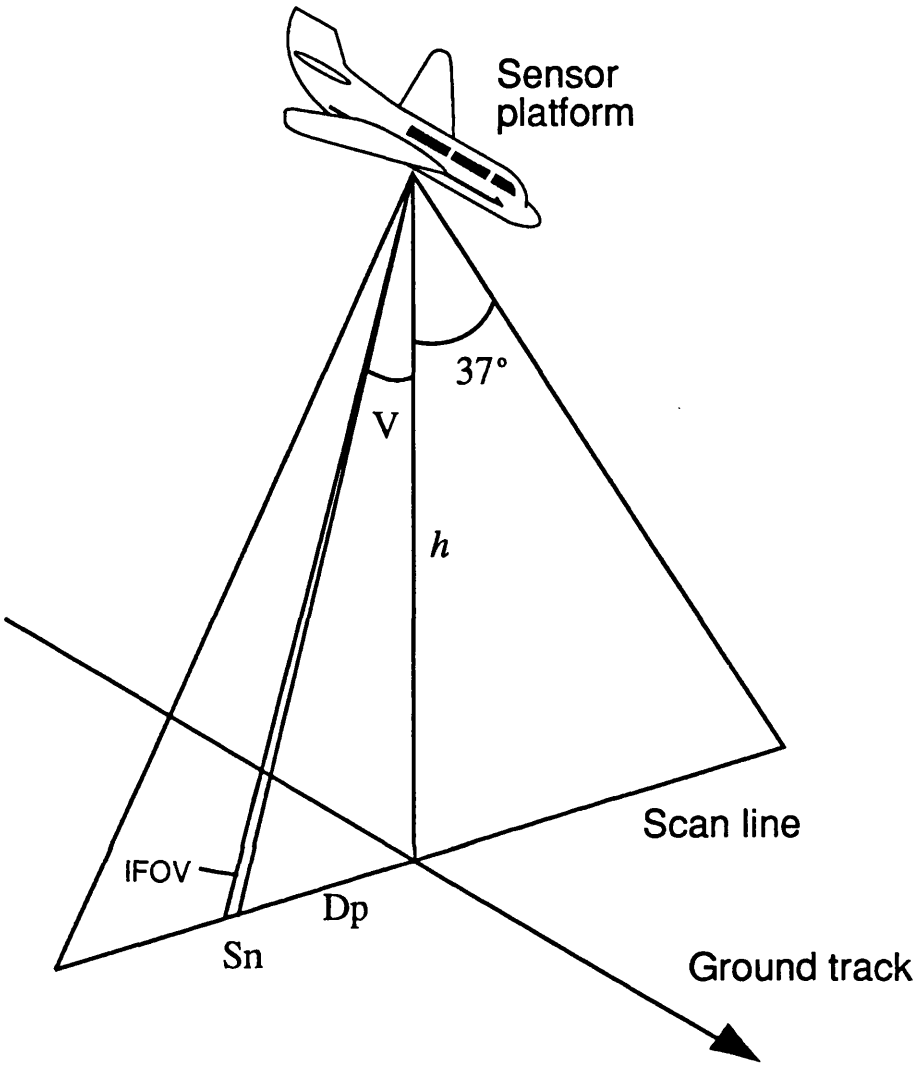


Figure 3.8: Daedalus ATM geometry used in this study. Flying height *h*, view angle V, sample number $S_n$, plane distance from nadir $D_p$.

indicate the variation in the GRE with changing sensor view angle. Before proceeding to the calculation of the GRE for the ATM scanner, it is important to give some definitions of standard concepts which are frequently used imprecisely in the remote sensing literature.

The **field of view** (FOV) of the sensor is the angle subtended by one scan line, while the **geometric instantaneous field of view** (IFOV) is defined as an angle which is a function of the detector size and the focal length of the system (Townshend, 1981). The IFOV can be used to determine the dimensions of the **ground resolution element** (GRE), which is the projection of the IFOV onto the Earth's surface (Slater, 1980). For a constant IFOV, the GRE varies as a function of the platform altitude and the sensor view angle (Barnsley and Kay, 1989).

**Pixel size** across track is equivalent to the ground distance between the centres of successive GRE's (Schowengerdt, 1983), which is controlled by the mirror angular velocity (constant on the ATM) and the sampling interval of the instrument (Slater, 1980, Swain and Davis, 1978). The implication of this, for a sensor sampling over a swath at a constant angular rate, is that pixel size would also become a function of view angle (Swain and Davis, 1978), and would thus increase towards the edges of the image. For this reason, the **S-bend** system correction is often applied to Daedalus ATM data to maintain a constant pixel size in the across track direction, by varying the sampling rate with view angle. This ensures that scale along an image scan line is constant. Pixel size in the along track direction is controlled by the scan rate of the sensor and the speed of the aircraft over the ground (Townshend, 1981).

### 3.4.2: Derivation of the ATM sensor geometry

When the NERC ATM instrument is operated in the S-bend correction mode, the FOV of the sensor is 74° (figure 3.8). Since there are 716 pixels in an ATM scan line, half a scan line (358 pixels) corresponds to 37°. Given the flying height of the aircraft ($h$, 2000m in this study), the dimension of a pixel across track ($P_{ac}$), ignoring terrain effects, is:

$$P_{ac} = h\tan(37°)/358 \qquad \text{Equation 3.1}$$

Which gives $P_{ac}$ the value of 4.21m in this instance. The dimension of a pixel along track ($P_{al}$) equals the ground-track velocity of the aircraft divided by the scan rate of the sensor (Townshend, 1981).

The plane distance ($D_p$) from the nadir to a given sample number ($S_n$) is, therefore, given by:

$$D_p = P_{ac}(S_n - 0.5) - h\tan(37°) \qquad \text{Eq. 3.2}$$

This gives $D_p$ a value of -1505.00m and +1505.00m for samples 1 and 716 respectively.

The view angle (V) for any value of $D_p$ is:

$$V = \text{atan}(D_p/h) \qquad \text{Eq. 3.3}$$

The dimension of the GRE along track ($G_{al}$) at any view angle is a function of the IFOV ($\phi$) and $h$:

$$G_{al} = (h.\phi)/\cos V \qquad \text{Eq. 3.4}$$

Assuming the distance on the ground between each scanline is constant, an increase in $G_{al}$ will increase the overlap between adjacent GREs in that direction.

The dimension of the GRE across-track ($G_{ac}$), at any view angle, is given by:

$$G_{ac} = h\,[\tan(V+\phi/2) - \tan(V+\phi/2)] \qquad \text{Eq. 3.5}$$

Once again, $G_{ac}$ varies as a function of sensor view angle. Now, by definition, the S-bend correction maintains a constant distance on the ground between centres of adjacent GREs in the across track direction (*cf.* 3.4 above). Therefore, an increase

in the size of $G_{ac}$ with view angle results in greater overlap between adjacent GREs towards the edges of the swath.

Finally, the area of the GRE ($G_{area}$) (figure 3.6, table 3.6) is approximated by:

$$G_{area} = G_{ac}.G_{al} \qquad \text{Eq. 3.6}$$

## 3.5: ATM view angle effects - some observations on image variance

With all sensors, several factors change as a result of changing view angle. First, a different profile of the target(s) is imaged. This will alter the ratio of shadowed/illuminated parts of the crop, and the perceived cover of the canopy over the substrate. Second, a different atmospheric component is acting upon the energy detected at the sensor, due to changing path lengths. Third, the sensor-target-sun geometry is altered. Detected canopy radiance at the sensor becomes a complex problem, concerning the radiative transfer interactions of the plant canopy, radiant flux and the illumination and viewing geometry (Barnsley and Kay, 1989).

With the ATM scanner, the level of oversampling between adjacent pixels increases, along and across track, towards the edge of the image. This has important implications concerning the resolving power of the sensor, and also the probability of two adjacent pixels having similar DN (the spatial autocorrelation between pixels), and therefore reducing the variance of the image. This reduction should be evident, in the image data set used in this study, when the same class occurs at different view angles within an image or a series of images. It has been possible to test this hypothesis with the ATM data presented here, since the flightline configuration has given five or six "looks" at individual fields, allowing the analysis of the DN within each field (sec. 5.2).

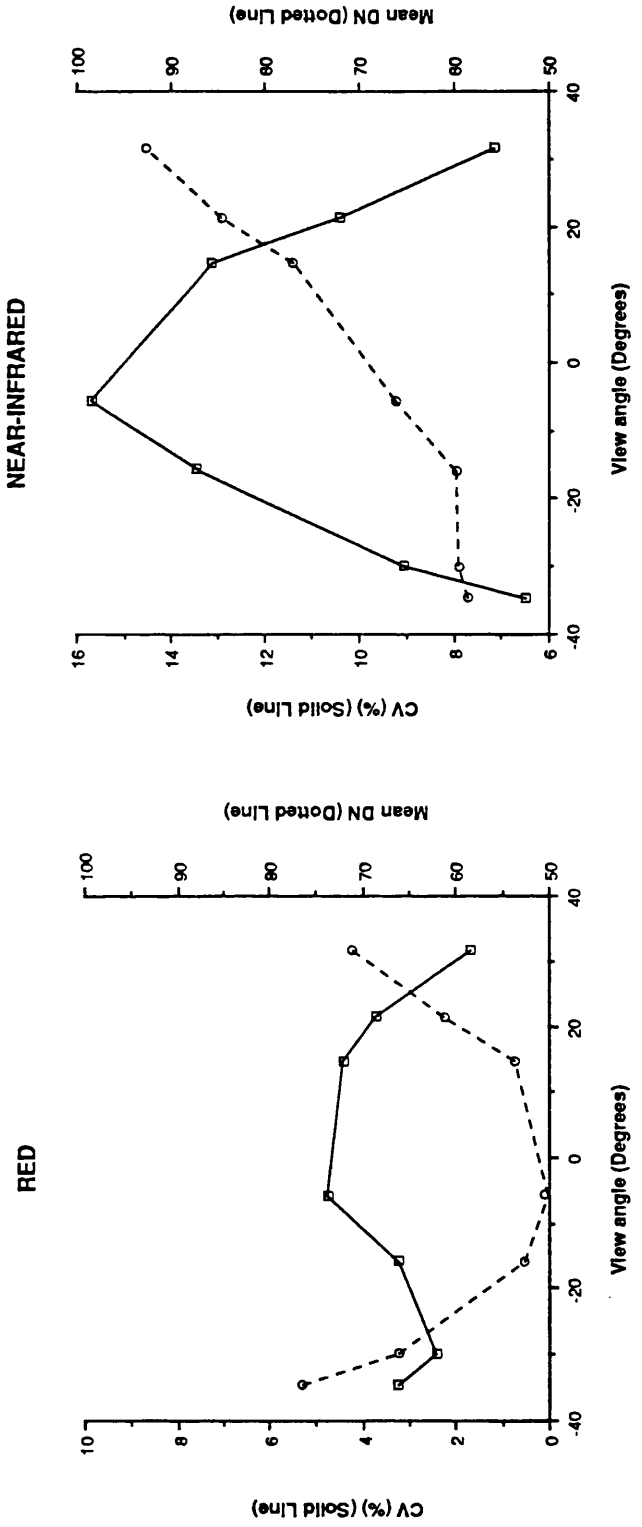


Figure 3.9: Variation of mean and CV with view angle for an apple orchard, for ATM bands 5 (red) and 7 (NIR).

Figure 3.9 shows the variation of mean DN and coefficient of variation for one sample area at a number of sensor view angles (from Barnsley and Kay, 1989). A noticeable decrease in image variance[7] occurs towards the edge of the swath. This results both from an increase in the area of the GRE and from the increased overlap between adjacent GRE's in the along and across track directions. In addition, at oblique view angles, the understorey becomes obscured, and thus reduces the range of scene elements detected.

This brief examination shows that sensor view angle has an effect not only upon the absolute value of the radiance detected by the sensor (Barnsley, 1984a and b), but also on the variability of the detected response. This results from three interacting (geometric) factors (Barnsley and Kay, 1989):

- An increase in area of the GRE towards the edges of the image.

- The consequent increased over-sampling between adjacent IFOV's with increasing view angle.

- For tall, spatially heterogenous cover types, a decreased proportion of understorey/soil will be viewed by the sensor at off-nadir angles, and therefore the spatial variability of the detected radiance will also decrease.

First-order correction algorithms designed to normalise image radiance to the nadir value do not take account of these effects (Morris and Barnsley, 1989). By implication, even where such corrections are applied, image data processing such as multispectral classification algorithms and vegetation indices will be affected by the position in the image of the target or land cover parcel. Attempts to extract information about the canopy geometry from multiple view angle imagery (Gerstl and Simmer, 1986) will need to isolate the effects of sensor geometry from those of the canopy (Barnsley and Kay, 1989).

---

[7] *cf.* sec. 5.1 for definitions and techniques for measuring image variance.

Figure 3.10: Overlay of digitised field boundaries on a false colour subscene of the study site (bands 7/red, 5/green and 4/blue). Mean error of fit of transformed boundaries was <10m.

A further important factor, when considering the effect of view angle upon image variance, is the scale of the discontinuities in the cover compared with their distribution and the size of the GRE (Strahler *et al.*, 1986). The exact relationship between sensor geometry and image variance is strongly dependent upon the interaction between the spatial variability of the surface under investigation and the spatial resolution of the sensor (Barnsley and Kay, 1989).

## 3.6: Geometric corrections and terrain distortion

The airborne data used in this study were difficult to geocode, mainly because non-parametric solutions had to be used. Geometric accuracy with airborne data is notoriously poor, and thus integration with DTM data, derived from 1:50,000 maps, proved to be of only moderate quality (figure 3.10). Also the resolution of the data (5m) was higher than that of the DTM (20m), since this was the highest resolution that could be justifiably generated from the digital contour data (10m contour interval). This means that the true variations in the terrain would not be modelled precisely enough for either parametric corrections for geometric distortions or the illumination algorithm described in chapter 4.

The ATM data required geocoding before research into radiometric modelling was able to take place. This rectification could have been attempted in several ways, although the problems inherent in airborne data probably prohibit any single method from being entirely successful. This is because airborne data have all the usual characteristics of geometric distortion that satellite imagery has, such as produced by pitch, roll, yaw, variations in altitude, relief displacements, velocity variations, side slip etc, at a considerable high rate of change and sometimes seemingly unpredictable frequency (for example when flying through turbulent air).

### 3.6.1: Magnitude of relief displacement

With nominally vertical-imaging satellite data (such as Landsat MSS and TM), relief displacement is not normally considered to be a significant problem because

the off-nadir view angles are small, the platform altitude high, and spatial resolution low (compared to relief displacement in the imagery) (Welch *et al.*, 1985, Bryant *et al.*, 1985, and others). However, the following expression helps illustrate two important relationships:

$$\delta r = \frac{r.h}{H} \qquad \text{Eq. 3.7}$$

Where $\delta r$ is the image displacement due to relief, r is the radial distance of the pixel from the nadir point, h the height of the Earth's surface above a datum, and H the altitude of the sensor above that same datum (Dowman, 1985, Kay, 1988).This shows that relief displacement is inversely proportional to sensor altitude, and directly proportional to magnitude of relief and position in the image (which, for many sensors, equates to view angle). For example, given a flying height of 2000m, relief of 100m and a position in the image 1000m from the nadir point/ground track, relief displacement would be of the order of 50m, or 12 pixels in the case of the data used in this study. At the edge of the image this figure would become 75m.

### 3.6.2: Parametric techniques

At first consideration, a parametric solution to the problem of geometric distortion would seem the most sensible approach (Kay, 1987, 1988), since complex polynomials (the alternative, non-parametric strategy) would be required to describe the geometric corrections. This modelling technique, however, is prohibited by three factors, (a) the mirror scan mechanism, (b) system corrections introduced by the instrument gyro, which delays or advances sampling (to preserve nominal nadir centre image position while the aircraft rolls up to ±6°), (c) across track sampling adjustments which preserve a standard pixel size on the image, such as the S-bend system correction.

Aerial photography, acquired simultaneous to the digital imagery could be used in a number of ways to assist geometric correction. Since, however, Daedalus makes

system corrections for roll that cannot be removed, the two datasets are essentially being collected in a different reference system. Also, since the periodicity of distortions (i.e. roll etc) is small and of unpredictable length and amplitude, the photo data may be a poorer source of control than the digital imagery, since it is relatively infrequent (one photo every 8-10 seconds). This precludes the use of the photography in a direct parametric solution of the orientation and resection of the digital image data to extract parameters of the instantaneous sensor position and attitude.

A second, indirect, use of the photography has been suggested by Muller *et al.* (*pers. comm.*, 1988) which uses the imagery to match and resample each pixel in the digital data with the (digitized) aerial photographs. Since the aerial photography is simple to model parametrically, a complete parametric model can be devised describing the correct geometric position for each point on the photograph; matching features on the image to the photographs, therefore, allows geocoding of the ATM imagery. However, this solution was still under development and therefore was not able to be used in this study.

### 3.6.3: Non-parametric transformations

For the reasons outlined above, non-parametric transformations become more appropriate to geometric correction in this study. Only affine and polynomial transformations, however, can provide the degree of accuracy required with such complicated geometric distortions (Dowman, 1985). Second-order polynomial transformations will correct first-order[8] and second-order[9] distortions. The only practicable method available in this study was to use the "WARP" algorithm on the I²S. This uses either method, depending upon the number of available control points. In this study, a data set of 90 control points was digitised from OS 1:10,000 map sheets, and used to rubber-sheet the DTM images to the ATM data.

---

[8]Scale differences in along and across track directions, non-orthogonality, rotation and translation (Dowman, 1985)

[9]Tilt, sub-platform track curvature, scan line convergence, some attitude variations of platform (Dowman, 1985).

Usually, between 20 and 30 control points were used, and average standard errors of less than pixel achieved.

The ATM image data have not been resampled; instead, the DTM image data have been transformed to fit to the ATM data. There are two main reasons for this. First, ten bands of image data exist for each DTM that has been processed (see chapter 4), so there are one tenth the number of images to transform this way. Although the problem of sampling strategy applies equally to both, with respect to corrupting the DN values in each of the data sets, the DTM image data are synthesised anyhow, and resampling is of less significance than for the original radiance values from the ATM data. The warp was carried out using the VAX CPU, rather than the I²S hardware, since the latter also introduced dropouts (with DN of zero). Unavoidably, this increased processing times, so the nearest neighbour resampling algorithm (Lillesand and Kiefer, 1979) was employed, since this provided the fastest means of generating the transformed images.

## 3.7: Radiometric calibration of the ATM data

Each channel on the scanner has an individual gain setting and calibration coefficient in order to utilise fully the 0-255 DN intensity range. However, band-to-band comparisons, ratios, or even classifications based on raw data can be misleading or absolutely incorrect, and in any case radiance image data must be used for the purposes of constructing reflectance images (see chapter 4). For this reason, calibration to equivalent units of radiance between bands is essential, and for multitemporal or multiple view imagery data sets, between image calibration is necessary (Wilson, 1986).

### 3.7.1: Method and data requirements

In the scanner, twelve analogue video inputs are digitized to 8-bit accuracy and recorded-on board on high density digital tape (HDDT). The twelfth channel is a result of the thermal infrared channel (11) being recorded twice with different gain

settings and band widths; these thermal bands are not considered in this study. Each channel has a gain switch of 0.5, 1, 2, 4 or 8 to that channel. The gain selection is made by the operator prior to the scanning flight on board the aircraft, and chosen to prevent saturation or under-exposure of sensor and to utilise fully the dynamic range of the DN. These gain settings, as well as the calibration data made on a test bench before and after each campaign, are essential to the construction of reflectance maps and the correct interpretation and use of band combinations (Wilson, 1986), for example vegetation indices, multispectral classification, and removal of topographic and atmospheric effects (Crippen, 1988, Holben and Justice, 1981).

**Table 3.7: Sensor calibration figures, 19/4/88**

| setting | .5 | | 1 | | 2 | | 4 | | 8 | |
|---|---|---|---|---|---|---|---|---|---|---|
| band | gain | base | g | b | g | b | g | b | g | b |
| 1 | 5.33 | 0.83 | 2.66 | 1.86 | 1.43 | 3.90 | 0.72 | 8.13 | **0.38** | **17.22** |
| 2 | 3.78 | 1.66 | 1.89 | 3.71 | 0.95 | 7.68 | **0.48** | **15.74** | 0.24 | 31.74 |
| 3 | 4.41 | 2.50 | 2.20 | 4.99 | 1.11 | 9.86 | **0.56** | **19.58** | 0.28 | 39.23 |
| 4 | 8.02 | 1.66 | 4.04 | 3.84 | 2.04 | 8.06 | 1.03 | 16.45 | **0.52** | **33.41** |
| 5 | 4.10 | 1.86 | 2.02 | 4.35 | 1.02 | 9.28 | **0.51** | **18.94** | 0.26 | 38.34 |
| 6 | 4.36 | 2.62 | 2.15 | 5.06 | **1.08** | **9.79** | 0.54 | 19.14 | 0.27 | 38.08 |
| 7 | 2.40 | 2.37 | **1.19** | **5.06** | 0.60 | 10.18 | 0.30 | 20.48 | | 41.22 |
| 8 | 3.39 | 2.05 | 1.68 | 4.48 | **0.84** | **9.28** | 0.42 | 18.88 | | 38.08 |
| 9 | 0.87 | 2.05 | 0.43 | 4.03 | 0.22 | 7.81 | **0.11** | **15.36** | | 30.59 |
| 10 | 0.21 | 2.62 | 0.11 | 5.12 | 0.05 | 9.98 | | **19.78** | | 39.36 |

Note: not all of these figures are available as the sensor was saturated at higher illuminations in certain bands.

### 3.7.2: Image processing

The algorithm to convert the NERC Daedalus ATM image data from raw DN to units of radiance outlined by Wilson (1986) is implemented locally on the I²S, where the only inputs required are the base and gain values, calculated from bench calibration tests, made before and after the campaign. The individual channel and gain setting values were calculated using the formulae listed by Wilson (1986), and used as input parameters to the I²S. These are listed in table 3.7 above; the values

in bold refer to those used for this dataset (gain settings were constant for each band on each flight line). Missing values exist because not all gains are calculated on the bench. One of the major problems is that, given the radiometric resolution of the sensor and the reflectance properties of the terrain, conversion to radiance units with this data set always resulted in a reduction in dynamic range, and a consequent loss in information caused by the quantisation effects of the $I^2S$ (sec. 4.4).

## 3.8: Summary and conclusions

By deriving the geometry of the ATM scanner used in this study, we have shown that multiple view angle data give rise to a series of effects which may be a cause of the complex radiative transfer interactions of the plant canopy and radiant flux. Standard image pre-processing has been carried out to prepare the image data for further analyses, also carried out in chapters 4 and 5, of these view angle effects. In chapter 4, the importance of using data which has been geometrically and radiometrically corrected to a high standard, is emphasised. In these later sections, reference back to the original ground data and the geometric characteristics of the sensor, both detailed in this chapter, will be made.

# CHAPTER 4: The use of reflectance images to process and correct ATM image data

## 4.1: Introduction to method

Modelling directional reflectance of Earth surface materials is, by implication, a complicated task. Terrestrial cover types are diverse, often spatially heterogenous at common scales of remote sensor instrument resolution, and have varying degrees of reflectance anisotropy, even for individual species or varieties. These characteristics may depend upon the organisation, development and arrangement of the cover in its environment.For example, arable crops have certain row spacing, orientation and growth stage for a given date, dependent upon the climate, soils and management strategy of the farmer.

There are perhaps then as many descriptions of directional reflectance as there are identifiable cover types; and this is the main problem with modelling such a phenomenon. The use of non-parametric techniques, where the behaviour of *all* cover types is used to describe an approximation of reflectance anisotropy for the whole image, is inappropriate when consideration of the directional reflectance characteristics of individual cover types is required. It is probable that the response (reflectance, radiance value etc.) of all cover types within the image will be modelled badly, since no one model could really be regarded as behaving in a 'mean' or average way, unless the image genuinely consists of one homogenous cover[1]. Similarly, crude models applying a theoretical description of (an)isotropy, such as diffuse (Lambertian) or specular models or even a combination of the two, will fail for the same reason. Canopy reflectance anisotropy is a problem too dependent upon specific cover type characteristics for general image descriptions to be effective.

---

[1]Although this technique could be adapted to account for specific segments within an image; the segmentation could be generated from other data (map data, GIS environments etc.). Even so, it demands a comprehensive multiple view angle data set if polynomial fitting is to be applied.

Parametric methods already exist for the correction of image data for atmospheric, sky radiance, topographic and view angle or canopy effects. The major limitation of these methods, however, is that the models can demand complex input data to determine the necessary correction. For the first three types of model, listed above, these data could be collected from a variety of sources, including field measurements, such as with an Automatic Weather Station (AWS) to measure irradiance at a point source, or computed data, output from a sky radiance model, or digital terrain data. Plant canopy models, however, demand less tangible information. These data are often cover type specific, for example leaf orientation and inclination distributions of a plant species or variety, and also vary both spatially and temporally, demanding parcels of homogeneous species, variety and development. Fortunately, some of these conditions are closely approximated in some forms of agriculture.

These specific requirements, of being able to describe in some detail the characteristics of a canopy for modelling purposes, have usually necessitated the undertaking of a considerable quantity of field work. The major problem is that this ground sampling must include and describe all cover types of interest that are to be examined in the image, since each parcel in the image demands an accurate description of the parameters required to model it; that is, it is important to know not only what the cover type is at a specific location in the image, but also the model parameters relating to that cover type. This is a difficult and time consuming task for areas where there are organised parcels of homogenous cover (farmland) and virtually impossible where cover types are basically complex, mixed, or highly spatially variable (natural/semi-natural rangelands). In this latter case, the image would have to be modelled on a per-pixel basis, and thus the ground sampling strategy would also have to cover each pixel on the ground. Strategies which apply general, non-parametric, models can never work in this circumstance because there is no systematic organisation of cover types in the

image[2]. This demand for ground data would negate the use of remote sensing instruments for this application using such a strategy.

It is desirable, therefore, to develop a strategy that overcomes this problem of excessive fieldwork; one that derives input data for the models remotely, preferably using the same sensor as by which the radiometric data is collected. To achieve this, two modifications must be made to the conventional method. First, a strategy for the collection of the input data must be devised, identifying what data can be collected feasibly, given current instrumentation and analysis facilities. Second, the models must be adapted and simplified to allow modest data inputs, compatible with realistic data collection strategies. These ideas are developed later in this thesis, in chapter 5 and 6.

It is evident that the data input to the new generation of invertible canopy models must not be dependent upon view angle, since it this effect that we are most interested in being able to overcome. Ideally we need to devise a strategy that circumvents the effects of view angle, for example on mean detected radiance. The strategy chosen in this study requires that a multi-angle dataset is available, since it is by using this extra dimension of data collection that the input data are to be generated.

The geometric properties of images, as regards the statistical description of cover types[3], allow the evaluation of a limited description of canopy parameters, as will be demonstrated further in chapter 5. The ATM sensor has significant artifacts within the image that are related to view angle, sensor geometry, and canopy parameters (Barnsley and Kay, 1989), and independent of atmospheric (in longer wavelengths), topographic and some, but not all, solar/target geometry effects.

---

[2]For example Jones *et al.* (1988), where the application of models was discussed and conclusions highlighting the paradox of requiring detailed data raised. However, it is obvious that in non-segmented datasets it would be extremely difficult to apply parametric models, because of the impossibility of identifying which model and what parameters should be applied to each parcel in the image - unless this information is acquired by another means.

[3]For example, examination and modelling of spatial variance by Li and Strahler (1985, 1986).

However, these latter effects can often be eliminated or modelled independently (for example row effects), since they can be identified in the imagery.

This chapter then, will illustrate, with examples from previous studies as well as this one, the response of a particular selection of cover types to view angle, and identify possible paths for the extraction of canopy information from geometric and statistical information in the imagery. It will then detail the method to remove other artifacts from the imagery, such as those due to differing topography and illumination, and explain the process by which reflectance maps can be used to analyse imagery for view angle effects. After assessing the performance of the topographic, atmospheric and illumination correction model, it will demonstrate that view angle artifacts are still dominant in the imagery and will identify the method by which canopy parameter extraction might proceed. Some of the preliminary results published in this chapter have been published previously in Kay (1989), Kay and Barnsley (1989) and Barnsley and Kay (1989).

### 4.1.1: Examples of change in detected vegetation canopy response with sensor view angle

Examples of vegetation canopy response have been acknowledged by remote sensing scientists for two decades. Salomonson and Marlatt (1971) examined the detected response of several cover types as a function of sensor view zenith angle, while Suits (1972a, Suits and Safir, 1972), in his early model of canopy reflectance, made particular reference to the change in reflectance with, among other parameters, view zenith and azimuth angles. Kimes (1984, 1987) examined directional reflectance of homogeneous coniferous woodland and, in this country, Barnsley (1984a and b) made a further detailed examination of detected spectral response of a variety of cover types with view angle. Foody (1988) summarises the results of these and other studies.

Data are presented here to illustrate the expected variation of detected radiance with view angle for a number of cover types, as derived from two airborne campaigns, both using a Daedalus ATM sensor. The effects of change in

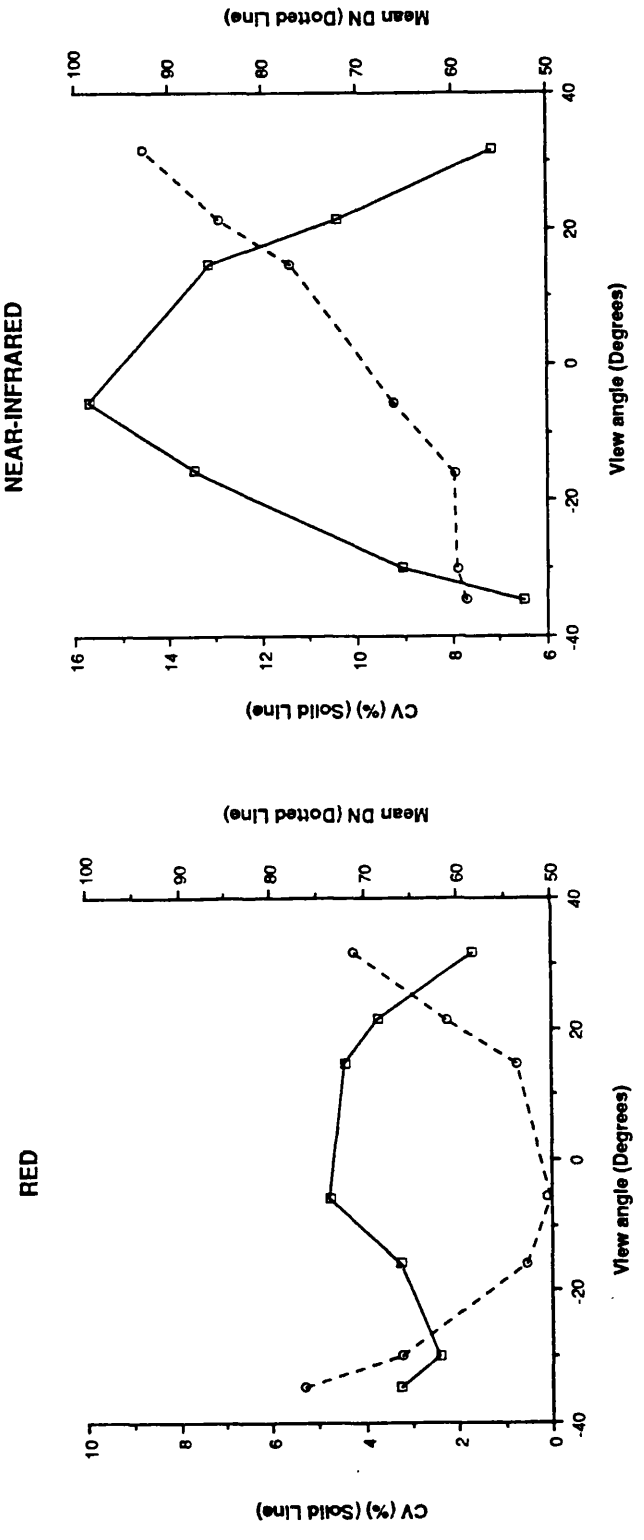


Figure 4.1: Variation of CV with view angle for an apple orchard, bands ATM 5 (red) and 7 (NIR). Solid lines CV, dotted lines mean DN. (From Barnsley and Kay, 1989)

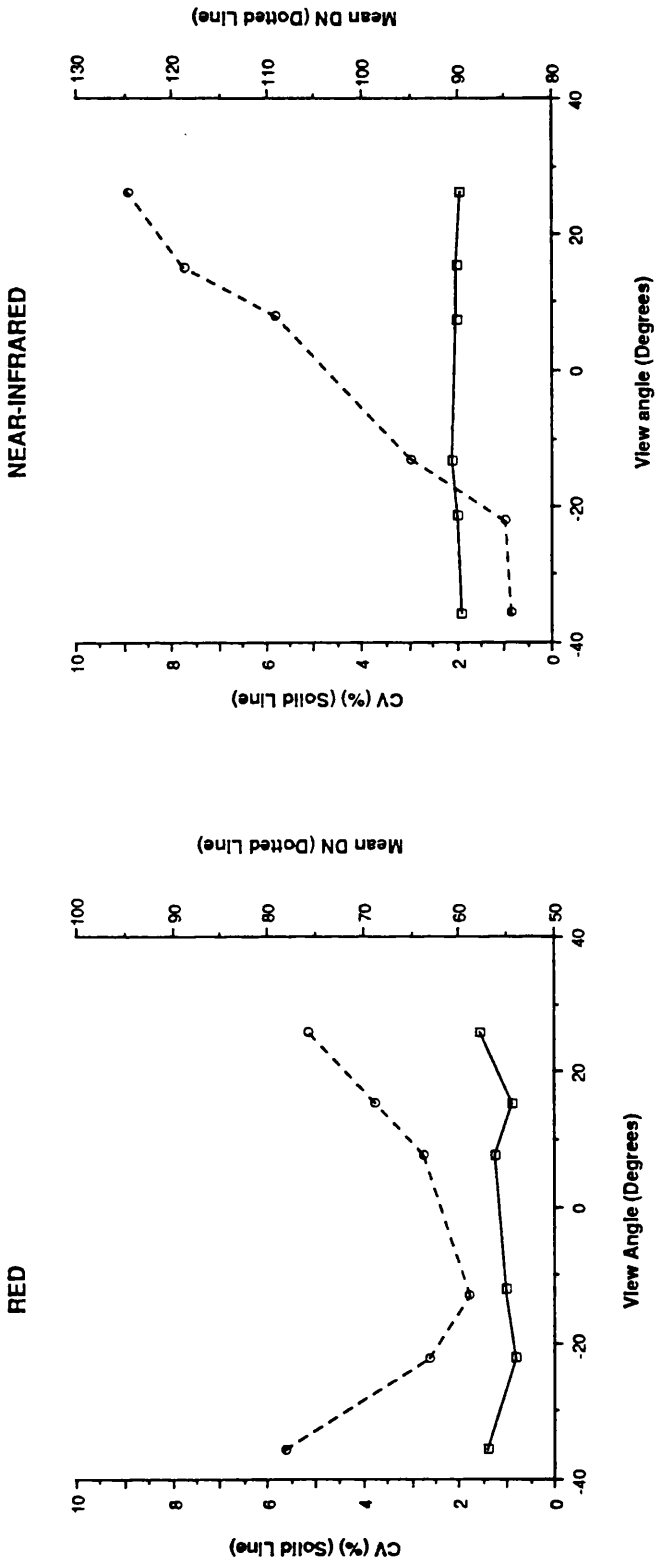


Figure 4.2: Variation of CV with view angle for a parcel of sugar beet, bands ATM 5 (red) and 7 (NIR). (From Barnsley and Kay, 1989)

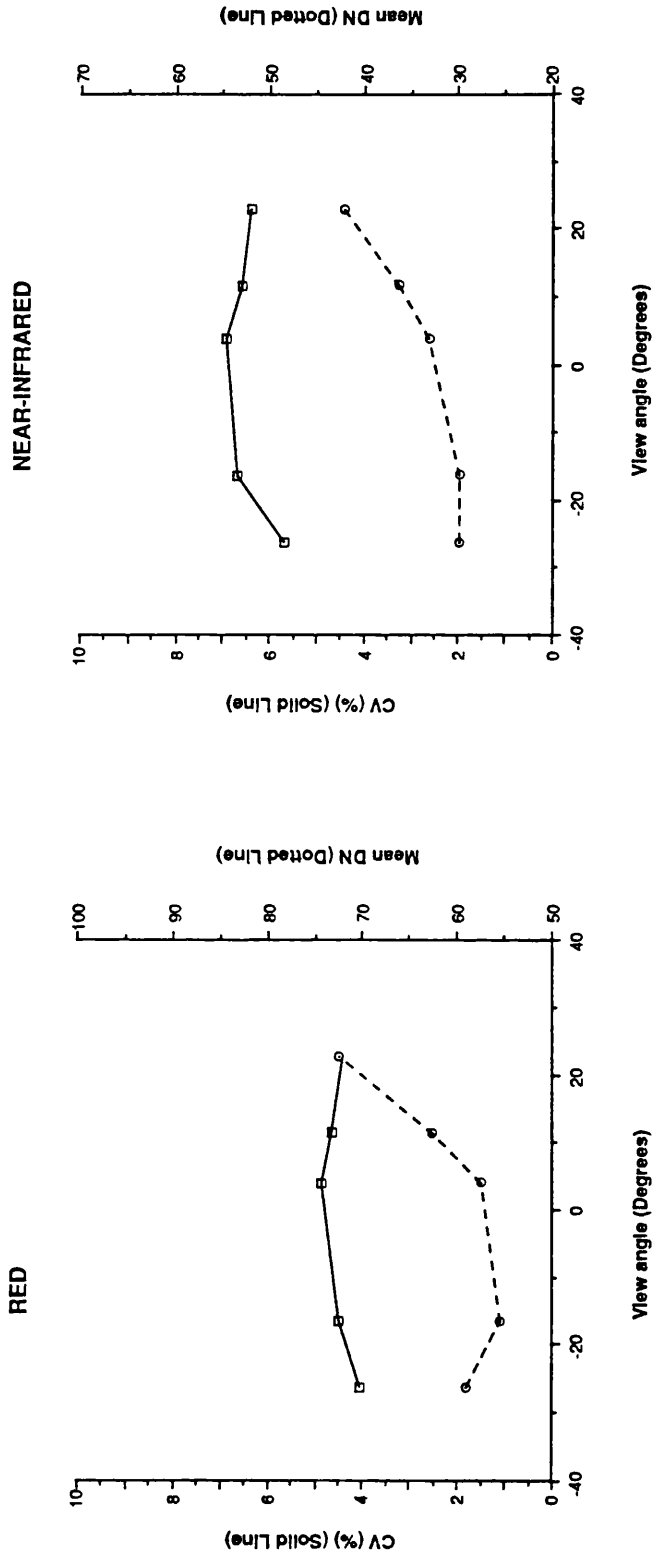


Figure 4.3: Variation of CV with view angle for a parcel of bare soil, bands ATM 5 (red) and 7 (NIR). (From Barnsley and Kay, 1989)

Coefficient of Variation (CV) are also illustrated, as are changes in measures of spatial autocorrelation (see 3.5, 5.1).

Figures 4.1 to 4.3 show the variance of Apple Orchard, sugar beet, and bare soil (Barnsley and Kay, 1989), for ATM bands 5 (red, 0.63-0.69μm) and 7 (NIR, 0.76-0.9μm) using data from a flat, fenland test site (Gedney Hill, Lincolnshire, *cf.* Barnsley, 1984a). The orchard consists of trees around 2.5m high and spaced at 10m intervals, with a mature grass understorey; the sugar beet is greater than 95% cover. Both the vegetative covers exhibit a similar response of detected radiance with view angle, a general increase in radiance with down-Sun view. Such a trend is typical of that found for green vegetation in the NIR, as will be apparent from the presentation of further results.

Of great interest to this study, however, is the variance of the DN in the parcels, when viewed from different angles. Variance of the datasets is represented here as the Coefficient of Variation (CV):

$$CV = 100(\text{Standard Deviation/mean}) \qquad \text{Equation 4.1}$$

and represents a normalised measure of image or parcel variance; hence it is not related to the magnitude of the mean. It can thus be used with equal relevance upon scaled data (DN), radiance data, and different wavebands, or for data acquired under differing irradiance - as is the case for multiple flightline datasets.

The orchard is mostly highly variable of the three cover types, as might be expected since the trees are not continuous in their cover. The sugar beet and bare soil cover types exhibit almost no change of CV with view angle. This contrast is extremely important, since it may allow the inference of canopy parameters at a qualitative level or even quantitatively. The change in CV due to view angle is a result of three interacting geometric effects (see sec. 3.5, Barnsley and Kay, 1989):

- An increase in the area of the GRE towards the edge of the image.

- The consequent increased over-sampling between adjacent IFOV's with increasing view angle.

- Changes in the proportions of different canopy elements visible to the sensor. This is particularly pronounced for tall, spatially heterogeneous cover types.

The first two effects are directly related to the sensor geometry, and are detailed for the Daedalus ATM sensor in Chapter 3. However, it is apparent from the results presented here that there must be variance within the scene for these effects to be manifest in the image at all; if there is little or no spatial variance in the cover, then there is nothing to be modulated by the geometry of the sensor. Hence we might expect the *degree* to which this modulation takes place to be an indicator of the spatial variance within a scene. For this reason, we will examine further the causes and mechanisms of spatial variance, and its co-existing concept of spatial autocorrelation, in greater detail in section 5.1.

It is also observed, in the case of bare soil (figure 4.3), that while a medium degree of variance is measured for the parcel as a whole (6-7% in the NIR), this variance does not change substantially with view angle. Note that the CV at off-nadir angles is the same as for the apple orchard in the NIR. The geometric effects of the sensor, increasing the area of the GRE and oversampling towards the edges of the swath **are the same for both datasets** - so the different trends observed **are due solely to the third effect**, that of the changing proportions of the canopy observed at off-nadir angles.

It is also important to note that the constant, significant level of variation in the soil parcel data implies that attenuation effects of the atmosphere are negligible at these longer wavelengths (in this dataset). Atmospheric attenuation would be expected to reduce image contrast at off-nadir view angles, due to an increased atmospheric path length, thereby reducing variance at the edges of the swath. This is observed, however, in only the shortest wavebands (ATM 1 and 2, see tables 5.3 to 5.11).

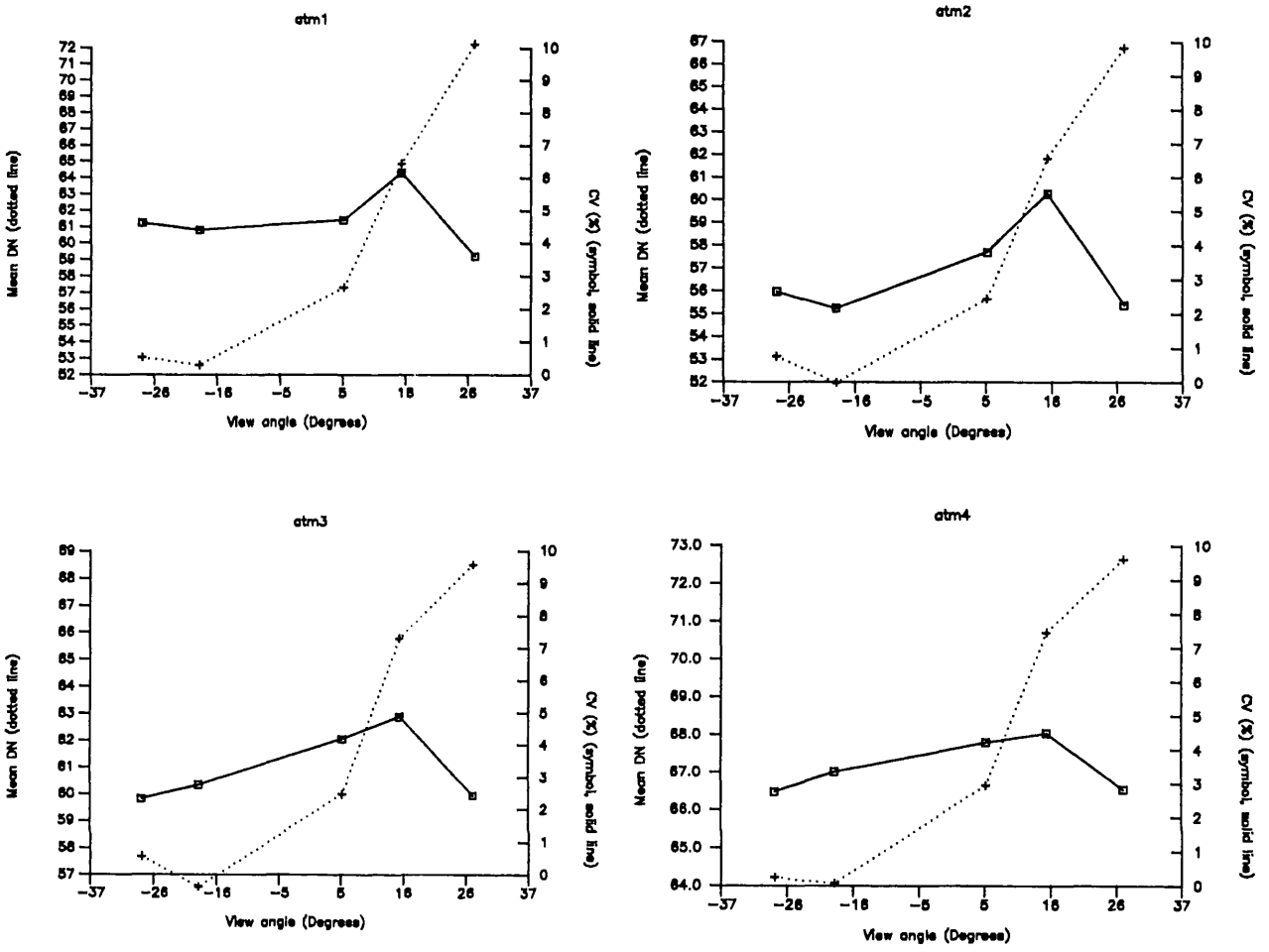


Figure 4.4: Variation of CV with view angle for field 29. Bands 1 to 4 are presented this page, 5-10 overleaf.

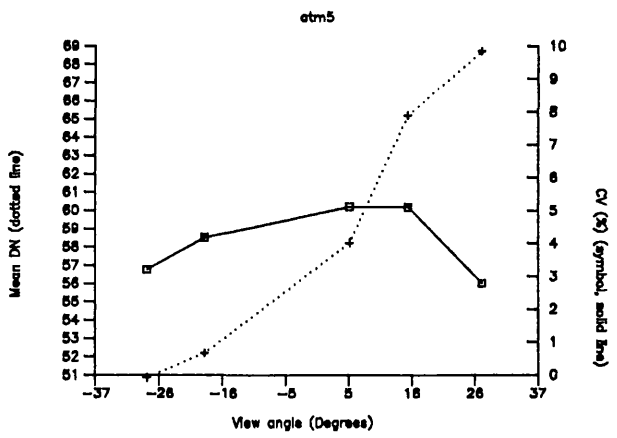
atm5
Mean DN (dotted line)
CV (%) (symbol, solid line)
View angle (Degrees)

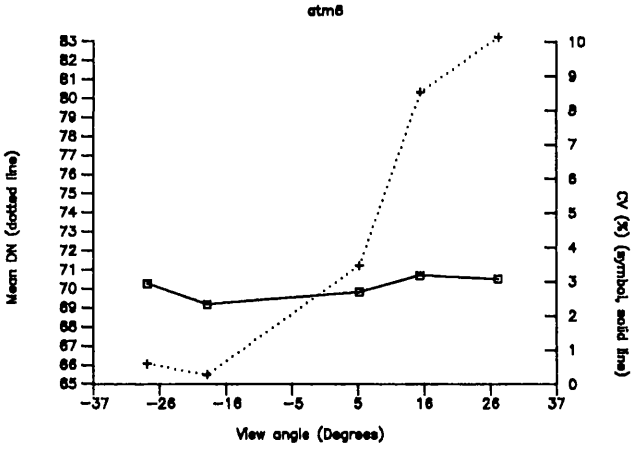
atm6
Mean DN (dotted line)
CV (%) (symbol, solid line)
View angle (Degrees)

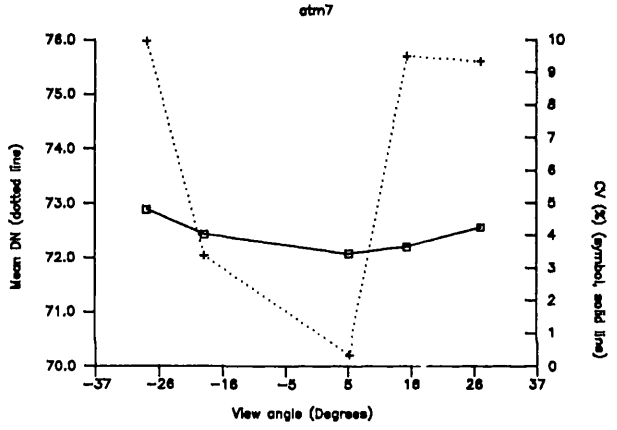
atm7
Mean DN (dotted line)
CV (%) (symbol, solid line)
View angle (Degrees)

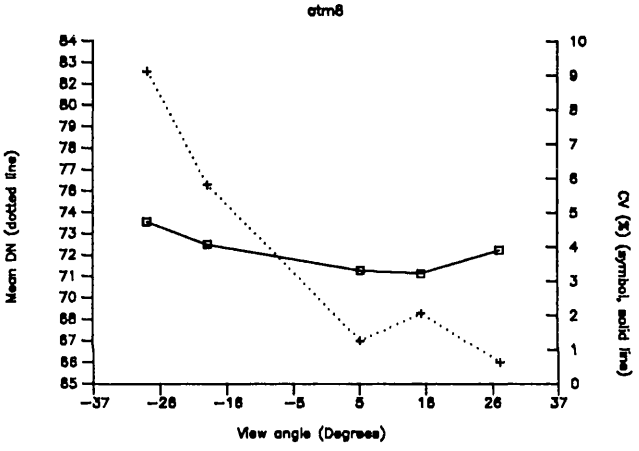
atm8
Mean DN (dotted line)
CV (%) (symbol, solid line)
View angle (Degrees)

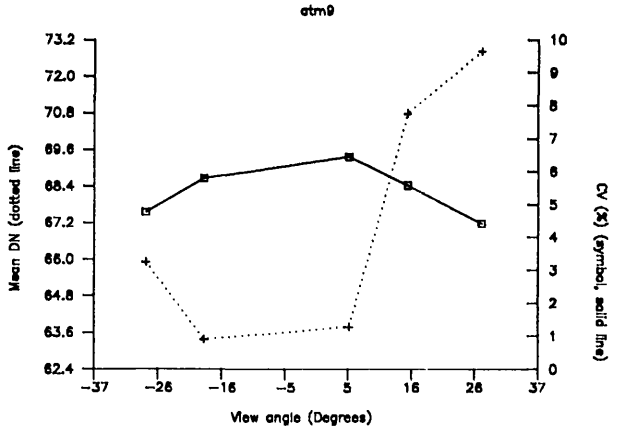
atm9
Mean DN (dotted line)
CV (%) (symbol, solid line)
View angle (Degrees)

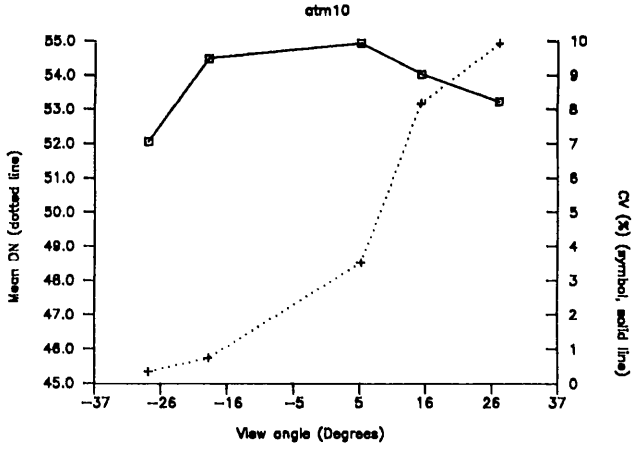
atm10
Mean DN (dotted line)
CV (%) (symbol, solid line)
View angle (Degrees)

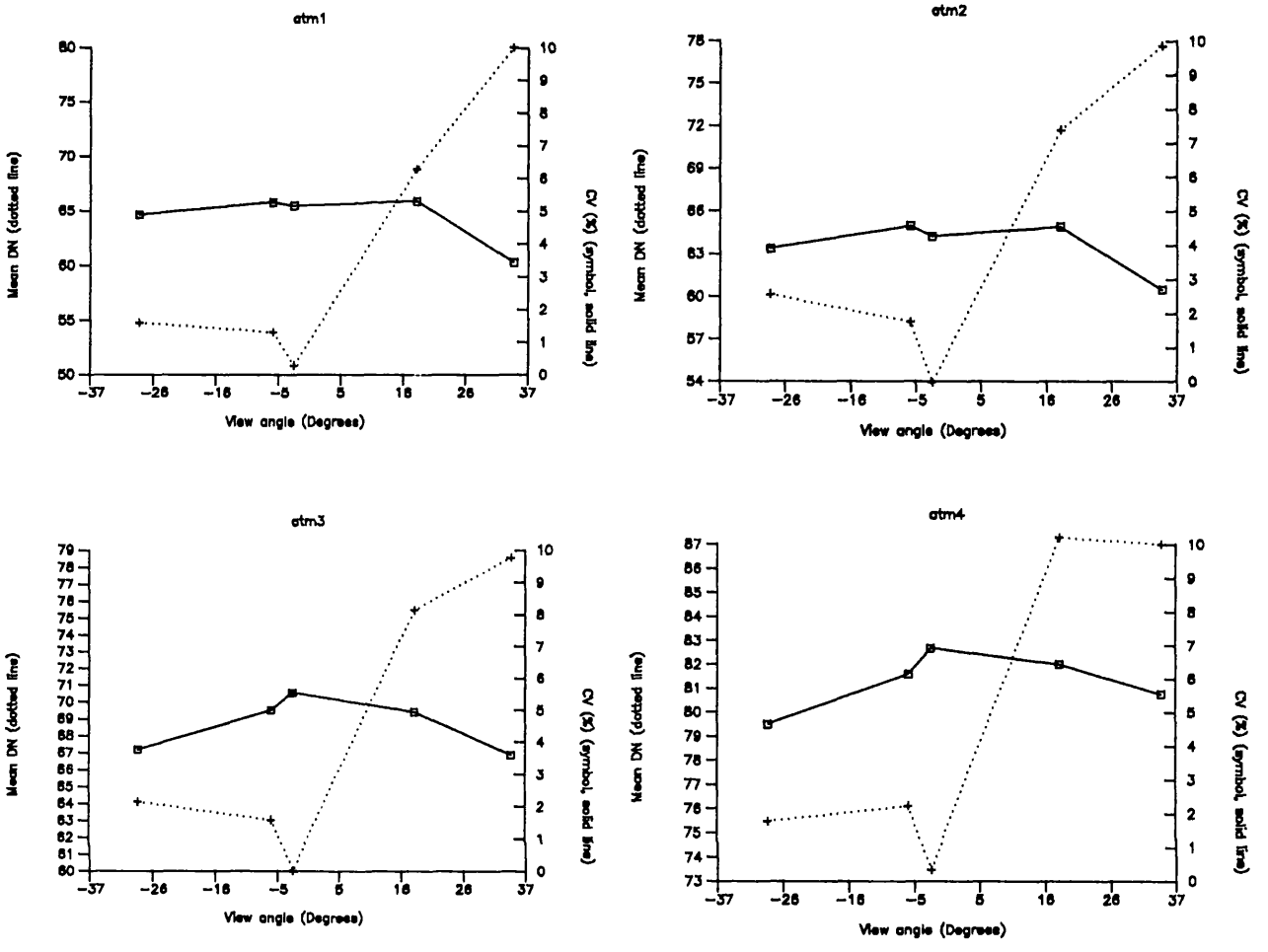


Figure 4.5: Variation of CV with view angle for field 21. Bands 1 to 4 are presented this page, 5-10 overleaf.

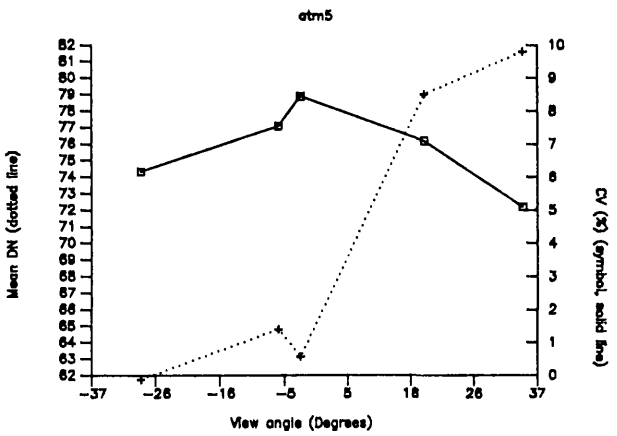
atm5
Mean DN (dotted line)
CV (%) (symbol, solid line)
View angle (Degrees)

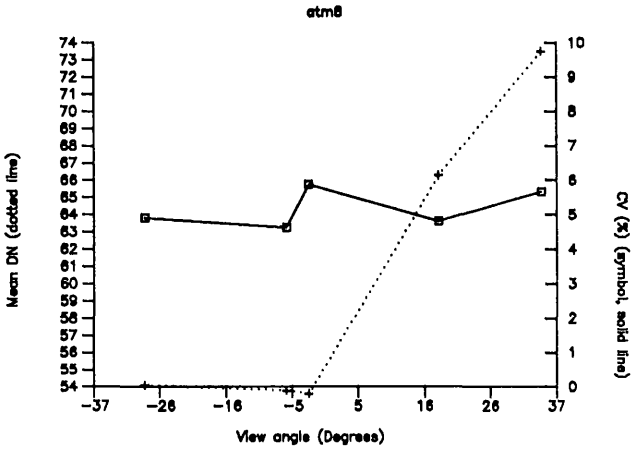
atm6
Mean DN (dotted line)
CV (%) (symbol, solid line)
View angle (Degrees)

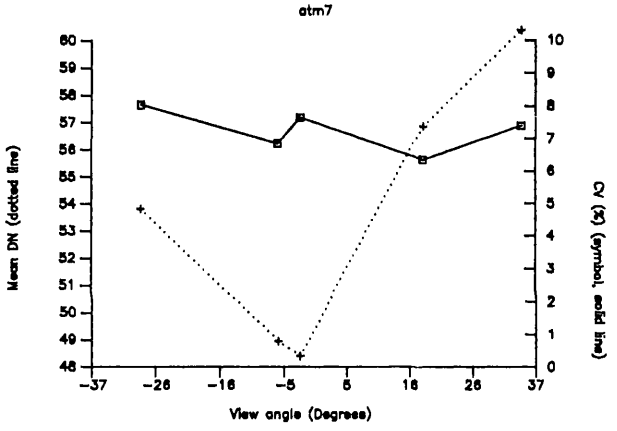
atm7
Mean DN (dotted line)
CV (%) (symbol, solid line)
View angle (Degrees)

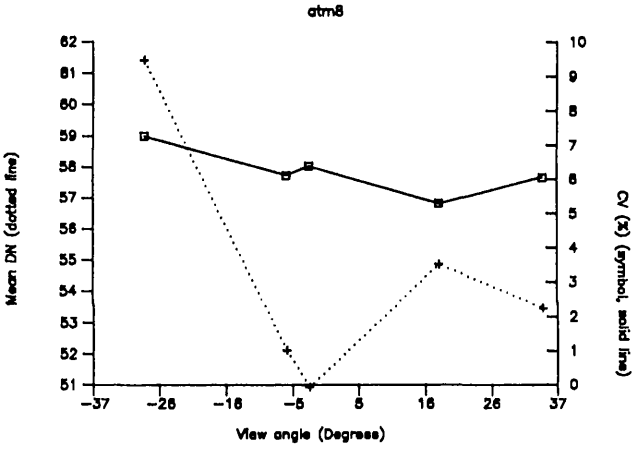
atm8
Mean DN (dotted line)
CV (%) (symbol, solid line)
View angle (Degrees)

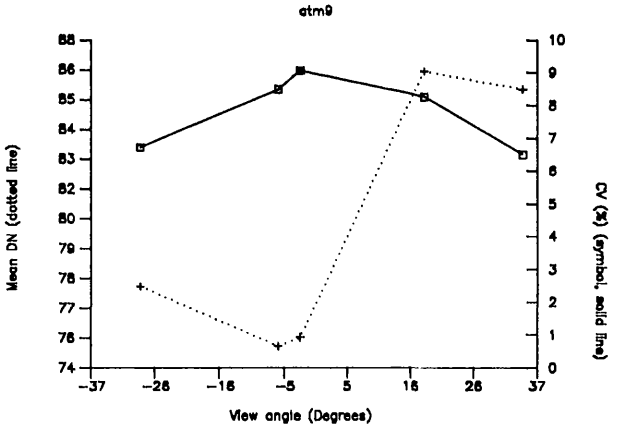
atm9
Mean DN (dotted line)
CV (%) (symbol, solid line)
View angle (Degrees)

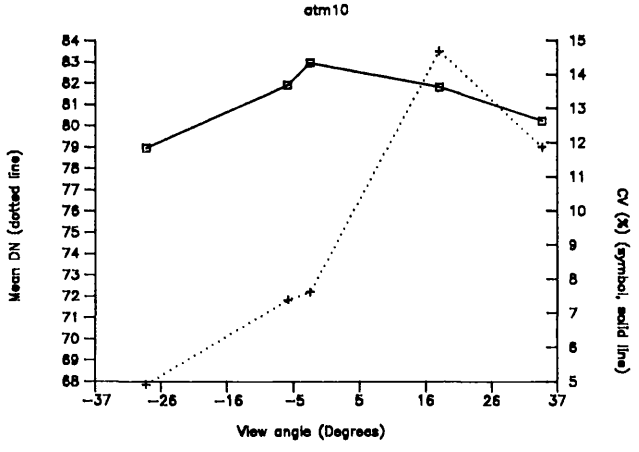
atm10
Mean DN (dotted line)
CV (%) (symbol, solid line)
View angle (Degrees)

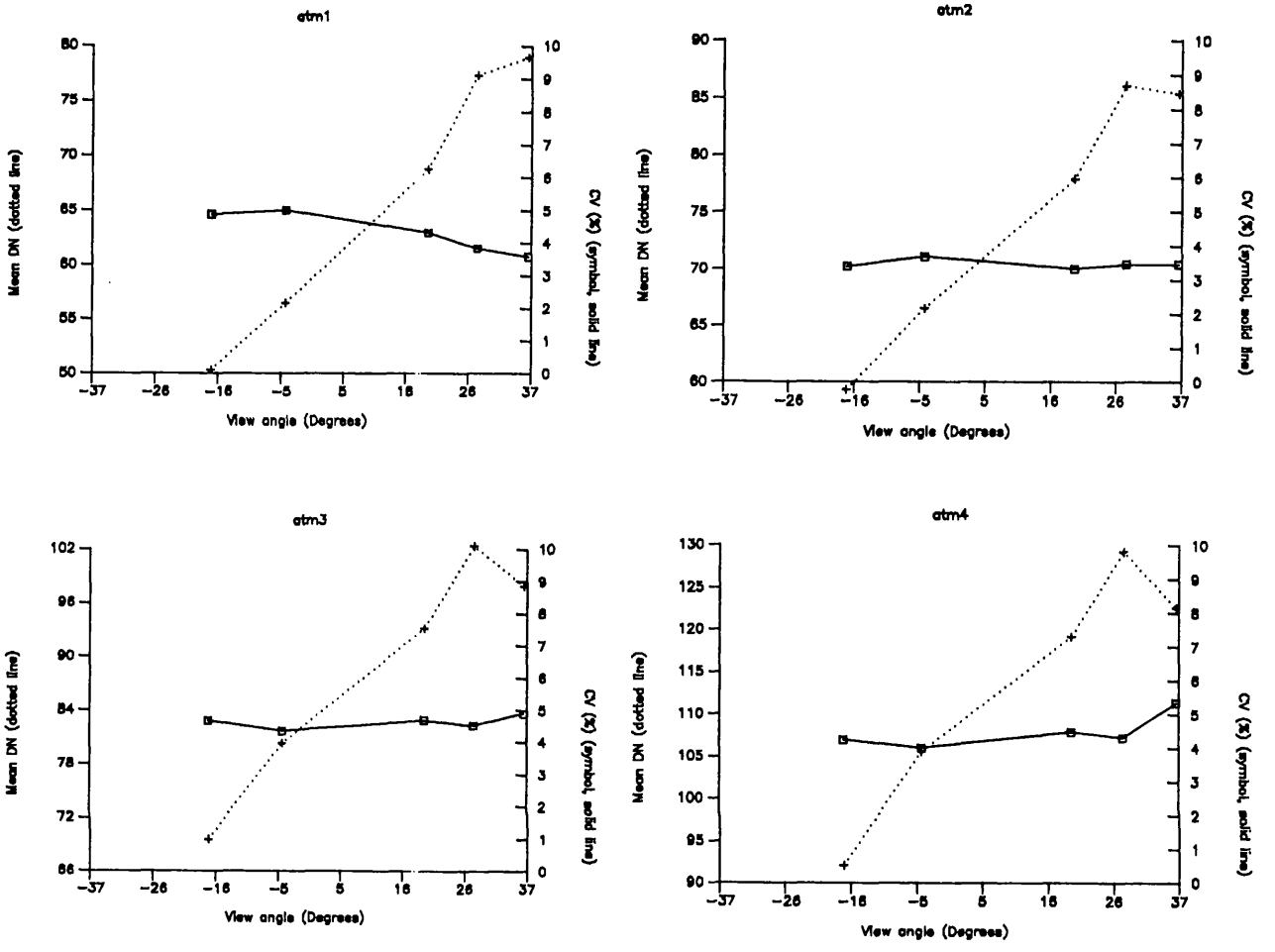


Figure 4.6: Variation of CV with view angle for field 30. Bands 1 to 4 are presented this page, 5-10 overleaf.

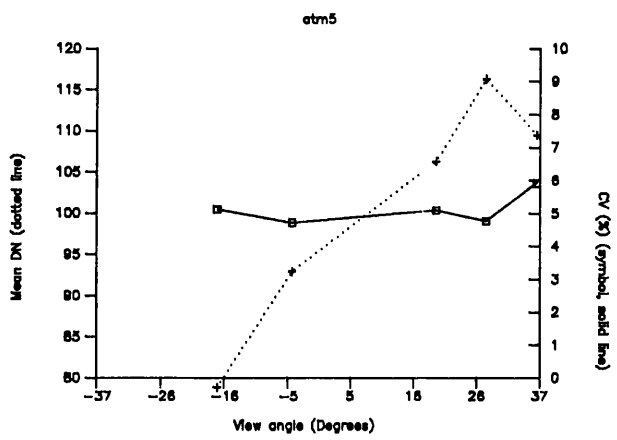
atm5
Mean DN (dotted line)
CV (%) (symbol, solid line)
View angle (Degrees)

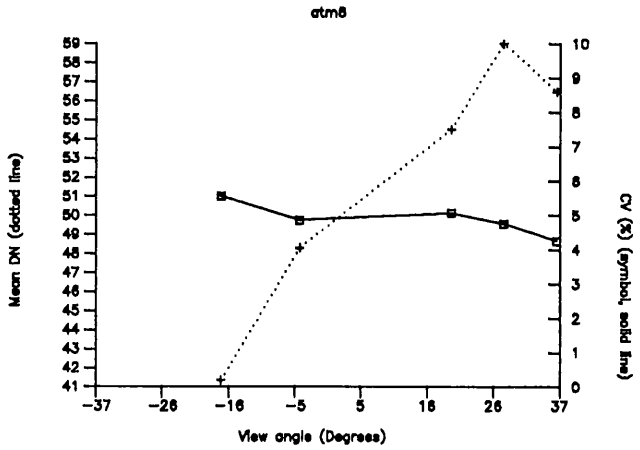
atm8
Mean DN (dotted line)
CV (%) (symbol, solid line)
View angle (Degrees)

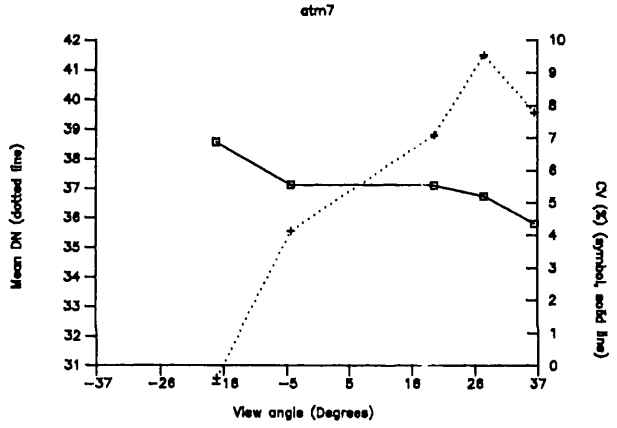
atm7
Mean DN (dotted line)
CV (%) (symbol, solid line)
View angle (Degrees)

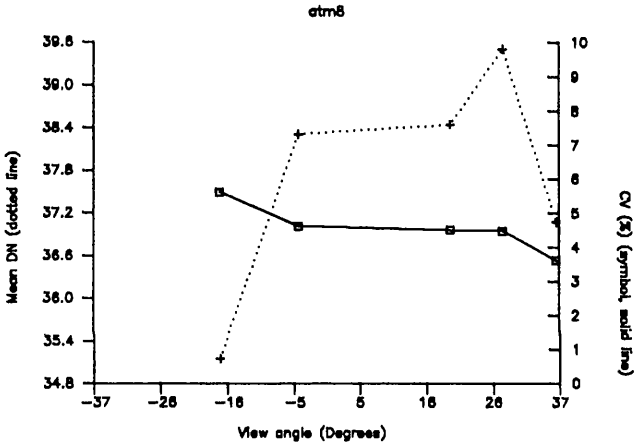
atm8
Mean DN (dotted line)
CV (%) (symbol, solid line)
View angle (Degrees)

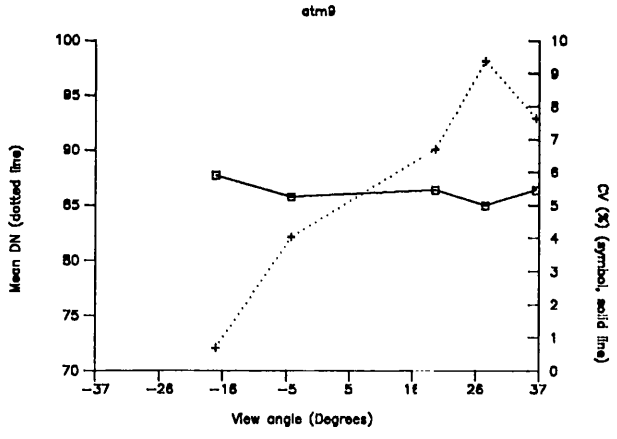
atm9
Mean DN (dotted line)
CV (%) (symbol, solid line)
View angle (Degrees)

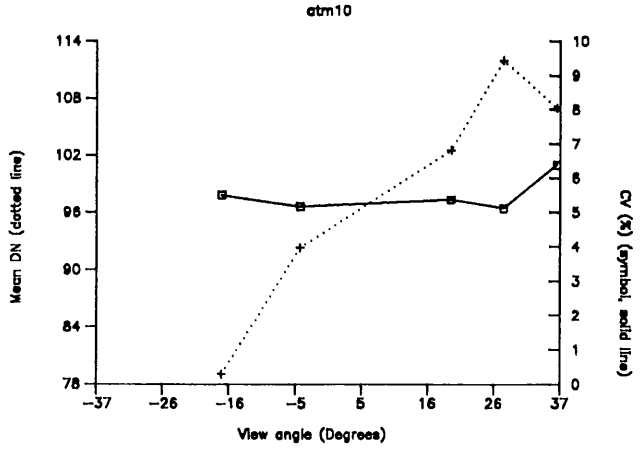
atm10
Mean DN (dotted line)
CV (%) (symbol, solid line)
View angle (Degrees)

Examples of the response of mean and CV of detected radiance for all ten bands used in this study, and for three cover types, are presented in figures 4.4 to 4.6. Field 29 (figure 4.4) (winter barley, 56% cover, growth stage 32 - see table 3.1) illustrates how the pattern of response can be broken down into three spectrums - visible bands, near infrared (NIR) and middle infrared (MIR). From a visual inspection, the shorter visible bands have a shallow curved response, with a weak relationship between view angle and CV. This response appears to become stronger in bands ATM 4 and 5, although the level of variation remains similar, between 3% and 5%. Band ATM 6, a transitional band between red and NIR, and the NIR bands ATM 7 and 8, show a second pattern, exhibiting even weaker view angle related responses, or in the case of bands ATM 7 and 8 and inverted response - CV increases with view angle. No explanation can yet be offered for this trend. Note the markedly changing mean response of the cover type in these bands. Finally, bands ATM 9 and 10 return to the expected response of view angle and CV, at a somewhat increased base level of variance.

Field 21 (winter wheat, table 3.1) illustrates similar view angle related trends of CV; again, it is convenient to classify the pattern of response into visible, NIR and MIR regions of the spectrum. Base levels of CV are in some cases higher than those recorded for field 29 (winter barley). These two fields represent, therefore, an intermediate level of response somewhere between the pattern observed for the apple orchard, bare soil and sugar beet parcels described above.

Finally, the response of a sparsely vegetated surface, field 30 (spring barley, 6% cover, growth stage 12, table 3.1), is presented. At the time of image acquisition this field was virtually bare soil, since the plants were at the tillering stage of development and very small. For this reason, response of both mean DN and CV is similar to that of the bare soil parcel above; no significant view angle related trend of CV is observed, in any of the bands. Fields 29 and 30 are included to allow comparison with the processed data at the end of this chapter.

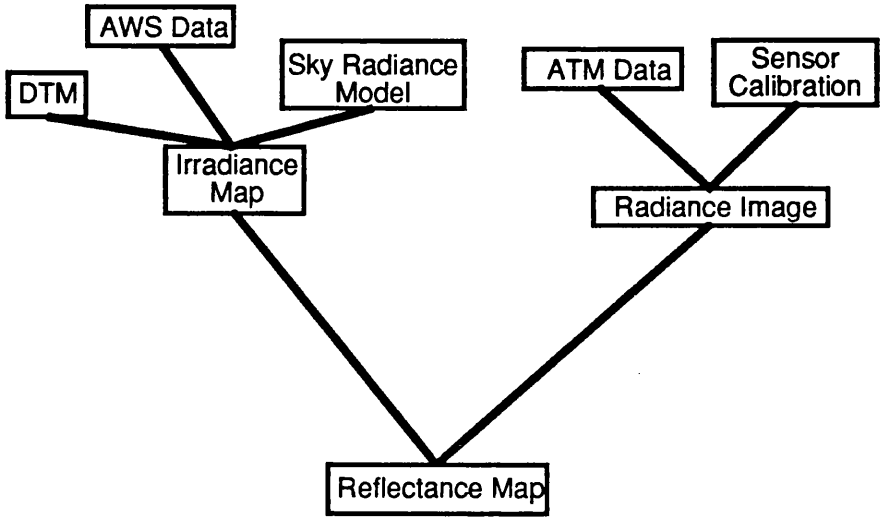


Figure 4.7: Reflectance image construction method. An irradiance map, or "potential radiance" image, was produced using measurements of sky radiance, a sky radiance model and the DTM. This was ratioed with the calibrated ATM radiance image to produce reflectance images.

## 4.2: Radiometric image corrections

### 4.2.1: Construction of reflectance images

The method used to correct the image data used in this study for illumination, topographic, sensor and sky radiance effects is most simply explained as the production of reflectance images, made by ratioing the "potential radiance" for a pixel in a synthesised image with the measured radiance value for the corresponding pixel in the ATM image (figures 4.7 and 4.8) (Kay, 1989). The standard procedure for the production of a reflectance image is to use simultaneous (or more likely contemporaneous) ground radiometer measurements to calculate reflectance for particular cover types within an image. This technique is limiting if many view angles are being considered, since this requires a similar range of ground measurements. Scales of variation of cover can also vary considerably between ground and airborne measurements, and this may affect the interpretation of the data. Large numbers of ground measurements may also be required to characterise reflectances for fields (Curran and Williamson, 1985, Atkinson, 1988).

In this study, irradiance data were recorded at a single ground location (using a pyranometer, see 3.2.1) and are combined with terrain model data to produce an irradiance image. A model of the angular distribution of sky radiance (4.2.3.1) has been used to improve upon the results obtained using a simple direct source illumination procedures. The resultant irradiance image, with the application of spectral sky radiance model (4.2.3.2), is used to produce an image of "potential radiance" for a specific bandwidth, in particular those of the ATM sensor. This procedure is carried out for each of the flightlines in the data set. These images express the maximum radiance that could be reflected in the direction of the sensor from each facet; they make no assumptions concerning the BRDF of the cover type. Hence the resulting reflectance images, produced by combining the "potential radiance" images with the remotely sensed data, contain the full compliment of reflectance anisotropy. However, because the effects of topography, solar zenith and azimuth angles, and sky radiance distributions have been

normalised between each flightline, the differences can be explained purely in terms of the canopy geometry.

### 4.2.2: Atmospheric corrections

Solar radiation detected at the Earth's surface is modified considerably by the atmosphere (section 2.3). Basically the atmospheric corrections are to adjust the detected radiance at the sensor for effects which occur between the exoatmospheric estimates of irradiance (derived from literature datasets), the target and the sensor. The main atmospheric problems come from the downward solar radiance being attenuated spectrally by an atmosphere (of unknown parameters), the upward target radiance being attenuated by the atmosphere of varying thickness, depending upon view angle, and the increased (asymmetric) backscatter at greater view angles. This first problem makes estimates of ground irradiance in discrete wavebands difficult to calculate, and the second two problems introduce errors into the image measurements of detected radiance.

The problem of modelling the effect of atmosphere on the flux between the target and the sensor is hard to quantify and resolve. Since the aircraft data are obtained at low altitude, the data could be considered to be only affected marginally by atmospheric attenuation. However, examination of the image data used in this study reveals that the major problem lies in the angular dependence of this attenuation, especially in the shorter wavebands. No method was developed to overcome this special problem in this study. Instead, the method used here relies upon the properties of the statistical test (CV) used, and the restriction of the data analysis to the longer wavebands (bands 5 to 10, red to infrared). While this may be a useful assumption here, it is acknowledged that this does not constitute a practicable method for general correction of all image data for this effect.

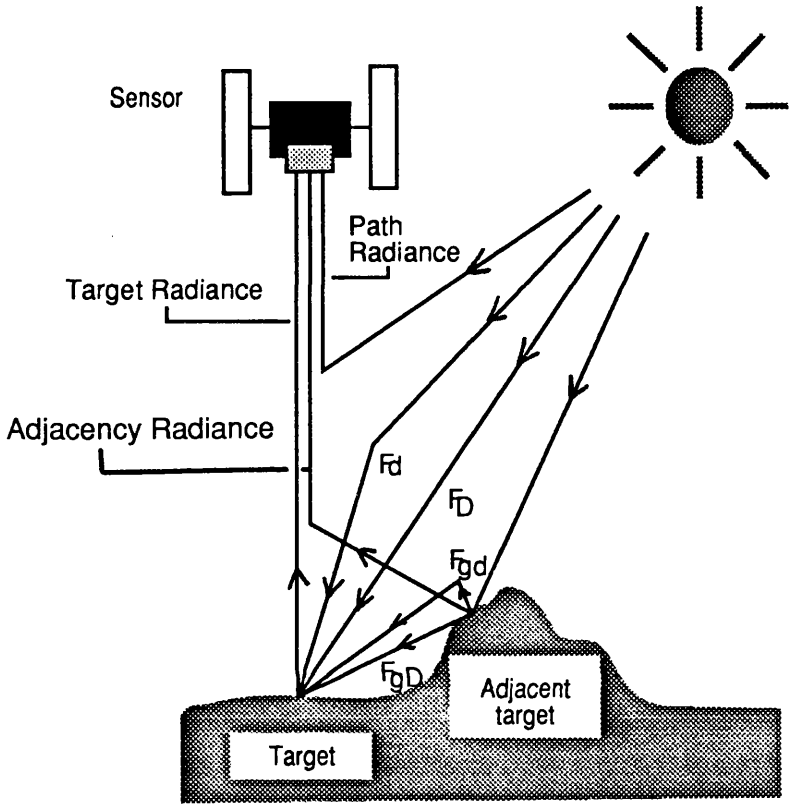


Figure 4.8: Component modelling of sky radiance - direct sky component $F_D$, diffuse sky component $F_d$, direct ground component $F_{gD}$, diffuse ground component $F_{gd}$. (After Woodham and Gray, 1987.)

### 4.2.3 Sky radiance corrections

#### 4.2.3.1: Spatial sky radiance distributions

The total flux of radiant energy (symbolised here as F) on a facet of ground is the simple addition of four components, direct radiation ($F_D$), diffuse sky radiation ($F_d$), the direct reflected ground component ($F_{gD}$), and a diffuse reflected ground component ($F_{gd}$) (figure 4.8 ) (adapted from Temps and Coulson, 1977, and Woodham and Gray, 1987).

$$F = F_D + F_d + F_{gD} + F_{gd} \qquad \text{Equation 4.2}$$

The significance of each component depends upon the state of the atmosphere, the terrain around each facet, and also the cover types associated with the neighbouring facets. Temps and Coulson (1977) estimate the importance of the diffuse sky element (in clear sky conditions) to be around 15% of the total irradiance; but this is a broad estimate, better estimates exist such as those given by McDowell (1974), Kondratyev (1969) and the 5S atmospheric modelling algorithm (*cf.* 4.3.1). The reflected ground component is recognised as influencing the anisotropic distribution of sky radiance, particularly near to the horizon, but contributes much less directly to the facet under consideration[4].

Precise modelling of the direct ground component ($F_{gD}$), given full terrain and local cover type characteristics, is extremely difficult for a number of reasons. First, an integration of the areas of all the terrain facets, and calculation of their relative orientations, that are visible from the GRE being modelled must be made. This is an extremely complicated and time-consuming task, even given the use of DTM data (Dozier and Frew, 1989). Second, the component cannot be calculated without the irradiance being modelled for each of these neighbouring components, so an iterative method is called for. Third, the implicit assumption is that the component is a reflected proportion of the total incident radiance, and that this proportion is computed by estimating the albedo of the surface (in Temps and Coulson's model).

---

[4]Temps and Coulson (1977), although this is not the opinion of Woodham (1989) or borne out by the model developed here - see 4.4

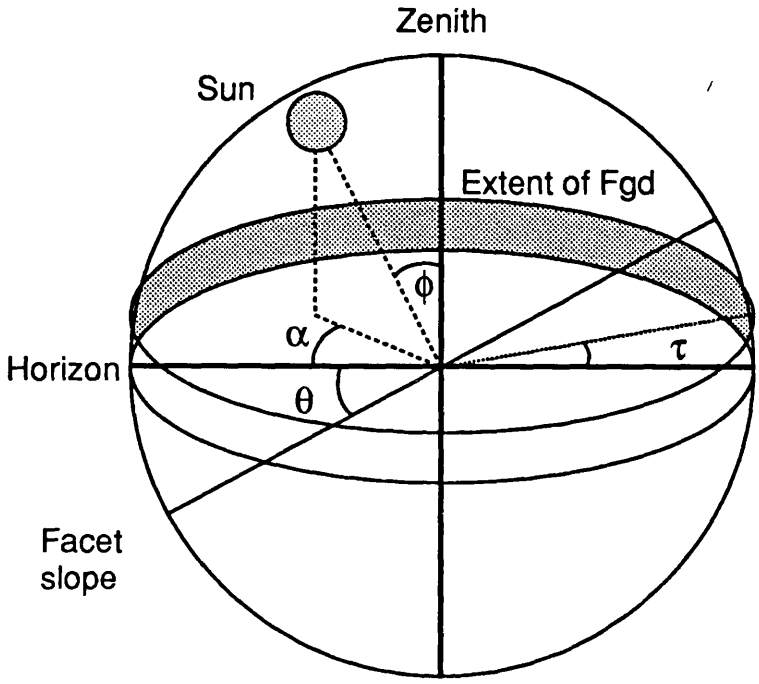


Figure 4.9: DTM facet geometry, used by the TL model. Facet slope $\theta$, solar azimuth $\alpha$, solar zenith angle $\phi$, and horizon brightening factor $\tau$.

This has several problems. While albedo may be a suitable estimate for the proportion of total radiation reflected, when considering discrete spectral bands this is not so. Albedo is not consistent for different cover types; so a variety of covers will introduce a variety of spectral reflectance types[5]. Lastly, the directional reflectance of each neighbouring facet will have to be taken into consideration, to determine how much radiance is to be derived from each facet. This finally renders the inclusion of a ground component at best impracticable given present computing capabilities.

In order to devise a practicable method, simplifying assumptions must be made. $F_D$ is computed using the DTM (4.2.4):

$$F_D = (1-\delta).E\cos i \qquad \text{Eq. 4.3}$$

Where E is the total incoming radiation, $\delta$ is proportion of diffuse to total incoming flux, determined from the spectral radiance model (*cf.* 4.2.3.2), and *i* is the incident angle between the Sun and the surface normal (*cf.* 4.2.4). This is equivalent to the standard cosine correction carried by many previous workers.

The distribution of $F_d$ is assumed isotropic, and hence proportional to the area of sky in view to the facet, sloping at angle $\theta$:

$$F_d = \delta.E(\pi-\theta)\pi^{-1} \qquad \text{Eq. 4.4}$$

If the relief is not great, and slopes moderate, it may be assumed that $F_{gD}$ is derived from a hemispherical field, extending only up to the horizontal in the field of view from the facet (see 4.2.5 for discussion of model assumptions) (figure 4.9). The proportion of the terrain in view is therefore given by $\theta/\pi$. This hemisphere is assumed to have average characteristics; that is it behaves as a Lambertian reflector and that its reflectance properties ($\sigma$) are given by a global

---

[5]For a large number of neighbouring facets this may cancel out, since the average albedo of other facets impinging upon the scene would approach the global average. However, this is unlikely in areas where there is a systematic bias towards particular cover types, such as in a farm landscape of near mono-cultivation.

(or locally derived) value for albedo. Hence the estimate for the direct ground component is:

$$F_{gD} = E\sigma\cos\phi(\theta/\pi) \qquad \text{Eq. 4.5a}$$

Where $\phi$ is the solar zenith angle, and $\alpha$ is the relative azimuth of the Sun and the facet.

The model can be extended further by scaling $F_{gD}$ by $[1-\sin\phi\cos(\alpha/2)]$, in order to account for shadowing, low-lighting and high-lighting. This is achieved by the combination of two scale factors (Equation 4.5b). The first, $\sin\phi$, accounts for the solar zenith angle. At the zenith, the Sun will cast no shadows, and as the solar zenith angle increases, shadowed components are more dominant, until all the surface is in shadow when it reaches the horizon; at this point $\sin\phi=1$, and $F_{gD}$ will be zero. The relative azimuth of the facet is also critical. This is accounted for by the second scale factor. Given the concept of an Egbert (1977) or Li and Strahler (1985) landscape, where the scene is made up of shadowed or non-shadowed (opaque) components, the proportion of illuminated terrain is very dependent upon the direction in which the terrain facet is oriented - looking down-Sun, mainly Sun-lit components will be observed, looking up-Sun, shadowed components will be dominant. Obviously, the shadowing will be dependent upon the solar zenith angle (a Sun at the zenith casts no shadows in this landscape), so the two scaling factors are combined. The $\alpha/2$ value is modified by the cosine of this angle, to try to allow for the fact that the facet views a segment of a 180° field of view and, in fact, never sees all shadowed or Sun-lit components; rather, this factor should account for low- and high-lighting effects.

$$F_{gD} = E\sigma\cos\phi(\theta/\pi)[1-\sin\phi\cos(\alpha/2)] \qquad \text{Eq. 4.5b}$$

If all four of the components are to be modelled, including $F_{gd}$, then (4.4) is actually equal to the total ground radiance (which we will term $F_g$), and:

$$F_{gD} = (1-\delta)F_g \qquad \text{Eq. 4.6}$$

again where $\delta$ is the proportion of diffuse to total incoming flux. Since it is only a fraction of the total incident radiation on any surface, simplifying assumptions are made to allow for easier computation of the diffuse ground component. $F_{gd}$ is assumed to be derived from a cylinder extending $\tau$ above the horizon (since $\tau$ is small, $\leq 10°$), and is isotropic with respect to azimuth and zenith angles[6]:

$$F_{gd} = \delta.F_g[1-\tan\theta(\pi\tan\tau)^{-1}] \qquad \{\text{for } \theta<\tau\} \qquad \text{Eq. 4.7a}$$

or

$$F_{gd} = \delta.F_g[1-(\pi\tan\tau)^{-1}\{\tan\theta-(\tan^2\theta-\tan^2\tau)$$

$$+\tan\tau\cos^{-1}(\tan\tau/\tan\theta)\}] \qquad \{\text{for } \theta>\tau\} \qquad \text{Eq. 4.7b}$$

Equation 4.7b approximates to

$$F_{gd} = \delta.F_g[1+(2\sqrt{2}/3\pi\tan\tau).\tan\theta.(1-\tan\tau/\tan\theta)^{3/2}$$

$$\{\text{for } \theta>\tau\} \qquad \text{Eq. 4.7c}$$

In this study, a number of factors allow the ground components to be computed in this way (Hall-Könyves, 1987, 1988), namely:

- the relatively low reflectance of the cover types
- the low, undulating relief (75% of facets sloping less than 10° (fig. 4.10)) and
- the elevation of the sun (approximately 45°), resulting in the lack of shadowed facets in the DTM.

---

[6]I am grateful to Paul Schooling, Department of Geography, UCL, for helping to prove equations 7a-7c.

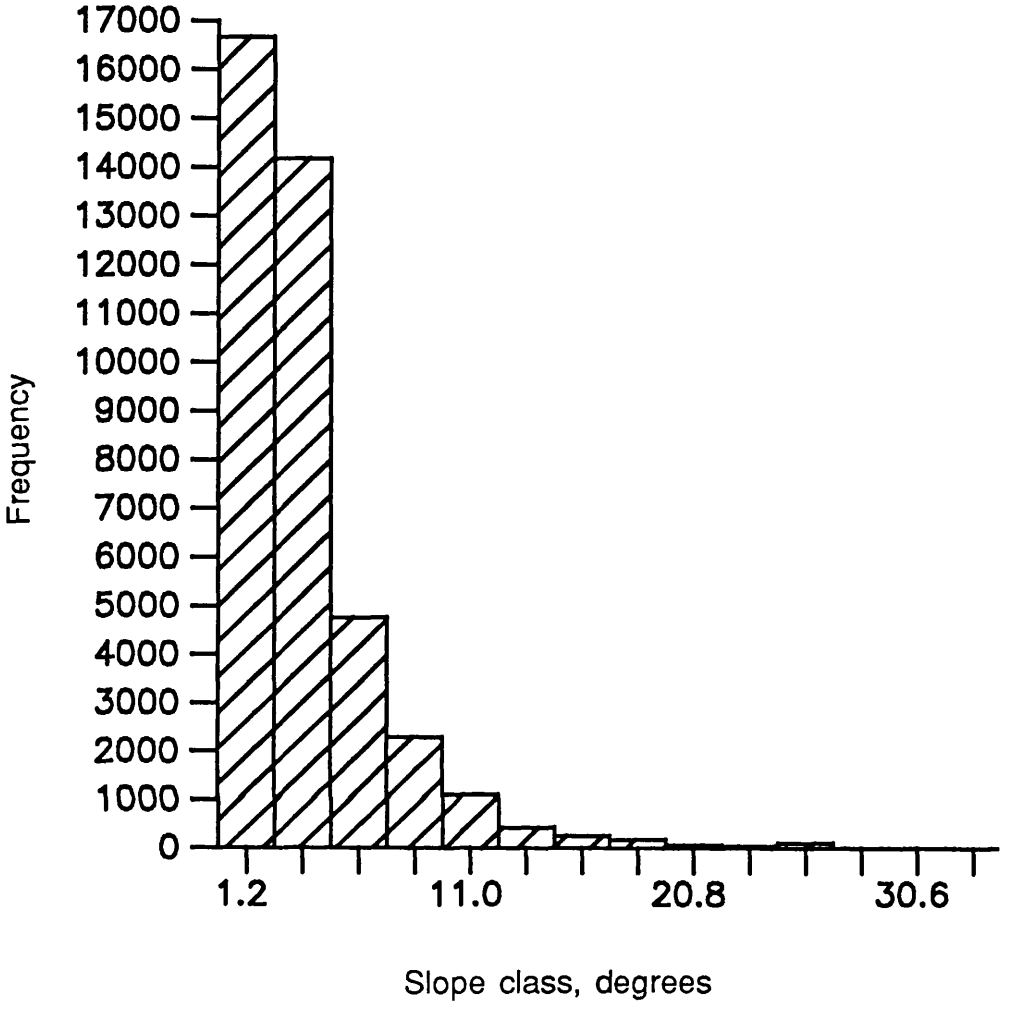


Figure 4.10: Distribution of slopes in the DTM dataset.

These formulae were programmed in Mapics[7] to allowing terrain model processing and image map generation. The algorithm and the program is called Terrain Lite (TL); several versions of this algorithm exist, and are outlined in 4.4.2.

4.2.3.2: Spectral sky radiance distribution

The optimum technique to evaluate irradiance data for each band is to make contemporaneous measurements of sky radiance intensities using a spectro-radiometer, integrating the values for each bandwidth, to simulate the endo-atmospheric irradiance values for the sensor in use. Ideally, these measurements should enable temporal spectral adjustments to the data, since changing atmospheric conditions will alter the spectral profile of the sky radiance. They should also measure the angular distribution of sky radiance over the hemisphere, rather than producing an integrated hemispherical measurement such as that obtained when using a pyranometer. Such measurement specifications demand specialist instrumentation, such as the PARABOLA instrument used by Ahmad *et al.* (1987), Middleton *et al.* (1987), and Deering (1988), or the multi-sensor pyranometer developed by Hämälainen *et al.* (1985). However, since such instruments and the capability to carry out such field work over a long field season (4 months) were unavailable, broad-band pyranometer measurements, combined with literature calculations and software modelling of the atmosphere were used to calculate and balance the total flux for each flightline.

Spectral irradiance was estimated in two ways; first, from published measurements and calculations of exo-atmospheric irradiance from the literature, and second using the 5S atmospheric transmittance model (Tanré *et al.*, 1986), based upon the LOWTRAN code (Prasad *et al.*, 1987).

In the first method, the ground measurements from the AWS pyranometer were converted to $W.m^{-2}.sr^{-1}$, and then the calculations from Woodham and Gray (1987) and Markham and Barker (1987) used to estimate the percentage of total incoming

[7]Mapics is a raster-based worksheet and mapping package.

radiation for each TM waveband. It is assumed that the measurement made by the pyranometer is equal to the total incoming radiation across the full spectrum of irradiance, since no detailed data upon the bandwidth and sensitivity function of the sensor is available. This will, in fact, produce a slight under-estimate of irradiance, since the bandwidth of the instrument is known to be not as broad as the full solar irradiance spectrum.

The transformation from measured irradiance to synthesised "potential radiance" is finally completed by dividing the value by the bandwidth, in μm, to produce standard units of the total incoming spectral irradiance E, in $W.m^{-2}.\mu m^{-1}.sr^{-1}$. Atmospheric attenuation to incoming flux was assumed to be a constant proportion across the entire spectrum, instead of being spectrally dependent. In otherwords, the exoatmospheric estimates, in percentages of the total flux, were applied to the measured flux on the ground. While this is obviously a gross over-simplistic assumption, without some model of what absorption and scattering is taking place in the atmosphere it is not possible to calculate the attenuation for each band. The effect of this will be to over-estimate the value of E in the equations above. This error will, in part, compensate for the under-estimate of the irradiance measured by the pyranometer.

The estimated spectral irradiance is then broken down for the TL models into proportions of diffuse to total spectral irradiance (the ratio δ), calculated from data recorded by McDowell (1974) and the 5S algorithm (*cf.* 4.4.1 below, Table 4.1), these being the two best sources available to the study. These values are essential for the calculation of $F_d$, $F_{gD}$, and $F_{gd}$. The second method calculates direct flux, diffuse flux, and "environmental" radiance (i.e. $F_{gD}$, but with no knowledge of the topography) for a flat, horizontal target. The program estimates detected radiance for off-nadir viewing sensors, which would implicitly make some assumptions about the directional, as well as spectral, reflectance properties of the target. In this instance the algorithm was used to calculate the proportions of direct and diffuse flux for each waveband, for specific irradiance, solar geometry and visibility conditions, corresponding to each flightline of the image data. The 5S program can also be used calculate absolute values of irradiance at ground level; these values have been compared to those estimated by method one (*cf.* 4.4.1

below), and exo-atmospheric calculations (Woodham and Gray, 1987, Markham and Barker, 1987).

### 4.2.4: Topographic corrections

Previous studies have concentrated upon topographic shading algorithms for digital terrain models, and methods of defining the reflectance characteristics of a target to model their behaviour, and hence correct them for image analysis (section 2.4). This method is inherently flawed in its logic. In order to make a useful and accurate correction, detailed characteristics of the target, including a descriptions of the BRDF of the target, are required. If this is so, then other useful knowledge of the target exist *a priori*, eg type, percentage cover, height, leaf orientation, and moisture content. Thus further analysis of the image data will reveal little more about the target than is already known.

A second misconception is that the target orientation, in particular the zenith direction for the BRDF, is achieved by calculating the normal to the terrain facet. This assumes that the directional effects of canopy reflectance are related to topography. The relationship is more complicated than may at first appear. Plant canopies do not organise themselves at a normal to the facet upon which they are located; rather they grow "upwards", although the packing of the individual components in the canopy may affect the macro-scale response of the canopy in a complicated manner (Leprieur *et al.*, 1988, Strahler *et al.*, 1988, Strahler, 1988). Thus it is not sufficient for the terrain model to be used simply to orient the canopy reflectance model.

The emphasis of the use of terrain information, in this study, has been to generate image maps determining irradiance, using DTM data calibrated with irradiance measurements. Three sources of terrain data were considered, 1:10,000 standard paper mapping, digital contour data digitised from 1:50,000 OS Landranger series (10m contour interval), and DEM data (on a 50m grid, generated to the nearest metre) derived from the digital contour data by the OS. Although digitised from the Landranger series, the digital contour data in fact originate from the 1:10,000

mapping, since it is this 5m contour dataset that is generalised in the production of the 1:50,000 series. No information upon the method used by the OS to derive the DEM was provided, although some estimates of accuracy were included with the data.

The algorithm employed here requires slope and aspect data to calculate the orientation of each terrain facet. This is used, in turn, to determine the irradiance on each facet. In order to achieve this, a DTM[8] dataset was computed from the digital contour data, using Mapics software package. Height-Gradient Grid files are computed, containing the necessary gradient information in East ($_eG$)and North ($_nG$) directions for each point (cell) in the model. A scaling value for each facet is determined by calculating the angle between the illumination vector and the normal vector for each facet. First the direction cosines[9] ($\underline{l}$, $\underline{m}$, $\underline{n}$) for the normal to the facet are calculated:

$$\underline{l} = -{}_eG/\sqrt{1+{}_eG^2+{}_nG^2} \qquad \text{Eq. 4.8}$$

$$\underline{m} = -{}_nG/\sqrt{1+{}_eG^2+{}_nG^2} \qquad \text{Eq. 4.9}$$

$$\underline{n} = 1/\sqrt{1+{}_eG^2+{}_nG^2} \qquad \text{Eq. 4.10}$$

And the dot product of the illumination vector and the facet normal is found to give the cosine of the incident angle, $i$:

$$\cos i = l\sin\alpha + m\cos\alpha + n\cos\phi \qquad \text{Eq. 4.11}$$

where $\alpha$ and $\phi$ are the solar azimuth and zenith angles, respectively.

Once this basic scaling factor has been determined for each facet (pixel) in the DTM image, it is then modified according to equations 4.2-4.7 above (4.2.3.1), and converted into potential radiance values by scaling the estimate of spectral irradiance, E (4.2.3.2).

---

[8]A DEM only models elevation as a function of position; a DTM models gradient information which can be used to derive slope and aspect information.

[9]Three dimensional vector describing the orientation of the normal

### 4.2.5: Model assumptions

In order for the model to function, several assumptions concerning the type of cover, topography, sky radiance, and the image data must be made; those assumptions concerning the development of the model have already been discussed in sections 4.2.1-4 above. The use of the reflectance images also requires some careful consideration about what exactly is taking place in the scene.

The use of reflectance images, generated by the method outlined in this study, normalises the variation in scene radiance due directly to topography. However, some indirect topographic artifacts may still remain, since some environmental factors, such as differential drainage conditions, or variable sunlight availability on steeper, north-facing slopes, may have an impact upon the canopy development. This may be manifest either as some difference in "health" of the plant, such as leaf development and (eventually) crop yield, or in the macro-canopy structure, for example the packing of each plant in the crop. While some reflectance models do recognise such differences (for example Franklin *et al.*, 1986, and Strahler *et al.*, 1988, who allows for shadowing changes in forest stands), few scientists consider that plant canopies would be altered significantly by such factors. It is evident, both from aerial photography and ground observations, crops such as wheat and barley are very sensitive to environmental factors, and that topographic effects may not be restricted purely to illumination differences, but could include physiological alterations in the plant canopy as well.

A further assumption that has to be made is that the flux from the target detected at the sensor is collimated, i.e. that it is derived from a common angular position with respect to the BRDF. Over a full image this is obviously not the case, since the ATM scanner has a very broad FOV. For individual parcels this is not such a poor assumption, since their extent across the imagery is usually limited to a few degrees. Consequently, changes in reflectance within a parcel can be attributed primarily to target parameters. The description of the reflectance of any parcel in an image can therefore be made using the statistics derived from the pixel values in the reflectance images. Multiple observations of fields, from several flightlines,

can then be compared on the basis of these statistics, and differences between datasets attributed to view angle effects alone.

## 4.3: Model performance

### 4.3.1: Parameter selection

Two important parameters have to be determined for the spatial and spectral sky radiance model: spectral albedo or reflectance, and the ratio of diffuse to direct flux, for each spectral band.

It is assumed (and observed) that for the season in which the image was obtained (spring), and that for a rural area, the surrounding cover type will be dominantly green leaf vegetation. Values of spectral reflectance estimated from Lillesand and Kiefer (1979) and Kondratyev (1969) for each band of the ATM sensor are given in Table 4.1. The 5S model (Tanré *et al.*, 1986) calculates average spectral reflectance for the pertinent sensor bandwidth from a "typical" green vegetation dataset; these values are included in the table. Estimates for spectral reflectance by Kondratyev are, for the longer wavebands, in the order of 5 percentage points lower than those from the 5S model, the values used in this study.

**Table 4.1: Terrain Lite model parameters**

| ATM Band | 1 | 2 | 3 | 4 | 5 | 6 | 7 | 8 | 9 | 10 |
|---|---|---|---|---|---|---|---|---|---|---|
| *Spectral reflectance* | | | | | | | | | | |
| $\sigma(\%)^{*}$ | >5 | 10 | 15 | 10 | 12 | 25 | 45 | 42 | 30 | 15 |
| $\sigma(\%)^{+}$ | n/a | 10.4 | 11 | n/a | 13.2 | n/a | 52.7 | n/a | 37.3 | 21.3 |
| *Diffuse irradiance* | | | | | | | | | | |
| $\delta(F_d/F^{\#})$ | 18 | 10 | 7 | 6 | 5 | 4.2 | 3-4 | 3 | n/a | n/a |
| $\delta(F_d/F^{+})$ | n/a | 39.1 | 31.2 | n/a | 25.5 | n/a | 17.5 | n/a | 6.6 | 4.5 |

*From Kondratyev (1969), and Lillesand and Kiefer (1979)
+Output from the 5S model, Tanré *et al.* (1986)
#From McDowell (1974)

Values for δ, the ratio of diffuse sky radiance ($F_d$) to total flux (F), were estimated from results measured by McDowell (1974), in which study sky conditions were stated to be "clear" and solar zenith angle similar to this experiment, around 45°. The 5S model, for the demonstration data presented here, was given parameter values of 45° for the solar zenith angle, 160° solar azimuth, 15km visibility. These values were, again, those used for the computation of the reflectance images.

It is important to remember that while the use of such parameters is essential to the functioning of the model, they do not in fact account for a large proportion of the flux incident on any facet. Hence any error introduced at this stage is likely to be reduced by a large amount (around an order of magnitude) when applied to the model. The gross differences between the 5S and McDowell estimates of diffuse sky radiance are likely to be a result of extremely clear skies at the "clear" test site used by the latter. Although it is impossible to tell exactly, or even to estimate, the state of the atmosphere when McDowell's observations were made, it would seem likely that such a test site (White Sands missile range) would produce very clear conditions.

**Table 4.2: Potential radiance, TM bands 1 to 7, $W.m^{-2}.sr^{-1}.\mu m^{-1}$**

| Band | 1 | 2 | 3 | 4 | 5 | 7 |
|---|---|---|---|---|---|---|
| Flightline | | | | | | |
| 1 | 182.429 | 161.191 | 137.716 | 96.580 | 20.657 | 7.419 |
| 2 | 176.607 | 156.046 | 133.321 | 93.498 | 19.998 | 7.182 |
| 3 | 182.429 | 161.191 | 137.716 | 96.580 | 20.657 | 7.419 |
| 4 | 172.726 | 152.617 | 130.391 | 91.443 | 19.559 | 7.024 |
| 5 | 190.192 | 168.050 | 143.577 | 100.690 | 21.536 | 7.735 |
| 6 | 176.607 | 156.046 | 133.321 | 93.498 | 19.998 | 7.182 |
| 7 | 178.548 | 157.761 | 134.786 | 94.525 | 20.218 | 7.261 |

Calculations were made for the potential radiance for each band, based upon the literature values of the percentage of the total exoatmospheric irradiance for each band of the Landsat TM sensor (Woodham and Gray, 1987, Markham and Barker, 1985, 1987). No such literature values exist for Earth surface measurements or

estimates, since these would be dependent upon changing atmospheric conditions. Such measurements would be preferable, but are dependent upon the opportunity to carry out further fieldwork at the time of imaging, and the availability of more sophisticated instrumentation, such as a spectrometer (*cf.* 4.2.3.2). Neither of these two options were available for this experiment, nor are they likely to be in most large area or long timescale studies, particularly those utilising satellite-borne sensors. The assumptions concerning this method are detailed in 4.2.5 above; in brief the method provides an over estimate of the potential radiance for each flightline, since it assumes equal attenuation across the entire spectrum. While this makes comparison with other studies difficult, it is acceptable for this study, in particular between flightlines, since the instrumentation and method is standardised. The actual values of potential radiance will in fact be over-estimates, but this is preferable to an underestimate, which could result in reflectance values greater than 1 being calculated.

**Table 4.3: Solar azimuth and zenith angles used in TL runs**

| Local time* | F/line | Azimuth | Zenith |
|---|---|---|---|
| 09:47:30 | 4 | 133.66° | 46.32° |
| 09:52:30 | 1 | 135.16° | 45.76° |
| 09:58:30 | 3 | 137.00° | 45.22° |
| 10:04:30 | 2 | 138.87° | 44.50° |
| 10:10:30 | 5 | 140.77° | 43.90° |
| 10:14:30 | 6 | 142.07° | 43.51° |
| 10:20:30 | 7 | 144.03° | 42.96° |

*Local solar time = GMT- ≈7.4 mins. Since each flightline takes between 40 and 50 seconds to image, these are approximate values. Position of the site was taken as 51.93°N 1.85°W. (Solar zenith and azimuth angles computed using an algorithm developed by J. Pearson, UCL)

### 4.3.2: Solar azimuth and zenith angles

Table 4.3 lists the values for solar azimuth and zenith angles calculated for input to the TL models. Over the 35 minute period of the imaging of the first seven

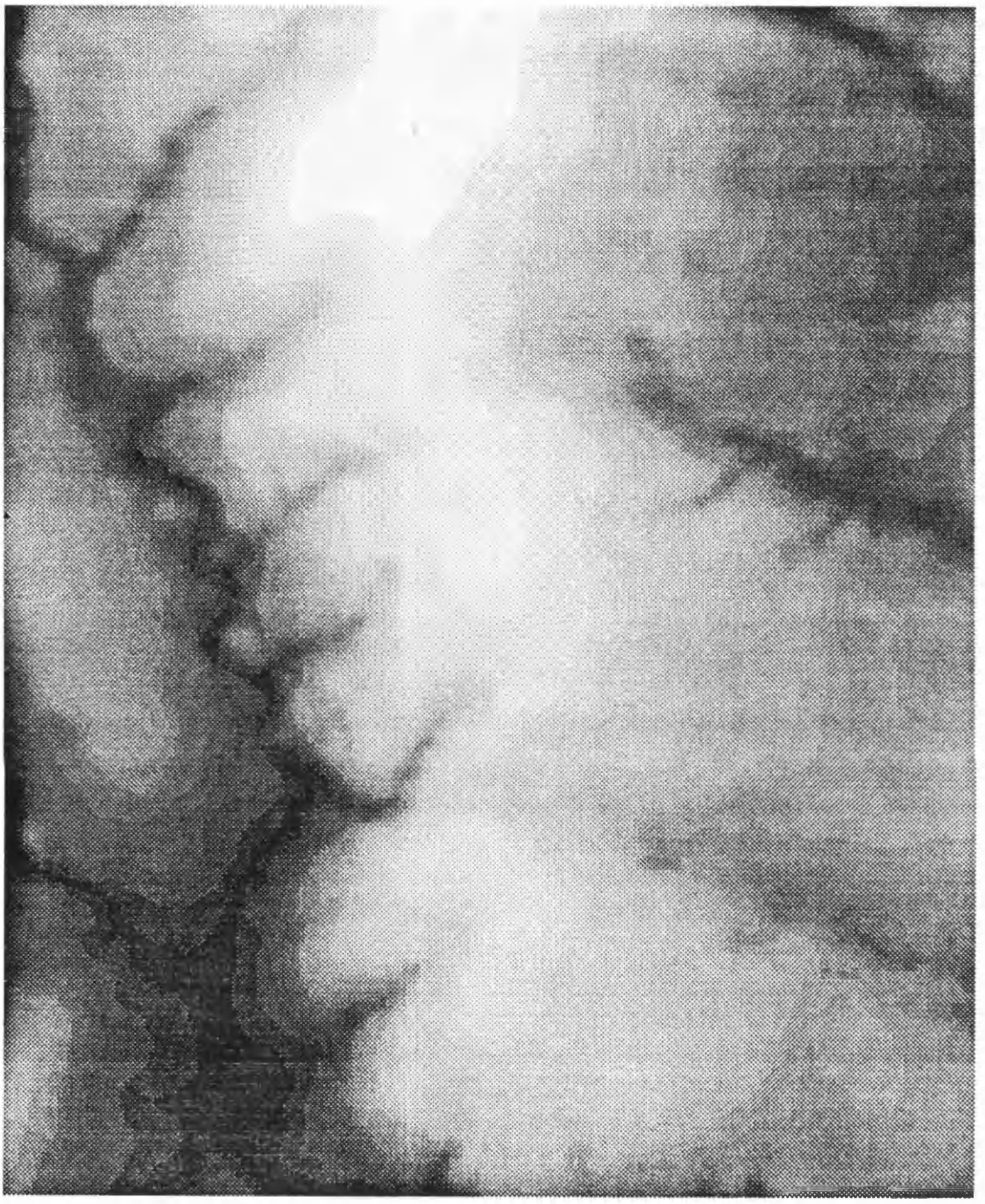

Figure 4.11: Laser print of the DEM used in the study; bright values correspond to high elevations, ranging up to 270m.

flightlines, the solar azimuth changed by 10.5°, and the zenith angle by around 3.5°; the former would likely be the more significant parameter.

### 4.3.3: Model results

Eight algorithms, of increasing complexity, were programmed in order to test the performance of the TL models. The description of each version is given in table 4.4 below.

**Table 4.4: Terrain Lite algorithms**

| | |
|---|---|
| **v1** | Calculation of $F_D$ alone, corrected by cos*i* only. |
| **v2** | $F_D$ + $F_d$; isotropic sky, proportion visible dependent upon facet slope, $F_d/F$ given by table 4.1 |
| **v3** | As v2, but additionally $F_{gD}$, proportion visible determined by facet slope, surface reflectance from table 4.1. |
| **v3a** | As v3, but solar zenith and azimuth corrections applied to $F_{gD}$ |
| **v4** | As v3, additionally accounts for $F_{gd}$; scattering given by table 4.1. |
| **v4a** | As v4, but solar azimuth and zenith corrections applied to $F_{gD}$. |
| **v4x/xa** | Fast algorithms to calculate $F_{gd}$ by approximation. |

Using the 20m resolution DTM, generated from the OS digital contour and point data covering the study site (figure 4.11), potential radiance images were generated using each of the versions of the TL algorithm in turn, up to version TL4x. A standardised solar geometry was used, with a solar zenith angle of 45°, and an azimuth of 160°. The ratio of diffuse to total flux was taken from McDowell (1974), and spectral reflectance of the surrounding terrain from Kondratyev (1969) (Table 4.1)[10]. Tables 4.5 to 4.10 and figures 4.12 to 4.16 show mean, standard deviation, minimum, maximum and median values of potential radiance for these images. The number of pixels in each image was 50,451 (201x251). Figure 4.17 shows the resulting synthesised potential radiance images for TL versions 1-4a.

[10]In the final production of the reflectance images, values of $F_d/F$ and $\sigma$ produced by the 5S model were used.

**Table 4.5: Band TM1 TL results**

| | Mean | SD | Min | Max | Med |
|---|---|---|---|---|---|
| v1 | 122.700 | 7.110 | 43.110 | 159.400 | 123.240 |
| v2 | 127.340 | 6.480 | 49.750 | 158.080 | 128.020 |
| v3 | 127.850 | 6.370 | 58.690 | 161.840 | 128.260 |
| v3a | 127.590 | 6.290 | 55.230 | 159.230 | 128.120 |
| v4 | 127.840 | 6.380 | 58.250 | 161.670 | 128.260 |
| v4a | 127.610 | 6.300 | 55.140 | 159.320 | 128.130 |

**Table 4.6: Band TM2 TL results**

| | Mean | SD | Min | Max | Med |
|---|---|---|---|---|---|
| v1 | 108.410 | 6.280 | 38.090 | 140.850 | 108.890 |
| v2 | 111.280 | 5.890 | 42.200 | 140.030 | 111.850 |
| v3 | 112.410 | 5.720 | 57.690 | 148.330 | 112.390 |
| v3a | 111.850 | 5.490 | 54.310 | 142.560 | 112.080 |
| v4 | 112.390 | 5.720 | 57.390 | 148.070 | 112.390 |
| v4a | 111.870 | 5.510 | 54.170 | 142.710 | 112.100 |

**Table 4.7: Band TM3 TL results**

| | Mean | SD | Min | Max | Med |
|---|---|---|---|---|---|
| v1 | 92.620 | 5.370 | 32.540 | 120.330 | 93.040 |
| v2 | 94.370 | 5.130 | 35.050 | 119.830 | 94.840 |
| v3 | 94.760 | 5.050 | 41.800 | 122.670 | 95.020 |
| v3a | 94.570 | 4.990 | 39.190 | 120.700 | 94.920 |
| v4 | 94.760 | 5.060 | 41.630 | 122.610 | 95.020 |
| v4a | 94.580 | 4.990 | 39.150 | 120.740 | 94.920 |

(All values in $W.m^2.sr^{-1}.\mu m^{-1}$)

**Table 4.8: Band TM4 TL results**

| | Mean | SD | Min | Max | Med |
|---|---|---|---|---|---|
| v1 | 64.960 | 3.770 | 22.820 | 84.390 | 65.250 |
| v2 | 65.820 | 3.650 | 24.050 | 84.140 | 66.680 |
| v3 | 66.900 | 3.550 | 36.230 | 92.110 | 66.680 |
| v3a | 66.360 | 3.290 | 35.660 | 86.580 | 66.350 |
| v4 | 66.890 | 3.550 | 36.080 | 91.980 | 66.680 |
| v4a | 66.370 | 3.300 | 35.600 | 86.640 | 66.360 |

**Table 4.9: Band TM5 TL results**

| | Mean | SD | Min | Max | Med |
|---|---|---|---|---|---|
| v1 | 13.890 | 0.810 | 4.880 | 18.050 | 13.960 |
| v2 | 13.950 | 0.800 | 4.960 | 18.040 | 14.010 |
| v3 | 14.090 | 0.780 | 6.750 | 19.100 | 14.080 |
| v3a | 14.020 | 0.750 | 6.510 | 18.360 | 14.040 |
| v4 | 14.090 | 0.780 | 6.750 | 19.090 | 14.080 |
| v4a | 14.020 | 0.750 | 6.510 | 18.360 | 14.040 |

**Table 4.10: Band TM7 TL results**

| | Mean | SD | Min | Max | Med |
|---|---|---|---|---|---|
| v1 | 4.990 | 0.290 | 1.750 | 6.480 | 5.010 |
| v2 | 5.010 | 0.290 | 1.780 | 6.480 | 5.030 |
| v3 | 5.060 | 0.280 | 2.420 | 6.860 | 5.060 |
| v3a | 5.030 | 0.270 | 2.340 | 6.590 | 5.040 |
| v4 | 5.060 | 0.280 | 2.420 | 6.860 | 5.060 |
| v4a | 5.030 | 0.270 | 2.340 | 6.590 | 5.040 |

(All values in $W.m^2.sr^{-1}.\mu m^{-1}$)

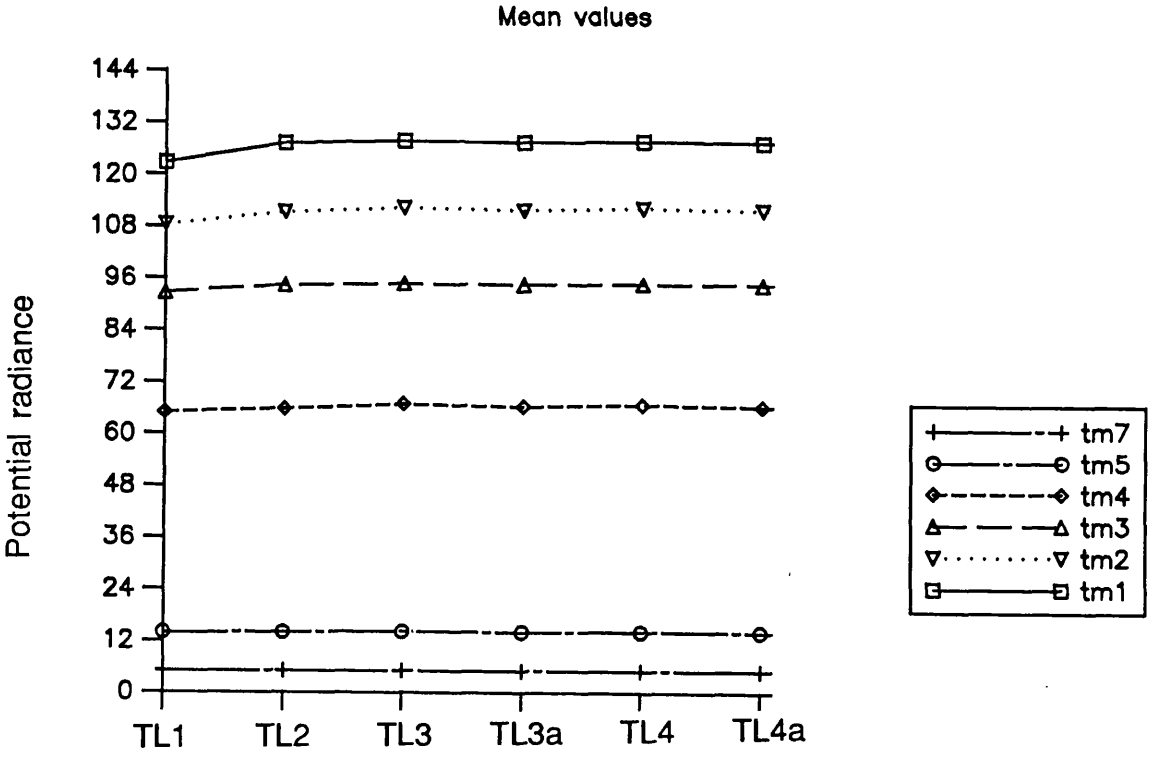


Figure 4.12: (above) Mean potential radiance values of the TL models. Figures 4.13-4.16 (overleaf) give Standard Deviation, Minimum, Maximum and Median results respectively.

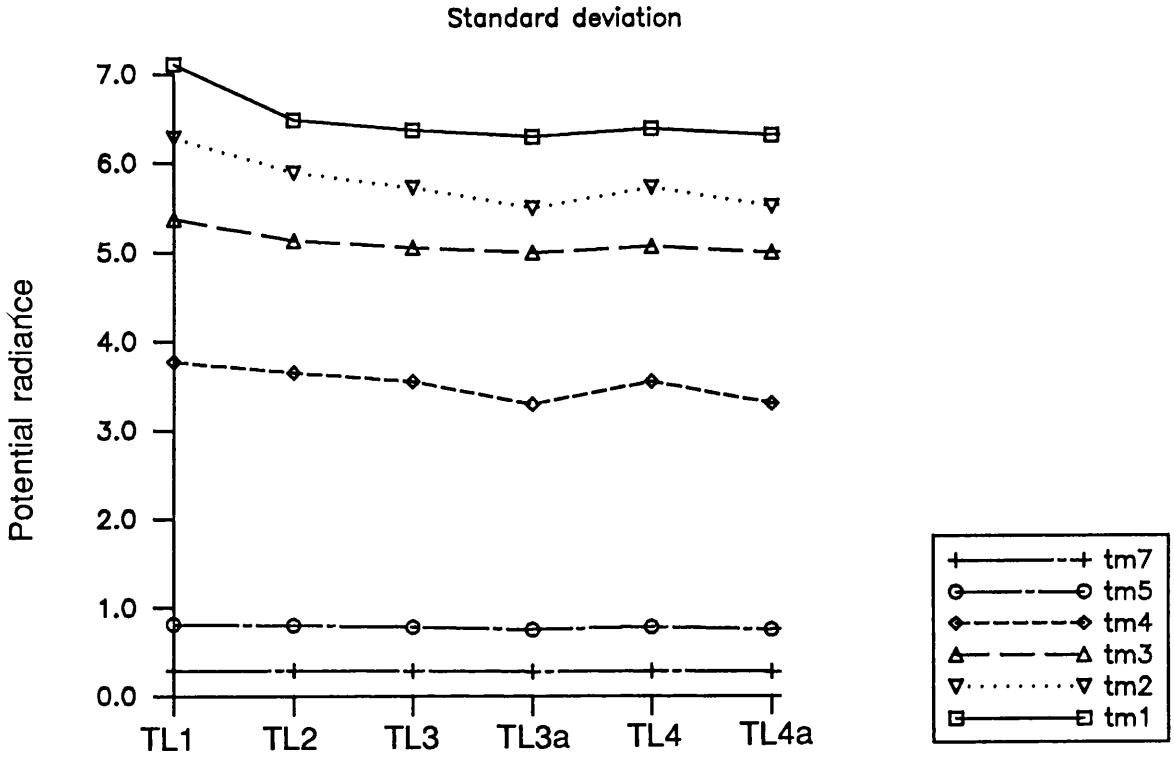
Standard deviation
Potential radiance
7.0
6.0
5.0
4.0
3.0
2.0
1.0
0.0
TL1
TL2
TL3
TL3a
TL4
TL4a
tm7
tm5
tm4
tm3
tm2
tm1

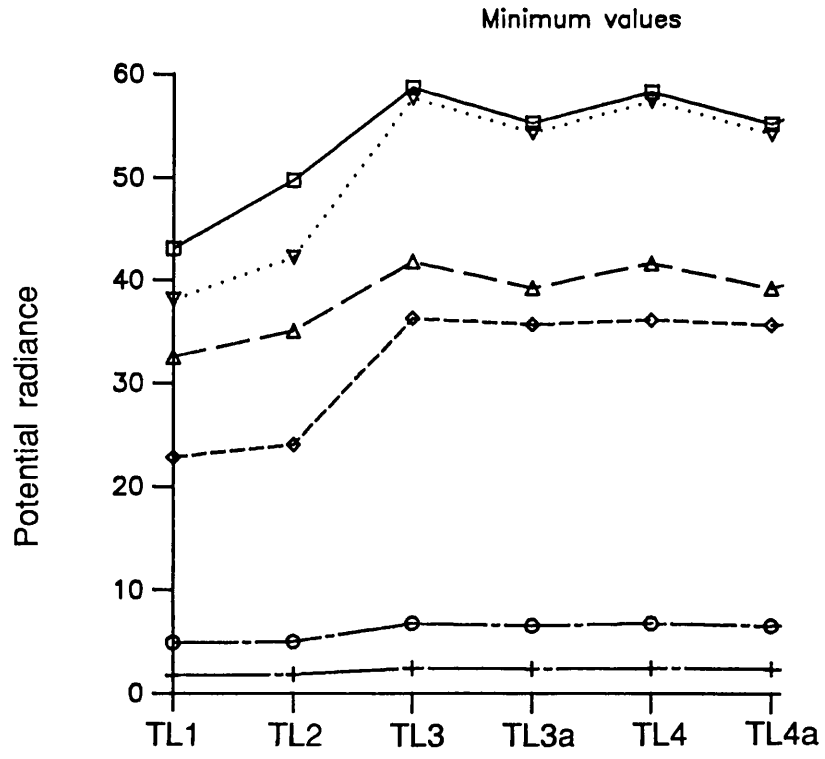
Minimum values
Potential radiance
60
50
40
30
20
10
0
TL1
TL2
TL3
TL3a
TL4
TL4a

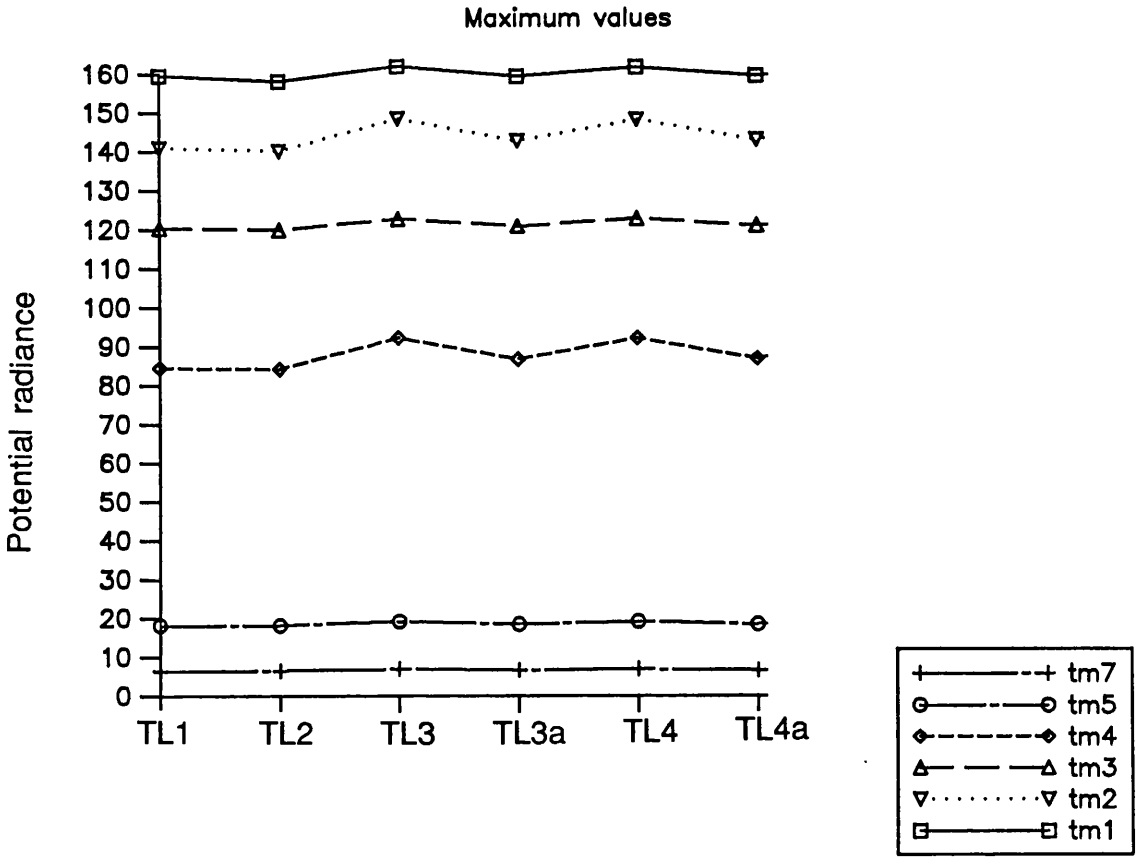
Maximum values
Potential radiance
160
150
140
130
120
110
100
90
80
70
60
50
40
30
20
10
0
TL1
TL2
TL3
TL3a
TL4
TL4a
tm7
tm5
tm4
tm3
tm2
tm1

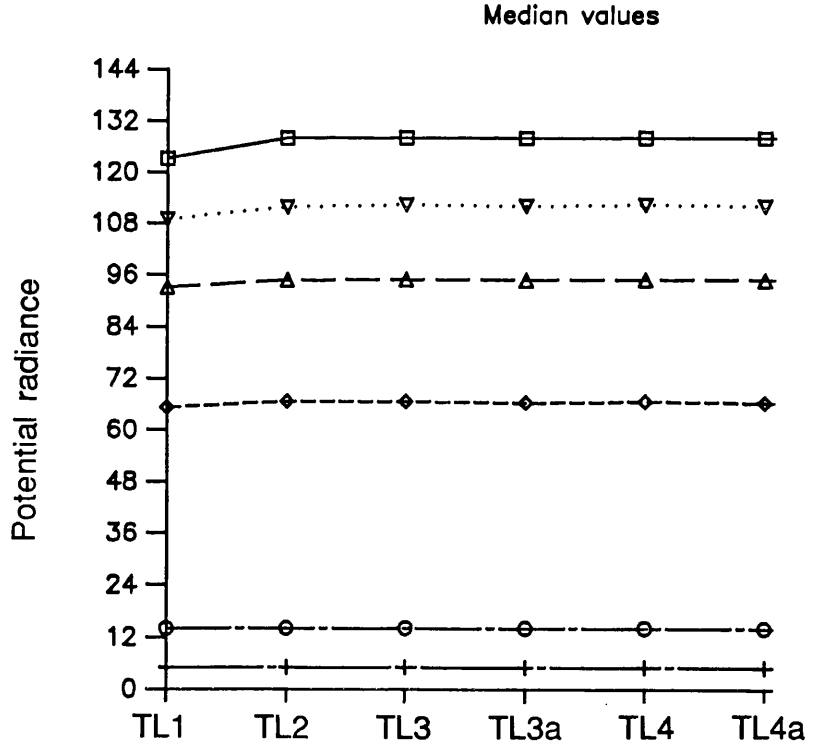
Median values
Potential radiance
144
132
120
108
96
84
72
60
48
36
24
12
0
TL1
TL2
TL3
TL3a
TL4
TL4a

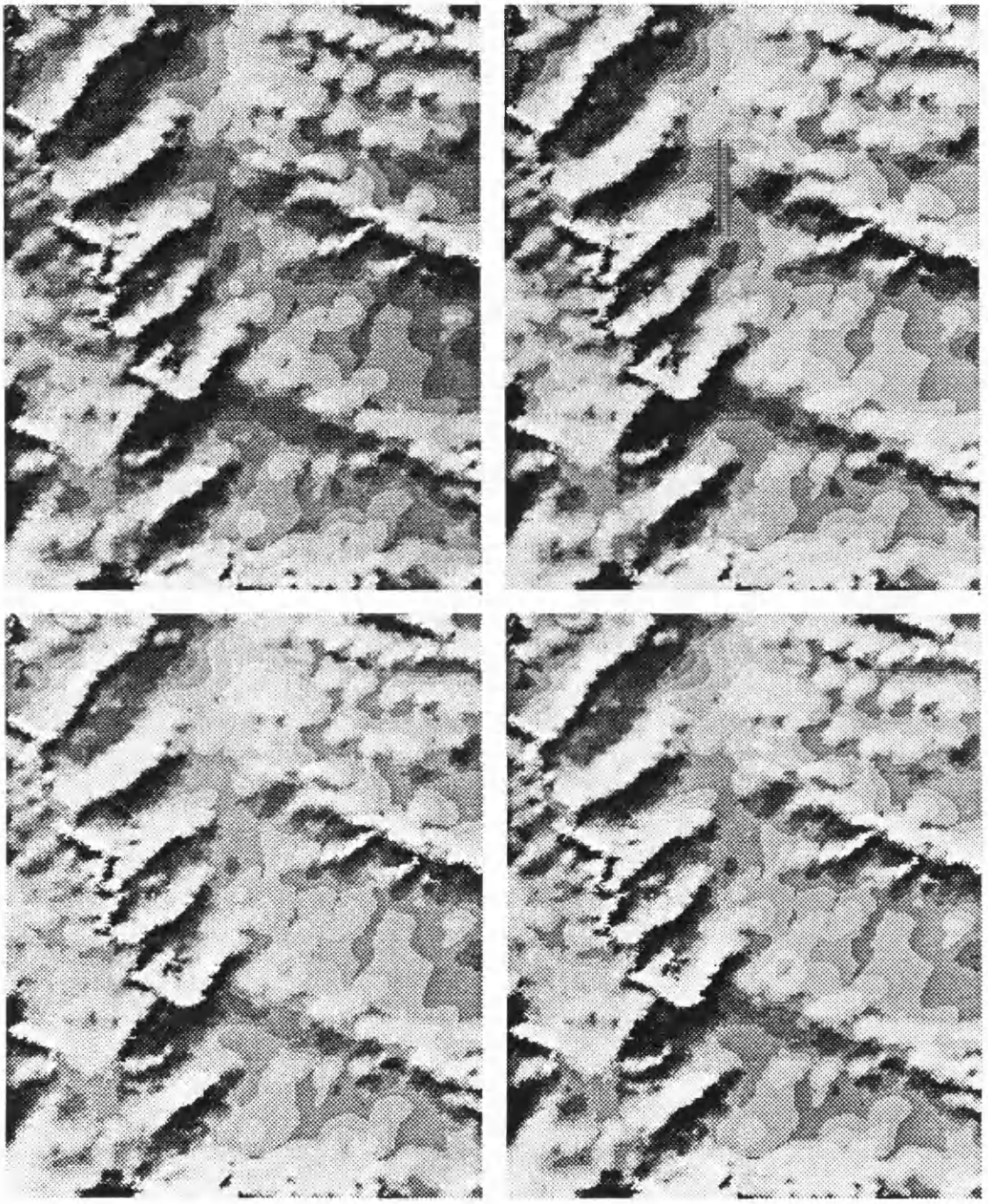

Figure 4.17: Laser print of potential radiance images from TL1 (top left), TL2 (top right), TL3a (bottom left) and TL4a (bottom right). North is up the page, illumination was from the bottom right corner.

In some previous uses of terrain modelling, to correct for differential illumination and reflectance map production, shaded or low-lit areas are in general under-illuminated, resulting in over-estimates of reflectance in these zones (for example, Jones *et al.*, 1988). This trend is counteracted by the more sophisticated versions (v3 onwards) of the TL model. While maximum values, particularly those from v3a and v4a, remain close to those calculated using v1, minimum values rise, as expected, when the diffuse sky component is included (v2), and further still for v3. The effect is most significant for bands where atmospheric scattering is strongest (i.e. short wavelengths) and terrain reflectance greatest (i.e. the NIR waveband). The addition of the $F_{gd}$ component (v4 onwards) makes little significant difference to potential radiance, suggesting that sky anisotropy is not a significant factor in this of study. This is a result of the moderate relief in the study area. Mean and median values (figures 4.12, 4.16) increase slightly for v2, but remain stable for further versions of the model.

The correction factor for facet aspect and shadowing appears to function favourably, moderating both maximum and minimum values. It does not greatly influence potential radiance values, the value of $F_{gD}$ is never large, contributing at most around 30% of the flux incident on the darkest facets. The aspect correction factor always slightly reduces the mean, SD, minimum, maximum and median values for the potential radiance images. This because the function, which we may recall is $[1-\sin\phi\cos(\alpha/2)]$, always returns a value of less than 1, except in the special cases of the solar zenith angle ($\phi$) being equal to zero or the relative azimuth angle being equal to 180°.

Of note, however, is the fact that the direct ground component does contribute rather more than the indirect ground component (back-scattered by the sky, manifest as horizon-brightening in the TL models TL4, TL4a). This is in contrast to the findings of Prasad *et al.* (1987), but similar to conclusions by Woodham (1989). It is sensible to recognise that the importance of this indirect component will be spectrally dependent, and be more significant in the shorter part of the spectrum; Prasad *et al.* (1987) were considering the full solar spectrum, and therefore made no spectral considerations regarding the relative importance of different components. In the red and NIR spectrum, the direct ground component

will be much more significant than the diffuse ground component, depending upon the reflectance properties of the local terrain.

As a result of this preliminary investigation, TLv3a was selected for all further analyses, as a compromise over computation time and the effectiveness of the algorithm in modelling the illumination of the terrain.

## 4.4: Reflectance image analysis and assessment

### 4.4.1: Analysis of the relationship between view angle and reflectance

Using reflectance images for two fields in the study area[11], the mean, minimum, and maximum pixel values, as well as standard deviation (SD) and coefficient of variation (CV) were calculated for five view angles and the six ATM bands corresponding to TM sensor bands (ATM 2, 3, 5, 7, 9 and 10). The data were analysed for trends that it was assumed would now be due solely to view angle - in particular, the relationship between view angle, mean pixel value, and CV of the samples in the parcel.

In section 4.1.1 the relationship between view angle and the detected response of various canopies is illustrated. In this section, the relationship between view angle and mean value of *reflectance* is compared with the earlier section. It would be expected that the trends evident in the raw DN data would remain in the reflectance data, since the major effect of reflectance image production is the removal of data scaling and offsets, achieved by data calibration.

A second comparison, that of the variance of the two datasets, is also made. There are two reasons why the relationship between view angle and CV, in this experiment at least, should be similar for both raw DN and reflectance data. CV is a measure of the ratio of the SD of a data set, assumed to be distributed normally,

[11]Fields 29 - winter barley, 56% cover - and 30 - spring barley, 6% cover.

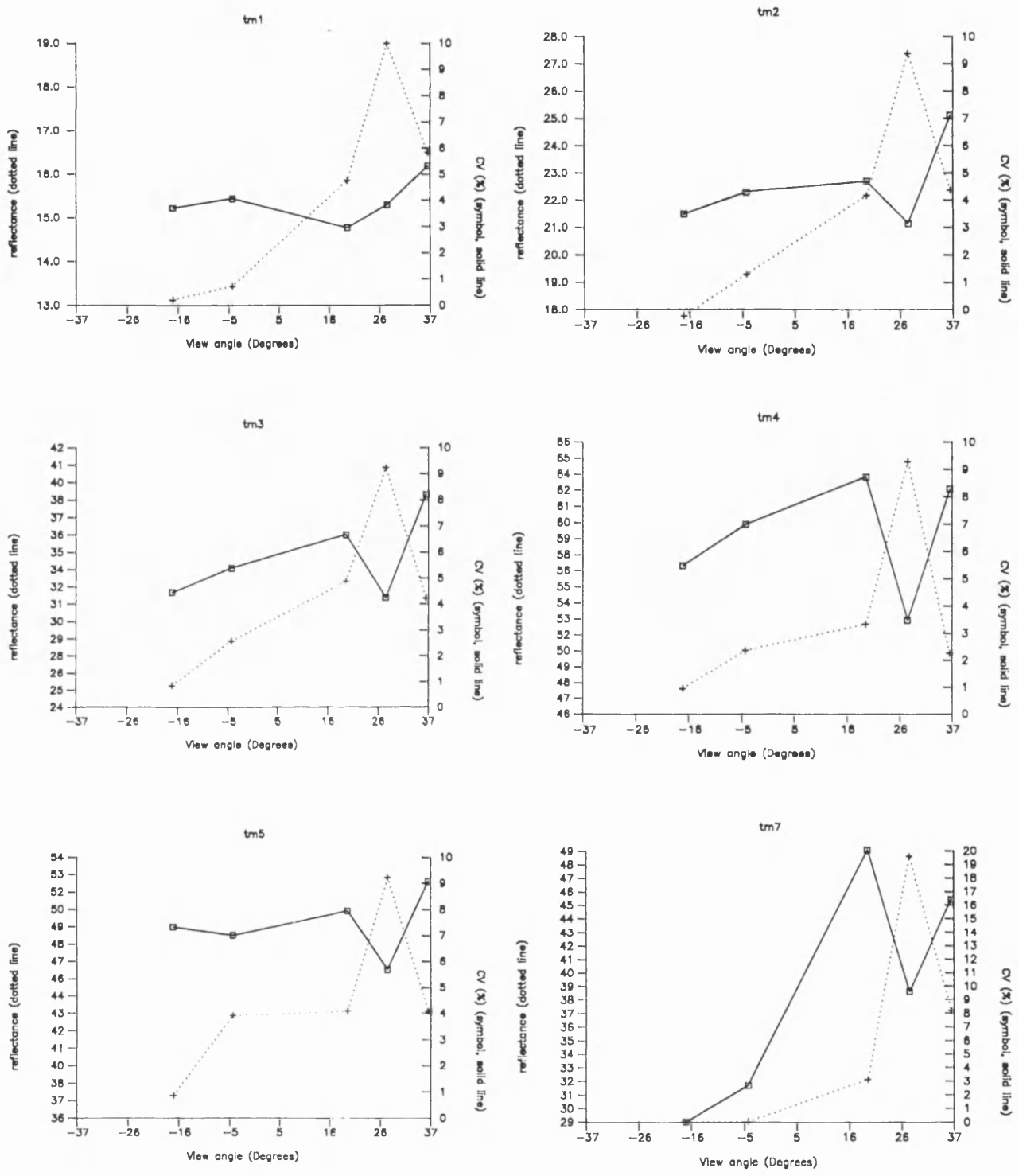


Figure 4.18: Field 30 reflectance, bands TM 1 to 7. Solid lines are CV, dotted lines mean DN.

to the mean. First, scaling the data, such as by converting the data values to radiance units, will not change the CV of the sample, excepting effects resulting from quantisation. Second, the act of ratioing radiance images with the potential radiance images, to produce reflectance images, will alter the distribution of the samples where the orientation of the facets is varied and extreme; the range of DN in parcels of single cover type in reflectance images will tend to be reduced. However, since parcels in managed agriculture are on moderate terrain, and are often a function of geomorphological and topographical units, the CV may be expected to remain similar, since over small areas the effect of generating reflectance images becomes approximately a scalar transformation.

4.4.1.1: Qualitative comparison

Figures 4.18 and 4.19 present the results of the reflectance data for two fields, 30 and 29 (see section 4.1.1, table 3.1). By comparison with figures 4.4 and 4.6, it can be seen that for field 30 (spring barley) the trend of both CV and mean reflectance for the visible bands shows a similar pattern, although the response of CV is a little more erratic. For the infrared bands, particularly band TM7, data reliability becomes doubtful. This is most evident in the measure of CV, which increases for several of the flightlines and bands. This is a direct result of the quantisation, caused as a result of the processing, corrupting the distribution of the data.

In figure 4.19, presenting the reflectance data for field 29 (winter barley) the pattern of response for the visible and NIR bands (TM1 to 4) is broadly the same as for the raw data; in TM4 even the inverted relationship noted in band ATM 7 (figure 4.4) is evident. The low radiance in the MIR bands (TM 5 and 7), however, causes serious quantisation problems when using calibrated data. As a result the statistical reliability of these bands is again doubtful (see section 4.4.2 below). A second problem is evident with TM4 - the high reflectance values (of greater than 100%) indicate that the gain setting on the instrument was incorrectly recorded during data collection. A gain setting of half this value would produce more acceptable results.

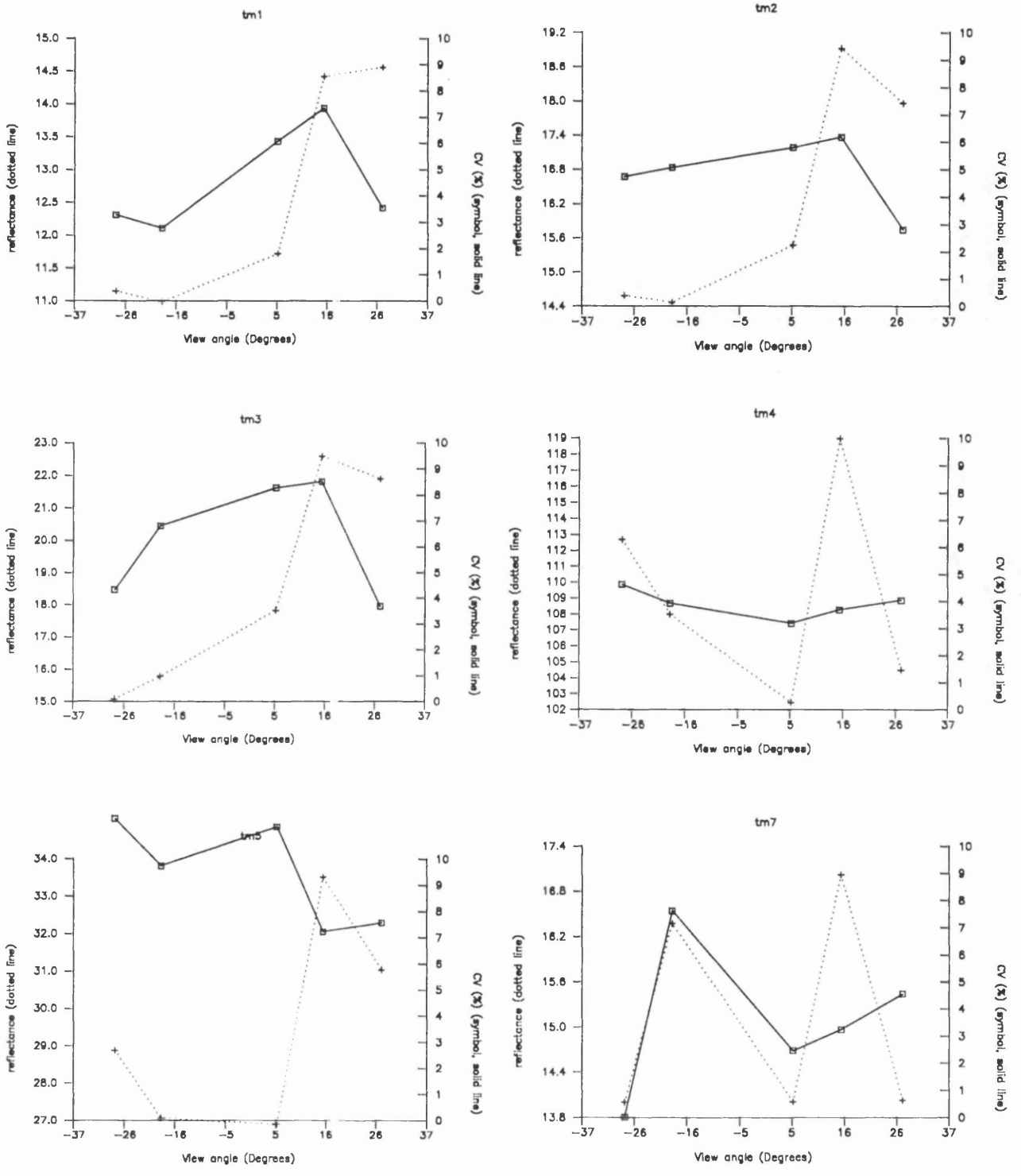


Figure 4.19: Field 29 reflectance, bands TM 1 to 7. Solid lines are CV, dotted lines mean DN.

4.4.1.2: Quantitative comparison - regression analysis

A further comparison is made between the raw and reflectance data, using the method outlined in the next chapter. Regression analysis is used to describe the trends of CV with view angle, and it is shown that for the shorter TM wavebands, no major differences in statistical explanation of the data are evident. For bands TM5 and TM7, however, corrupted data distributions do not allow the use of these bands in analysis. For a full explanation of the method, refer to the later sections (5.2 and 5.3).

The results of the regression analysis are presented in tables 4.11, 4.12, 5.3 and 5.4. For field 30 reflectance data (table 4.11), non-linear regression fit is not significant when tested at a 90% confidence level for all six TM bands; and in no case does non-linear regression produce a result with >70% significance when compared with linear regression. Linear regression also produces poor results, but this is to be expected since $r^2$ values are also low, and the *b* coefficients in the regression equations (indicating the gradient of the regression line) are also small. For bands TM5 and TM7, the assumptions concerning the normal distribution of the data do not hold, so in fact these results are probably invalid in any case. For the other four bands, however, the results are similar to those derived from analysis of the raw data (see section 5.3, table 5.3).

In the case of field 29 reflectance data (table 4.12), non-linear regression provides a significantly improved explanation of data variance[12] for bands TM3 and TM4; in both cases the fit is significant at the 95% confidence level when compared to the linear regression results. Of note is that the *c* coefficients for TM4/ATM7 are both positive, an anomaly peculiar to this kind of vegetation cover in this study. Again, results for bands TM5 and TM7 are invalid due to corrupted data distributions. Results for TM1 and TM2 are similar to those obtained with raw data, although only significant at a lower confidence level.

---

[12]Note: this is a measure of the variance of the observed dependent variable from the predicted value - and in this case our dependent variable is, perversely, also a measure of variance, CV.

**Table 4.11: Field 30, reflectance - linear and non-linear regression of view angle and coefficient of variation**

| Band | TM1 | TM2 | TM3 | TM4 | TM5 | TM7 |
|---|---|---|---|---|---|---|
| Linear Regression | | | | | | |
| a | 3.79 | 4.07 | 5.25 | 6.38 | 7.24 | 5.81 |
| b | 0.014 | 0.038 | 0.043 | 0.017 | 0.013 | 0.315 |
| $r^2$ | 0.143 | 0.295 | 0.340 | 0.030 | 0.057 | 0.680 |
| t-test | 40% | 60% | 60% | 20% | 30% | 80% |
| Non-linear Regression | | | | | | |
| a | 3.14 | 3.45 | 4.93 | 6.69 | 6.70 | 7.98 |
| b | -0.023 | 0.002 | 0.025 | 0.034 | -0.018 | 0.439 |
| c | 0.002 | 0.002 | 0.001 | -0.001 | 0.002 | -0.007 |
| $r^2$ | 0.590 | 0.419 | 0.368 | 0.046 | 0.206 | 0.729 |
| f-test | ns | ns | ns | ns | ns | ns |
| Significance of use of non-linear regression | | | | | | |
| t-test | 70% | 40% | 20% | 10% | 30% | 30% |

**Table 4.12: Field 29, reflectance - linear and non-linear regression of view angle and coefficient of variation**

| Band | TM1 | TM2 | TM3 | TM4 | TM5 | TM7 |
|---|---|---|---|---|---|---|
| Linear Regression | | | | | | |
| a | 4.59 | 4.92 | 6.32 | 3.89 | 9.48 | 3.57 |
| b | 0.042 | -0.015 | 0.009 | -0.011 | -0.065 | 0.019 |
| $r^2$ | 0.247 | 0.068 | 0.008 | 0.246 | 0.561 | 0.025 |
| t-test | 60% | 30% | 10% | 60% | 80% | 10% |
| Non-linear Regression | | | | | | |
| a | 6.18 | 6.35 | 9.11 | 3.31 | 9.95 | 4.27 |
| b | 0.034 | -0.023 | -0.007 | -0.008 | -0.067 | 0.015 |
| c | -0.004 | -0.003 | -0.006 | 0.001 | -0.001 | -0.002 |
| $r^2$ | 0.618 | 0.766 | 0.922 | 0.951 | 0.591 | 0.062 |
| f-test | ns | ns | 90% | 95% | ns | ns |
| Significance of use of non-linear regression | | | | | | |
| t-test | 70% | 80% | 95% | 95% | 20% | 10% |

Notes: ns= not significant at 90%; $r^2$ is a measure of explained variance; f-test is a comparable significance test to the t-test.

Where non-linear regression provides a better explanation, it may be noted that the *b* and *c* coefficients of the equation are not always the same in the analysis of raw and reflectance data. Such changes are almost certainly due to the corruption of data distributions in the image correction processing. In this data set, the effect is least evident for band TM4[13], and for this band the coefficients are virtually identical. Reducing the number of grey levels in the reflectance image, without reducing the overall dynamic range of the image commensurately, appears to result in spuriously large values of CV (*cf.* data for bands TM5 and TM7). The net result of this process, therefore, is to increase the value of the *c* coefficient in the regression equation; this effect is observed in band TM3.

### 4.4.2: Quantisation problems and data set distributions

Despite promising a useful means of determining reflectance properties for a wide range of surfaces and applications (Yang and Vidal, 1989, Woodham, 1989, Dozier and Frew, 1989), the reflectance images produced in this study do not provide the quality of data that are required for further analysis in the context of this investigation (see Chapter 5). The main problem is the effect of quantisation upon the images at different stages of the correction.

The first problem arises with the radiometric calibration of the data. In all bands imaged by the ATM sensor in this experiment the gain setting was 1 or greater, enhancing the dynamic range of the DN values in the image. The effect of calibrating the data to radiance, and still displaying and manipulating these data on an image processor that will only operate with integer values, is a net decrease in the dynamic range of the data. In some bands, particularly ATM9 and ATM10 (TM5 and TM7), this may have a dramatic effect of reducing the dynamic range by a factor of 4.

[13]This band was had a gain setting of near unity, so little dynamic range was lost in conversion to radiance units

**Table 4.13: Data distributions before and after conversion to reflectance**

| column | minimum | maximum | median | count |
|---|---|---|---|---|
| DN, tm3 | 57.00 | 81.00 | 68.50 | 24 |
| Reflectance, tm3 (%) | 18.00 | 31.00 | 24.50 | 14 |
| DN, tm7 | 44.00 | 95.00 | 66.50 | 46 |
| Reflectance, tm3 (%) | 17.00 | 33.00 | 25.00 | 2 |

This table shows that the distribution of the image data for a vegetative parcel (Field 29) is severely corrupted during the conversion to reflectance values. In particular, band TM7 is reduced from 46 grey levels to just two.

The second effect is a result of the terrain model potential radiance images also being integer; for example, band TM7 has a maximum DN of 6, although 4 is a more common value. This means that the calculation of reflectance can only produce values of 0%, 17%, 33%, 49%, 51%, 83%, and 100%[14], for pixels with a radiance value of 6.

The same effect can arise in the calculation of reflectance values. While this is done using real arithmetic, in a FORTRAN program developed to do this, the conversion of the reflectance values to byte data for display and image processing means that the nearest integer value must be chosen for the value written out by the program. Since reflectance values are also represented in terms of percentage, the most convenient system to display images is using a possible 100 grey levels, each level representing one percent. Obviously, making better or full use of the grey level range on the image processing system could reduce this problem (for example see Yang, 1989, who used 256 grey levels), but this does not solve the problem of the radiometrically corrected image data being essentially 2-bit. Such a system is also a less convenient to work with.

The combined effect of these two quantisation stages is to produce an image with a reduced dynamic range, and in some cases only 4 or 5 different grey levels. The effect is the reduction of integrity of the data, especially when it is to be used for the calculation of variance, since this measure relies upon assumptions concerning the normal distribution of the data. Quantisation, and in particular reducing the number of available grey levels used in an image, can alter data distributions dramatically (table 4.13).

Reflectance images, however, can provide a valuable method for the removal of illumination, atmospheric and topographic effects in remotely sensed data, and could become essential elements of multitemporal and multiple view angle data set analyses (Yang, 1989, Woodham, 1989). It has been shown, in this study, that the main limitation in the production of such images is the computational facilities available; for accurate, quantitative analysis, access to a floating point processing

[14]In fact even these values are not calculated exactly, due to rounding errors with both the image processor and the use of byte arithmetic in FORTRAN.

system, such as is usually the case with software rather than hardware systems, is essential.

## 4.5: Conclusions on the use of reflectance images for further analysis

An attempt has been made here to show that production of reflectance images can provide a useful, and indeed in some cases necessary, method for the analysis of view angle effects. A method of production that simplifies some of the more difficult conceptual problems has been derived and introduced, and some results analysed. In particular, the response of coefficient of variance (CV) of DN within parcels with view angle has been investigated, and found to be similar for both raw image and reflectance image data.

The development of a simplified sky radiance model, incorporating both angular and spectral characteristics, has been a key factor in this section. A version of the model that attempts to account for illumination differences according to the aspect of each terrain facet relative to that of the Sun was introduced and used in analysis. It is interesting to note that such an idea has been published elsewhere (Dozier and Frew, 1989; subsequent to the work here)

The major disadvantage of the use of the reflectance images produced in this study is the effect of quantisation and reduction of dynamic range in the intermediate images that are generated in the process, namely the radiance image and the synthesised potential radiance image. The use of an image processing system that could compute such transformations in floating point format would evade such difficulties. Ideally, the final image should have more than 100 grey levels to display the reflectance image. This would preserve DN data distributions, allowing statistical analysis of the reflectance images to proceed with a greater level of confidence concerning the integrity of the data.

It has also been ascertained, however, that the view angle effect of greatest interest to this study, namely the coefficient of variation of DN in parcels, is not affected

significantly by atmosphere, topography, and instrument calibration; at least not so far as they apply to this study. With this in mind, and the justification of maintaining the statistical integrity of the data so far as is possible, further analysis to understand the relationship between view angle and image variance (undertaken in Chapter 5) has been carried out on the raw, uncorrected data.

# CHAPTER 5: Measures of spatial variance in remotely sensed digital images as a new method for information extraction

The analysis of image statistics has been shown to allow the numerical inversion of models to extract characteristics of scene components, in particular for forestry applications (for example, Li and Strahler, 1985, 1986, Franklin and Strahler, 1988). In the first section of this chapter, the concepts underlying one such statistic, scene variance, are reviewed, and the interaction of scene variance and image resolution assessed in an experiment (section 5.1.4) using ATM imagery of the study area. In section 5.2, a new method for the extraction of agrophysical canopy parameters from imagery, using the relationship between view angle and image variance, is explained. Section 5.3 presents the results of this method when applied to Daedalus ATM data, in particular the general description of the canopy, correct interpretation of the regression analysis, and the influence of crop row geometry. The final section discusses new options that could be explored using such a method and other techniques of measuring image variance.

## 5.1: Theoretical background to modelling and measuring spatial variance in images

### 5.1.1: Spatial variance in scenes

Remotely sensed data represent a discretely sampled model of the Earth's surface, measured at a sampling interval determined by the geometry of the sensor. For any one region of the Earth's surface, many scales of examination and evaluation could possibly exist. For example, at a "global" scale, an image of the whole earth may be described as a combination of like areas that are logically defined (segmented) by the human observer: oceans, continents (land or ice) and cloud (weather systems). By enlarging the scale at which the examination takes place, more subdivisions may be distinguished; for example at a continental scale, mountain ranges, plains, river systems.

By moving to a regional scale, one commonly associated with remotely sensed data, more complicated spatial relationships become apparent. With a scene comprised of agricultural components, that is fields or parcels of homogeneous land cover types separated by boundaries, the predominant factor determining whether or not a field may be distinguished is the relationship between the size of the field and the sampling interval. That is, if the size of the ground resolution element is smaller (perhaps several times smaller) than the field, then the field will be identifiable. But it is wholly possible that at such a sampling scale, spatial variations in other components of the scene, such as soil moisture variations or variations in canopy density, will also influence measurements. If the size of ground resolution elements is reduced further, other factors will also become important. Plant row structure, individual plants, plant components (leaves, stalks, ears), and cells will in sequence become identifiable.

It can, therefore, be argued that we use variance in an image to help us to identify scene characteristics, at all scales of examination. Some of this interpretation is based upon textural analysis, but statistical analogies are hard to formulate. This is an important area of information extraction in image understanding that has long been recognised; in this chapter, we attempt to follow one strategy for the extraction of canopy parameter characteristics, based upon the evaluation of image variance, in a multiple view angle dataset.

### 5.1.2: Measures of spatial variance

Several measures of spatial variance have been proposed (Woodcock and Strahler, 1987, Curran, 1987, Atkinson, 1988). The simplest, used in this study, is to extract pixel values (DN) from a parcel within an image, and calculate the statistical measure of the coefficient of variation (CV) (4.1.1, Eq. 4.1) of the total population of pixels in that region; we shall refer to this technique as the **coefficient of variation method**, or CV method. This has the advantage of being simple to implement on an image processing system. Results from this technique, using ATM data collected at the Bemborough Farm study site, are given in figure 5.7

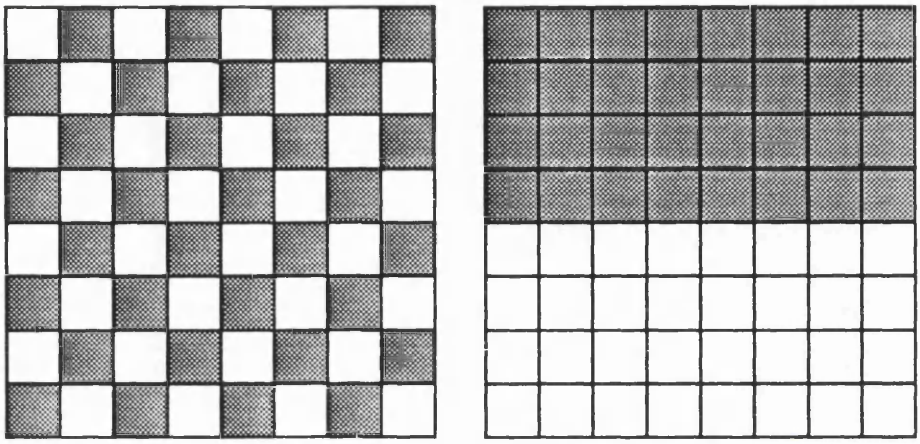

Figure 5.1: Assumptions concerning the distribution of objects in a scene for the CV method. These two parcels have the same CV, but the left one is variable at a higher frequency. The CV method assumes that objects are distributed as in the left parcel for results to be comparable. The regression strategy described in sections 5.2 and 5.3, however, explains how this assumption can also be used to identify the nature of the distribution of the objects in the scene when using a multiple view angle dataset.

below, and in greater detail in section 5.2. A basic assumption is made when using this technique, however, that the spatial distribution of DN is random within the parcel, or that it is described by a periodic function of similar spatial frequency to the sampling frequency of the sensor[1], i.e. that despite the parcel being classified as a single cover type the likelihood of a pixel having the *same value as its neighbour* is normally distributed. Spectrally pure parcels, that is DN of a single cover type, will have a narrow distribution of values; those from a less pure sample area will have a broader, perhaps even bimodal distribution. In regions where the distribution of DN does not meet these criteria, the assumptions concerning the assessment of spatial autocorrelation, using the surrogate of CV, would be false (figure 5.1).

A further reason for using the CV to measure image variance is that measures such as the Standard Deviation (SD) are sensitive to differences between the mean values of sample populations. Since the analysis of the data was taking place upon non-calibrated, or raw, image data, it was important that fluctuations in the mean values of sample datasets - of the same parcel on the ground - from each of the flightlines would not effect the analysis of variance.

Woodcock and Strahler (Woodcock, 1985, Woodcock and Strahler, 1987) measured local variance by passing a 3x3 kernel over an image, calculating the SD of the pixels within the kernel, and averaging the SD of all positions of the kernel within the image to produce a measure of variance for the whole image. This technique (which we will term the **Woodcock SD method**) provides a better measurement of the spatial autocorrelation and variance of neighbouring pixels in an image than the CV technique, since it does not make any implicit assumptions concerning the distribution of pixels within an image. It also has the advantage of providing a measurement of variance for each pixel in the image, rather than one based on parcels that appear spectrally homogeneous. Several examples of images processed in this manner are presented here (figure 5.3).

---

[1]This case will later be termed an *M-resolution model* case, in section 5.1.5

The Woodcock SD method actually emulates the action of a high-pass filter (e.g. Laplacian) on an image by identifying pixels which fall upon or near to edges. However, whereas convolving an image to produce a high-pass filtered image produces a graphical representation of variance or spatial autocorrelation characteristics of the original image, Woodcock's method quantifies variance exactly. A second difference is that the magnitude of all edges is represented in the same (positive) direction, i.e. the stronger the edge, the greater the statistical measure of local variance. Nevertheless, it is marginally harder to implement this technique on an image processor than the CV method, and an interpretation of the significance of the results still demands further understanding of the effect of scene structure upon image variance. As will be seen, moreover, some of the results presented here output using this algorithm (implemented in FORTRAN 77, not on the image processor) produced some surprising results (see 5.1.4).

Woodcock (1985), Curran (1987), Atkinson (1988) and Atkinson and Danson (1988) have proposed the use of semi-variograms as a means of characterising the spatial variability of scenes. This more complicated computational technique permits the identification of the "optimal" sampling strategy for remote sensing of different cover types, and should indicate the general level of variability of that cover at differing scales of measurement. It would be difficult, however, to build the oversampling and canopy effects produced by the ATM sensor in to such a modelling mechanism. For these reasons the modelling of image variance using this technique has not been attempted.

### 5.1.3: The rôle of models in evaluating scene spatial variance

It is important, for the purpose of this study, to establish terms and concepts which can be used to describe and classify the interaction of scene spatial variance and image sampling. This has been attended to, in great detail by other workers (Jupp *et al.*, 1988, 1989, Woodcock *et al.* 1988a & b, Woodcock and Strahler, 1987, Cliff and Ord, 1973), and in a general biogeographical (and specifically remote sensing) context by Strahler *et al.* (1986) and Woodcock (1985). This paper reviewed and discussed the derivation and application of scene and image spatial

variance models in general use in remote sensing. Much of this understanding and knowledge is used as a background to applications of invertible models, used to estimate parameters of forest canopies (Li and Strahler 1985, 1986, 1988, Franklin and Strahler, 1988, Strahler *et al.* 1988). Of most relevance here is the following review of the paper (Strahler *et al.*, 1986), as applied to the modelling of the behaviour of parcels of land planted with wheat or barley crops.

5.1.3.1: Definitions based upon sampling scale

Scene models can also be classified depending upon the relationship between the size of the elements in the scene model and the resolution cell size. *H-resolution* models are defined as being those in which the scene elements are larger than the resolution cells, and are thus detectable; conversely, *L-resolution* models are those where the elements are smaller than the resolution cell, and so cannot be distinguished in the image. With regard to spatial autocorrelation, for *H*-resolution models it is likely that each resolution cell will have a similar reflectance to its neighbour, since adjacent cells are likely to be imaging the same element. With *L*-resolution models, there is no reason to suppose that neighbouring cells will resemble each other since the scene elements are smaller than the cells. However, in extreme cases of *L*-resolution models, where elements are much smaller than the resolution cell, high spatial autocorrelation is likely due to the effect of resolution cell integrating over a large number of individual elements. Even in scenes of diverse cover types, if the scene element size is small then many cover types will be integrated over one resolution cell, and hence cells are likely to be correlated.

High spatial variance is likely to be observed, therefore, when the element size approximates[2] the resolution cell size. Strahler *et al.* (1986) do recognise such a circumstance, but only acknowledge the difficulty of characterising such a model; in this study we will term such a model *M-resolution.*

[2]Probably 0.5-2 times the size of the resolution cell.

5.1.3.2: Model definitions incorporating considerations of scene components

At a low level, scene models can be considered as either *discrete* or *continuous*. In the former case, the scene is considered to be made up of two or more different types of object, each of which interacts in a unique way with the energy impinging upon it. For this reason, it is assumed that detectable boundaries exist in the spatial pattern of flux exiting from the scene; hence, it may be possible to identify the objects in the scene, given suitable sensor resolution. In this study, the concept of a discrete model is most appropriate, since in the image we are able to distinguish between features at the sampling scale of the sensor.

Continuous models consider the spatial variation of flux, as measured in the image, to be continuous; while this is unrealistic when considering natural surfaces at all scales, for images where the scene objects are much smaller than the sensor resolution cell it may be a suitable assumption to treat the model as continuous. For example, atmospheric models which consider the interaction of gases with incoming radiation could be considered as discrete models (they are made up of different gaseous molecules) but when allowing for the scale of spatial variation they are more straightforward to treat as continuous.

A *simple* model is one which considers the scene to consist of one class of *element* (or type of object) partially obscuring another, spatially continuous or homogeneous, element, termed the *background. Complex* models assume that more than one class of element exist in the scene. In mono-cultivation, however, this is an unnecessary concept, and we can consider the parcels in the scene to be modelled adequately using the concept of a simple model.

*Nested* models are useful when examining the composition of objects at different scales (5.1.1 above). For example, a cultivated field fits the structure of a simple, discrete model; it consists of a single vegetative species, (partially) obscuring a continuous soil background. But, at increasingly higher scales of examination, the vegetation, although predominantly barley or wheat, could include weeds, the crop is systematically arranged in rows, each plant is also regularly spaced and identifiable as an object, and comprised of physically unique objects (leaves, stalks,

ears) which are capable of having identifiable interactions with irradiant energy fluxes. The soil substrate, too, could breakdown further to stones and soil, moisture differences, mineral discontinuities etc. The structure of canopy models at most levels, therefore, are best described by the concept of a nested model.

## 5.1.4: Testing the effect of spatial resolution and scene structure on the spatial variance of images

### 5.1.4.1: Literature background and tests using synthesised images

Townshend (1981) concluded that increasing spatial resolutions did not necessarily equate to improved classification accuracies, the reason being that increased within-class variance diminishes the ability of spectral algorithms to distinguish between classes (Woodcock and Strahler 1987). Thus while increased spatial sampling frequencies will reduce the effects of adjacent parcels of dissimilar cover types, they will also reveal **greater heterogeneity within each parcel.**

Strahler *et al.* (1986) and Woodcock and Strahler (1987) have also examined the issue of scale on remotely sensed imagery. In the latter paper, *simulated* images of a sparse forest, made up of non-overlapping canopies generated using a simplified Li-Strahler conifer forest canopy model[3], were assessed for their local variance at differing scales of measurement. The results indicated that variance peaked when the sampling interval was 0.5 to 0.75 that of the size of the objects within the scene. But in their experiment, as the sampling interval increased, the scale of the *objects* or elements remained constant, i.e. it did not progress from tree, to branch, to leaf etc. Thus the spectral definition of an entity remained intact throughout the experiment, and the complications caused by the constant need to redefine an "entity", as is the case in real scenes, were not introduced.

---

[3]This treats conifers as cones casting shadows on a contrasting background; the scale at which the model operates is essentially at the level of individual tree scale, since no account is made of variations in canopy or background structure. (Li and Strahler, 1985, 1986.)

In reality, therefore, variance within an image is complex interaction of sensor resolution, or more precisely size of ground resolution elements, and the scale and distribution of the objects that make up the scene. Scene element scale is not just determined by the physical dimension of the element, but also by the spectral contrast between the element and the background. This will vary from one region of the electromagnetic spectrum to another, as is shown with the response of different cover types in this study to different wavebands.

The second factor, distribution of objects within the scene, is also important, especially if there is some systematic arrangement (at the scale of the GRE) that may bias the spectral response of individual scene element. A natural forest acts as a good example; it is made up of trees (which are made up of leaves, branches, trunk and gaps) and understorey (grass {leaves, stalks}, soil, and litter), both of which (and all of their composite components) can be sunlit or in shadow. We can consider these two major components (tree, understorey) to be spectrally distinguishable from each other. However, if we consider the examination of this scene at the scale of the *tree*, these components are systematically arranged to form trees, and understorey. Assuming a GRE somewhat smaller than the tree (say at the scale of the Nyquist[4] frequency or slightly smaller), then it is likely that a pixel in our image will represent either "tree" or "understorey" - because of the systematic arrangement of the components in the scene - and image variance will be relatively high, since adjacent pixels will represent different spectral classes. But at smaller image scales, i.e. where the GRE is much larger than a tree, approaching the size of or larger than the average spatial period between trees, and the distribution of components is no longer systematic, image variance would be reduced.

Woodcock and Strahler (1987) considered the sequence of scene elements with reference to sparsely-stocked Pine forest (*Pinus Jeffreyi* and *P. Ponderosa*). They anticipated a peak of image variance at image scales smaller[5] than tree scale due

---

[4]The Nyquist sampling theorem indicates that the sampling frequency must be double the frequency of the spatial variation in the scene for it to be resolved in the image - in practice, higher sampling frequencies are preferable. (Slater, 1980)

[5]That is, for a GRE between 20 and 100m.

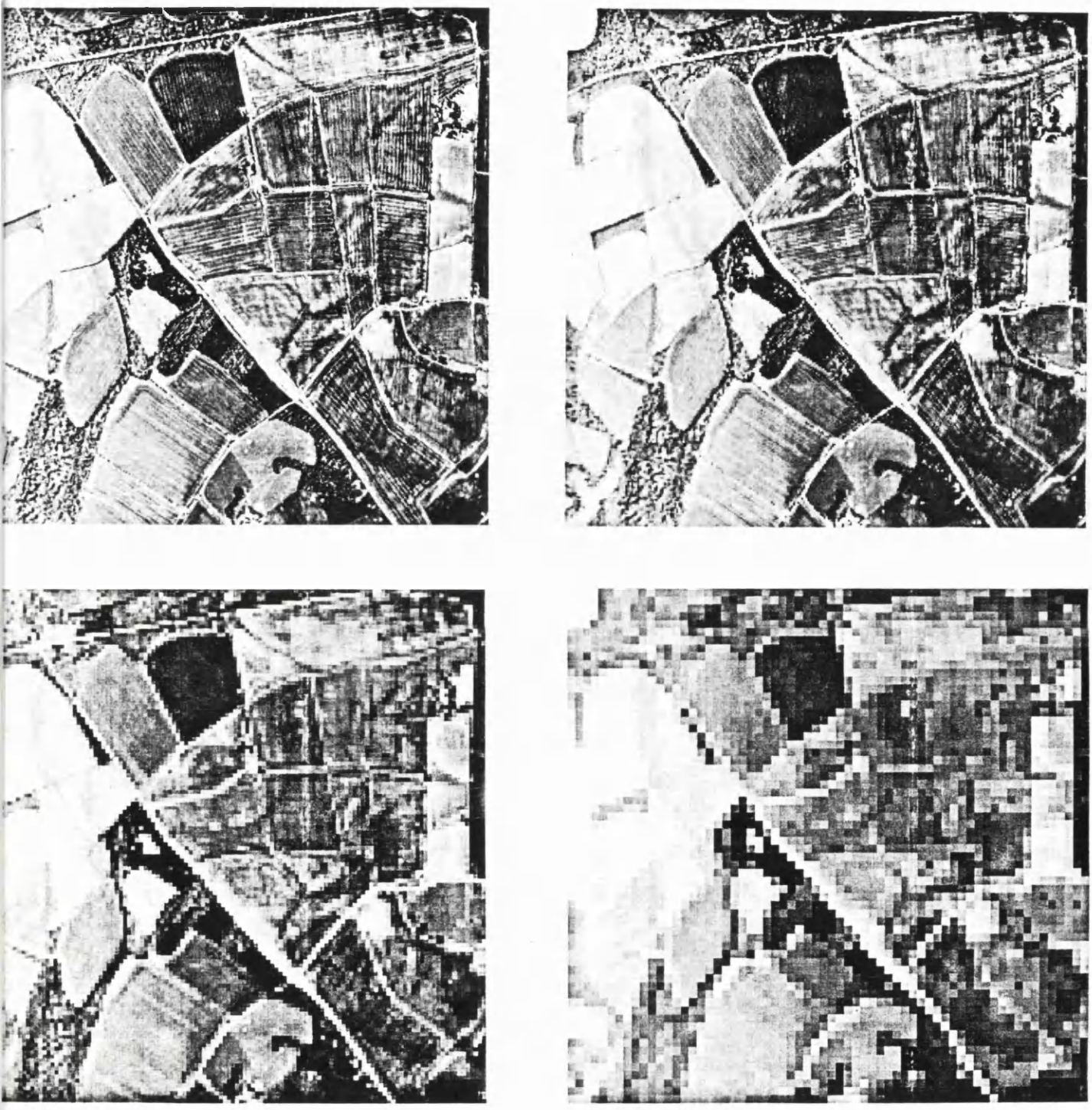

Figure 5.2: ATM subscene at four (nominal) spatial resolutions: 5m (top right), 10m (top left), 20m (bottom left) and 40m (bottom right).

to the systematic clustering of trees in "stands". They found that because stand size varied widely there was not one size class dominant enough to generate such a peak. However, it is apparent that peaks could occur in some scenes, either where stands have a narrow size range or where the trees are arranged systematically, such as in a managed forest. Examples of repetitive or cyclic measures of spatial variance of different scales can be observed in the data presented by Atkinson and Danson (1988).

5.1.4.2: Method

ATM image data for the Bemborough study site were examined to analyse the spatial variance of data acquired by this sensor, and to see if they fitted the expected trends reported in the literature. Examination of the variance of individual fields has already been made, and discussed in earlier sections (4.1.1); in this instance the images were analysed to see if any "peaks" in variance were evident, as reported by Woodcock and Strahler (1987). In addition, thereby, an estimate could be made of the spatial dimensions of the phenomena causing such an effect.

Bands 5 (red), 9 and 10 (MIR) were chosen for evaluation, although only the results for band 5 are presented here[6]. It was noted from section 4.1.1 that these bands show the typical relationship between view angle and image variance. Figure 5.2 is a laserprint of the section of the image used in this experiment. The spatial dimensions of the image are 512x512 pixels, at a nominal GRE of 5x5 metres at nadir. Individual fields can be seen clearly, and a number of different cover types identified.

The effect of lower sensor spatial resolution has been simulated by the simple process of averaging groups of 2x2 pixels, to form a single value representing twice the area in the original image. This technique does not take into account the point spread function[7] of the sensor, or the effect of differences in the signal-to-

[6]Bands ATM9 and 10 also showed similar results in this experiment.

[7]Not available for the ATM scanner used by NERC

Figure 5.3: Laser print of SD (Woodcock method) filtered 5m resolution subscene.

Figure 5.4: Laser print of SD (Woodcock method) filtered 10m resolution subscene.

-noise ratio at different spatial resolutions (Townshend, 1981). It is easy to implement, however, and the same technique has been used by Woodcock and Strahler (1987) and indeed by Townshend (Townshend and Justice, 1989). Thus it is a useful technique for the analysis of the relationship between variance and spatial resolution for a particular image, although the extrapolation of the results derived from these data, to other scenes and sensors, should only be made with caution.

5.1.4.3: Results

Figure 5.3 shows the result of SD filtering, using the standard 3x3 kernel, of the original image. Bright values indicate high local variance. Obvious marked contrast exists on roads and other distinct boundaries, such as between fields (hedgerows) and other cover types exhibiting spectral contrast, as would be expected. Within fields of higher percentage cover, much of the row structure caused by the tramlines is apparent, as well as some aliasing[8]. There is some evidence to show that for certain field orientations, row structure in the image is better preserved. Fields with rows parallel to the scanline (left to right in the image) show a better patterned row structure than those oriented perpendicular to the scanline. This may be explained by the increased oversampling between scan lines, as compared to the across-track direction, on ATM data.

The woodland and pasture areas are of particular interest, exhibiting high and low spatial variance, respectively. These results confirm some of the findings of Woodcock and Strahler (1987). In the bare soil parcels, highly complicated structural patterns are visible that are not distinguishable on the original (digital) image. Of particular significance is the division down the centre of the 'D' shaped

[8]Aliasing is the interference pattern caused by the interaction of the spatial variation of features in the scene and the sampling pattern of the sensor. It is usually manifested in the image as a periodic pattern which is of lower frequency than the true scene spatial frequency.

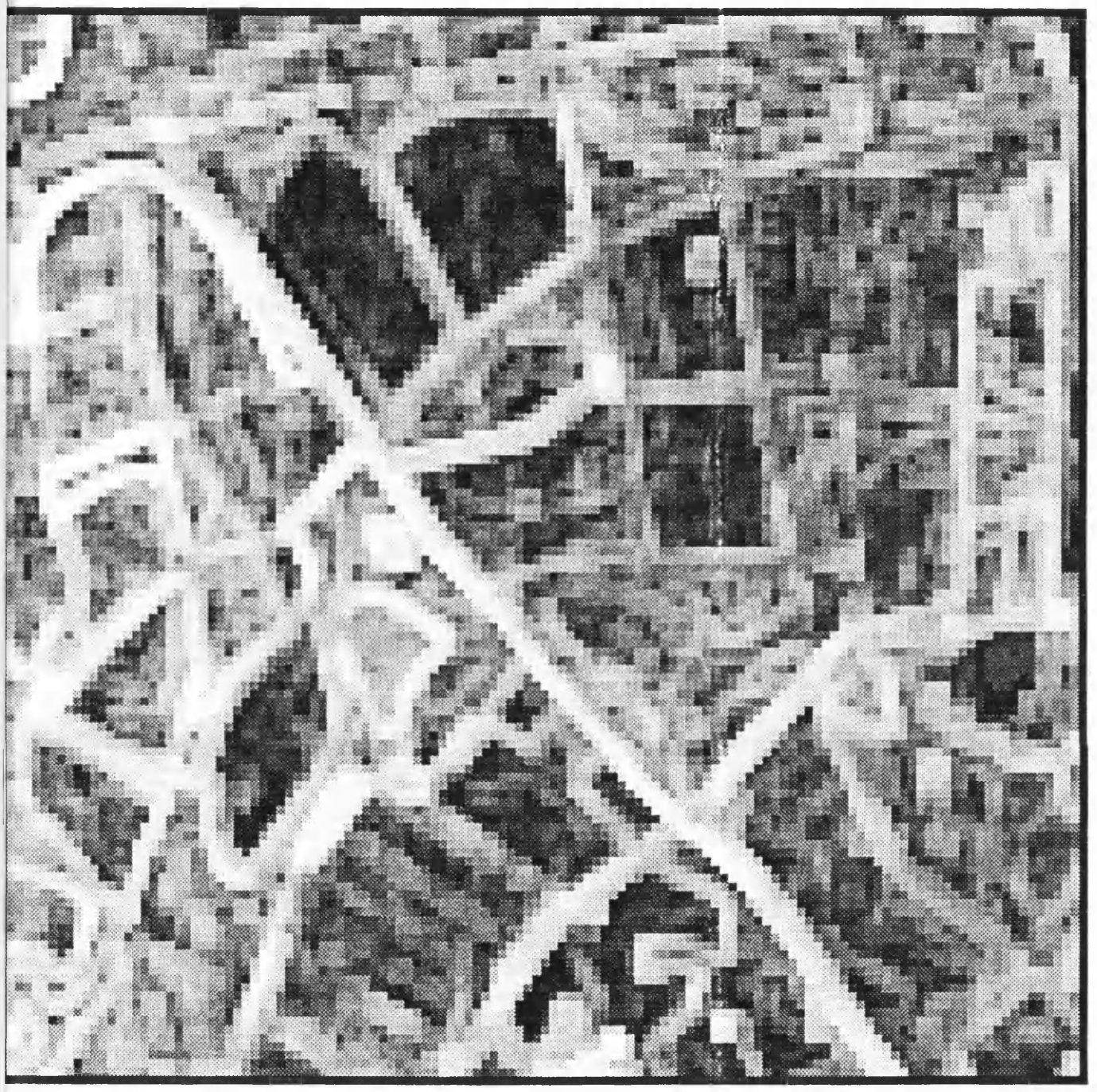

Figure 5.5: Laser print of SD (Woodcock method) filtered 20m resolution subscene.

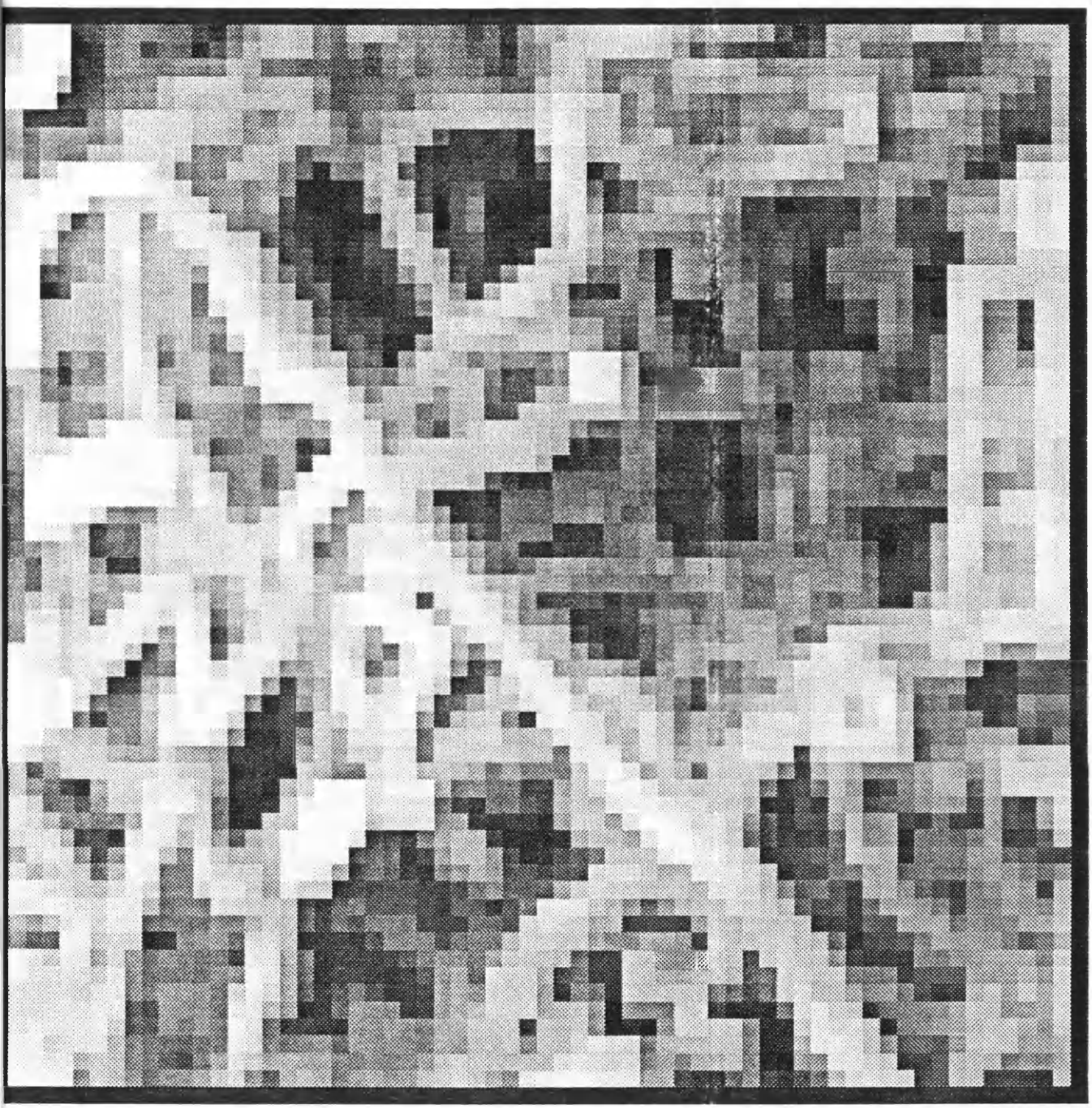

Figure 5.6: Laser print of SD (Woodcock method) filtered 40m resolution subscene. Note how this image begins to resemble the original image as the spatial resolution of the sensor approaches the size of the objects (fields are increasingly dominant).

field[9] in the top left corner of the image, visible on figure 5.2 as a tonal difference in soil colour. This boundary follows that of a geological fault line, and separates two slightly different soil types overlying similar oolitic limestones (see section 3.1).

Figures 5.4 to 5.6 show a continued decrease in complexity of variance for most cover types with further degradation of the image resolution. By degrading spatial resolution to 20x20m (figure 5.5), row structure, whether direct or caused by tramlines, is not evident in any field, bar one (Big Ground, field 2 on figure 3.2, highlighted on figure 5.5). This implies a row structure of higher period than in other fields, or a more pronounced aliasing produced by the spatial resolution of the sensor and the scene variance interacting. The structure of variation in most fields, in the simulated 20x20m image, does not appear to be related directly to the tramline structure. Significant variance, however, is still evident in most fields.

**Table 5.1: Aggregate variance, fields 18 and 2**

| Field 18 | | | | Field 2 | | |
|---|---|---|---|---|---|---|
| Res[n] | Mean | SD | Pop[n] | Mean | SD | Pop[n] |
| 5m | 57.024 | 3.110 | 3775 | 67.617 | 4.104 | 6992 |
| 10m | 56.630 | 2.844 | 846 | 67.940 | 3.783 | 1608 |
| 20m | 56.940 | 2.674 | 200 | 67.788 | 3.726 | 400 |
| 40m | 56.157 | 1.735 | 57 | 67.675 | 3.145 | 74 |

Table 5.1 and figure 5.7 show the change in variance, resulting from a degradation of image resolution, obtained by calculating the SD of DN for two fields, both winter barley. A near-linear relation between "resolution" and SD can be observed. While these results can indicate the strength of the relationship, they are not entirely reliable since only four pairs of data are available. However, it is not

[9]D Ground and Long Ground, fields 30 and 31 on the sketch map at end of document.

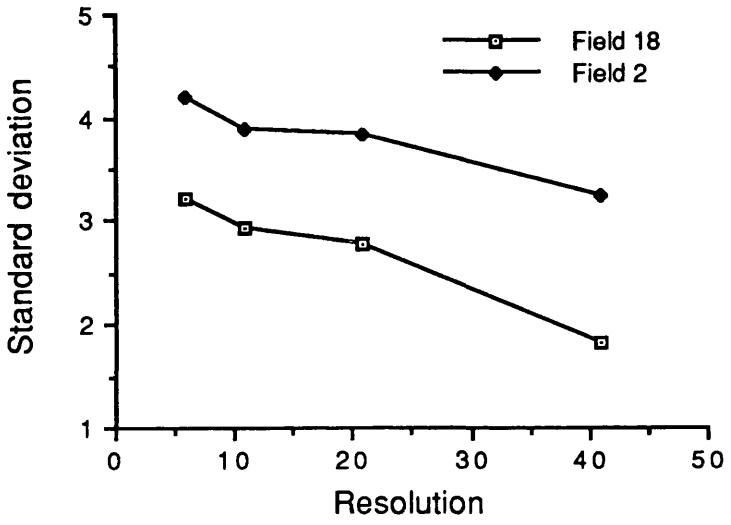


Figure 5.7: SD of the DN within fields 18 and 2

possible to degrade the imagery further, because of the increasing influence of integration of boundaries and adjacent parcels, producing "mixels", would also result in increased variance.

No peaks of the kind reported by Woodcock and Strahler occur. This may be for two reasons. First, a peak in variance may occur at a resolution higher than that included in this dataset, i.e. it results from a scene element of period less than 5m. Second, defining scene variance at any particular scale is, in reality, impossible since the scale of the objects within the scene is continuously variable (see 5.1.1 and 5.1.4).

**Table 5.2: Average local variance, fields 20, 18, 29, 2, and whole image**

| | Full resolution (5m) | | Degraded (10m) | | Degraded (20m) | |
|---|---|---|---|---|---|---|
| Field | Mean SD | {SD}[10] | Mean SD | {SD} | Mean SD | {SD} |
| 20 | 11.50 | 5.286 | 7.84 | 2.7 | 6.88 | 2.436 |
| 18 | 9.04 | 6.826 | 10.79 | 9.0 | 10.79 | 8.127 |
| 29 | 9.99 | 4.258 | 9.31 | 4.4 | 8.02 | 4.382 |
| 2 | 13.04 | 4.844 | 12.69 | 4.4 | 12.15 | 4.319 |
| whole | 28.32 | 31.85 | 33.15 | 34.9 | 37.45 | 35.89 |

Table 5.2 and figure 5.8 describe local variance calculated by the Woodcock SD method for four fields (all winter barley) and the 512x512 scene containing these fields as a whole. The "mean" value in the table refers to the mean of the SD values for every pixel in the SD filtered images. The SD value in table 5.2 refers to the distribution of these values. The sample population, in fact, will not be normally distributed, since the program calculates positive values of variance; it is more likely that the data will approximate a Poisson distribution. This will also be distorted because the filtered image is scaled for display, so areas of high variance are represented as grey level 255. For restricted parcels where variance is relatively

[10]Note: this is SD of the values in the SD image.

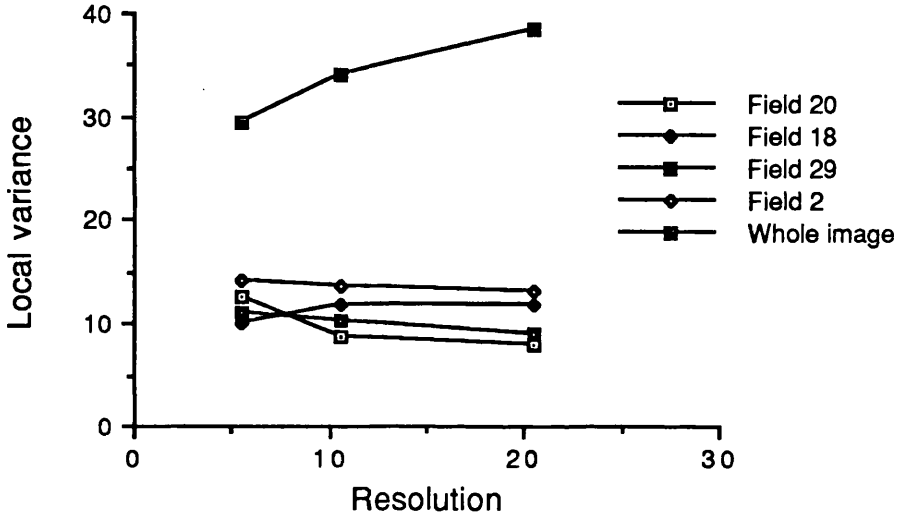


Figure 5.8: Variance measured by the Woodcock method for fields 20, 18, 29, 2 and the whole subscene.

low, however, this will not be a difficulty, but should be taken into account when considering the significance of the SD of these values. This, and the fact that SD is correlated to the mean value of the DN in the original image, is also an example of why such data are difficult to interpret.

Field 20 exhibits high variance initially, at 5m resolution, falling to half its original value by 20m degradation. However for fields 2 and 29, little decrease in mean SD is observed, nor is there much change in the distribution of these values (SD). The pattern of spatial variance in the sequence of images is maintained. Field 18 shows a slight increase in variance, but this is caused by a patch in the parcel[11] which becomes increasingly significant on the sequence of images. For the image as a whole, variance *increases* as the images are degraded. This is understandable since the dominant features in the image are a tessellation of parcels, divided by distinct, narrow boundaries - indicated in the SD images as high frequency, variable features - which become more significant as the number of pixels in the image decreases (as a function of degradation). As the resolution cell size approaches that of the field, there is a suggestion that peaks in variance do occur, as identified by Woodcock and Strahler.

### 5.1.5: Conclusions - modelling scene spatial variance for ATM imagery

The major criticism of the concepts outlined by Strahler *et al.* (1986) is that any scene could be considered to fit any of the *H*, *M*, or *L*-resolution scene models simultaneously, as the discussion in 5.1.1 implies. The data presented here can be modelled as *H*-resolution if fields are described as entities, *L*-resolution if the elements are treated as individual plant canopies, and probably *M*-resolution if the row structure of the crop is defined as the unit in the model. Examination of the relationship of local variance per field and as a whole image (figure 5.8) reveals quite simply that within a field, local variance is probably similar at all scales, once *H*-resolution has been attained; and that for the image as a whole, if a systematic structure is present (fields, boundaries) then the important factor is the

[11]Probably water-logging retarding plant development

proportion of boundary pixels as a fraction of the whole image. This will achieve a maximum depending upon the spatial frequency and distribution of boundaries, and thus the topology of the land cover units making up the landscape (Townshend, 1981).

Figure 5.7 illustrates these conclusions effectively. Reduced within-class variance is to be expected with decreasing resolution. This is supported by Townshend's work (1981) on resolution and classification accuracies. Local variance, however, can increase with degraded resolution (for this dataset) so far as this is tested here. To an extent, this confirms observations by other workers (Woodcock and Strahler 1987), with the caveat that their conclusions are far from complete, since scant consideration is made of scales outside an artificial minimum definition (say, a tree as an entity or finite element), and do not consider images where the cover types are not conceptually infinite in extent (i.e. the images are of one class only). This limits the complexity apparent in more normal images, where nested models should be applied to describe any object in the scene. The effect of reducing image scale on these images is likely to enhance a cyclic pattern of alternating spatial autocorrelation and variance, depending upon the scale and configuration of features within the scene.

Finally, it has been shown (with reference to section 4.1.1 and 5.3) that the effect of degraded spatial resolution on image variance is far outweighed by other geometric effects of off-nadir viewing by the ATM scanner - namely, the enhanced autocorrelation caused by the increased overlap between adjacent GREs, and view geometry affecting the canopy components in view, as well as the larger area of the GRE, at the swath edges (section 4.1.1).

## 5.2: Alternative strategies: Coefficient of Variation

### 5.2.1: Introduction

In Chapter 3, the effect of view angle upon image variance was hypothesised; Chapter 4 illustrates this effect, showing that it is a positive manifestation of view

angle; section 5.1 explains the effect of scale of elements in a scene and image variance in greater detail. In this section the method of evaluating image variance using the coefficient of variation (CV) is described, sampling strategies outlined, and regression analysis explained.

### 5.2.2: Method

Data from several overlapping flightlines, providing up to six views of any area on the ground, were used to calculate image variance for seven different parcels. In addition, two further parcels were chosen from a second dataset (Kay and Barnsley, 1989), a complete sugar beet canopy, and an apple orchard planted in a regular lattice, to provide two extremes of canopy architecture not present in the main study site. The view angle for each sample area was taken to be that to the centre of the parcel on the respective flightline. Parcels in the raw image were analysed by calculating the mean and standard deviation (SD) of DN within each area of apparent homogeneity of cover. The coefficient of variation (CV) was calculated for each parcel (see sec. 4.1.1), to provide five or six pairs of view angle and CV, between which the degree of correlation was tested statistically using linear and non-linear regression analysis (Croxton *et al.*, 1967). The results of these analyses were tested for statistical significance using the Student t-test and the F-test. These two tests take into account sample size in the calculation of degrees of freedom for the sample, in this case between 2 and 4.

#### 5.2.2.1 Sampling

Parcels were identified in the images by visual inspection and knowledge of field boundaries acquired from ground observations, aerial photography, farm maps and 1:10,000 OS mapping[12]. In most instances, these did equate to fields in the scene,

---

[12]It could be a valid strategy to use automated image segmentation techniques, particularly where image variance (as a surrogate perhaps for texture, and implicitly cover type and characteristics) was used in the algorithm. This would enable some of the assumptions made above (section 5.1.2) concerning distributions

(continued...)

except for the samples of sugar beet and apple orchard, which were a standardised 24x24 pixels. Headlands and field boundaries, where inconsistent applications of fertilizer, pesticides and regulators, would have irregular effects upon crop development, were excluded as a result of this method. "Mixels", pixels containing boundary elements or an unpredictable number of model elements, were also excluded by this process.

Each parcel contained, in general, between four and five thousand pixels. The number varied, however, between flightlines because the geometric properties of each image varied as a function of flight parameters (height, speed, yaw etc.; see section 3.3.3). The data collected included the number of DN, minimum and maximum values in each sample population. Mean, median, standard deviation and CV values were calculated for all ten bands used in this study (ATM1 to ATM10).

5.2.2.2 Regression analysis

After visual inspection of the data, paired values of view angle and CV were analysed. Three tests were applied to each dataset. First, the data were tested for linear fit to a regression model of the form:

$$y = a + bx \qquad \text{Equation 5.1}$$

and the t-test value for significance of fit calculated. Second, the data were analysed for the fit of a non-linear ($2^{nd}$-order polynomial) regression model, of the type:

$$y = a + bx + cx^2 \qquad \text{Eq. 5.2}$$

---

[12](...continued)
of DN within a parcel, and how this affects variance, to be applied rigorously.

and the F-test value[13] for overall significance of the regression line computed. Third, the significance of the improvement in fit of the use of the non-linear regression equation was tested, using the t-test - but note that non-linear regression will **always** produce a result as good as, or more likely better than, that of linear regression. It is this result that is often of greatest interest in this study.

The coefficients for the equations, and the results of the various tests are presented in tables 5.3 to 5.11. Figures 5.9 to 5.17 illustrate the fit of the regression lines to the CV data for bands 5, 9 and 10. By the perspicacious inspection of these coefficients and their associated significance test results, it is possible in certain cases to deduce information concerning the nature of the cover type.

Notes to tables 5.3-5.11: ns= not significant at 90%; nt=not testable; *a*, *b*, and *c* are coefficients of the regression equations; $r^2$ is a measure of explained variance; f-test is a comparable significance test to the t-test.

**Table 5.3: Field 30 - linear and non-linear regression of view angle and coefficient of variation**

| Band | 1 | 2 | 3 | 4 | 5 | 6 | 7 | 8 | 9 | 10 |
|---|---|---|---|---|---|---|---|---|---|---|
| Linear Regression | | | | | | | | | | |
| a | 4.65 | 3.49 | 4.57 | 4.26 | 5.00 | 5.12 | 5.95 | 4.91 | 5.51 | 5.38 |
| b | -0.026 | -0.001 | 0.004 | 0.016 | 0.010 | -0.017 | -0.036 | -0.028 | -0.008 | 0.010 |
| $r^2$ | 0.897 | 0.047 | 0.209 | 0.52 | 0.224 | 0.677 | 0.806 | 0.774 | 0.312 | 0.191 |
| t-test | 98% | 20% | 50% | 80% | 50% | 90% | 95% | 95% | 60% | 50% |
| Non-linear Regression | | | | | | | | | | |
| a | 4.85 | 3.51 | 4.42 | 3.95 | 4.62 | 5.17 | 5.94 | 4.91 | 5.31 | 4.95 |
| b | -0.015 | 0.000 | -0.004 | -0.002 | -0.011 | -0.014 | -0.037 | -0.028 | -0.019 | -0.014 |
| c | -0.001 | 0.000 | 0.000 | 0.001 | 0.001 | 0.000 | 0.000 | 0.000 | 0.001 | 0.001 |
| $r^2$ | 0.977 | 0.075 | 0.635 | 0.823 | 0.691 | 0.687 | 0.81 | 0.774 | 0.584 | 0.708 |
| f-test | 95% | ns | ns | ns | ns | ns | ns | ns | ns | ns |
| Significance of use of non-linear regression | | | | | | | | | | |
| t-test | 80% | <20% | <75% | <80% | <80% | <20% | <<10% | <<10% | 70% | 80% |

[13]The F-test is a comparable test to the Student T-test, but simpler to calculate (Croxton *et al.*, 1967).

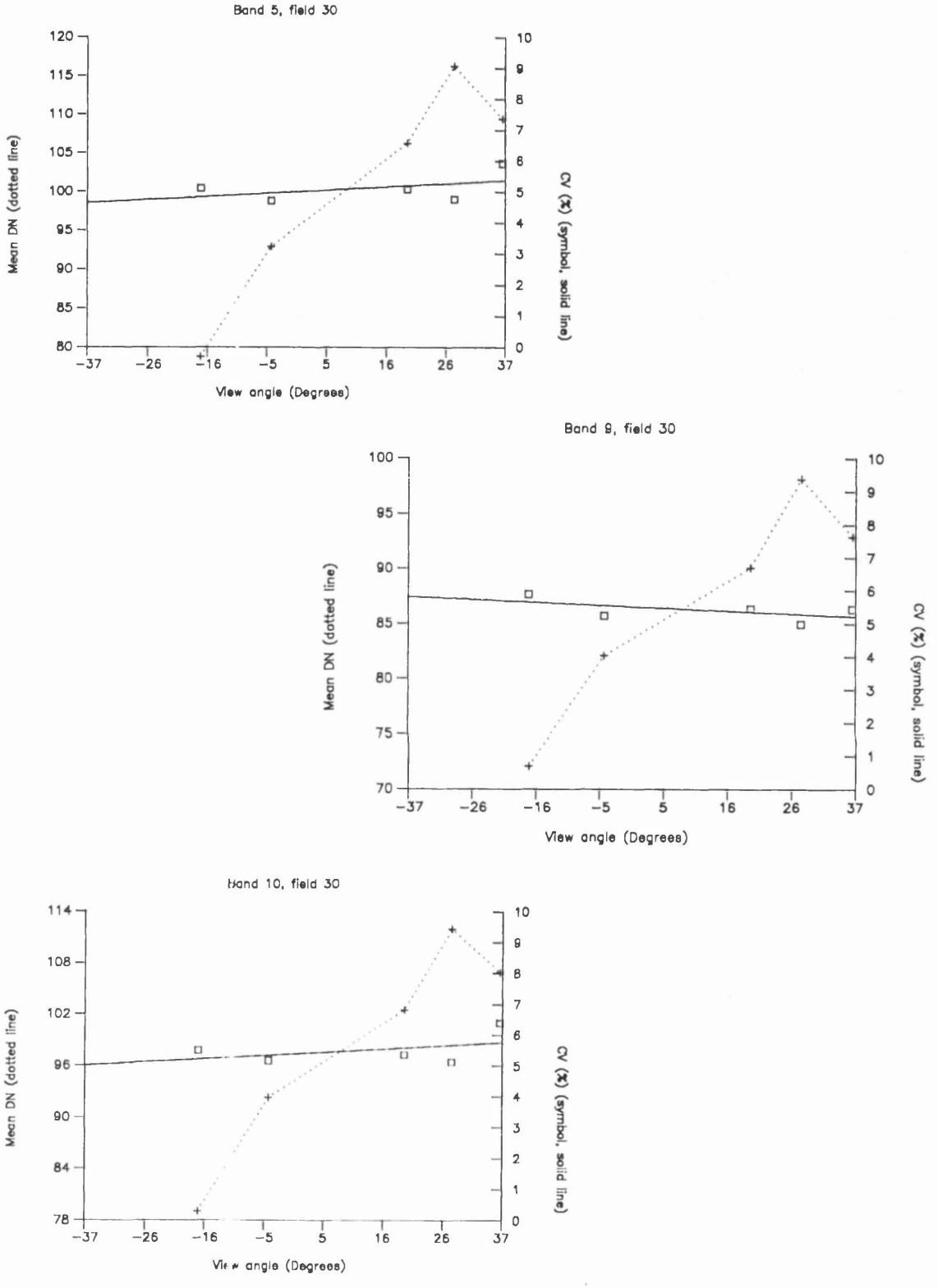


Figure 5.9: Field 30 regression analysis, bands 5, 9 and 10. Mean DN dotted line, CV symbols, solid line gives regression equation fit. Negative view angles are up-sun.

~ bare soil

**Table 5.4: Field 29 - linear and non-linear regression of view angle and coefficient of variation**

| Band | 1 | 2 | 3 | 4 | 5 | 6 | 7 | 8 | 9 | 10 |
|---|---|---|---|---|---|---|---|---|---|---|
| Linear Regression | | | | | | | | | | |
| a | 4.69 | 3.26 | 3.31 | 3.52 | 4.07 | 2.84 | 4.035 | 3.85 | 5.40 | 8.74 |
| b | 0.000 | 0.022 | 0.019 | 0.011 | 0.004 | 0.008 | -0.012 | -0.018 | -0.003 | 0.014 |
| $r^2$ | 0.000 | 0.132 | 0.155 | 0.108 | 0.008 | 0.310 | 0.257 | 0.492 | 0.010 | 0.080 |
| t-test | nt | 40% | 40% | 40% | 10% | 60% | 60% | 80% | 10% | 30% |
| Non-linear Regression | | | | | | | | | | |
| a | 5.35 | 4.28 | 4.47 | 4.42 | 5.42 | 2.65 | 3.43 | 3.28 | 6.45 | 10.05 |
| b | -0.003 | 0.016 | 0.013 | 0.006 | -0.003 | 0.009 | -0.008 | -0.015 | -0.009 | 0.006 |
| c | -0.001 | -0.002 | -0.003 | -0.002 | -0.003 | 0.000 | 0.001 | 0.001 | -0.002 | -0.003 |
| $r^2$ | 0.293 | 0.431 | 0.751 | 0.856 | 0.924 | 0.487 | 0.998 | 0.983 | 0.983 | 0.845 |
| f-test | ns | ns | ns | ns | 90% | ns | 99% | 97.5% | 97.5% | ns |
| Significance of use of non-linear regression | | | | | | | | | | |
| t-test | 50% | 50% | 80% | 90% | 95% | 50% | 99.5% | 98% | 99% | 90% |

**Table 5.5: Small stand, mixed woodland - linear and non-linear regression of view angle and coefficient of variation**

| Band | 1 | 2 | 3 | 4 | 5 | 6 | 7 | 8 | 9 | 10 |
|---|---|---|---|---|---|---|---|---|---|---|
| Linear Regression | | | | | | | | | | |
| a | 4.75 | 3.07 | 4.64 | 3.85 | 5.55 | 9.60 | 11.23 | 10.02 | 9.87 | 10.43 |
| b | -0.011 | 0.001 | 0.009 | 0.011 | 0.008 | 0.000 | -0.021 | -0.034 | 0.000 | 0.025 |
| $r^2$ | 0.248 | 0.001 | 0.051 | 0.117 | 0.023 | 0.000 | 0.070 | 0.188 | 0.000 | 0.113 |
| t-test | 50% | nt | 20 | 40% | 10% | nt | 30% | 50% | nt | 40% |
| Non-linear Regression | | | | | | | | | | |
| a | 5.19 | 3.57 | 5.53 | 4.54 | 6.74 | 11.13 | 12.96 | 11.65 | 11.63 | 12.09 |
| b | -0.003 | 0.010 | 0.025 | 0.023 | 0.029 | 0.027 | 0.01 | -0.005 | 0.031 | 0.055 |
| c | -0.001 | -0.001 | -0.002 | -0.001 | -0.002 | -0.003 | -0.004 | -0.003 | -0.004 | -0.003 |
| $r^2$ | 0.964 | 0.924 | 0.969 | 0.982 | 0.976 | 0.959 | 0.967 | 0.985 | 0.997 | 0.994 |
| f-test | 95% | 90% | 95% | 97.5% | 97.5% | 95% | 95% | 97.5% | 99% | 90% |
| Significance of use of non-linear regression | | | | | | | | | | |
| t-test | 97.5% | 95% | 98% | 98% | 98% | 97.5% | 98% | 99% | 99.5% | 95% |

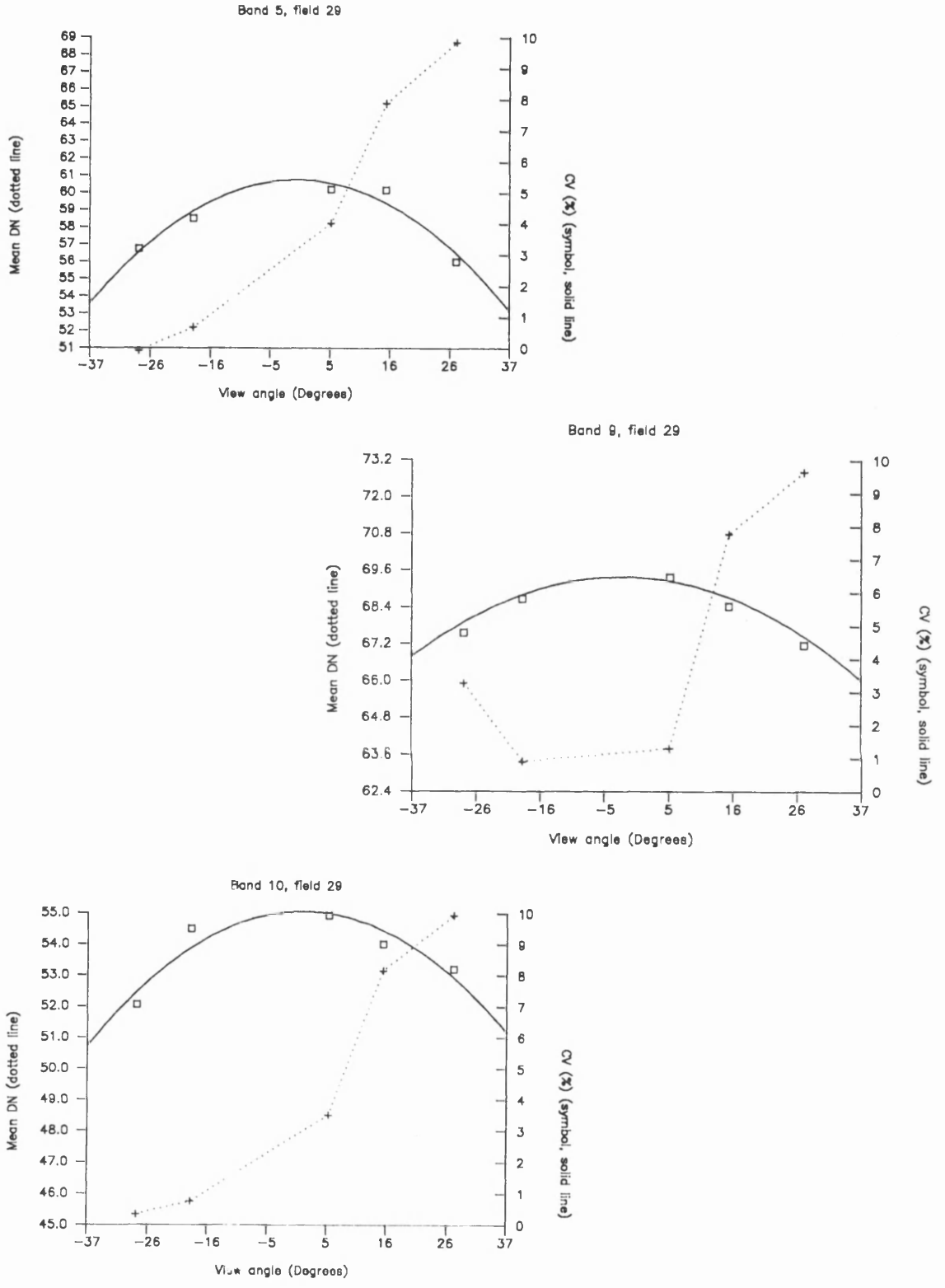


Figure 5.10: Field 29 regression analysis, bands 5, 9 and 10. Mean DN dotted line, CV symbols, solid line gives regression equation fit.

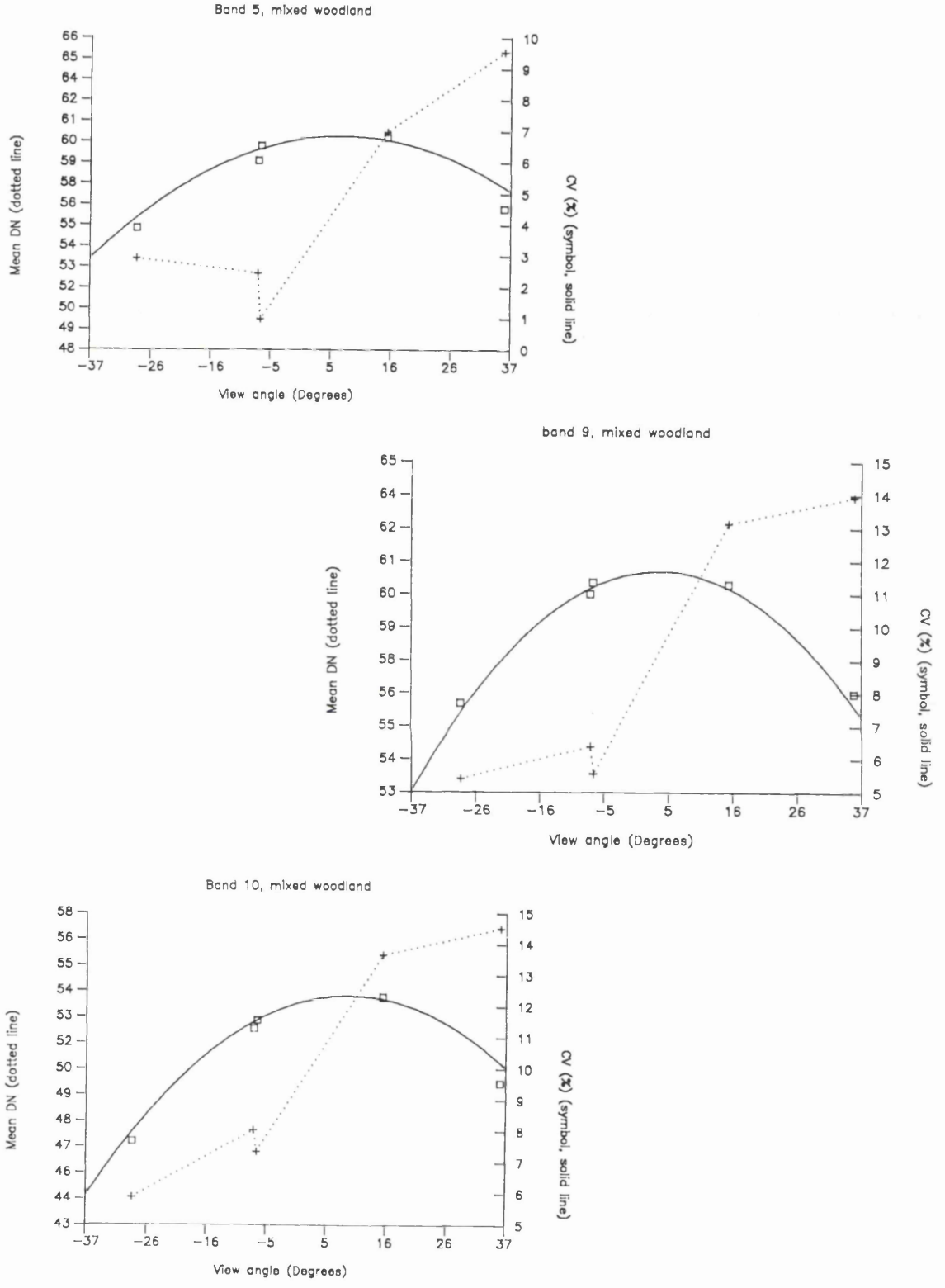


Figure 5.11: Small stand of mixed woodland, regression analysis bands 5, 9 and 10. Mean DN dotted line, CV symbols, solid line gives regression equation fit.

**Table 5.6: Field 21 - linear and non-linear regression of view angle and coefficient of variation**

| Band | 1 | 2 | 3 | 4 | 5 | 6 | 7 | 8 | 9 | 10 |
|---|---|---|---|---|---|---|---|---|---|---|
| Linear Regression | | | | | | | | | | |
| a | 4.86 | 4.04 | 4.58 | 5.90 | 6.92 | 5.14 | 7.30 | 6.26 | 7.82 | 13.20 |
| b | -0.019 | -0.015 | -0.004 | 0.012 | -0.019 | 0.008 | -0.014 | -0.022 | -0.006 | 0.009 |
| $r^2$ | 0.342 | 0.237 | 0.013 | 0.112 | 0.131 | 0.133 | 0.260 | 0.575 | 0.015 | 0.048 |
| t-test | 60% | 50% | 10% | 40% | 40% | 40% | 60% | 80% | 10% | 20% |
| Non-linear Regression | | | | | | | | | | |
| a | 5.38 | 4.60 | 5.35 | 6.64 | 8.01 | 5.10 | 6.95 | 5.94 | 8.86 | 14.06 |
| b | -0.011 | -0.007 | 0.007 | 0.023 | -0.003 | 0.007 | -0.019 | -0.027 | 0.010 | 0.022 |
| c | -0.001 | -0.001 | -0.002 | -0.002 | -0.002 | 0.000 | 0.001 | 0.001 | -0.002 | -0.002 |
| $r^2$ | 0.847 | 0.833 | 0.962 | 0.929 | 0.945 | 0.140 | 0.568 | 0.837 | 0.978 | 0.948 |
| f-test | ns | ns | 95% | 90% | 90% | ns | ns | ns | 97.5% | 90% |
| Significance of use of non-linear regression | | | | | | | | | | |
| t-test | 80% | 80% | 98% | 95% | 95% | nt | 60% | 75% | 98% | 95% |

**Table 5.7: Field 10 - linear and non-linear regression of view angle and coefficient of variation**

| Band | 1 | 2 | 3 | 4 | 5 | 6 | 7 | 8 | 9 | 10 |
|---|---|---|---|---|---|---|---|---|---|---|
| Linear Regression | | | | | | | | | | |
| a | 4.29 | 2.72 | 3.10 | 3.29 | 3.96 | 3.40 | 4.97 | 4.91 | 4.40 | 6.65 |
| b | -0.011 | 0.009 | 0.019 | 0.122 | 0.005 | 0.016 | -0.003 | -0.001 | 0.012 | 0.015 |
| $r^2$ | 0.181 | 0.084 | 0.281 | 0.192 | 0.017 | 0.388 | 0.010 | 0.051 | 0.080 | 0.068 |
| t-test | 60% | 40% | 70% | 60% | 20% | 80% | 10% | 30% | 40% | 30% |
| Non-linear Regression | | | | | | | | | | |
| a | 4.85 | 3.37 | 4.09 | 4.16 | 5.42 | 4.05 | 5.52 | 5.62 | 5.93 | 8.956 |
| b | -0.009 | 0.011 | 0.023 | 0.015 | 0.011 | 0.018 | -0.001 | -0.007 | 0.017 | 0.023 |
| c | -0.001 | -0.001 | -0.001 | -0.001 | -0.002 | -0.001 | -0.001 | -0.001 | -0.002 | -0.003 |
| $r^2$ | 0.475 | 0.372 | 0.704 | 0.763 | 0.747 | 0.787 | 0.168 | 0.232 | 0.874 | 0.970 |
| f-test | ns | ns | ns | ns | 90% | 90% | ns | ns | 95% | 99% |
| Significance of use of non-linear regression | | | | | | | | | | |
| t-test | 70% | 60% | 80% | 90% | 90% | 90% | 40% | 50% | 97.5% | 99.5% |

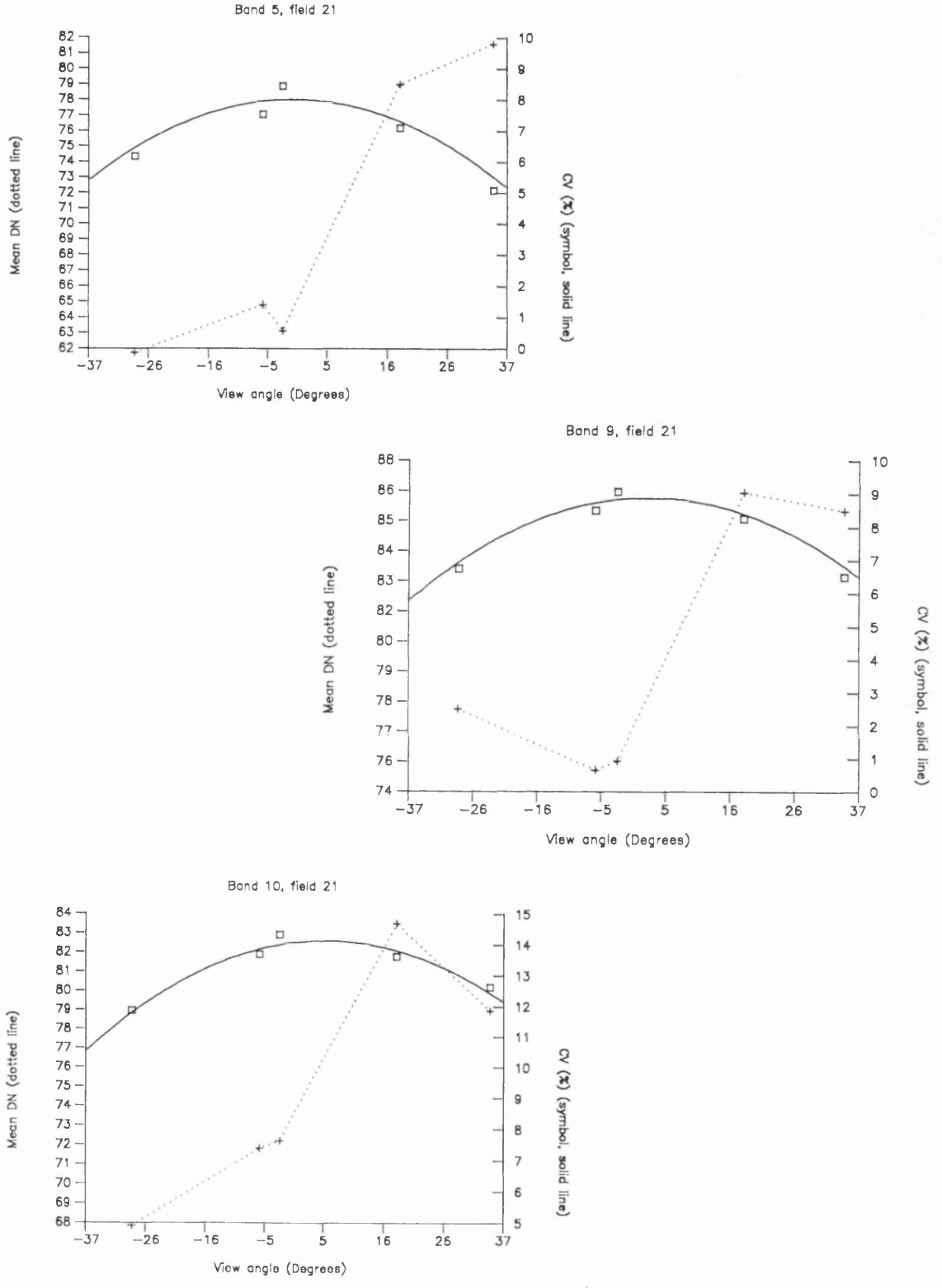


Figure 5.12: Field 21 regression analysis, bands 5, 9 and 10. Mean DN dotted line, CV symbols, solid line gives regression equation fit.

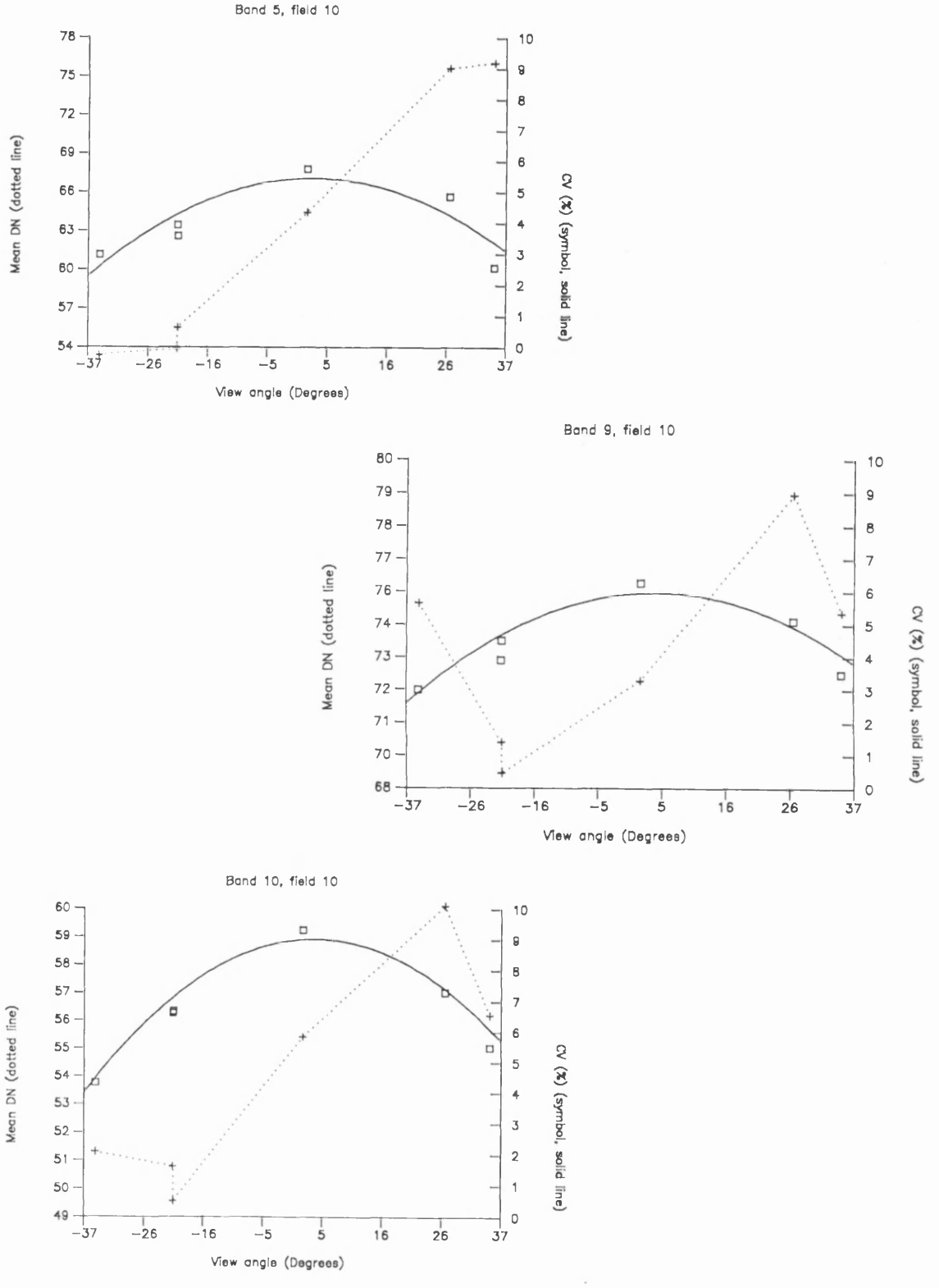


Figure 5.13: Field 10 regression analysis, bands 5, 9 and 10. Mean DN dotted line, CV symbols, solid line gives regression equation fit.

**Table 5.8: Field 3 - linear and non-linear regression of view angle and coefficient of variation**

| Band | 1 | 2 | 3 | 4 | 5 | 6 | 7 | 8 | 9 | 10 |
|---|---|---|---|---|---|---|---|---|---|---|
| Linear Regression | | | | | | | | | | |
| a | 3.83 | 1.69 | 1.49 | 1.42 | 1.52 | 1.99 | 2.55 | 2.43 | 2.65 | 2.43 |
| b | -0.007 | 0.012 | 0.003 | 0.009 | 0.009 | -0.004 | -0.009 | -0.011 | 0.009 | 0.012 |
| $r^2$ | 0.685 | 0.287 | 0.160 | 0.601 | 0.670 | 0.157 | 0.479 | 0.573 | 0.551 | 0.868 |
| t-test | 90% | 60% | 40% | 80% | 80% | 40% | 80% | 80% | 80% | 97.5% |
| Non-linear Regression | | | | | | | | | | |
| a | 3.845 | 1.29 | 1.34 | 1.29 | 1.43 | 2.02 | 2.65 | 2.57 | 2.75 | 2.51 |
| b | -0.007 | 0.024 | 0.007 | 0.013 | 0.011 | -0.005 | -0.012 | -0.015 | 0.006 | 0.011 |
| c | 0.000 | 0.001 | 0.000 | 0.000 | 0.000 | 0.000 | 0.000 | 0.000 | 0.000 | 0.000 |
| $r^2$ | 0.697 | 0.902 | 0.873 | 0.828 | 0.807 | 0.187 | 0.591 | 0.757 | 0.672 | 0.947 |
| f-test | ns | 90% | ns | ns | ns | ns | ns | ns | ns | 90% |
| Significance of use of non-linear regression | | | | | | | | | | |
| t-test | 10% | 95% | 90% | 75% | 60% | 10% | 40% | 60% | 50% | 75% |

**Table 5.9: Field 27 - linear and non-linear regression of view angle and coefficient of variation**

| Band | 1 | 2 | 3 | 4 | 5 | 6 | 7 | 8 | 9 | 10 |
|---|---|---|---|---|---|---|---|---|---|---|
| Linear Regression | | | | | | | | | | |
| a | 4.49 | 3.61 | 5.09 | 5.84 | 7.35 | 5.43 | 6.00 | 5.19 | 6.89 | 8.18 |
| b | -0.010 | 0.021 | 0.029 | 0.030 | 0.014 | -0.001 | -0.015 | -0.011 | 0.000 | 0.001 |
| $r^2$ | 0.605 | 0.738 | 0.853 | 0.968 | 0.883 | 0.004 | 0.523 | 0.879 | 0.017 | 0.053 |
| t-test | 80% | 90% | 97.5% | 99.5% | 98% | nt | 80% | 98% | 10% | 20% |
| Non-linear Regression | | | | | | | | | | |
| a | 4.73 | 3.79 | 5.26 | 5.91 | 7.39 | 5.59 | 5.94 | 5.21 | 6.90 | 8.16 |
| b | -0.007 | 0.023 | 0.025 | 0.031 | 0.015 | 0.001 | -0.016 | -0.011 | 0.000 | 0.001 |
| c | 0.000 | 0.000 | 0.000 | 0.000 | 0.000 | 0.000 | 0.000 | 0.000 | 0.000 | 0.000 |
| $r^2$ | 0.833 | 0.776 | 0.888 | 0.971 | 0.888 | 0.209 | 0.527 | 0.883 | 0.071 | 0.064 |
| f-test | ns | ns | ns | 95% | ns | ns | ns | ns | ns | ns |
| Significance of use of non-linear regression | | | | | | | | | | |
| t-test | 75% | 30% | 40% | 30% | 20% | 40% | nt | 10% | 20% | 10% |

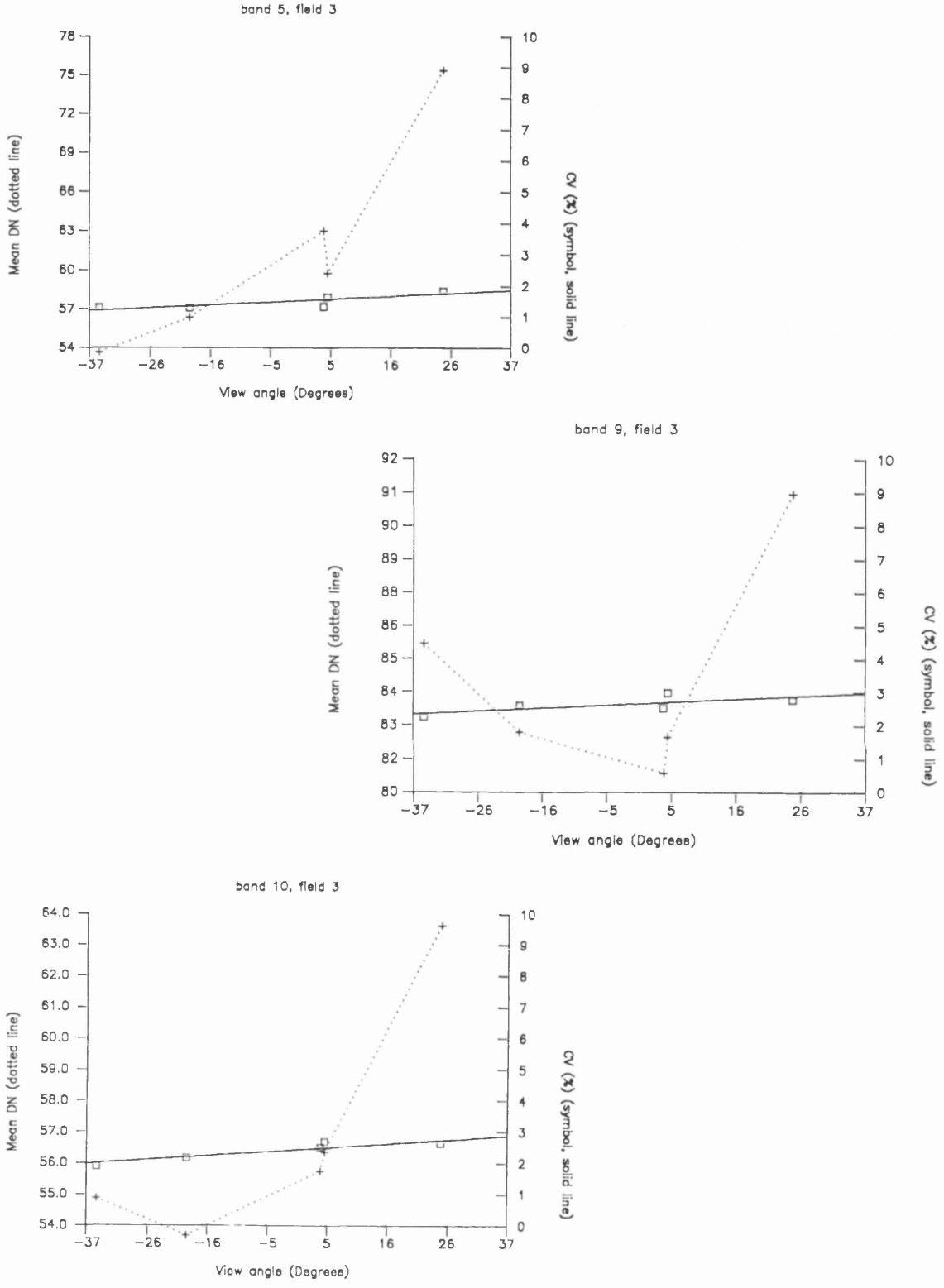


Figure 5.14: Field 3 regression analysis, bands 5, 9 and 10. Mean DN dotted line, CV symbols, solid line gives regression equation fit.

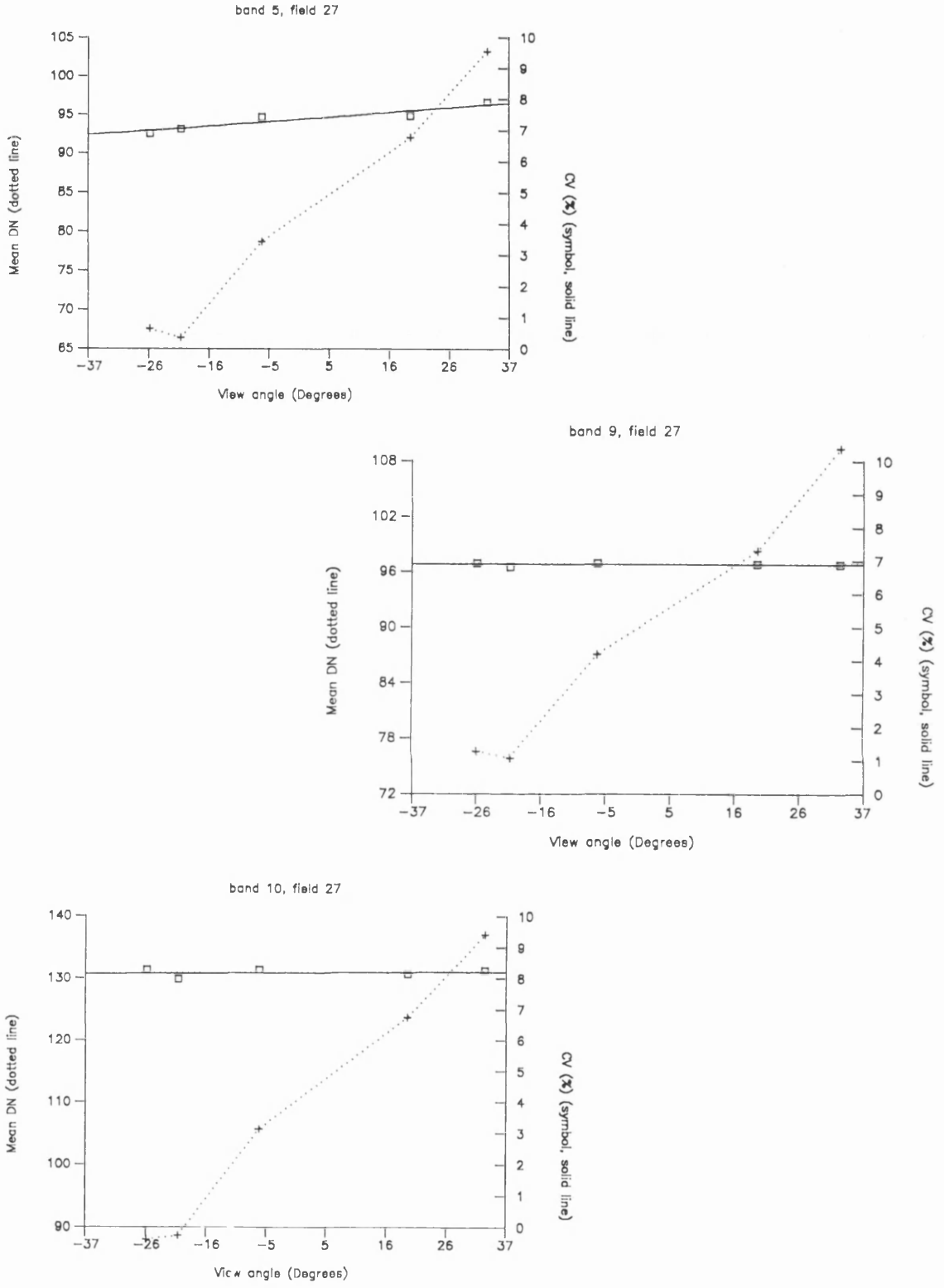


Figure 5:15: Field 27 regression analysis, bands 5, 9 and 10. Mean DN dotted line, CV symbols, solid line gives regression equation fit.

**Table 5.10: Sugar beet - linear and non-linear regression of view angle and coefficient of variation**

| Band | 1 | 2 | 3 | 4 | 5 | 6 | 7 | 8 | 9 | 10 |
|---|---|---|---|---|---|---|---|---|---|---|
| Linear Regression | | | | | | | | | | |
| a | 2.04 | 1.40 | 1.30 | 1.25 | 1.16 | 1.78 | 2.00 | 1.64 | 2.85 | 2.19 |
| b | -0.003 | -0.005 | 0.000 | 0.003 | 0.003 | -0.001 | 0.000 | 0.002 | -0.008 | 0.018 |
| $r^2$ | 0.107 | 0.058 | 0.000 | 0.051 | 0.052 | 0.012 | 0.004 | 0.336 | 0.692 | 0.744 |
| t-test | 40% | 30% | nt | 30% | 30% | 10% | nt | 75% | 90% | 95% |
| Non-linear Regression | | | | | | | | | | |
| a | 1.96 | 0.99 | 1.00 | 0.97 | 0.909 | 1.95 | 2.08 | 1.66 | 2.99 | 2.46 |
| b | -0.001 | 0.003 | 0.007 | 0.009 | 0.008 | -0.005 | -0.001 | 0.001 | -0.011 | 0.012 |
| c | 0.000 | 0.001 | 0.001 | 0.001 | 0.001 | -0.000 | 0.000 | 0.000 | 0.000 | -0.001 |
| $r^2$ | 0.235 | 0.515 | 0.609 | 0.885 | 0.552 | 0.431 | 0.866 | 0.430 | 0.956 | 0.982 |
| f-test | ns | ns | ns | 95% | ns | ns | 95% | ns | 99% | 99% |
| Significance of use of non-linear regression | | | | | | | | | | |
| t-test | 40% | 80% | 80% | 98% | 80% | 75% | 98% | 40% | 97.5% | 99% |

**Table 5.11: Apple orchard - linear and non-linear regression of view angle and coefficient of variation**

| Band | 1 | 2 | 3 | 4 | 5 | 6 | 7 | 8 | 9 | 10 |
|---|---|---|---|---|---|---|---|---|---|---|
| Linear Regression | | | | | | | | | | |
| a | 2.58 | 1.93 | 2.58 | 2.39 | 3.36 | 8.70 | 10.78 | 10.30 | 12.81 | 10.40 |
| b | -0.017 | -0.023 | -0.004 | 0.000 | -0.001 | 0.021 | 0.010 | 0.019 | 0.014 | 0.041 |
| $r^2$ | 0.689 | 0.552 | 0.038 | 0.000 | 0.000 | 0.033 | 0.006 | 0.025 | 0.022 | 0.255 |
| t-test | 97.5% | 90% | 30% | nt | nt | 30% | 10% | 20% | 20% | 75% |
| Non-linear Regression | | | | | | | | | | |
| a | 2.74 | 1.47 | 2.71 | 2.44 | 4.49 | 12.48 | 15.23 | 14.24 | 15.94 | 12.62 |
| b | -0.019 | -0.019 | -0.005 | 0.000 | -0.009 | -0.008 | -0.024 | -0.012 | -0.010 | 0.024 |
| c | 0.000 | 0.001 | 0.000 | 0.000 | -0.002 | -0.007 | -0.008 | -0.007 | -0.006 | -0.004 |
| $r^2$ | 0.741 | 0.757 | 0.076 | 0.006 | 0.630 | 0.981 | 0.983 | 0.986 | 0.955 | 0.908 |
| f-test | 90% | 90% | ns | ns | ns | 99.9% | 99.9% | 99.9% | 99% | 99% |
| Significance of use of non-linear regression | | | | | | | | | | |
| t-test | 50% | 80% | 20% | 10% | 90% | 99.9% | 99.9% | 99.9% | 99.9% | 99% |

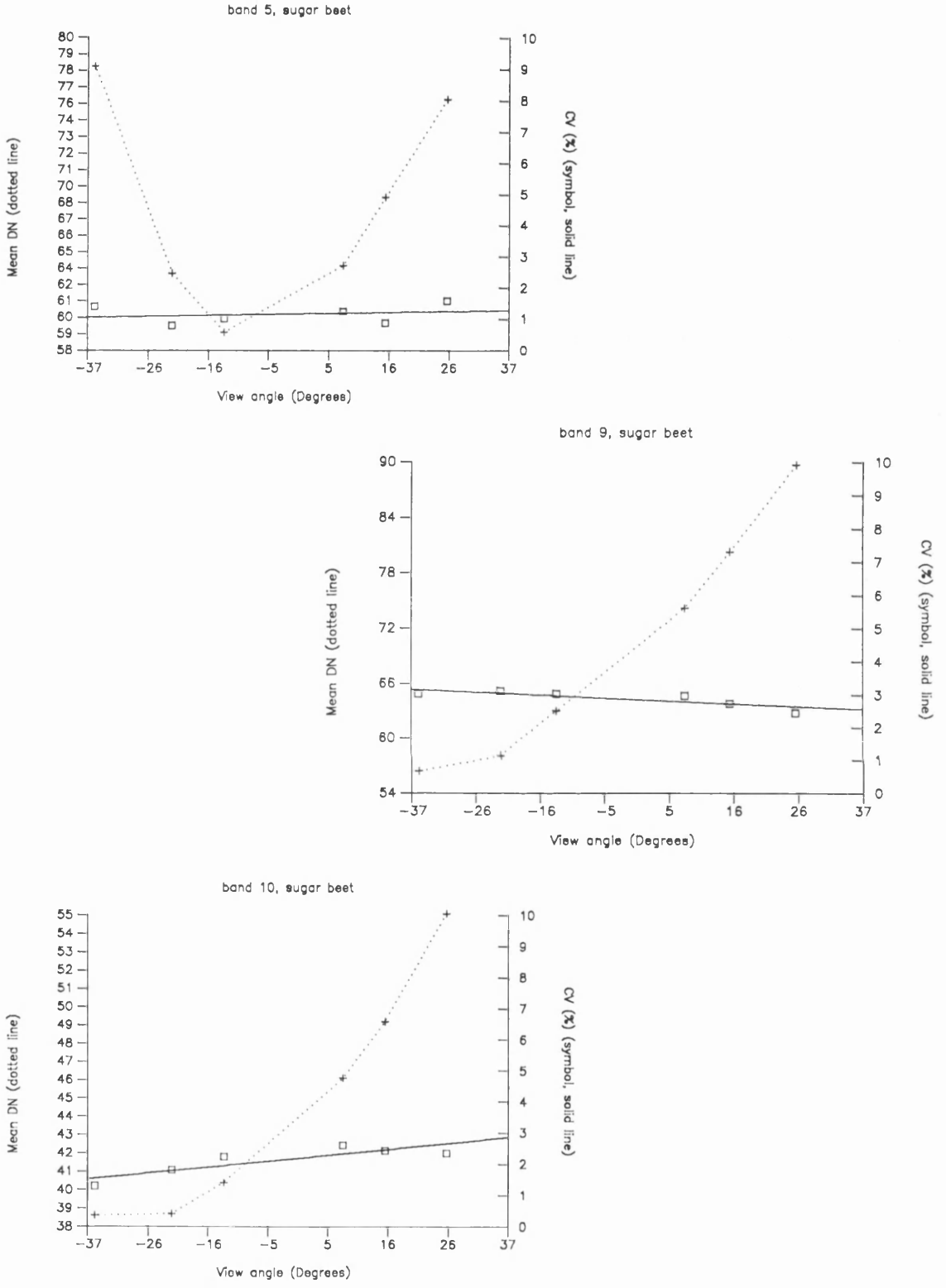


Figure 5.16: Sugar beet parcel, regression analysis, bands 5, 9 and 10. Mean DN dotted line, CV symbols, solid line gives regression equation fit.

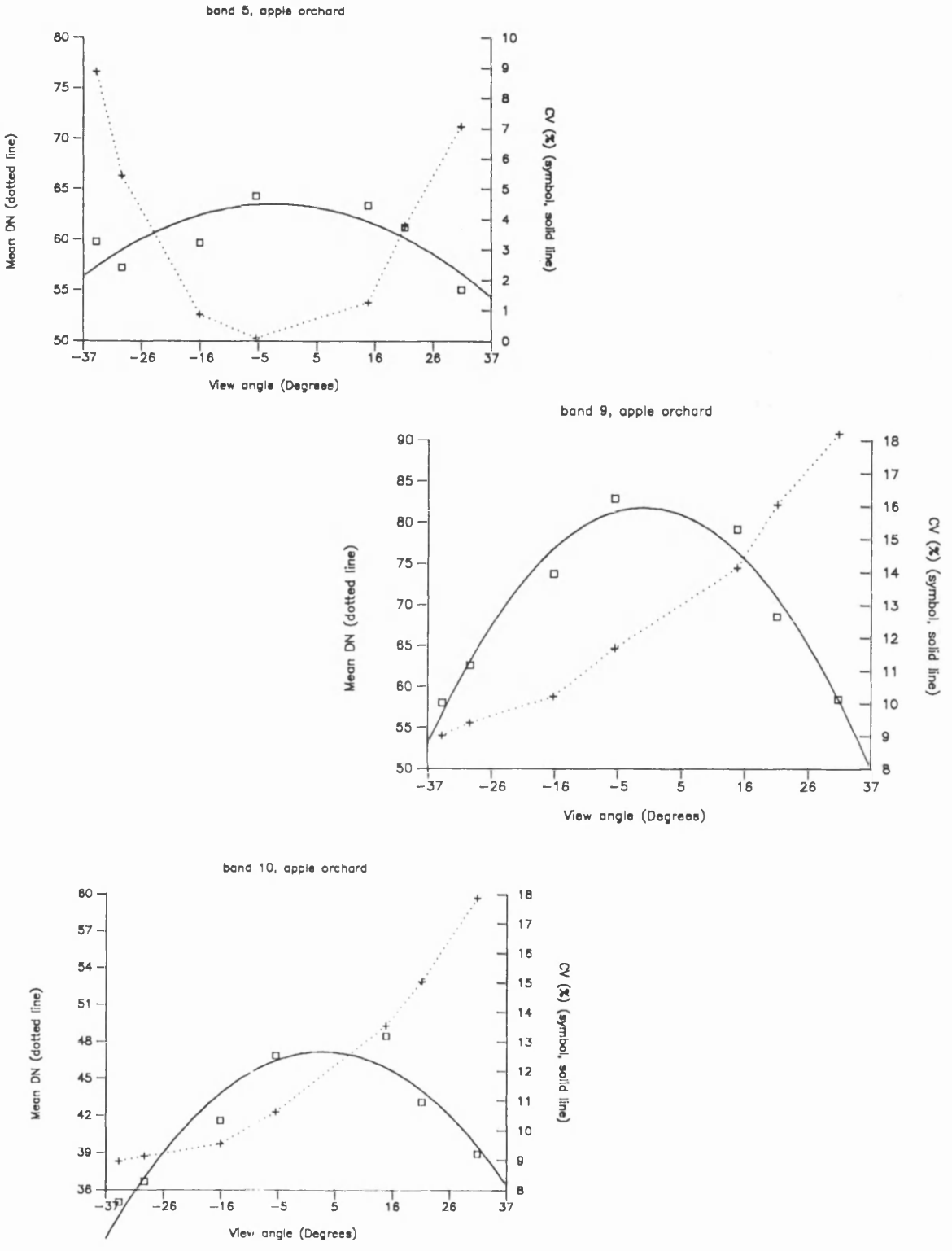


Figure 5.17: Apple orchard, regression analysis, bands 5, 9 and 10. Mean DN dotted line, CV symbols, solid line gives regression equation fit.

## 5.3: Results

### 5.3.1: Introduction

In this section we will first examine, for two distinct cover types, the relationship between CV and view angle, and then evaluate one technique, regression analysis, to characterise and quantify this relationship. Results for nine different cover types are presented in tables 5.3 to 5.11, for each band of the raw DN data, and figures 5.9 to 5.17 show how image variance (represented by the CV of the DN in each field) varies with view angle, for bands 5, 9 and 10; these bands show the strongest and most consistent relationship between view angle and image variance. No radiometric corrections of any kind have been made to these data.

The main findings of this section are that view angle has a significant effect upon the variance of ATM data. Three interacting factors - namely the increased area of the GRE, the increased overlap between adjacent GREs, and the changed canopy components viewed by the sensor (section 4.1.1) - act to modify the spatial variance as measured by the coefficient of variation. Extending the conclusions from the previous section (5.1.5) it is shown here that this effect is a direct result of the canopy geometry, by comparing the relationship between homogeneous and non-homogeneous cover types of various canopy structures. It is concluded that such a relationship may be inverted to deduce information concerning the structure of the canopy, given image variance data for a number of different view angles.

### 5.3.2: General description of the results

The two major trends which can be observed are best illustrated by fields 30 (spring barley, mostly bare soil) and 29 (winter barley) (tables 5.3 and 5.4). For field 30[14], linear regression produces good results in bands 1, 6, 7 and 8. Non-linear regression is only significant for band 1; this is probably due to view angle-

[14]Spring barley, 6% cover, growth stage 12; this field is essentially bare soil.

dependent atmospheric path radiance reducing image variance in the shorter wavebands. The t-test result, of whether the relationship between view angle and CV is better explained by non-linear regression than linear regression, is not significant at the 90% confidence level for any of the ten channels. The low t-test values for linear regression are a result of low $r^2$ values and the *b* coefficient in the regression equation; a coefficient of zero would produce an $r^2$ value of zero - and thus the significance of the result would be very low. By inspection of the data, however, it is apparent that a linear fit is acceptable for field 30; and that there is no significant relationship between view angle and image variance for this field.

For field 29[15] the results are very different. Linear regression produces consistently poor results. Non-linear regression, however, explains a significant degree of the relationship between view angle and CV, and is also a significant improvement over linear regression for bands 5, 7, 8,9 and 10 (although this is in part due to the poor results from linear regression in these bands). Fields 21 (winter wheat, 22% cover, growth stage 32) and 10 (winter barley, 58 %, 37) show similar results.

The differing response of these two densities of cover (spring barley and winter barley) indicate, therefore, that there could be a mechanism for information extraction based upon the effect of view angle on the CV of a sample of DN from a parcel. Importantly, this relationship appears relatively unaffected by topography or by the atmosphere in the longer wavebands (ATM 5-10, *cf.* 4.4). If these factors had been important they would be manifested as an asymmetric relationship of CV with view angle, or some displacement of the parabola (determined by the regression analysis) origin with respect to the nadir view angle. The *b* coefficient in the non-linear regression equation is the factor determining this position, and in most cases this is small, causing a displacement of just a few degrees. Much of this displacement could be the result of the limited size of the dataset used to construct the parabola.

[15]Winter barley, 56% cover, growth stage 32.

### 5.3.3: Description of results for further cover types

Further analysis is restricted to the longer wavelength bands (ATM 5-10), since it is recognised that atmospheric effects are less likely to alter image contrast, and thus mask scene variance, in these wavebands. Bands ATM 1-4, nevertheless, are included in the tables for the purpose of comparison. It is essential also to ascertain which bands are most suitable for the analysis of variance of the data. Bands 5, 9, and 10 have been chosen to illustrate the relationship between view angle and CV, since in these channels the spectral contrast between the *element* (the canopy) and the *background* (soil, except for the apple orchard where it is grass) (section 5.1.3) is great, the background having a higher reflectance than the element in these wavebands. This configuration is significant, because the architecture of the element controls the amount of background "seen" at any view angle. If the *background* has low reflectance then there would, therefore, be a weaker relationship between view angle and any measured dependent variable based upon detected radiance, since the *background* will not be seen at any view angle.

Dividing the results in terms of non-homogeneous or homogeneous canopies, the results can be listed as follows:

i) **Non-homogeneous**: for field 29, bands ATM 5, 7, 8 and 9 are better explained by a non-linear model. Field 10, with similar canopy parameters to field 29, also shows a significant non-linear relationship between view angle and CV for bands ATM 5, 9 and 10. Field 21 has significant explanation of variance by non-linear regression for five bands; as does the area of mixed woodland for all ten bands. The apple orchard produces significant non-linear modelling for bands ATM 6-10.

ii) **Homogeneous**: For field 30 non-linear regression does not provide a significantly better explanation of image variance than a linear model for any band. Field 3 has a similar response to modelling as field 30, although the $a$ coefficients for each band are lower. Field 27 has no band for which non-linear regression is significant at more than the 75% confidence level.

The results, then, fall into two categories: types of cover where non-linear regression provides a significant explanation of the relationship between view angle and image variance, and those where it does not and a linear fit to the data is good[16], because there is only a poor relationship between view angle and image variance. Into the first category fall fields 29, 21, 10, the area of mixed woodland, the apple orchard, and (exceptionally, since it is nearly 100% cover) the field of sugar beet. Into the second category fall fields 30, 27, 3. This group is characterised by low spatial frequency of variance in the scene, by comparison with the sampling frequency of the instrument. The description of soil and grass cover types in the scene may therefore be considered as a **continuous, single element, *H*-resolution model**, using the terminology introduced in 5.1.3 above. The former group, where the interaction of the sensor sampling frequency and the spatial variance of the cover in the scene is manifest as a significant relationship between view angle and CV, are best described by **discrete, simple (two-element), *M*-resolution models.**

The parcel of sugar beet produces a more complex result. Non-linear regression appears significant, notably for bands ATM 9 and 10, but in fact the *c* coefficients are small or nearly zero (meaning shallow curves). This trend is also very weak when compared with other data, for example the apple orchard. The parcel is virtually 100% cover, and therefore may be thought to be single element, like field 3 (grass). But the large leaf structure may provide a condition in which in fact a two-element description is preferable, since larger areas of illuminated and shadowed leaves would be apparent at some wavelengths. This implies, more importantly, that the scale of the spatial frequency of the variation is approaching *M*-resolution. But the sugar beet canopy has a very low base coefficient (*a*), and it therefore is not, indeed, highly variable within the parcel - a characteristic of the *M*-resolution case. Also, the significance of the non-linear fit is exaggerated by the low $r^2$ values for the linear regression, where the *b* coefficient is low. It is therefore most suitable to consider this cover type as continuous, *H*-resolution.

---

[16]This, however, does not imply that linear regression produces a significant result.

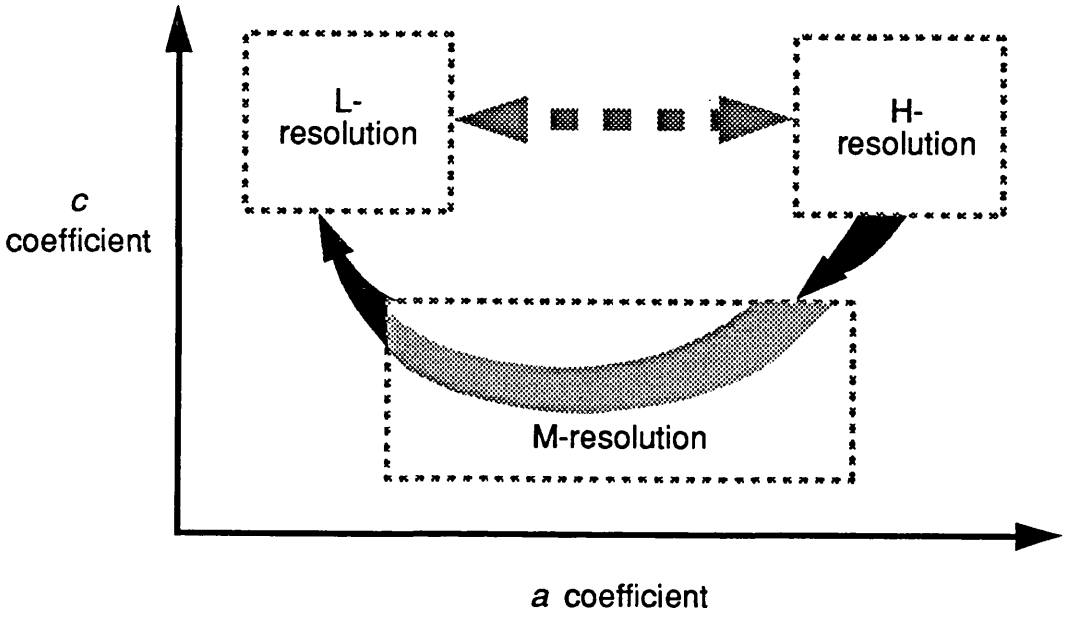


Figure 5.18: Variance characteristics of a developing crop. Initially the predominant variance of the parcel characteristics are *H*-resolution; as the crop develops it becomes *M*-resolution; and finally, as it nears maturity, it becomes *L*-resolution, when complete vegetative cover is obtained. At this stage, however, it may also be possible to describe the parcel as *H*-resolution, depending upon whether the objects in the scene are taken to be plants (by definition then, *L*-resolution) or variations at a broader scale, say due to moisture or soil differences (therefore *H*-resolution). These states can be determined by analysing the regression coefficients.

### 5.3.4: Parameter evaluation

By distinguishing which resolution model (see 5.1.3) is best applied to describe parcel variance, parcel characteristics can be inferred. The most direct measurement is crude - whether the cover type is mostly soil (such as the spring barley fields), 100% uniform cover (sugar beet, grass), or some intermediate stage (winter wheat and barley, woodland and orchard). Attempts have also been made to identify further methods for extracting other canopy parameters, such as row orientation, percentage cover, crop height or spacing.

#### 5.3.4.1: Crude inferences

Valuable information regarding the structure of the scene can be inferred from the combined analysis of the *a* and *c* coefficients of the non-linear regression models. Each of the three scene variance models, described in section 5.1.3, should produce a particular combination of the two parameters. A high value for *a*, combined with a low value[17] for *c*, would imply an *H*-resolution target, with greater variance of radiance values within the parcel, albeit of low spatial frequency - typically soil in this dataset. High *a* and *c* coefficients imply a canopy or target spatially variable at around the scale of the resolution cell, as illustrated by the orchard and winter crops in this study, modelled as *M*-resolution. Finally, a low value for *a* and *c* would imply an *L*-resolution canopy, with little variance in radiance values within the parcel; this would typically be a high-density, closed, vegetative canopy. This is the first step toward classifying and assessing cover type using image variance alone.

As well as a method for deducing the type of canopy under investigation, analysis of CV could be used in much the way that Kauth and Thomas (1986) developed the tassled-cap model of arable crop development. This is because at each stage of growth the scene will have particular spatial variance characteristics, and will

[17]Low value in this description implies a value near to zero - the relationship between *c* and view angle is in fact negative, a large negative number being referred to as a large number here.

follow a trajectory through the variance "feature space". Figure 5.21 illustrates this hypothesis with relation to a developing winter barley canopy. Because of the limited number of dimensions (two) applied in this analysis, however, it would be sensible to apply this technique with other, conventional spectral techniques, synergistically.

5.3.4.2: Interpretation of magnitude and scale of variance (*a* and *c* coefficients)

It has been noted in 5.1.2 above that the spatial distribution of the DN in the parcel is critical in determining the variance of the sample population. For this reason, CV can only be used indirectly as a measure of the spatial variability of elements within a scene. High values of CV do not necessarily equate with variability of high spatial frequency. Of greater importance, however, is the relationship between view angle and CV. A significant, non-linear, model - i.e. with a large *c* coefficient - implies that the scene is spatially variable (at the scale of the resolution cell), because there is changing interaction between the sampling frequency of the resolution cell, the sensor geometry, the canopy geometry.

By examining three of the fields in the dataset, each of the three resolution models can be illustrated.

i) ***H*-resolution**: Field 27 (newly sown spring barley, virtually bare soil) produces quite high values of CV (*a* coefficient) between 7.39 and 8.16, but values for *c* are all <0.001 (table 5.9).

ii) ***M*-resolution**: Field 29 results show values of *a* varying between 5.42 and 10.05, and *c* between -0.002 and -0.003 (table 5.4, bands ATM 5, 9, and 10). The marked change in CV with view angle indicates that the parcel is more spatially variable (measured at the scale of the resolution cell) than field 27, as well as the more obvious comparison of the magnitude of *a*, which would otherwise give a similar interpretation if made on this basis alone.

iii) ***L*-resolution**: Field 3 (grazed permanent pasture) has a low CV value (the coefficient *a*, between 1.43 and 2.65) for bands ATM 5-10, and *c* coefficients of <0.001 (table 5.8); i.e. there is no change of CV with view angle. Low CV values would be expected, as there is very little within field variation of DN.

Thus, while the sample populations of the *H*-resolution models have a (relatively) high variance, as measured by the CV, the distribution of the sample values is such that no significant change in variance is measured by the sensor at different view angles. It is likely, therefore, that adjacent pixels will have similar values, and that the image will be dominated by clusters or blocks of like pixels, forming groups that are *significantly larger than the ground resolution element.* This is confirmed by inspection of the image (figure 5.2).

Rather than presenting a further complication, testing for the relationship between view angle and image variance through the magnitude of the *c* coefficient allows sampling strategies to be more relaxed. In effect, it normalises for the sampling strategy; while the magnitude of the *a* coefficient is likely to give a measure of the spatial variability of the cover type (when the assumptions made in 5.1.2 are met), it is the value of *c* that gives a full insight into the spatial *autocorrelation* of the scene, as measured at the (changing) sensor sampling frequency.

5.3.4.3: Influence of crop row geometry on image variance

Two fields, 18 and 20, were analysed for cover type characteristics. Bands ATM 5, 9 and 10 were used, since these presented the greatest spectral contrast between the model element (canopy) and the background (soil). The results for regression analysis are given in table 5.12 below.

We are able to state, based upon the argument presented in 5.3.4.2 above, that the spatial scene variance in both these fields is explained by the *M*-resolution model; i.e. they are an intermediate developing canopy, not soil, or continuous uniform cover. This is despite the fact that the base coefficient *a* is somewhat different for

the two populations. In fact they are both parcels of winter barley (variety *Plaisant*), planted on the same day, are adjacent fields, and yielded a harvest within 50kg per hectare of each other. The row orientation of the crop in the two fields are perpendicular to each other; in the case of field 18 the rows are parallel to the flightline direction. The effect of row geometry on these data is instantly recognisable, since no other major differences in the canopy exist between these two fields.

**Table 5.12: Fields 18 and 20, regression analysis**

| | Field 18 | | | Field 20 | | |
|---|---|---|---|---|---|---|
| Band | 5 | 9 | 10 | 5 | 9 | 10 |
| *Significance* | | | | | | |
| non-linear regression | 97.5% | 97.5% | 97.5% | 97.5% | 99% | 97.5% |
| comparison with linear | 98% | 99% | 99% | 99% | 99.5% | 99% |
| *Coefficients*: | | | | | | |
| *a* | 5.37 | 8.77 | 13.25 | 3.14 | 4.26 | 5.65 |
| *b* | -0.010 | 0.012 | 0.013 | -0.008 | -0.002 | 0.000 |
| *c* | -0.0017 | -0.0032 | -0.0033 | -0.0009 | -0.0011 | -0.0015 |

To an extent, the observations of these two fields are complicated by the differences in relative solar azimuth of the rows in the two parcels. This may cause some of the differences in the magnitude of the coefficients calculated in the analysis (table 5.12). Two conclusions may be inferred, however: first, the row orientation of the crop, relative to the Sun, for field 20 restricts the illumination of the background, which in turn affects image variance; and second, that some target-sensor geometry effects, in particular the increased over-sampling between adjacent GRE's, are also in operation. If the sensor is viewing along the crop row direction (i.e. crop row and scanline directions are parallel), then the proportions of background and canopy elements, in resolution cells across the swath, are likely to be similar for whatever view angle is chosen. The reduction in image variance at

increased view angles will be a function more completely of the sensor geometry, i.e. the increased oversampling resulting from the S-bend system correction.

For a scan line direction perpendicular to the crop row orientation, canopy components will become increasingly dominant with increased oblique view angle. Thus, image variance will decrease at a greater rate than in the former case, since more than one of the geometric factors will be in operation. This hypothesis is confirmed by inspection of the analysis of fields 18 and 20.

Row orientation, therefore, becomes a limiting factor when attempts to infer canopy characteristics from image variance are made. In extreme cases, where *M*-resolution scene models apply and viewing geometry is parallel to row orientation (for example, viewing straight down the rows of the apple orchard presented in this study), the effect of view angle upon canopy geometry may be diminished to a completely insignificant level by comparison with the sensor geometry effects on image variance (increased oversampling and GRE area). In such a case, however, it would be possible to identify the row orientation from the imagery, and this information must be used if the image variance (and therefore canopy structure) is to be determined correctly.

The illumination geometry of the target may become as important as the relative canopy-sensor geometry in determining image variance. Diurnal variations, represented as changes in solar zenith and relative azimuth angles, will have a marked effect upon image variance. Interestingly, these two factors are represented in the second-order polynomial equation coefficients. Changing solar zenith angle will affect the magnitude of image variance; for example, at low illumination angles the increased likelihood of incoming flux being intercepted by part of the canopy will cause the background element to be in more shadow than at near zenith illumination angles.

Modifications to the relative azimuth of any regular structure in the parcels, such as rows, will be also be manifest in the $a$ and $c$ coefficients, because again different proportions of the canopy and background element will be illuminated; as the relative azimuth approaches 90°, less background would be illuminated and the

image variance would be reduced, since image variance relies upon the significance of spectral contrast between the element and the background. This would reduce the magnitude of both the coefficients. To an extent, therefore, the factors of (relative) solar azimuth and zenith angles, and the row orientation with respect to the sensor, are inter-related. In this mono-temporal dataset, however, it has not been possible to test for this relationship.

## 5.4: Discussion and conclusions

### 5.4.1: Extensions to crop modelling

While crude inferences from variance data are a significant new step toward extracting information from multiple view angle image datasets, for this technique to be generally applicable more specific and detailed information must also be surmised. The time available to this study has not permitted the further development of the areas, listed below, but they are included to give an insight to the information that might be forthcoming from such an analytical procedure.

#### 5.4.1.1: Extracting crop height and spacing parameters

The most straightforward parameter, after the determination of the best scene resolution model (*H*-, *M*-, or *L*-resolution), is the ratio of crop height to row spacing. If the crop row structure is perpendicular to the view direction, then this ratio becomes:

$$R = s/h \qquad \text{Eq. 5.3}$$

Where $s$ is the *effective* row spacing, $h$ is the average *effective* canopy height (figure 5.19), and $R$ is the ratio of these two values. This ratio is important, because from it we can calculate the view angle, $V_0$ at which the sensor effectively sees no background element:

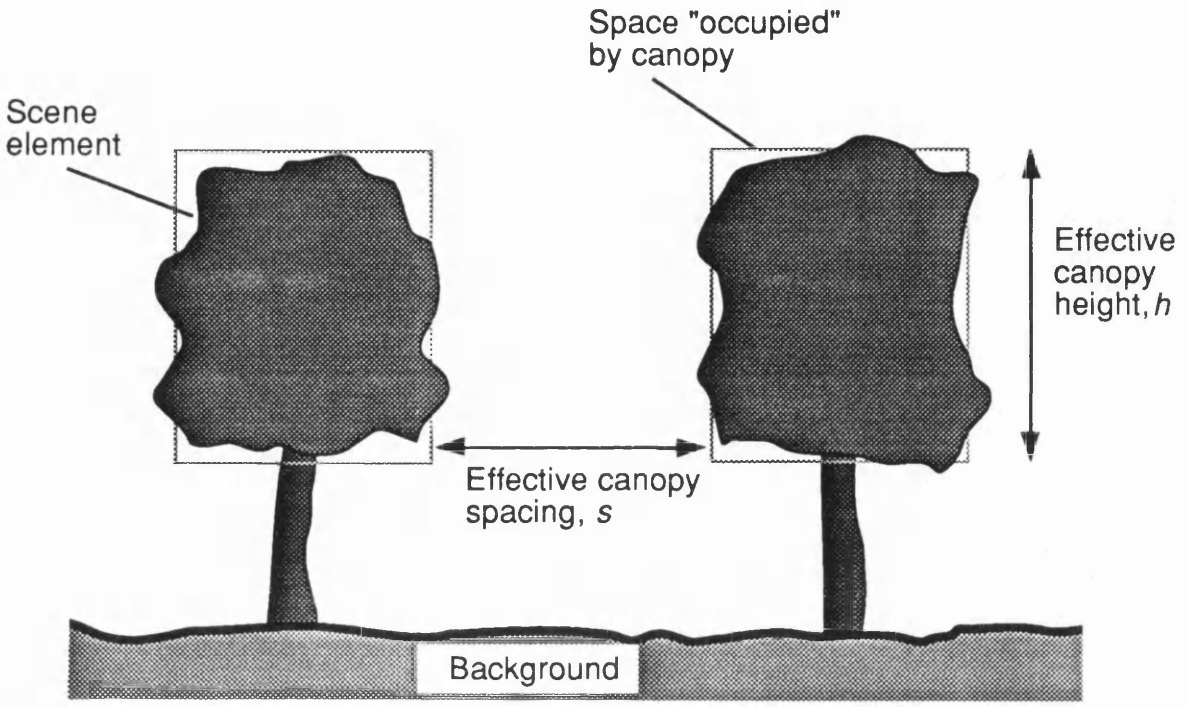


Figure 5.19: "Effective" canopy spacing. The variable that it may be possible to determine would be the gap between the canopy elements, in this case a tree, and not necessarily the spacing between the planting of the trees. Similarly, canopy height may also be affected in the same way. Knowledge of the typical morphology of the canopy must be available in order to determine factors such as planting density with any degree of accuracy.

$$V_0 = \tan^{-1}(R) \qquad \text{Eq. 5.4}$$

Where the row orientation is not perpendicular with the view direction, $V_0$ is modified by the relative azimuth, $\alpha$, of the view and row orientations to become:

$$V_0 = \tan^{-1}(R/\sin\alpha) \qquad \text{Eq. 5.5}$$

At this angle, we could expect the introduction of an asymptotic relationship between view angle and CV. If we extend the observations of continuous cover type (for example, field 3 and sugar beet parcel), beyond $V_0$, CV will not decrease significantly in the manner observed for intermediate M-resolution parcels for view angles within $V_0$. Rather than the parabolic second order polynomial function used to model the view angle/CV relationship in the analysis above, a higher order equation, of the form:

$$y = (a + bx + cx^2)^{-1} \qquad \text{Eq. 5.6}$$

could be used to describe an asymptotic bell-shaped curve. The position of $V_0$ could be ascertained by identifying the point at which the curve tends towards the asymptote. This would demand a greater number of data values, since the polynomial has a larger number of coefficients, and would probably demand a greater FOV, in order to actually record an image where view angle was guaranteed to exceed $V_0$.

In order to extract either $s$ or $h$, however, the complementary parameter must be known. In some cases of $M$-resolution modelling it may be possible to estimate $s$ from the image data; alternatively, two orientations of multiple view angle flightline datasets could be used to produce simultaneous equations, which could then be solved to produce estimates for both parameters.

5.4.1.2: Estimating percentage cover using variance analysis

It is evident from the results presented here that as percentage cover increases, distinct trends in the values of the *a* and *c* coefficients of the regression equations can be identified (figure 5.18). Without external knowledge of the phenology of the crop, however, it may prove impossible to estimate percentage cover from the variance statistics alone. For this reason, it has not been attempted in this study. Given that CV is a valid means of comparing the spatial variance of two remotely sensed datasets, and that all other factors are equal between the two parcels, then the values of the coefficients should indicate the relative cover of the two parcels.

5.4.1.3: Inverse relationships between view angle and image variance

Examination of tables 5.4 and 5.6 reveal that for bands ATM 6, 7 and 8 fields 29 (winter barley) and 21 (winter wheat) have a positive *c* coefficient; i.e. spatial variance increases as a function of sensor view angle. This relationship is difficult to explain, since all the geometric factors considered in this study have the effect of *attenuating* image variance. It is also apparent that these two parcels are the only two giving such a result in this dataset. Possibly, therefore, these examples represent unreliable data, or give an indication as to the accuracy of the technique used to compute image variance in this instance.

**5.4.2: Other techniques for measuring image variance**

5.4.2.1: Local image variance; Woodcock and Strahler

Woodcock and Strahler (1987) measured image variance by passing a 3x3 kernel over an image, computing the SD of the kernel matrix (see 5.1.2 above). This algorithm was implemented in FORTRAN 77, to enable some analysis of the imagery in a similar manner to Woodcock and Strahler (1987) (section 5.1.4). The results depend upon two factors: first, the magnitude of the difference between DN in adjacent pixels, the greater the difference the greater the calculation of

'variance' for the image or parcel; and second, the proportion of these variable features in the image or parcel as a percentage of the total number of pixels. It can be expected that greatest variance will be recorded when the frequency of spatial variance in the image is close to the Nyquist frequency.

In this case, again, the aim is to estimate the *spatial autocorrelation* characteristics of the parcel. When averaged, the processed pixel values in the parcel should correspond to the degree of autocorrelation - higher mean values would correspond to lower autocorrelation. The significance that can be read into such figures, however, is extremely dependent upon the proportion of the 'edge' pixels in the parcel as a whole, as well as the magnitude of the edge - an extremely strong edge in a small parcel would give the (wrong) impression of an extremely variable cover type.

#### 5.4.2.2: Formal measures of spatial autocorrelation

For the reasons explained above, both the CV and Woodcock methods fall short of producing formal measurements of spatial autocorrelation in images. In order to achieve some surrogate estimate, measures of image variance are used instead which can only be allowed if certain criteria are met. It would be more useful, and more generally applicable, if formal measures were developed which allowed the true autocorrelation characteristics to be quantified. A major advantage of such techniques would be that results from different sensors, dates and of different cover types would be directly comparable. It is apparent, however, that the use of such statistical measures (Cliff and Ord, 1973) is a complex task which has not been attempted in this study.

### 5.4.3: Conclusions

In this chapter, the effect of scene structure upon image was hypothesised, and a number of models to describe this interaction defined. Several studies using synthesised degraded data were used to illustrate the relationship between spatial

resolution and image variance. It was found that image variance decreased with resolution within specific classes, or parcels; but for whole images, comprised of a number of different objects, image variance increased[18] as a result of the boundary pixels in the images becoming an increasing proportion of the total pixels in the image. These results were as expected from some of the available literature. Section 5.1 concluded that despite the general within-parcel decrease in variance, the decrease in image variance observed for some cover types in multiple view angle datasets could not be explained by decreased spatial resolution alone. Indeed, it is reasonable to conclude that the remaining factors, of increased over-sampling of the sensor and changed proportions of canopy elements viewed by the instrument at off-nadir angles, are much more dominant.

By comparing the response of different cover types imaged in a multiple view angle dataset, sections 5.2 and 5.3 explain how canopy geometry has a significant effect on the relationship between view angle and image variance, as measured by the technique developed in this study, termed CV (5.1.2). This relationship is analysed using linear and non-linear regression analysis, and a method for interpreting the regression equation coefficients outlined. This is used to interpret the results according to the model definitions made in the opening section (5.1.3). A number of extraneous factors, namely row orientation and illumination geometry, are discussed to identify the factors that may effect image variance not accounted for by differences in canopy structure.

In the final section (5.4), practical extensions to the extraction of canopy parameters (crop height and spacing, percentage cover) are discussed briefly, along with other techniques for improving upon the measurements of image variance.

In conclusion, it has been shown that a formal approach to the analysis of image variance, in a multiple view angle dataset, allows the extraction of valuable information that could enhance conventional, non-parametric, techniques of image analysis for estimating agro-physical canopy parameters.

---

[18]Up to the resolution tested - 40m

# CHAPTER 6: Capabilities of current and future sensors for use in multiple view angle image strategies

## 6.1: Introduction and criteria

In this chapter the feasibility of a multiple view angle image strategy for the extraction of agrophysical parameters is assessed on the basis of the capabilities of current and future sensors. In this first section, the demands of such a strategy on sensor design, and some general design considerations are outlined. A list of criteria, upon which assessment of various instruments can be made, is then constructed. The second and third sections match these criteria to current and future sensors, respectively, attempting to identify which instruments can be used as data sources and to what degree of effectiveness, cost and efficiency. Finally, in the concluding section, the practicality of this strategy is reviewed.

### 6.1.1: Application of image variance analysis

It was identified in Chapter 1 that economic demands and the need for regional, national and global logistical planning, to provide a stable market and prevent shortfalls in food supply have resulted in the development of the field of agro-meteorological modelling. Because of the broad spatial scales at which the information is required, remote sensing has become an obvious data source for the science. It might be noted, however, that the design of most sensors, in particular the Landsat series so widely used in such agronomic projects, has been compromised by the need to provide data for other applications and technological constraints. These data are often of a far from ideal nature, usually providing only an indirect means of predicting the agro-physical parameters required for the task of crop assessment. This is because the input from remote sensing has relied upon assumptions concerning the relationship between spectral reflectance and these various parameters, such as leaf reflectance and transmittance, leaf area index, leaf angle distribution, planting density, row orientation, biomass and productivity (Woodham, 1989). Using present systems and operational models, none of these parameters can be measured directly with confidence - they are estimated, or

interpreted, using assumptions concerning the scene under investigation. While in many cases the models produce good results, in other situations parameter predictions may be in gross error, because the assumptions required by the model are not justified; and thus the generality of these models becomes questionable.

It makes greater sense, therefore, to try to make more direct measurements of these parameters. If the required input for the agro-meteorological modelling is biomass and growth stage, then it is these two parameters that should be measured, not just reflectance in the red and near infrared wavebands. In this study we have tried to show how this might take place, with further improvements to the method presented here.

### 6.1.2: Demands of new data collection strategies upon sensor design

With new methods, new strategies for data collection must be devised. In turn, this could mean new sensor designs to maximise the potential of developing techniques. In order to allow stereo coverage and bidirectional reflectance analysis, for example, off-nadir sensors for space-borne platforms have been developed, such as SPOT-HRV and HIRIS. Technological developments are often useful to a number of disciplines: along-track off-nadir viewing sensors (such as HIRIS) will be useful to ocean scientists, atmospheric modellers, as well as biological scientists studying anisotropic canopy reflectance. The greatest benefit will be derived from such technological developments when the scientific direction is coordinated and the emphasis is multi-disciplinary.

Compromise over sensor design, however, can lead to an inadequate data product. The SPOT-1 sensor typifies such a situation: by trying to meet the requirements of both the Earth sciences and the topographic mapping communities, the sensor design has been compromised, perhaps to the detriment of the majority of users. Topographic mapping applications demanded stereo capability and high spatial resolution, whereas Earth science applications also required multispectral channels and high temporal coverage. The compromise resulted in limited areal coverage of a scene, across-track pointing, reasonable spatial resolution, and only three

multispectral channels. The stereo facility has been disappointing in many instances due to problems with temporal changes between images of the same scene. This results in difficulties to produce good stereo models as well as limiting the use of these data for directional reflectance studies. The choice and performance of the spectral channels for the multispectral sensor has been poor, despite initial claims of improvements over other instruments (Chevrel *et al.*, 1981); although the signal-to-noise ratio of SPOT-HRV is apparently better than that of Landsat TM (Slater *pers. comm.*), the dynamic range of DN over some surfaces is extremely low. It has also been shown that temporal resolution, supposed to be more frequent due to the pointing capability of the sensor, has improved little over that offered by Landsat TM in cloudy temperate regions such as Europe (Cushnie, 1988).

If the analysis of image variance is the main technique to be used for estimating scene parameters, then an instrument which carries out on-board processing of data could be devised. This could allow data compression, and therefore overcome a major problem with designing a high spectral, spatial and temporal resolution sensor - data transmission rates. Filtering, such as that used by Woodcock and Strahler (1987), in conjunction with image segmentation could produce a radical product describing the spatial pattern of scene variance. Such a strategy, however, has several limitations. From a practical aspect, on-board processing means an increased demand for space on the platform, power, and technical reliability. Synergistic operation with other techniques, such as spectral analysis, would be reduced; and single-product (and, therefore, single-user) sensors are less economic than multi-user systems. Finally, much information can be interpreted from the original data before variance analysis is carried out. Pre-processing data on-board would not allow this to take place.

The requirements upon a sensor for a multiple view angle strategy to be operational can be summarised in the following four criteria:

- The image dataset must contain a number of different views of the object, preferably in the same view azimuth plane.

- Multiple coverage, ideally, should be near-simultaneous, image data should be acquired preferably from the same orbit.

- The spatial resolution of the sensor (or more precisely the size of the ground resolution element) should be as high as possible; although a range of sensors could provide examination of the scene at different spatial scales and resolutions.

- A number of spectral bands should be collected, to ensure that scene element contrast is high for a variety of ground cover types.

There are several ways of configuring sensors for a data collection strategy that meets these criteria. All involve the ability to view off-nadir, but this could be achieved using a broad-swath or a pointable capability of the sensor. The list of possible sensors, therefore, includes a number not designed for "off-nadir" reflectance studies. The following sections in this chapter (6.2, 6.3) assess the capability of current sensors in carrying out such a data collection task using the criteria listed above, and examine the prospects offered by future instruments on the NASA Earth Observing System (EOS) project due to be launched in 1996.

## 6.2: Current sensors

Most sensors, by virtue of having a field of view, are capable of off-nadir viewing to a greater or lesser degree. Other factors, namely repeat cycle and spatial resolution can restrict the potential of certain instruments otherwise capable of collecting multiple view angle datasets. Table 6.1 below lists some of the characteristics of current sensors relevant to the collection of such data.

### 6.2.1: Landsat TM

While the GRE size is suitable for image variance analysis, and the number of spectral channels enough to ensure good spectral contrast between scene elements,

the low repeat cycle and restricted overlap allow only two views of a limited area of the Earth's surface. For these reasons, Landsat TM cannot be considered as having any potential for analysing image variance in the manner advocated by this study, since more than four views are required to compile the dataset.

**Table 6.1: Application of some current visible and IR sensors to image variance analysis**

| | Landsat TM | SPOT XS | SPOT Pan | AVHRR |
|---|---|---|---|---|
| GRE size | 30m | 20m | 10m | 1.1-2.4x6.9km |
| Channels | 7 | 3 | 1 | 2* (5) |
| Spectral coverage | Vis, NIR, MIR | Vis, NIR | Vis | Vis, NIR MIR, Thermal |
| Off-nadir# | (±7°) V | ±27° P | ±27° P | ±55.4° V |
| Repeat | 14 days | <26 days | <26 days | daily[1] |

* Only two of general use to vegetative studies

# V - off-nadir *viewing*, P - off-nadir *pointing*

### 6.2.2: SPOT-HRV multispectral

Like Landsat TM, the SPOT-HRV multispectral sensor has a small GRE size, although it collects data in a more limited number of spectral channels. The capability to collect data from oblique view angles, however, is an important feature in the context of this study. While the full repeat cycle of the platform is 26 days, the off-nadir geometry of the sensor allows seven images of a scene per cycle to be acquired at the Equator, eleven at latitude 45°, increasing to ≈13 at latitude 55° (Cutler, *pers. comm.*). Despite such theoretical abundance of imagery,

[1]Twice daily, but with more than one platform and instrument. This causes problems because the Sun-target-sensor geometry varies between images because local times of imaging will be different. As we have seen in section 5.3.4.3, illumination geometry of the target is likely to affect image variance.

these data would be far from perfect for multiple image analysis because the data are acquired from successive orbital paths rather than from a single pass. As a consequence, a large proportion of the differences between the images could be explained by atmospheric and illumination effects, and even changes in the target characteristics that the analysis is attempting to describe. For this reason, SPOT XS can only be considered as having a very limited potential for such an application.

### 6.2.3: SPOT-HRV Panchromatic

While the decreased size of the GRE of the panchromatic mode of SPOT-HRV improves the usefulness of this instrument over the multispectral mode, this is to some extent offset by the decreased spectral contrast of some Earth surface materials in this single, broad channel. The capability of this sensor for scene variance analysis is, therefore, only marginally improved over the SPOT XS instrument.

### 6.2.4: NOAA AVHRR series

The broad-swath geometry of the AVHRR series of instruments is well-suited for the type of data collection strategy proposed here. High off-nadir view angles of up to 55.4°, resulting in a large degree of overlap between images acquired from adjacent passes and the capability to collect multiple view angle datasets of 9 scenes in a 10 day cycle[2], would allow significant work to take place concerning the relationship between view angle and image variance.

Two factors, however, severely limit this capability. First, despite showing an impressive change in area across the swath, the very coarse GREs may limit the assessment of variance to be at a broad ecological unit level rather than provide

---

[2]The number of orbits per day is 14.1, giving a 10 day repeat cycle of 140 unique orbits, at an average spacing at the Equator of 2.57°. A 2700km swath would therefore generate an average of 9 views of any point on the Earth's surface. NASA have calculated that three images in a nine day cycle is the more likely practicable limit (NASA, 1986)

any realistic capability for the extraction of canopy parameters. Some studies have been carried out investigating the nature of variance in AVHRR derived products (Townshend and Justice, 1989), but the results of these studies have been inconclusive. Second, since adjacent orbits will have to be used to gather multiple angle data the Sun-target-sensor geometry will vary considerably between images, because the platforms are sun-synchronous and the swath widths are 2700km wide. Study areas would be imaged at various local times in order to build up a multiple view angle dataset. While the effect of solar geometry upon scene variance has not been fully investigated in this study, it is interpreted from the data collected here and elsewhere that image variance is likely to change with solar zenith angle, and azimuth depending upon the spectral contrast between the scene elements.

### 6.2.6: Airborne sensors

Despite their intrinsically complex geometries, airborne sensors provide useful data sources for the understanding of scene structure through the analysis of image variance. In general, they can operate at a good spatial resolution, produce multiple coverage from different oblique view angles within a short space of time, and are usually equipped with a good choice of spectral bands. In a number of other ways, however, airborne sensors are not a flexible operational data source.

The first of these difficulties is the limited extent of coverage provided by airborne imagery. While the spatial resolution is high, the low altitude of the aircraft and the speed of the platform mean that only small areas on the ground can be surveyed quickly - one of the criteria for data collection listed above. Coverage is usually non-systematic, depending upon weather conditions and equipment availability. The cost of airborne data too, while not high when assessed with respect to image quality (approximately 40 pence per line for that collected by the NERC Daedalus ATM campaigns), is prohibitive when applied to large areas.

Platform geometry may vary between flightlines, and is relatively unstable compared to a satellite, causing many problems with image geometry. Relief effects will also be more severe because of the low altitude of the platform.

Although the sensors are often designed as test instruments for satellite-borne sensors (for example, AIS, AVIRIS, HIRIS) the possibilities of synergistic operation with other sensors can be limited because of the atmospheric, illumination and geometric differences between sensors. It would be necessary to remove these effects, or to work with image products, before combined analysis can be made from any two sources.

A final problem with airborne data is navigation. This has implications for the analysis of multiple view datasets for two reasons. First, locating the platform over the correct area of ground. This may need to be achieved with great precision, as in this study. Second, low altitude airspace can be very restricted, demanding constant attention to other airspace users and sometimes special permission to enter zones. In some cases, permission may be unobtainable; it would (and should) be impossible to obtain airborne imagery of foreign countries unwilling to cooperate with overflights.

This said, airborne sensors probably present the best system currently available for the collection of multiple view angle datasets.

## 6.3: Future sensors; the Earth Observing System platform, and SPOT 2-4

In the mid-1990's, the United States' National Aeronautics and Space Administration (NASA) will launch a multi-sensor platform, including one broad swath and two pointable image spectrometer instruments, the fixed view Moderate-Resolution Imaging Spectrometer (MODIS-N), the tilting Moderate-Resolution Imaging Spectrometer (MODIS-T) and the High-Resolution Imaging Spectrometer (HIRIS) (table 6.2), and the less sophisticated Multi-angle Imaging Spectroradiometer, MISR.

**Table 6.2: General specification of the MODIS-N, MODIS-T, HIRIS and MISR instruments**

| | GRE (Nadir) | Swath width | View angle capability *along* | *across* | Spectral Channels |
|---|---|---|---|---|---|
| MODIS-N | 0.25-1km | 1500km | n/a | (90° FOV) | 40 0.47-12μm |
| MODIS-T | 0.25-1km | 1500km | ±60° | (90° FOV) | 64 0.41-1.04μm |
| HIRIS | 30m | 30.0km | +60°/-30° | ±24° | 192 0.4-2.5μm |
| MISR | 0.216 -1.73km | 210km | ±72.5° | n/a | 4 0.44-0.86μm |

(Source: NASA, 1986, 1987, Diner *et al.*, 1988)

### 6.3.1: MODIS

Two sensors of moderate spatial resolution are planned for the EOS platform of the 1990's to provide data coverage similar to that currently acquired by the AVHRR sensor. Despite having similar spatial resolution and areal coverage, MODIS-N and MODIS-T are in fact quite different instruments in terms of image geometry, optics and detector design, spectral characteristics and their intended applications (NASA, 1986). MODIS-N, termed the "nadir" viewing part of the package despite having broad swath characteristics like AVHRR, will contain 40 channels extending from the visible to thermal spectrum. MODIS-T will provide 64 channels more applicable to terrestrial science, oceanography, and atmospheric studies.

It is not certain that data acquired by the MODIS sensors would provide any useful multiple angle datasets which could be used for the analysis of image variance. While some studies have examined image variance at these (and coarser) spatial resolutions (Townshend and Justice, 1989), these have been inconclusive and provided no explanation for the trends of changing image variance with

degraded spatial resolutions. By comparison, it seems unlikely that the processes identified by this study as the mechanism for changing *image variance*, i.e. canopy geometry and the spatial distribution of canopy elements in the scene, would be able to operate at the coarse spatial resolutions provided by either of the MODIS instruments. Changes in image variance do occur at coarser scales though, and it remains to be seen what information multiple view angle image analysis with such data would reveal. In addition to studies in isolation, MODIS imagery could be used in conjunction with HIRIS data to extrapolate the more detailed analysis capable with this instrument to larger areas, in line with the synergistic operation of the EOS sensor payload (see 6.3.3).

### 6.3.2: HIRIS

HIRIS is a 192 band imaging spectrometer, capable of pointing off-nadir by a considerable margin in both the along and across-track directions (NASA, 1987). Although the instrument will not be operational until the launch of the EOS platform in 1996, the specification for the instrument gives a spatial resolution similar to Landsat TM, with a varied brief of applications in various disciplines. Among these criteria has been the requirement to collect data from off-nadir view angles for estimates of the Bidirectional Reflectance Distribution Function (BRDF) of vegetative canopies.

Assuming that it is possible to target the sensor quickly using the along-track pointing facility, ten 30x30km images could be acquired of a single scene in the space of 4.75 minutes (table 6.3). This would be achieved by successively pointing the instrument down-track, collecting 1000 scan lines of data, slewing the pointing system, waiting for the instrument to settle, and restarting data acquisition at the appropriate instant. Based upon the experience of this study, images acquired at 10° intervals would be suitable for the analysis of variance; since the off-nadir tilt capability is between +60° to -30°, this means ten images could be acquired.

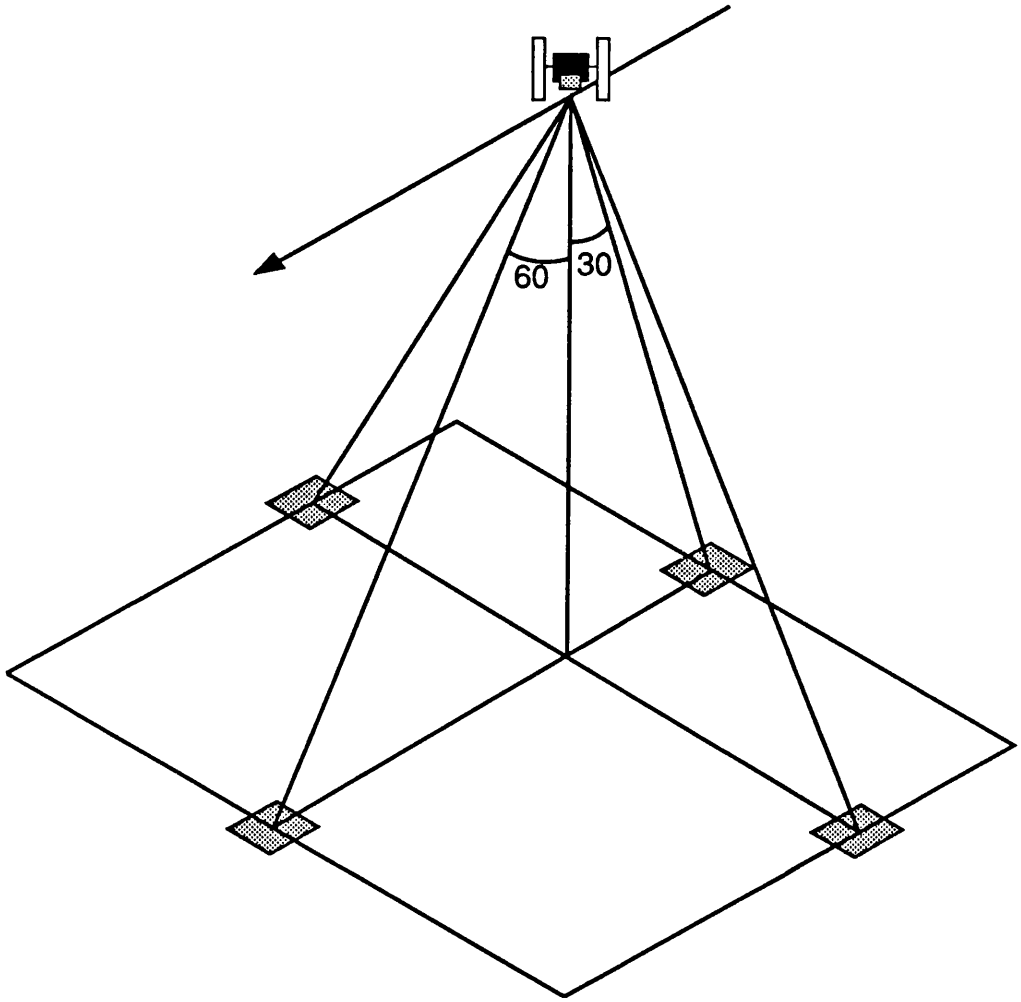


Figure 6.1: The HIRIS sensor geometry. HIRIS points off-nadir in both the along- and across-track directions.

**Table 6.3: Tracking capability of HIRIS**

| | |
|---|---|
| Nominal Altitude | 824km |
| Slew rate (max) | $5° s^{-1}$ (down-track), $2^{o-1}$ (cross-track) |
| Settling time | 0.5 sec |
| Ground speed | $6.67 km.s^{-1}$ |

(NASA, 1987)

The variation of the size of the GRE, in both the down- and cross-track directions, is given in figures 6.1 and 6.2 and table 6.4. Unlike the ATM scanner, this is easier to calculate because HIRIS is a pushbroom sensor, sampling one line of the image at a time using a solid-state array. GRE size in the cross-track direction is therefore equal to pixel size, since the detectors abut each other, and is proportional to view angle. In the down-track direction pixel size is constant, irrespective of the down-track viewing angle, because it is determined by the speed of the sensor over the ground and the sampling rate (Barnsley and Kay, 1989, Townshend, 1981). The size of the GRE down-track, however, will increase with the change in view angle geometry in both these directions. While oversampling between adjacent GREs will not take place cross-track, in the down-track direction oversampling between lines will be proportional to the viewing angle. Based upon the figures calculated in table 6.4, scan lines will overlap nearly by 50% at 60° down-track view angles.

The spatial resolution offered by HIRIS is probably not high enough to allow the assessment of canopies in the manner outlined in this study without modification. For semi-natural or natural vegetation communities, however, 30m may provide a suitable initial resolution for image variance analysis.

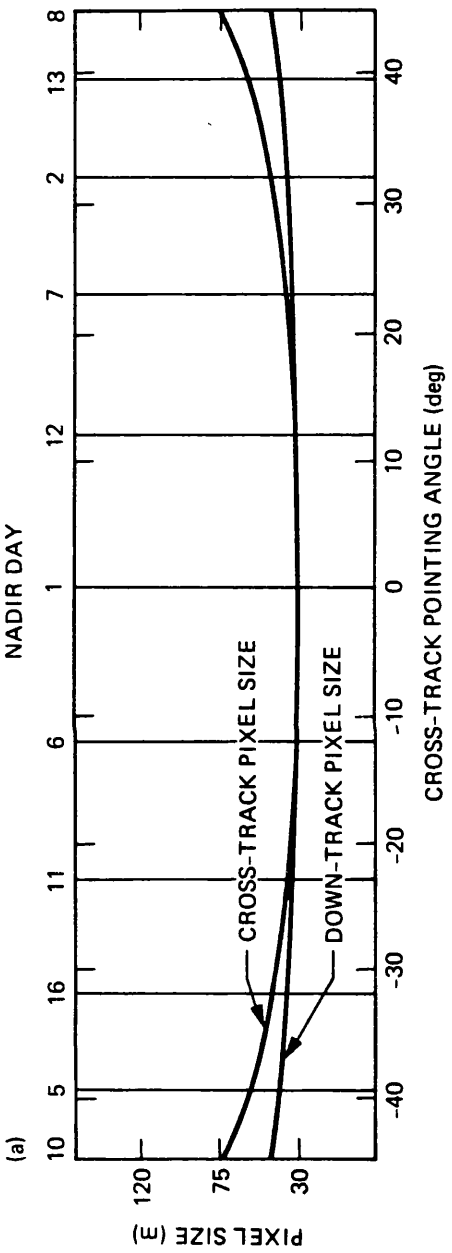


Figure 6.2: HIRIS sensor GRE size. (From NASA, 1987)

**Table 6.4: Variation in GRE size of HIRIS (meters)**

| | | | | | | | | | | |
|---|---|---|---|---|---|---|---|---|---|---|
| Down-track angle | +60° | +50° | +40° | +30° | +20° | +10° | 0° | -10° | -20° | -30° |
| GRE size along-track* | 59.3 | 46.1 | 38.7 | 34.3 | 31.6 | 30.1 | 29.7 | 30.1 | 31.6 | 34.3 |
| Cross-track angle | +24° | +20° | +15° | +10° | +5° | 0° | | | | |
| GRE size cross-track• | 32.5 | 31.6 | 30.7 | 30.1 | 29.8 | 29.7 | | | | |

* Pixel size constant at 30m

• Pixel size equals GRE

The HIRIS instrument will provide excellent data collection possibilities in general for off-nadir studies of vegetation in the future. The down-track pointing capability allows a multiple image dataset to be collected in one view azimuth plane, with the minimum of variation in illumination geometry since local time will change by less than five minutes. Good temporal coverage (four to five day revisit at the Equator; NASA, 1987) is provided by the across-track pointing facility. Effects of changing atmospheric composition and changing irradiance conditions will be minimised, since the short data collection periods will reduce temporal variations in conditions and the off-nadir strategy will allow better modelling of the effects. A large number of spectral channels covering a broad spectrum will ensure the best possible choice of bands for a wide variety of Earth surface materials. Finally, the synergistic capabilities with other EOS instruments, in particular MODIS-N and MODIS-T, will allow the extrapolation of the fine resolution analysis to a broader regional scale.

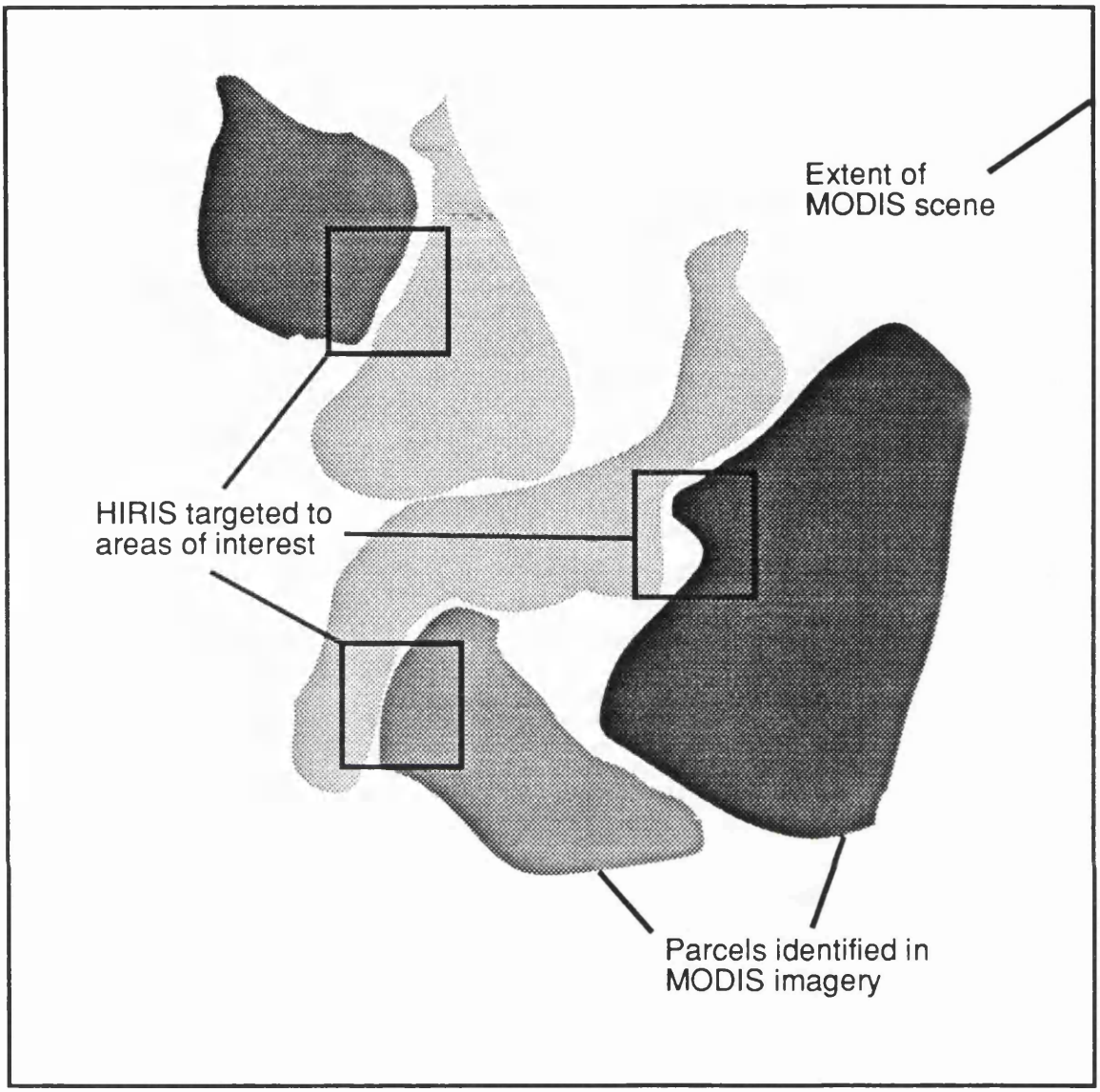


Figure 6.3: Synergistic use of MODIS and HIRIS.

### 6.3.3: Synergistic operation of the HIRIS and MODIS instruments

It is desirable to devise a strategy to combine the broad, high temporal resolution overview capabilities of the MODIS instruments with the greater spectral and spatial resolutions of the HIRIS sensor. The complementary designs of these two instruments provides for an examination of Earth surface phenomena at two distinct scales. The potential of each of the datasets is increased when the instruments are used synergistically, and data collection strategies should reflect these possibilities.

Using MODIS, spectral analysis of image data at a regional scale can be made, in order to define regions of interest as a function of homogeneity, heterogeneity, or temporal variation. Once "target areas" are identified, HIRIS can be used to examine sections of these regions in detail, in order to facilitate extrapolation of interpretation over a wider area. While HIRIS offers a greater number and range of spectral channels, as well as increased spatial resolution, over the MODIS sensors, the off-nadir capability would mean that multiple angle analysis of image variance could also take place. Hence, while MODIS could be used to identify a homogeneous parcel in an ecosystem, say a forest, HIRIS could be used to estimate canopy parameters such as tree height and density. These estimates could then be extrapolated to other similar parcels identified by the MODIS imagery (figure 6.3).

### 6.3.4: Multi-angle Imaging SpectroRadiometer (MISR)

The Multi-angle Imaging SpectroRadiometer (MISR) is a further experiment on board EOS, intended primarily to address the effects of geophysical processes and human activities on the Earth's ecology and climate (Diner *et al.*, 1988). One of the named areas of investigation is the inference of vegetation canopy structural parameters by the utilisation of the multiple view angle imaging system. Eight identical CCD-based pushbroom cameras acquire data at four viewing angles - 25.8°, 45.6°, 60.0° and 72.5° - in the fore and aft directions. Data will be collected in four narrow (20-60 nm) spectral bands, at 440, 550, 670 and 860 nm,

with a choice of two spatial resolutions - 'Global' mode, 1.73km, and 'Local' mode, 216m.

MISR offers a good opportunity for the collection of multiple view angle datasets, since the hardware system may prove to be more reliable than HIRIS due its simpler design. The reduced number of spectral channels and spatial resolution and the lack of a nadir view, however, decrease its potential when compared to the more sophisticated spectroradiometer instruments planned for the EOS platform.

### 6.3.5: SPOT 2-4

Further versions of the SPOT-HRV sensor are planned for the 1990's. Although the later instruments will have an increased number of spectral channels, and improved spatial resolution in the red band, the off-nadir pointing capability will remain cross-track. These instruments will not provide a significant improvement over the current SPOT-1 sensor for the purposes of collecting multiple view angle image data.

## 6.4: Conclusions

In this chapter the suitability of different sensors for multiple view angle data collection strategy has been assessed. Only one current sensor configuration, airborne sensors with wide fields of view, satisfies the four criteria of view angle, near simultaneous coverage, spatial and spectral resolution well enough to be considered as an operational source of data. The problems of using airborne data, in particular data quantity, quality and cost, are also highlighted. The AVHRR series of satellite sensors are also considered to be useful for the collection of multiple view angle datasets, although further research would be required to examine the effect of different illumination geometries, and the sampling of cover types by coarse scale resolution cells, upon the variance of image data.

With the launch of the EOS platform in 1996, more off-nadir viewing sensors will become available. In particular, the HIRIS instrument will provide excellent quality data for the implementation of a multiple view angle strategy, minimising the atmospheric, illumination and temporal effects on the target restricting the application of current sensors in such a method. In conjunction with the two MODIS instruments, HIRIS will provide an operational capability of extending interpretation of cover type characteristics over a global scale, improving upon the synergistic capabilities presently available with sensors like Landsat TM and AVHRR.

The launch date of the EOS platform is still some years away, however, and some doubt as to the final specification of the sensors to go on board the platform still remain. From current information (November 1989), MODIS-N is likely to go ahead as planned; MODIS-T may have the tilt mechanism restricted to ±20°, severely limiting its usefulness for off-nadir studies; and HIRIS could be launched on a different platform (if at all), due to the problems caused by the extremely high data-rate from the instrument.

Two final considerations need to be made in assessing the practicality of multiple view angle image data methods. First, the cost of multiple angle datasets is very high, since it is directly proportional to the number of views required. The collection of such datasets would need to be justified on economic grounds before they could be considered feasible. Second, it needs to be established more precisely exactly what information is required by the Earth science and agriculture communities. Only when these two questions have been answered can the development of new sensors take place.

# CHAPTER 7: Summary and conclusions

It has been demonstrated in this study that multiple view angle image data acquired by an airborne sensor have characteristics relating to the anisotropic reflectance properties of variety of vegetative and bare soil cover types. Rather than these characteristics always presenting a problem, it is considered possible to use them to determine qualitative and quantitative information regarding the nature of these surfaces. In some instances, this approach may have advantages over more conventional radiometric procedures that assume nadir data collection geometries.

A number of different ways of extracting quantitative information concerning agro-physical parameters of vegetative Earth surface materials have been developed, and are recorded in the literature. In particular, reflectance models which account for the anisotropic reflectance characteristics of these surfaces have been developed; however, in general they still only allow the relation of measurements of reflected radiance indirectly to these parameters. For these reasons such models are unsatisfactory, and the requirement of a more direct means of assessing canopy characteristics arises. A number of studies, in particular those carried out by Strahler *et al.* (Li and Strahler, 1985, 1986, Woodcock, 1985, Strahler *et al.*, 1986, Woodcock and Strahler, 1987, Franklin and Strahler, 1988, Strahler *et al.*, 1988) have examined the geometric structure of scenes, developing an understanding of the relationship between scene structure, sensor characteristics and the image. It is concluded that by understanding these relationships it would be possible to devise a method by which image variance could be used to extract quantitative information concerning the geometric structure of the surface.

This study extends the area of earlier research by examining the relationship between view angle and image variance, for a number of agricultural cover types. As well as the expected changes in variance as a result of degraded spatial resolutions off-nadir, canopy geometry was predicted to play an important part in the variance of the radiance detected by the sensor. The intention of the study, therefore, was to examine the possibility of identifying the effect of canopy geometry on image variance at different view angles, and explore the possibilities

of developing a method for extracting information concerning agro-physical parameters of the surface under observation.

The data used in this study were acquired using an airborne sensor, the Daedalus Airborne Thematic Mapper. Airborne instruments in general, and the ATM in particular, have complex sensor geometries. The exact geometry for this sensor, including the size of the GRE and view angle for each sample in the image, was derived. Initial results demonstrated that changes in image variance could be expected for the same parcel on the ground when viewed from different view angles; image variance would be expected to decline with increased sensor view angle.

A number of other effects could also account for changing variance in images acquired from a number of parallel flightlines, as in this study. Here, the use of reflectance images was developed to remove the differences between flightlines due to changed illumination geometry, atmospheric effects and topography. The remaining differences between the images could then be explained purely in terms of the different sensor geometry. It was established that in this study, in fact, these external factors were less important than expected and analysis proceeded using the raw data, since the reflectance image data suffered from quantisation effects and corrupted data distributions, rendering the data unreliable for the analysis of variance.

Several geometric factors affect the variance of remotely sensed image data; these include the effects of scene structure as well as the interaction of the sensor sampling frequency and scene spatial variability. In particular, with Daedalus ATM data three interacting factors are important:

- The enlarged area of the GRE with increased sensor view angle
- The increased spatial autocorrelation between adjacent GREs, resulting from increased overlap of adjacent GREs at off-nadir viewing angles
- And the changing proportions of canopy elements when viewed obliquely

It was determined in this study that this third factor will cause the change in image variance with view angle to be directly related to canopy structure. Further, it was demonstrated that general descriptions of canopy type, based upon the concepts of *H*- *M*- and *L*- relative resolution models proposed by Woodcock and Strahler (Woodcock, 1985, Strahler *et al.*, 1986), can be made from the analysis of these results. In this study, this interpretation is carried out by quantifying the relationship between the two parameters of view angle and image variance, measured as the Coefficient of Variation of a parcel, by using linear and non-linear regression techniques. By interpreting the coefficients of these regression equations it is possible to identify whether a parcel is homogeneous vegetative cover, partial cover or bare soil, based upon knowledge of the sampling frequency of the sensor (or spatial resolution) and the expected variation of different Earth surface materials. While this technique is not developed significantly further in this study, in order to extract quantitative information concerning the nature of the canopy, extensions to the model are discussed and ways in which this could be achieved outlined.

Finally, it was established that although the method of multiple view angle data analysis developed here would be difficult to implement using current sensors, future instruments such as HIRIS and MISR, both to be launched upon the NASA EOS platform in 1996, would provide high quality data which could easily be used in such a strategy. Considerations of cost and suitability of such data products that could be obtained from such a strategy should be made before the general application of this method or the investment in future bespoke technology.

A number of areas of further work are necessary in order to evaluate exactly the nature of the relationship between view angle and image variance. These are as follows:

- Rigorous methods should be devised to improve upon the assumption of negligible atmospheric attenuation in the red and NIR spectral regions, in order to construct a more generally applicable method.

- Data collection of irradiance should be carried out using a pointable spectrometer, in order to gather better data to input into the Terrain Lite model devised in this study. These data could also be used in the empirical validation of the assumptions in this model concerning the spectral and spatial distributions of sky radiance.

- More effective methods of production should be devised for the generation of reflectance images, that avoid the problems of increased quantisation of data and thereby degrading the reliability of such data in the use of variance analysis.

- The effect of row structure and the associated illumination and sensor geometries upon image variance is not yet fully understood. Such an understanding would be a prerequisite to the operational use of this multiple view angle data strategy in the assessment of cultivated vegetative surfaces.

- Further studies using sensors capable of increased off-nadir viewing, beyond 37°, should be made in order to ascertain whether it is possible to extract parameters of row spacing and canopy height, where these are applicable.

In conclusion, this study has demonstrated two major points. First, it has confirmed that the analysis of variance in image data could provide a useful source of information concerning scene structure. Second, it has shown that multiple angle image data can also be used to extract quantitative information concerning vegetative Earth surface materials, by virtue of the effects of canopy geometry upon the radiance detected by the sensor.

# References


Ahmad, S.P., Middleton, E.M., and Deering, D.W. (1987). Computation of diffuse sky irradiance from multidirectional radiance measurements. *Remote Sensing of Environ.*, Vol. 21, pp. 185-200.

Allen, W.A., Gayle, T.V., and Richardson, A.J. (1970). Plant-canopy irradiance specified by the Duntley equations. *J. Opt. Soc. Am.*, 60, pp. 372-376.

Asrar, G., Kanemasu, E.T., Miller, G.P., and Weiser R.L. (1986). Light interception and leaf area estimates from measurements of grass canopy reflectance. *IEEE Trans. Geosc. Remote Sensing*, Vol. GE-24, No. 1, pp. 76-81.

Atkinson, P.M. (1988). Optimal sampling for remote sensing: estimating the regional mean. *Proceedings of IGARSS '88 Symposium, Edinburgh, Scotland, 13-16 Sept. 1988*, pp. 1793-1796. (*ESA SP-284.*)

Atkinson, P.M., and Danson, F.M. (1988). Spatial resolution for remote sensing of forest plantations. *Proceedings of IGARSS '88 Symposium, Edinburgh, Scotland, 13-16 Sept. 1988*, pp. 221-223. (*ESA SP-284.*)

Badhwar, G.D., Verhoef, W., and Bunnik, J.J. (1985). Comparative study of Suits and SAILS canopy reflectance models. *Remote Sensing of Environ.*, Vol. 17, pp. 179-195.

Baret, F., Champion, I., Guyot, G., and Podaire, A. (1987). Monitoring wheat canopies with a high spectral resolution radiometer. *Remote Sensing of Environ.*, Vol. 22, pp. 367-378.

Barnsley, M.J. (1984a). Effects of off-nadir view angles on the detected spectral response of vegetation canopies. *Int. J. Remote Sensing*, Vol. 5, No. 4, pp. 715-728.

Barnsley, M.J. (1984b). Integration of multispectral data obtained at different view angles for vegetation analysis. *Proc: Integrated Approaches in Remote Sensing, Guildford, UK, 8-11 April 1984*, pp. 135-142. (*ESA SP*-214).

Barnsley, M.J. (1985). Classification accuracy of land cover types as a function of sensor view angle. *Proceedings of the International conference of the RSS and CERMA, University of London, 9-12th September, 1985*, Vol. 2, pp. 143-152.

Barnsley, M.J., and Kay, S. (1989). The relationship between sensor geometry, vegetation canopy geometry, and image variance. *Int. J. Remote Sensing.* (In press.)

Barnsley, M.J., and Muller, J-P. (1989). *Angular variations of reflectance in multiple look-angle satellite and aircraft imagery.* Interim report to the NERC on Grant No. GR3/7020, 20p.

Baudoin, A., and Brossier, R. (1983). The SPOT programme at IGN-F. *Int. Archives of Photogrammetry*, Vol. 24, Part 1, pp. 174-179.

Bird, R.E. (1982). Terrestrial Solar spectral Modelling. *Solar Cells*, Vol. 7, pp. 107-118.

Bird, R.E., and Hulstrom, R.L. (1983). Terrestrial Solar spectral data sets. *Solar Energy*, Vol. 30, No. 6, pp. 563-573.

Bryant, N.A., Zobrist, A.L., Walker R.E., and Gokhman, B. (1985). An analysis of Landsat thematic mapper P-product internal geometry and conformity to Earth surface geometry. *Photogramm. Engng. Remote Sensing*, Vol. 51, No. 9, pp. 1435-1447.

Callison, R.D., Blake, P., and Anderson, J.M. (1987). The quantitative use of airborne thematic mapper thermal infrared data. *Int. J. Remote Sensing*, Vol. 8, No.1, pp. 113-126.

Campbell, N.A., De Boer, E.S., and Hick, P.T. (1987). Some observations on crop profile modelling. *Int. J. Remote Sensing*, Vol. 8, No. 2, pp. 193-201.

Chevrel, M., Courtois, M., Weill, G. (1981). The SPOT satellite remote sensing mission. *Photogramm. Engng. Remote Sensing*, Vol. 47, No. 8, pp. 1163-1171.

Clevers, J.G.P.W. (1986). Application of remote sensing to agricultural field trials. Ph.D. thesis, Agricultural University Wageningen papers, 86-4.

Clevers, J.G.P.W. (1988). The derivation of a simplified reflectance model for the estimation of leaf area index. *Remote Sensing of Environ.*, Vol. 25, pp. 53-69.

Cliff, A.D., and Ord, J.K. (1973). *Spatial Autocorrelation*, 178pp. Pion Ltd., London.

Crippen, R.E. (1987). The regression intersection method of adjusting image data for band ratioing. *Int. J. Remote Sensing*, Vol. 8, No. 2, 137-155.

Crippen, R.E. (1988). The dangers of underestimating the importance of data adjustments in band ratioing. *Int. J. Remote Sensing*, Vol. 9, No. 4, pp. 767-776.

Croxton, F.E., Cowden, D.J., and Klein, S. (1967). *Applied General Statistics*, 754pp. Pitman, London, New York, Toronto.

Curran, P.J. (1987). What is a semi-variogram? *Proceedings of the 13th annual conference of the RSS, Nottingham 7th-11th, 1987*, pp. 36-45. (Remote Sensing Society, Nottingham.)

Curran, P.J., and Williamson, H.D. (1985). The accuracy of ground data used in remote sensing investigations. *Int. J. Remote Sensing*, Vol. 6, No. 10, pp. 1637-1651.

Curran, P.J., and Williamson, H.D. (1987). Airborne MSS data to estimate GLAI. *Int. J. Remote Sensing*, Vol. 8, No. 1, pp. 57-74.

Cushnie, J. (1988). The acquisition of SPOT-1 HRV imagery over southern Britain and northern France, May 1986-May 1987. *Int. J. Remote Sensing*, Vol. 9, No. 1, pp. 159-167.

Danson, F.M. (1987). Estimating forest stand parameters using airborne MSS data. *Proceedings of the 13th annual conference of the RSS, Nottingham 7th-11th, 1987*, pp. 46-54. (Remote Sensing Society, Nottingham.)

Dave, J.V. (1978). Extensive datasets of the diffuse radiation in realistic atmospheric models with aerosols and common absorbing gases. *Solar Energy*, Vol. 21, pp. 361-369.

Deering, D.W. (1988). PARABOLA directional field radiometer for aiding in space sensor data interpretations. [publication unknown]

Deering, D.W., and Eck, T.F. (1987). Atmospheric optical depth effects on angular anisotropy of plant canopy reflectance. *Int. J. Remote Sensing*, Vol. 8, No. 6, pp. 893-916.

Diner, D.J., Bruegge, C.J., Martonchik, J.V., Ackerman, T.P., Davies, R., Gerstl, S.A.W., Gordon, H.R., and Sellers, P.J. (1988). Geophysical and climatological research using a Multi-angle Imaging SpectroRadiometer (MISR). *Flight proposal to NASA by JPL*, JPL, Pasadena, California.

Dowman, I.J. (1985). Space Cartography. *Proc. University Dundee summer school Remote Sensing Appns. in Civil Engineering, Dundee 19 Aug. - 8 Sept. 1984.* (ESA SP-216, 1985)

Dozier, J., and Frew, J. (1989). Rapid calculation of terrain parameters from digital elevation data. *Proceedings of IGARSS'89; 12th Canadian symposium on Remote Sensing, Vancouver, July 10-14, 1989*, Vol. 3, pp. 1796-1774.

Duggin, M.J. (1985). Factors limiting the discrimination and quantification of terrestrial features using remotely sensed radiance. *Int. J. Remote Sensing*, Vol. 6, No. 1, pp. 3-27.

Duntley, S.Q. (1942). The optical properties of diffusing materials. *J. Opt. Soc. Am.*, 32, pp. 61-70.

Dymond, J.R. (1988). Nonparametric modeling of radiance in Hill Country. *Remote Sensing of Environ.*, Vol. 25, pp. 3-21.

Egbert, D.D. (1977). A practical method for correcting bidirectional reflectance variations. *Proc. Symp. Machine Processing Remotely Sensed Data.* LARS, Purdue University, pp. 178-185.

Escadafal, R., Girard, M-C, and Courault, D. (1989). Munsell soil color and soil reflectance in the visible spectral bands of Landsat MSS and TM data. *Remote Sensing of Environ.*, Vol. 27, pp. 37-46.

Foody, G.M. (1988). The effects of viewing geometry on image classification. *Int. J. Remote Sensing*, Vol. 9, No. 12, pp. 1909-15.

Forgan, B.W. (1980). The influence of sky radiance distributions on the measurement of diffuse irradiance with shadowbands. *Arch. Met. Geoph. Biokl., Ser. B*, Vol. 28, pp. 373-384.

Franklin, J., Logan, T.L., Woodcock, C.E., and Strahler, A.H. (1986). Coniferous forest classification and inventory using Landsat and digital terrain data. *IEEE Trans. Geosc. Remote Sensing*, Vol. GE-24, No. 1, pp. 139-149.

Franklin, J., and Strahler, A.H. (1988). Invertible canopy reflectance modeling of vegetation structure in semiarid woodland. *IEEE Trans. Geosc. Remote Sensing*, Vol. 26, No. 6, pp. 809-824.

Fraser, R.S., and Kaufman, Y.J. (1985). The relative importance of aerosol scattering and absorption in remote sensing. *IEEE Trans. Geosc. Remote Sensing*, Vol. GE-23, No. 5, pp. 625-633.

Gallo, K.P., and Flesch, T.K. (1989). Large-area crop monitoring with the NOAA AVHRR: estimating the silking stage of corn development. *Remote Sensing of Environ.*, Vol. 27, pp. 73-80.

Gerstl, S.A.W., and Simmer, C. (1986). Radiation physics and modelling for off-nadir satellite-sensing of non-Lambertian surfaces. *Remote Sensing of Environ.*, Vol. 20, pp. 1-29.

Goel, N.S. (1988). A perspective on vegetation canopy reflectance models. *Proceedings of the 4th International Colloquium on Spectral Signatures of Objects in Remote Sensing*, Aussois, France, 18-22 January 1988. (*ESA SP-287*, pp. 77-85.)

Goel, N.S. and Deering, D.W. (1985). Evaluation of a canopy reflectance model for LAI estimation through its inversion. *IEEE Trans. Geosc. Remote Sensing*, Vol. GE-23, No. 5, pp. 674-684.

Goel, N.S., and Grier, T. (1986). Estimation of canopy parameters for inhomogeneous vegetation canopies from reflectance data I. Two-dimensional row canopy. *Int. J. Remote Sensing*, Vol. 7, No. 5, pp. 665-681.

Goel, N.S., and Grier, T. (1987). Estimation of canopy parameters of row planted vegetation canopies using reflectance data for only four view directions. *Remote Sensing of Environ.*, Vol. 21, pp. 37-51.

Goel, N.S., and Grier, T. (1988). A model for radiative transfer in heterogeneous three-dimensional canopies. *Proceedings of the 4th International Colloquium on Spectral Signatures of Objects in Remote Sensing*, Aussois, France, 18-22 January 1988. (*ESA SP-287*, pp. 133-136.)

Goel, N.S. and Reynolds, N.E. (1989). Bidirectional canopy reflectance and its relationship to vegetation characteristics. *Int. J. Remote Sensing*, Vol. 10, No. 1, pp. 107-132.

Goel, N.S., and Strebel, D.E. (1983). Inversion of vegetation canopy reflectance models for estimating agronomic variables. I.. problem definition and initial

results using the Suits' model. *Remote Sensing of Environ.*, Vol. 13, pp. 487-507.

Goel, N.S., and Thompson, R.L. (1984a). Inversion of vegetation canopy reflectance models for estimating agronomic variables. III. Estimation using only canopy reflectance data as illustrated by the Suits' model. *Remote Sensing of Environ.*, Vol. 15, pp. 223-236.

Goel, N.S., and Thompson, R.L. (1984b). Inversion of vegetation canopy reflectance models for estimating agronomic variables. IV. Total inversion of the SAIL model. *Remote Sensing of Environ.*, Vol. 15, pp. 237-253.

Grant, L. (1987). Diffuse and specular characteristics of leaf reflectance. *Remote Sensing of Environ.*, Vol. 22, pp. 309-322.

Gratzki, A., and Gerstl, S.A.W. (1989). Sensitivity of an atmospheric correction algorithm for non-Lambertian vegetation surfaces to atmospheric parameters. *IEEE Trans. Geosc. Remote Sensing*, Vol. 27, No. 3, pp. 326-331.

Gueymard, C. (1987). An anisotropic solar irradiance model for tilted surfaces and its comparison with selected engineering algorithms. *Solar Energy*, Vol. 38, No. 5, pp. 367-386.

Hall-Könyves, K. (1987). The topographic effect on Landsat data in gently undulating terrain in Southern Sweden. *Int. J. Remote Sensing*, Vol. 8, No. 2, pp. 157-168.

Hall-Könyves, K. (1988). *Remote Sensing of cultivated lands in the south of Sweden.* Ph.D. thesis. (Lund University Press, Sweden)

Hämälainen, M., Nurkkanen, P., and Slåen, T. (1985). A multisensor pyranometer for determination of the direct component and angular distribution of solar radiation. *Solar Energy*, Vol. 35, No. 6, pp. 511-525.

Hartung, R.E., and Lloyd, W.J. (1969). Influence of aspect on forests of the Clarksville soils in Dent county, Missouri. *J. Forestry*, Vol. 26, pp. 178-182.

Hatfield, J.L., Kanemasu, E.T., Asrar, G., Jackson, R.D., Pinter, P.J., Reginato, R.J., and Idso, S.B. (1985). Leaf area estimates from spectral measurements over various planting dates of wheat. *Int. J. Remote Sensing*, Vol. 6, No. 1, 167-175.

Henricksen, B.L. (1986). Reflections on drought: Ethiopia 1983-1984. *Int. J. Remote Sensing*, Vol. 7, no. 11, pp. 1447-1451.

Heydorn, R.P., and Takacs, H.C. (1986). On the design of classifiers for crop inventories. *IEEE Trans. Geosc. Remote Sensing*, Vol. GE-24, No. 1, pp. 150-156.

Hinzman, L.D., Bauer, M.E., and Daughtry, C.S.T. (1986). Effects of nitrogen fertilization on growth and reflectance characteristics of winter wheat. *Remote Sensing of Environ.*, Vol. 19, pp. 47-61.

Holben, B.N. (1986). Characteristics of maximum-value composite images from temporal AVHRR data. *Int. J. Remote Sensing*, Vol. 7, no. 11, pp. 1417-1434.

Holben, B.N., and Fraser, R.S. (1984). Red and near-infrared sensor response to off-nadir viewing. *Int. J. Remote Sensing*, Vol. 5, No. 1, pp. 145-160.

Holben, B.N., and Justice, C.O. (1980). The topographic effect on spectral response from nadir pointing sensors. *Photogramm. Engng. Remote Sensing*, Vol. 46, No. 9, pp. 1191-1200.

Holben, B.N., and Justice, C.O. (1981). An examination of spectral band ratioing to reduce the topographic effect on remotely sensed data. *Int. J. Remote Sensing*, Vol. 2, No. 2, pp. 115-133.

Holben, B., Kimes, D., and Fraser, R.S. (1986). Directional reflectance response in AVHRR red and near-IR bands for three cover types and varying atmospheric conditions. *Remote Sensing of Environ.*, Vol. 19, pp. 213-236.

Hook, S.J., and Donoghue, N.M. (1988). Calibration and correction of view angle effects in the Visible/Near Infrared and Thermal data. *Proceedings of the NERC 1986 Airborne campaign workshop, 24th February 1988*, pp. 187-202.

Huete, A.R., Jackson, R.D., and Post, D.F. (1985). Spectral response of a plant canopy with different soil backgrounds. *Remote Sensing of Environ.*, Vol. 17, pp. 37-53.

Hugli, H., and Frei, W. (1983). Understanding anisotropic reflectance in mountainous terrain. *Photogramm. Engng. Remote Sensing*, Vol. 49, No. 5, pp. 671-683.

Ineichen, P., Perez, R., and Seals, R. (1987). The importance of correct albedo determination for adequately modelling energy received by tilted surfaces. *Solar Energy*, Vol. 39, No. 4, pp. 301-305.

Irons, J.R., Johnson (Jr.), B.L., and Linebaugh, G.H. (1987). Multiple-angle observations of reflectance anisotropy from an airborne linear array sensor. *IEEE Trans. Geosc. Remote Sensing*, Vol. GE-25, No. 3, pp. 372-383.

Irons, J.R., and Labovitz, M.L. (1982). A data analytic approach to look-angle radiance adjustment. *J. Applied Photogramm. Engng.*, Vol. 8, pp. 128.

Jackson, R.D., and Pinter (Jr.), P.J. (1986). Spectral response of architecturally different wheat canopies. *Remote Sensing of Environ.*, Vol. 20, pp. 43-56.

Jackson, R.D., Pinter, P.J., Reginato, R.J., and Sherwood B.I. (1986). Detection and evaluation of plant stresses for crop management decisions. *IEEE Trans. Geosc. Remote Sensing*, Vol. GE-24, No. 1, pp. 99-106.

Jones, A.R., Settle, J.J., and Wyatt, B.K. (1988). Use of digital terrain data in the interpretation of SPOT-1 HRV multispectral imagery. *Int. J. Remote Sensing*, Vol. 9, No. 4, pp 669-682.

Jones, A.R., and Wyatt, B.K. (1989). Remote sensing for monitoring and inventory of protected landscapes: resources management in a less favoured area. *Proceedings of the 15th Annual Conference of the Remote Sensing Society, University of Bristol, 13-15 September 1989*, pp. 193-200. (Remote Sensing Society, Nottingham)

Jupp, D.L.B., Strahler, A.H., Woodcock C.E. (1988). Autocorrelation and regularization in digital images; I. Basic Theory. *IEEE Trans. Geosc. Remote Sensing*, Vol. GE-26, No. 4, pp. 463-473.

Jupp, D.L.B., Strahler, A.H., Woodcock, C.E. (1989). Autocorrelation and regularization in digital images II. Simple image models. *IEEE Trans. Geosc. Remote Sensing*, Vol. GE-27, No. 3, pp. 247-258.

Justice, C.O., Wharton, S.W., and Holben, B.N. (1981). Application of digital terrain data to quantify and reduce the topographic effect on Landsat data. *Int. J. Remote Sensing*, Vol. 2, No. 3, pp. 213-230.

Kalayeh, H.M., and Landgrebe, D.A. (1986). Utilizing multitemporal data by a stochastic model. *IEEE Trans. Geosc. Remote Sensing*, Vol. GE-24, No. 5, pp. 792-795.

Kaufman, Y.J. (1988). Atmospheric effect on spectral signature - measurements and corrections. *IEEE Trans. Geosc. Remote Sensing*, Vol. GE-26, No. 4, pp. 441-450.

Kauth, R.J., and Thomas, G.S. (1976). The tasselled cap - a graphic description of the spectral-temporal development of agricultural crops as seen by Landsat. *Proc. 2nd Int. Symp. Machine Processing Remotely Sensed Data.* LARS, Purdue University, pp. 4B- 41-45.

Kay, S. (1987). The differential rectification of SPOT HRV panchromatic data using a Digital Elevation Model. M.Sc. Thesis, University of London.

Kay, S. (1988). The differential rectification of SPOT HRV panchromatic and multispectral imagery using a digital elevation model. *Proceedings of IGARSS '88 Symposium, Edinburgh, Scotland, 13-16 Sept. 1988, pp. 479-481. (ESA SP-284.)*

Kay, S. (1989). A holistic methodology for the pre-processing of multiple view angle image data. *Proceedings of the 15th Annual Conference of the Remote Sensing Society, University of Bristol, 13-15 September 1989*, pp. 201-206. (Remote Sensing Society, Nottingham)

Kay, S., and Barnsley, M.J. (1989). The relationship between vegetation canopy geometry and image statistics in a multiple view angle data set. *Proceedings of the 15th Annual Conference of the Remote Sensing Society, University of Bristol, 13-15 September 1989*, pp. 207-213. (Remote Sensing Society, Nottingham)

Kimes, D.S. (1984). Modeling the directional reflectance from complete homogeneous vegetation canopies with various leaf-orientation distributions. *J. Opt. Soc. Am.*, Vol. 1, No. 7, pp. 725-737.

Kimes, D.S., Holben, B.N., Tucker, C.J., and Newcomb, W.W. (1984). Optimal directional view angles for remote sensing missions. *Int. J. Remote Sensing*, Vol. 5, No. 6, 887-908.

Kimes, D.S., and Newcomb, W.W. (1987). Directional scattering properties of a wintering deciduous hardwood canopy. *IEEE Trans. Geosc. Remote Sensing*, Vol. GE-25, No. 4, pp. 510-515.

Kimes, D.S., Newcomb, W.W., Nelson, R.F., and Schutt, J.B. (1986). Directional reflectance distributions of a hardwood and pine forest canopy. I.E.E.E. Trans. on Geoscience and Remote Sensing, Vol. GE-24, No. 2, pp. 281-293.

Kimes, D.S., Sellers, P.J., and Diner, D.J. (1987). Extraction of spectral hemispherical reflectance (albedo) of surfaces from nadir and directional reflectance data. *Int. J. Remote Sensing*, Vol. 8, No. 12, pp. 1727-1746.

Kimes, D.S., Smith, J.A., and Ranson, K.J. (1980). Vegetation reflectance measurements as a function of solar zenith angle. *Photogramm. Engng. Remote Sensing*, Vol. 46, No. 12, pp. 1563-1573.

Kirchner, J.A., Schnetzler, C.C., and Smith, J.A. (1981). Simulated directional radiances of vegetation from satellite platforms. *Int. J. Remote Sensing*, Vol. 2, No. 3, pp. 253-264.

Kondratyev, K.Ya. (1969). *Radiation in the atmosphere.* (Academic Press, New York and London, 912 pp.)

Kouremenos, D.A., Antonopoulos, K.A., and Doulgrakis, S. (1987). Direct and diffuse solar radiation correlations for tilted surfaces in Athens, Greece. *Solar Energy*, Vol. 38, No. 3, pp. 203-217.

Kriebel, K.T. (1978). Measured spectral bidirectional reflectance properties of four vegetated surfaces. *Applied Optics*, Vol. 17, No. 2, pp. 253-259.

Kubelka, P., and Munk, F. (1931). Ein beitrag zur optek der farbonstriche. *Zeitschrift fur technische physik*, 12, pp. 593-601.

Langer, R.H.M., and Hill, G.D. (1982). *Agricultural Plants.* Cambridge University Press, 344pp.

Lee, T.Y., and Kaufman, Y.J. (1986). Non-lambertian effects on remote sensing of surface reflectance and vegetation index. *IEEE Trans. Geosc. Remote Sensing*, Vol. GE-24, No. 5, pp. 699-708.

Leprieur, C.E., Durand, J.M., and Peyron, J.L. (1988). Influence of topography on forest reflectance using Landsat Thematic Mapper and digital terrain data. *Photogramm. Engng. Remote Sensing*, Vol. 54, No. 4, pp. 491-496.

Lewis, G. (1987). The applicability of diffuse solar radiation models to Huntsville, Alabama. *Solar Energy*, Vol. 38, No. 1, pp. 55-57.

Li, X., and Strahler A.H. (1985). Geometric optical modelling of a conifer forest canopy. *IEEE Trans. Geosc. Remote Sensing*, Vol. GE-23, No. 5, pp. 705-719.

Li, X. and Strahler, A.H. (1986). Geometric-optical bidirectional reflectance modelling of a conifer forest. *IEEE Trans. Geosc. Remote Sensing*, Vol. GE-24, No. 6, pp. 906-919.

Li, X., and Strahler, A.H. (1988). Modelling the gap probability of a discontinuous vegetation canopy. *IEEE Trans. Geosc. Remote Sensing*, Vol. GE-26, No. 2, pp. 161-170.

Lillesand, T.M., and Kiefer, R.W. (1979). *Remote sensing and image interpretation.* (1st edition) John Wiley & Sons, New York, 612 pp.

Lord, D., Desjardins, R.L., and Dube, P.A. (1985). Influence of wind on crop canopy reflectance measurements. *Remote Sensing of Environ.*, Vol. 18, pp. 113-123.

Lovelock, J.E. (1979). *Gaia: A new look at life on Earth.* (1989 reprint) Oxford University Press, Oxford, New York, 154 pp.

MacDonald, R.B., and Hall, F.G. (1980). Global crop forecasting. *Science*, Vol. 208, pp. 670-679.

Markham, B.L. and Barker, J.L. (1985). Spectral characterisation of the Landsat thematic mapper sensors. *Int. J. Remote Sensing*, Vol. 6, No. 5, pp. 697-716.

Markham, B.L. and Barker, J.L. (1987). Thematic Mapper bandpass solar exoatmospheric irradiances. *Int. J. Remote Sensing*, Vol. 8, No. 3, pp. 517-523.

May, G.A., Holko, M.L. and Jones Jr., N. (1986). Landsat large-area estimates for land cover. *IEEE Trans. Geosc. Remote Sensing*, Vol. GE-24, No. 1, pp. 175-184.

McDowell, D.Q. (1974). Spectral distribution of skylight energy for two haze conditions. *Photogramm. Engng.*, Vol. 40, pp. 569-571.

Middleton, E.M., Deering, D.W., and Ahmad, S.P. (1987). Surface anisotropy and hemispheric reflectance for a semiarid ecosystem. *Remote Sensing of Environ.*, Vol. 23, pp. 193-212.

Moran, M.S., Jackson, R.D., Hart, G.F., Slater, P.N., Bartell, R.J., Biggar, S.F., and Santer, R.P. (1988). Surface reflectance factors derived from SPOT-1 HRV data at two view angles. [Place of publication unknown.]

Morris, K.P., and Barnsley, M.J. (1989). An assessment of various procedures for the radiometric correction of the sensor view angle effect. *Proceedings of the $15_{th}$ Annual Conference of the Remote Sensing Society, University of Bristol, 13-15 September 1989.* (RSS)

National Aeronautics and Space Administration (1986). Moderate-Resolution Imaging Spectrometer. *Earth Observing System Instrument Panel Report*, Vol. IIb. NASA, Washington, D.C., 59pp.

National Aeronautics and Space Administration (1987). High-Resolution Imaging Spectrometer: Science opportunities for the 1990s. *Earth Observing System Instrument Panel Report*, Vol. IIc. NASA, Washington, D.C., 74pp.

Nicodemus, F.E. (1970). Reflectance nomenclature and directional reflectance and emissivity. *Applied Optics*, Vol. 9, No. 6, pp.1474-1475.

Oke, T.R. (1978). *Boundary layer climates*. Methuen, London, 372p.

Pinter, P.J., Jr., Jackson, R.D., Ezra, C.E., and Gausman, H.W. (1985). Sun-angle and canopy-architecture effects on the spectral reflectance of six wheat cultivars. *Int. J. Remote Sensing*, Vol. 6, No. 12, pp. 1813-1825.

Pinter, P.J., Jr., Jackson, R.D., Idso, S.B., and Reginato, R.J. (1981). Multidate spectral reflectance as predictors of yield in water stressed wheat and barley. *Int. J. Remote Sensing*, Vol. 2, No. 1, pp. 43-48.

Prasad, C.R., Inamdar, A.K., and Venkatesh, P. (1987). Computation of diffuse solar radiation. *Solar Energy*, Vol. 39, No. 6, pp. 521-532.

Prince, S.D. (1987). Measurement of canopy interception of solar radiation by stands of trees in sparsely wooded savanna. *Int. J. Remote Sensing*, Vol. 8, No. 12, pp. 1747-1766.

Ranson, K.J., Daughtry, C.S.T., Biehl, L.L., and Bauer, M.E. (1985a). Sun-view angle effects on reflectance factors of corn canopies. *Remote Sensing of Environ.*, Vol. 18, pp. 147-161.

Ranson, K.J., Biehl, L.L., and Bauer, M.E. (1985b). Variation in spectral response of soybeans with respect to illumination, view and canopy geometry. *Int. J. Remote Sensing*, Vol. 6, No. 12, pp. 1827-1842.

Reyna, E., and Badhwar, G.D. (1985). Inclusion of specular reflectance in vegetation canopy models. *IEEE Trans. Geosc. Remote Sensing*, Vol. GE-23, No.5, pp. 731-736.

Richardson, A.J., and Wiegand, C.L. (1977). Distinguishing vegetation from soil background information. *Photogramm. Engng. Remote Sensing*, Vol. 43, No. 12, pp. 1541-1552.

Riordan, C., Myers, D., Rymes, M., Hulstrom, R., Marion, W., Jennings, C., and Whitaker, C. (1989). Spectral Solar radiation data base at SERI. *Solar Energy*, Vol. 42, No. 1, pp. 67-79.

Royer, A., Vincent, P., and Bonn, F. (1985). Evaluation and correction of viewing angle effects on satellite measurements of bidirectonal reflectance. *Photogramm. Engng. Remote Sensing*, Vol. 51, No. 12, pp. 1899-1914.

Salomonson, V.V., and Marlatt, W.E. (1971). Airborne measurements of reflected solar radiation. *Remote Sensing of Environ.*, Vol. 2, pp. 1-8.

Schowengerdt, R.A. (1983). Techniques for image processing and classification in remote sensing, 249pp. (Academic Press, London, New York etc.)

Shibayama, M., and Wiegand, C.L. (1985). View azimuth and zenith, and solar angle effects on wheat canopy reflectance. *Remote Sensing of Environ.*, Vol. 18, pp. 91-103.

Simmer, C., and Gerstl, S.A.W. (1985). Remote sensing of angular characteristics of canopy reflectances. *IEEE Trans. Geosc. Remote Sensing*, Vol. GE-23, No. 5, pp. 648-658.

Sirén, K.E. (1987). The shadow band correction for diffuse irradiation based on a two-component sky radiance model. *Solar Energy*, Vol. 39, No. 5, pp. 433-438.

Sjoberg, R.W., Horn, B.K.P. (1983). Atmospheric effects in satellite imaging of mountainous terrain. *Applied Optics*, Vol. 22, No. 11, pp. 1702-1716.

Slater, P.N. (1980). *Remote Sensing: Optics and Optical Systems.* Addison-Wesley, Reading, Massachusetts.

Smith, J.A., Tzeu Lie Lin, and Ranson, K.J. (1980). The Lambertian assumption and Landsat data. *Photogramm. Engng. Remote Sensing*, Vol. 46, No. 9, pp. 1183-1189.

Steven, M.D. (1977). Standard distributions of clear sky radiance. *Quart. J. R. Met. Soc.*, 103, pp. 457-465.

Steven, M.D., and Rollin, E.M. (1985). Estimation of atmospheric corrections from multiple aircraft imagery. *Proceedings of the 3rd International Colloquium on Spectral Signatures of Objects in Remote Sensing, Les Arcs, France, 16-20 Dec., 1985.* (*ESA* SP-247)

Steven, M.D., and Rollin, E.M. (1986). Estimation of atmospheric corrections from multiple aircraft imagery. *Int. J. Remote Sensing*, Vol. 7, no. 4, pp. 481-497.

Stohr, C.J., and West, T.R. (1985). Terrain and look angle effects upon Multispectral Scanner response. *Photogramm. Engng. Remote Sensing*, Vol. 51, No. 2, pp. 229-235.

Strahler, A.H. (1977). Response of woody species to site factors in Maryland, U.S.A.: Evaluation of sampling plans and continuous and binary measurement techniques. *Vegetatio*, Vol. 35, pp. 1-19.

Strahler, A.H. (1978). Response of woody species to site factors of slope angle, rock type, and topographic position in Maryland as evaluated by binary discriminant analysis. *J. Biogeogr.*, Vol. 5, pp. 403-423.

Strahler, A.H. (1988). Mapping spectral directional radiance, spectral directional surface radiance, and spectral bidirectional reflectance distribution functions

for land surface covers using MODIS-T. *Research proposal submitted to the NASA, 6/30/88.* (Department of Geography, Boston University.

Strahler, A.H., Woodcock, C.E., and Smith J.A. (1986). On the nature of models in Remote Sensing. *Remote Sensing of Environ.*, Vol. 20, pp. 121-139.

Strahler, A.H., Yecheng Wu, Franklin, J. (1988). Remote estimation of tree size and density from satellite imagery by inversion of a geometric-optical canopy model. Paper presented at *the 22nd International Symposium on Remote Sensing of the Environment, Abidjan, Côte d'Ivoire*, October 20-26, 1988.

Suits, G.H. (1972a). The calculation of the directional reflectance of a vegetative canopy. *Remote Sensing of Environ.*, Vol. 2, pp. 117-125.

Suits, G.H. (1972b). The cause of azimuthal variations in the directional reflectance of vegetative canopies. *Remote Sensing of Environ.*, Vol. 2, pp. 175-182.

Suits, G.H. and Safir, G.R. (1972). Verification of a reflectance model for mature corn with applications to corn blight detection. *Remote Sensing of Environ.*, Vol. 2, pp. 183-192.

Swain, P.H., and Davis, S.M. (1978). *Remote sensing: the quantitative approach.* McGraw-Hill, New York.

Tanré, D., Deroo, C., Duhart, P., Herman, M., Morcrette, J.J., Perbos, J., and Deschamps, P.Y. (1986). Simulation of the satellite signal in the solar spectrum (5S). *User Guide, January 1986. Laboratoire d'Optique Atmospherique, Université des Sciences et Techniques de Lille, 59655 Villeneuve d'Ascq Cédex, France.*

Teillet, P.M. (1986). Image correction for radiometric effects in remote sensing. *Int. J. Remote Sensing*, Vol. 7, No. 12, pp. 1637-1651.

Temps, R.C., and Coulson, K.L. (1977). Solar radiation incident upon slopes of different orientations. *Solar Energy*, Vol. 19, pp. 179-184.

Townshend, J.R.G. (1981). The spatial resolving power of earth resources satellites. *Prog. in Physical Geography*, Vol. 5, pp. 33-55.

Townshend, J.R.G., and Justice, C.O. (1986). Analysis of the dynamics of African vegetation using the normalized difference vegetation index. *Int. J. Remote Sensing*, Vol. 7, no. 11, pp. 1435-1445.

Townshend, J.R.G., and Justice, C.O. (1989). The spatial variation of land cover at very coarse scales. *Proceedings of the 15th Annual Conference of the Remote Sensing Society, University of Bristol, 13-15 September 1989*, pp. 415-420. (Remote Sensing Society, Nottingham)

Tucker, C.J., and Choudhury, B.J. (1987). Satellite remote sensing of drought conditions. *Remote Sensing of Environ.*, Vol. 23, pp. 243-251.

Tucker, C.J., and Sellers, P.J. (1986). Satellite remote sensing of primary production. *Int. J. Remote Sensing*, Vol. 7, no. 11, pp. 1395-1416.

Tucker, C.J., Townshend, J.R.G., and Goff, T.E. (1985). African land-cover classification using satellite data. *Science*, Vol. 227, pp. 369-375.

Verhoef, W. (1984). Light scattering by leaf layers with application to canopy reflectance modelling: the SAIL model. *Remote Sensing of Environ.*, Vol. 16, pp. 125-141.

Verhoef, W. (1985). Earth observation modeling based on layer scattering matrices. *Remote Sensing of Environ.*, Vol. 17, pp. 165-178.

Walthall, C.L., Norman, J.M., Welles, J.M., Campbell, G., and Blad, B.L. (1985). Simple equation to approximate the bidirectional reflectance from vegetative canopies and bare soil surfaces. *Applied Optics*, Vol. 24, No. 3, pp. 383-387.

Wardley, N.W. (1984). Vegetation index variability as a function of viewing angle geometry. *Int. J. Remote Sensing*, Vol. 5, No. 5, pp. 861-870.

Welch, R., Jordan, T.R., and Ehlers, M. (1985). Comparative evaluations of the geodetic accuracy and cartographic potential of Landsat-4 and Landsat-5 thematic mapper image data. *Photogramm. Engng. Remote Sensing*, Vol. 51, No. 9, pp. 1249-1262

Wiegand, C.L., Richardson, A.J., Jackson, R.D., Pinter, P.J., Aase, J.K., Smika, D.E., Lautenschlager, L.F., and McMurtrey, J.E. (1986). Development of agrometeorological crop model inputs from remotely sensed information. *IEEE Trans. Geosc. Remote Sensing*, Vol. GE-24, No. 1, pp. 90-97.

Williams, D.F. (1984). Overview of the NERC airborne thematic mapper campaign of September 1982. *Int. J. Remote Sensing*, Vol. 5, No. 4, pp. 631-634.

Williamson, H.D. (1989). The discrimination of irrigated orchard and vine crops using remotely sensed data. *Photogramm. Engng. Remote Sensing*, Vol. 55, No. 1, pp. 77-82.

Wilson, A.K. (1986). Calibration of ATM data. *Proceedings of the 1985 NERC airborne campaign workshop, 26th November 1986*, pp. E25-E40. (NERC)

Woodcock, C.E. (1985). *Understanding spatial variation in remotely sensed imagery.* Ph.D. thesis, University of California, Santa Barbara, 136p. University Microfilms International, Ann Arbor, USA.

Woodcock, C.E., and Strahler, A.H. (1987). The factor of scale in remote sensing. *Remote Sensing of Environ.*, Vol. 21, pp. 311-332.

Woodcock, C.E., Strahler, A.H., and Jupp, D.L.B. (1988). The use of variograms in remote sensing: I. Scene models and simulated images. *Remote Sensing of Environ.*, Vol. 25, pp. 323-343.

Woodcock, C.E., Strahler, A.H., and Jupp, D.L.B. (1988). The use of variograms in remote sensing: II. Real digital images. *Remote Sensing of Environ.*, Vol. 25, pp. 349-379.

Woodham, R.J. (1989). Determining intrinsic surface reflectance in rugged terrain and changing illumination. *Proceedings of IGARSS'89; 12th Canadian symposium on Remote Sensing, Vancouver, July 10-14, 1989*, Vol. 1, pp. 1-5.

Woodham, R.J., and Gray, M.H. (1987). An analytic method for the radiometric correction of satellite multispectral scanner data. *IEEE Trans. Geosc. Remote Sensing*, Vol. GE-25, No. 3, pp. 258-271.

Yang, C., and Vidal, A. (1989). Removal of the topographic effect from SPOT-1 HRV multispectral imagery in mountainous terrain. *Proceedings of IGARSS'89; 12th Canadian symposium on Remote Sensing, Vancouver, July 10-14, 1989*, Vol. 2, pp. 471-474.

Zangvil, A., and Aviv, O.E. (1987). On the effect of latitude and season on the relation between the diffuse fraction of solar radiation and the ratio of global extraterrestrial radiation. *Solar Energy*, Vol. 39, No. 4, pp. 321-327.

# GLOSSARY

**AIS:** Airborne Imaging Spectrometer

**Albedo:** Reflectance of a target over the full solar spectrum

**Analogue:** The use of a continuously varying signal to represent a measurement; in RS usually a photograph is considered an analogue image of the object.

**Anisotropic:** Not constant with angle.

**ATM:** **Airborne Thematic Mapper**; an instrument built by Daedalus to simulate the Landsat TM sensor series, used from an aircraft.

**AVHRR:** Advanced Very High Resolution Radiometer, on board NOAA series of platforms

**AVIRIS:** Airborne Visible and Infrared Imaging Spectrometer

**AWS:** **Automatic weather station**, several meteorological sensors connected to a (digital) data logger, needing periodic attention for down-loading of data, batteries *etc*..

**BRDF:** Bidirectional Reflectance Distribution Function; the theoretical description of radiance from a target over infinitesimally small angles (Nicodemus, 1970).

**Canopy:** Generic term for vegetative structures, eg the organisation of leaves and branches making up a tree.

**CPU:** Central Processing Unit.

**CV:** Coefficient of Variation.

**DEM:** A **digital elevation model** is a matrix of reference coordinates, with associated height information only; *cf.* **DTM**.

**Digital:** Data represented as sampled discrete values measured upon a quantised scale.

**Diffuse:** A diffuse surface reflects an equal amount of radiance in every direction, according to Lambert's law.

**Directional Reflectance:** Term to describe the anisotropic reflectance characteristics of a target

**DTM:** A **digital terrain model** is usually a matrix of reference coordinates, with associated information on height and gradient, and/or slope and aspect information; *cf.* **DEM.**

**EOS:** Earth Observing System; multi-sensor satellite platform to be launched 1996.

**FOV:** The **field of view** is defined as the angle subtended by one scan line at the perspective centre of the sensor.

**GRE:** The **ground resolution element** is determined by the projection of the IFOV onto the Earth's surface. For a constant IFOV, the size of the GRE varies as a function of platform altitude and sensor view angle (Slater, 1980).

**HDDT:** **High density digital tape.**

**HIRIS:** High Resolution Imaging Spectrometer, to be launched on board EOS platform 1996.

***H*-res$^n$:** A basic scene model where the size of the elements in the scene are significantly larger than the resolution cells of the sensor and therefore can be resolved (Woodcock, 1985, Woodcock and Strahler, 1987).

**I$^2$S:** **International Imaging Systems**[1]; usually used to refer to the image processing system.

**IFOV:** The geometric **instantaneous field of view** is defined as an angle which is a function of the detector size and the focal length of the optical system (Townshend, 1981).

**Image:** Collection of measurements from sensor, arranged in a systematic fashion (Strahler *et al.* 1986). Can be either **analogue** or **digital.**

---

[1]Trademark

**Irradiance:** Energy impinging on the object, usually from the sky.

**Isotropic:** Constant relationship with angle; see diffuse.

***L*-res$^n$:** A basic scene model where the size of the elements in the scene are significantly smaller than the resolution cells of the sensor, and therefore cannot be resolved (Woodcock, 1985, Woodcock and Strahler, 1987).

**LAI:** **Leaf Area Index**; the ratio of leaf area to ground area.

**Lambertian:** A surface behaving according to Lambert's law; see **diffuse**.

**Landsat:** A series of satellites first launched 1972. Landsat 1 to 3 carried (among other sensors) the MSS; Landsat 4 (1982) and 5 carried the MSS and more importantly the TM sensor.

***M*-res$^n$:** A basic scene model where the size of the elements in the scene are approximately the same as the resolution cells of the sensor. This special case has a significant effect upon image variance.

**MAFF:** **Ministry of Agriculture, Fisheries and Food.**

**Mapics:** Digital mapping and general purpose graphics package[1]; some GIS capabilities and integration with image data.

**Model:** A framework, description of systems for the calculation or simulation of phenomena.

**MODIS:** Moderate Imaging Spectrometer, N (nadir) and T (tilt) versions to be launched on EOS platform 1996.

**MISR:** Multi-angle Imaging SpectroRadiometer, to be launched on EOS platform 1996.

**MSS:** **Multi-Spectral Scanner**, four spectral bands, 50x80m GRE; *cf.* **Landsat**.

**Nadir:** Sub-platform point on datum; has equivalent point on image.

**NASA:** National Aeronautics and Space Administration

**NERC:** Natural Environment Research Council.

**NOAA:** National Oceanic and Atmospheric Administration

**Normalisation:** Strategy that corrects data to a normal, in view angle corrections often the nadir view.

**OS:** **Ordnance Survey**, main UK national mapping service, government body.

**Object:** Feature, or collection of features, of which measurements are made by the sensor, eg the surface of the Earth.

**Off-nadir:** Any angle that is not nadir; an oblique view

**Parcel:** An area of the object generally defined as homogeneous (at the image scale) in the distribution of features within the region; generally relates to a field, forest, land cover type.

**Parametric:** The use of parameters in a physical model, for example of sky radiance.

**Pixel:** A **pixel** is a *picture element* that makes up a digital image; its size is determined by the ground distance between the centres of successive GRE's (across-track), and between successive scan lines (along-track).

**PSF:** The **Point Spread Function** defines how the **radiance** from an object is integrated over the **IFOV**.

**PVI:** **Perpendicular Vegetation Index**, measures the distance, in feature space, of a cover type response from the soil line (Richardson and Wiegand, 1977).

**Radiance:** Upwelling radiant flux from the object to the sensor.

**Scene:** The spatial distribution (at the **object**) of **features** from which measurements of energy flux are made by the sensor.

**Spectral Reflectance:** Often termed "reflectance", actually meaning reflectance of a target over a given spectral range.

**Specular:** Surface with mirror-like reflectance properties.

**SPOT:** *Systeme Probatoire d'Observatoire de la Terre*; French multi-spectral (three bands, 20m GRE) and panchromatic (green/visible band width, 10m GRE) passive sensor, launched 1986, oblique imaging capability up to ±27° off-nadir; *cf.* Chevrel *et al.*, 1981.

**S-bend:** Correction applied to ATM image data to preserve pixel size, and therefore scale, across-track.

**TL:** **Terrain Lite**, the algorithm developed here to model differential terrain illumination, using a **DTM** and spectral and spatial sky radiance distribution models (*cf.* Kay, 1989).

**TM:** **Thematic Mapper**, seven spectral bands, 30m GRE; *cf.* **Landsat**.

**Utilisation:** Strategy that attempts to use the anisotropic reflectance characteristics of targets to obtain information.

# Appendix 1: Field index

This section indexes the main fields used in this study on Bemborough Farm. For location map see figure 3.2, p63.

(Field number, name, crop and variety, sowing date, yield cwt/acre)

Field 2: Big Ground, winter barley *Marinka* C2, 29/9/87, 53

Field 3: Main Ground, ley grass, grazed.

Field 10: Sheffield Thorns, winter barley *Plaisant* C2, 24/9/87, 45.5

Field 18: Far Lotts, winter barley *Plaisant* C3, 22/9/87, 52

Field 20: Lotts Pool, winter barley *Plaisant* C3, 22/9/87, 52.5

Field 21: Hanging Post, winter wheat *Brimstone* C2, 19-23/10/87, 43.5

Field 27: Big Cooks, spring barley *Triumph* C2, 7-9/3/88, 44.5

Field 29: Lotts Barrow Ground, winter barley *Plaisant* C3, 22/9/87, 54

Field 30: D Ground, spring barley *Natasha* C2, 9/3/88, 42.5

Figure 3.1: Location of study site

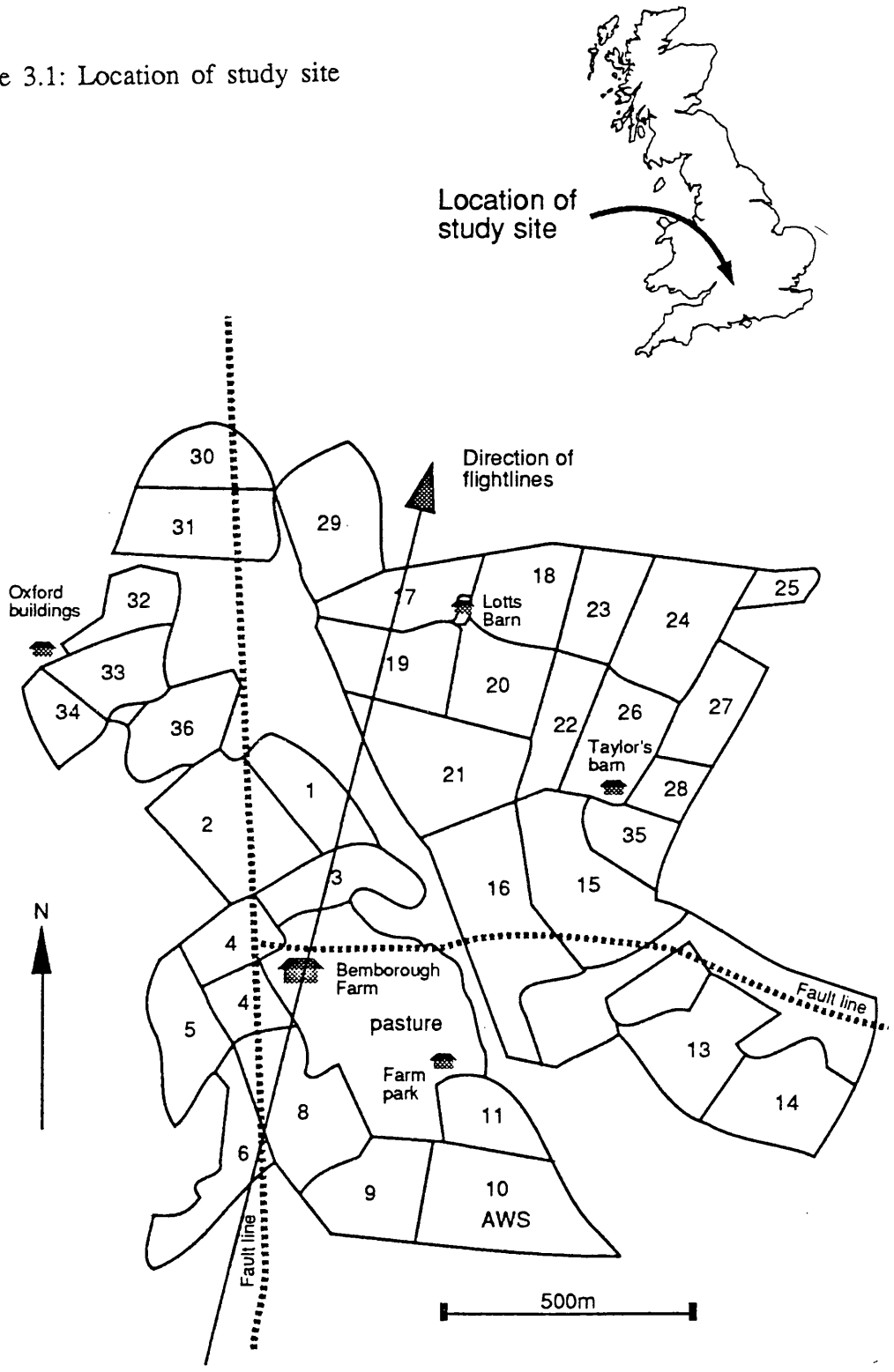


Figure 3.2: Map of study site, including field index (see Appendix 1)

## Appendix 2: Example of Terrain Lite model 3a, encoded in a Mapics command file

```
echo off
define pi 3.141529
define E %3 $ incoming radiation
define albedo %4
$
let c11=(-c4/sqrt(1+c4*c4+c5*c5))
let c12=(-c5/sqrt(1+c4*c4+c5*c5))
let c13=(1/sqrt(1+c4*c4+c5*c5))
$
let c6=sqrt(c4*c4+c5*c5)              $ compute slope
$
let c7=(atan(c5/c4))                  $ compute aspect
$
$ calculate quadrant for aspect
$
make c8 if (c4 lt 0) then ((pi*0.5)-c7) \
   else ((pi*1.5)-c7)
$
let c89=pi*((%2)/180)
let c88=pi*((%1)/180)
label c89 zen
label c88 azi
label c8 asp
eras c1 to c5
$
let c17=c13/c13 $ create a unit column
let c16=c17*cos(zen)
let c17=c17*sin(zen)
let c14=sin(azi)*c17
let c15=cos(azi)*c17
$
$ make the relative aspect column c87
$
let c87=azi-asp
label c87 Raz
$
```

```
$
$The first make is for all facets with some inclination directly at the Sun;
$the else is for all those in shadow
$
$This version FD, Fd, FgD
$
make c21 if (c20 gt 0) then (E*(c20*%5 \
        +(pi-c6)*%6/pi \
        +albedo*cos(zen)*(c6/pi)*(1-sin(zen)*cos(Raz/2)))) \
  else (E*((pi-c6)*%6/pi + albedo*cos(zen)*(c6/pi) \
        *(1-sin(zen)*cos(Raz/2))))
$
$
outgrid 201 251 1 1 201 251 c21 idisk:[rs.simonk.models]temp.hog
$ output in IMO  RS directory
define pi
define albedo
define E
```